'THE TIMING NOT TO RESPOND'

Spatio-temporal high-resolved analysis of the neural response inhibition network in healthy subjects and its changes in psychiatric disease models.

Dissertation
Zur Erlangung des Grades
Doktor der Naturwissenschaften

Am Fachbereich Biologie

Der Johannes Gutenberg-Universität Mainz

Lena Schmüser

geb. am 15.07.1984 in Bad Schwalbach

Mainz, 2016

Dekan:

1. Berichterstatter:

2. Berichterstatter:

Tag der mündlichen Prüfung: 12. Mai 2016

D77: Dissertation Johannes Gutenberg-Universität Mainz

Ich erkläre, dass ich die vorgelegte Thesis selbständig, ohne unerlaubte fremde Hilfe und nur mit den Hilfen angefertigt habe, die ich in der Thesis angegeben habe. Alle Textstellen, die wörtlich oder sinngemäß aus veröffentlichten oder nicht veröffentlichten Schriften entnommen sind, und alle Angaben, die auf mündlichen Auskünften beruhen, sind als solche kenntlich gemacht. Bei den von mir durchgeführten Untersuchungen habe ich die Grundsätze guter wissenschaftlicher Praxis, wie sie in der Satzung der Johannes Gutenberg - Universität Mainz zur Sicherung guter wissenschaftlicher Praxis niedergelegt sind, eingehalten.

Lena Schmüser

(Mainz, den 23. März 2016)

'Dass etwas neu ist und daher gesagt werden sollte, merkt man erst, wenn man auf scharfen Widerspruch stößt.'

Konrad Lorenz (1903-1989)

Danksagung

This page was removed for data privacy protection reasons.

This page was removed for data privacy protection reasons.

Zusammenfassung

Die Fähigkeit, das eigene Verhalten in Reaktion auf komplexe Umweltveränderungen anzupassen, ist essentiell für jedes Lebewesen. Eine wichtige Komponente ist hierbei die Fähigkeit, Verhaltensimpulse umzulenken, aufzuhalten oder zu unterbrechen - man bezeichnet dies als Reaktionsinhibition. Bei gesunden Erwachsenen werden die inhibitionsbezogenen neuronalen Prozesse mit der Aktivität in einem ausgedehnten fronto-striatalen Netzwerk assoziiert. Elektrophysiologisch sind diese inhibitorischen Prozesse mit einem markanten negativen Ausschlag um 150–400 ms nach Stimulusbeginn, gefolgt von einem positiven Ausschlag um 300–500 ms, assoziiert. Die separate Analyse von funktionellen magnetresonanztomographischen Daten (fMRT) und elektrophysiologischen ereigniskorrelierten Potentialen (EKP) liefert jedoch nur Informationen entweder in der räumlichen (fMRT) oder in der zeitlichen (EKP) Domäne. Die kombinierte Auswertung von simultanen elektroenzephalographischen (EEG) Daten und fMRT-Daten ist hingegen ein wirkungsvolles Verfahren, um die neuronalen Reaktionen unterschiedlicher Aspekte und/oder Phasen der Informationsverarbeitung während der Reaktionsinhibition zu entschlüsseln.

Ziel der vorliegenden Dissertation war die umfangreiche Charakterisierung der Dynamik des neuronalen Netzwerkes der Reaktionsinhibition in verschiedenen Gruppen erwachsener Probanden - bei gesunden Erwachsenen sowie in Patientengruppen, die durch defizitäre Inhibitionskontrolle charakterisiert sind, d.h. bei Patienten mit dem Aufmerksamkeitsdefizit-/Hyperaktivitätssyndrom (ADHS) und bei Patienten mit der Borderline-Persönlichkeitsstörung (BPS). Dies ermöglichte neue Einblicke in die räumlich-zeitliche Dynamik der neuronalen Prozesse der Reaktionsinhibition bei gesunden Probanden (Studie 1, Kapitel 3) und trug zu einem umfangreicheren Verständnis der Neuropathophysiologie der defizitären Reaktionsinhibition in den unterschiedlichen Krankheitsmodellen (AHDS und BPS, Studie 2, Kapitel 4) sowie bei gesunden Probanden, die durch eine impulsivere Persönlichkeitseigenschaft charakterisiert sind (Studie 3, Kapitel 5), bei. Zu diesem Zweck wurde ein neues, datengesteuertes Analyseverfahren eingeführt und zunächst anhand einer Stichprobe gesunder Probanden validiert (Studie 1, Kapitel 3) und anschließend auf die Daten von ADHS- und BPS-Patienten angewandt (Studie 2, Kapitel 4).

Dieses neu entwickelte Analyseverfahren selektiert automatisch aufgabenspezifische elektrophysiologisch unabhängige Komponenten (engl. independent components, ICs), welche reliabel mit der Reaktionsinhibition in unterschiedlichen Phasen der Aufgabenausführung zusammenhängen. Da diese inhibitionsbezogenen ICs auf der Ebene der Einzelprobanden identifiziert wurden, garantiert dieser Ansatz, dass die Variabilität der gewählten elektrophysiologischen Komponenten spezifisch für die anvisierten neurophysiologischen Prozesse auf Gruppenniveau und auf der Ebene der Einzelprobanden ist. Das Verfahren steht im deutlichen Gegensatz zu bisherigen kombinierten EEG-/fMRT-Analysen, da diese Methoden darauf ausgerichtet waren, bekannte EKP-Komponenten zu vermessen, die auf Gruppenniveau bestimmt wurden, ungeachtet der interindividuellen Unterschiede. Der Vergleich dieses konventionellen Verfahrens mit dem neuentwickelten IC-basierten

Verfahren zeigte für Letzteres eine größere Spezifität für aufgabenbezogene neuronale Aktivität. Einzeltrial-Korrelationen dieser automatisch selektierten inhibitionsspezifischen ICs mit der fMRT-Antwort zeigten, dass die Aktivität in den fronto-striatalen Regionen in einer frühen Phase der Aufgabenausführung stärker ausgeprägt war verglichen mit einer späten Phase der Aufgabenausführung.

Dieses neue IC-basierte Analyseverfahren wurde anschließend dazu verwendet, die zeitliche und räumliche Dynamik der neuronalen Prozesse zu untersuchen, die der defizitären Reaktionsinhibition bei ADHS-Patienten, zugrunde liegen, im Vergleich zu den ebenfalls impulsiven BPS-Patienten und gesunden Probanden (Studie 2, Kapitel 4). Dies ermöglicht es, gezielt zu untersuchen, ob nur bestimmte, zeitlich abgrenzbare Phasen der neuronalen Verarbeitung in einer bestimmten Patientengruppe wie den erwachsenen ADHS-Patienten beeinträchtigt sind. Defizitäre Impulskontrolle, also die Tendenz zu impulsiven (Re-)Aktionen und impulsiven Entscheidungen, wird als zentrales Element bei psychiatrischen Störungen wie ADHS und BPS angesehen. Ungeachtet solider Befunde von klinisch relevantem impulsiven Verhalten bei BPS-Patienten deuten neuste fMRT-Studien darauf hin, dass das neuronale Impulskontrollnetzwerk bei BPS-Patienten weitestgehend intakt ist. Daher wird diskutiert, ob das impulsive Verhalten von BPS-Patienten aus einer Interaktion zwischen negativen Emotionen/defizitärer Emotionsregulation und der Impulskontrolle resultieren könnte. Im Gegensatz dazu wird angenommen, dass Dysfunktionen im fronto-striatalen Netzwerk eine zentrale Rolle in der ADHS-Pathophysiologie innehaben, auch wenn dies kaum durch unimodale fMRT-Studien bestätigt wird. In Übereinstimmung damit zeigten die unimodalen fMRT-Analysen der Studie 2 (Kapitel 4) eine Unteraktivierung in striatalen Regionen bei ADHS-Patienten, aber keine Unterschiede zwischen BPS-Patienten und gesunden Kontrollprobanden. Einzeltrial-EEG-/fMRT-Korrelationen enthüllten signifikante Unteraktivierungen in fronto-striatalen Regionen bei ADHS-Patienten im Vergleich zu gesunden Kontrollprobanden und BPS-Patienten, aber nur geringe Unterschiede zwischen BPS-Patienten und gesunden Kontrollprobanden. Dies liefert erste Hinweise darauf, dass kritische Regionen des neuronalen Reaktionsinhibitionsnetzwerkes bei erwachsenen ADHS-Patienten zeitlich nicht gut abgestimmt sind, während dieses Netzwerk bei BPS-Patienten nur geringfügig beeinträchtigt ist, was auf einen ADHS-spezifischen Pathomechanismus hinweist.

Man nimmt an, dass interindividuelle Unterschiede in der intraindividuellen Variabilität einen zentralen pathologischen Prozess bilden, welcher der defizitären Impulskontrolle bei psychiatrischen Störungen zugrunde liegt. Durch die zeitliche Auflösung des EEG's im Millisekunden-Bereich wird es ermöglicht, die neuronalen Korrelate kognitiver Prozesse mit einem genau definierten zeitlichen Zusammenhang zu einem gegebenen Ereignis zu bestimmen. Dies ermöglicht die Analyse von Trial-zu-Trial-Variabilität und, basierend darauf, eine detaillierte Analyse interindividueller Unterschiede. Diese Information kann für die Klassifikation neurokognitiver Unterschiede in der interindividuellen neuronalen Variabilität genutzt werden, nicht nur zwischen gesunden Kontrollprobanden und Patientengruppen, sondern auch innerhalb einer Gruppe gesunder Probanden. Dennoch existiert bislang keine kombinierte EEG-/fMRT-Studie, welche diese Information über die neuronale Variabilität für

eine Subgruppenklassifikation genutzt hat. Das Vorhandensein oder Fehlen spezifischer ICs, welche mit inhibitionsspezifischen Prozessen zu einem frühen Zeitpunkt der Reaktionsinhibition assoziiert sind (Studie 1, Kapitel 3), können für eine vollkommen datengesteuerte Subgruppenklassifikation genutzt werden (Studie 3, Kapitel 5). Anschließend durchgeführte unimodale EEG- und fMRT-Analysen sowie konventionelle Einzeltrial-EKP/fMRT-Analysen zeigten, dass die beobachteten interindividuellen Unterschiede in einem elektrophysiologischen Korrelat der Reaktionsinhibition mit verschiedener neuronaler Aktivität assoziiert sind. Dies könnte ein Hinweis auf das Vorhandensein elektrophysiologisch trennbarer Phänotypen der verhaltensbezogenen und neuronalen Reaktionsinhibition sein, sogar in einer Gruppe gesunder Probanden. Es kann die Hypothese aufgestellt werden, dass der Phänotyp, der durch die Existenz von mit frühen inhibitorischen Prozessen assoziierten ICs charakterisiert ist, protektiv gegen impulsivitätsbezogene Dysfunktionen sein könnte. Dies zeigt, dass die Verwendung eines Verfahrens, das sensitiv für interindividuelle Unterschiede ist, bei gesunden Probanden eine Subgruppenklassifikation ermöglicht und somit auch eine Identifizierung und Charakterisierung der neuronalen Korrelate interindividueller Unterschiede in der Reaktionsinhibition. Dies wiederrum kann wichtige Informationen für unser Verständnis der Defizite in der Reaktionsinhibition heterogener psychiatrischer Störungen wie ADHS und BPS liefern.

Summary

The ability to adapt their own behavior in response to complex environmental changes is essential for living beings. An important component of this is the ability to redirect, withhold or interrupt behavioral impulses—known as response inhibition. In adult healthy subjects, inhibition-related neural processes are associated with activity in a broad fronto-striatal network. Electrophysiologically, these inhibitory processes have been associated with a prominent negative deflection around 150–400 ms after stimulus onset followed by a large positive deflection at 300–500 ms. However separate analyses of functional magnetic resonance imaging (fMRI) data or electrophysiological event-related potentials (ERPs) provide information only on the spatial (fMRI) or temporal (ERP) domain. A combined analysis of simultaneous electroencephalographic (EEG) and fMRI data is a powerful tool to disentangle neural responses related to different aspects and/or stages of information processing during response inhibition.

The aim of the present thesis was to comprehensively characterize the dynamics of the neural response inhibition network in several groups of adult subjects, healthy adults as well as patients characterized by deficient inhibitory control, i.e., Attention-Deficit/Hyperactivity Disorder (ADHD) or Borderline Personality Disorder (BPD). This provided new insights into the spatio-temporal dynamics of neural processes in healthy controls (Study 1, Chapter 3) and contributed to a more comprehensive understanding of neural pathophysiology of deficient inhibitory control in the different disease models (ADHD and BPD, Study 2, Chapter 4) as well as in healthy controls characterized by a higher impulsive personality trait (Study 3, Chapter 5). To this end a new data-driven analysis procedure was introduced and first validated in a sample of healthy controls (Study 1, Chapter 3) and then applied to the data of ADHD and BPD patients (Study 2, Chapter 4). This newly developed analysis procedure automatically selects task-specific electrophysiological independent components (ICs) which are reliably related to response inhibition at different phases of task execution. Since inhibition-related ICs are identified on the single-subject level, this approach guarantees that the variability of the chosen electrophysiological component is specific for the targeted neurophysiological process on the group and single-subject level. This procedure is in clear distinction to previous applications of combined EEG/fMRI analyses, as these approaches aimed to measure known ERP components defined on the group level, irrespective of inter-individual differences. Comparisons between this conventional approach and the newly developed IC-based approach revealed that the latter provides greater specificity for task-related neural activity. Single-trial correlations of automatically selected inhibition-related ICs with fMRI responses revealed activity in fronto-striatal regions which was more pronounced in an early compared to a late phase of task execution.

This new IC-based analysis procedure was then used to examine the temporal and spatial dynamics of neural processes underlying response inhibition deficits in adult patients with ADHD compared to impulsive patients with BPD and healthy control subjects (Study 2, Chapter 4).

This procedure allows to specifically examine whether only certain, temporally distinct phases of neural processing are affected in a specific patient group, e.g., in adult ADHD patients. Deficient impulse control, i.e., the tendency towards impulsive (re-)actions and impulsive choices is viewed as a key element in psychiatric disorders such as ADHD and BPD. Despite robust findings of clinically relevant impulsive behaviors in BPD patients, recent fMRI studies point towards an almost intact neural response inhibition network in BPD patients. Thus it is said that impulsive behaviors in BPD patients may arise from an interaction between negative emotions/deficient emotion regulation and impulse control. In contrast, in adult ADHD patients, dysfunctions in the fronto-striatal network are thought to be central in ADHD pathophysiology although this is rarely confirmed by unimodal fMRI studies. In line with this, unimodal fMRI data analysis of Study 2 (Chapter Chapter 4) revealed a hypoactivation of striatal regions in ADHD compared to healthy controls, but no differences between BPD and healthy controls. Single-trial EEG/fMRI correlations unveiled significantly reduced activity in frontal-striatal regions in ADHD in comparison to both BPD and healthy controls, but only marginal differences between healthy controls and BPD. This provides initial evidence that critical regions of the neural response inhibition network are temporally not well orchestrated in adult ADHD patients while this network was only mildly affected in BPD patients, hence pointing to an ADHD-specific pathomechanism.

Between-subject differences in the intra-individual variability have been said to be a key to pathological processes underlying deficient impulse control in psychiatric disorders. Due to its millisecond-scale temporal resolution, EEG allow for an assessment of the neural correlates of cognitive processes with precisely defined temporal relationship relative to a given event and thus for the analysis of trial-to-trial neural variability and, based on that, for detailed inter-individual difference analysis. This information can be used to classify neurocognitive differences in inter-individual neural variability not only between healthy controls and patient groups but also within a group of healthy subjects. Nevertheless, at present no combined EEG/fMRI studies used this neural variability information for subgroup classification. Using the existence or absence of ICs related to inhibition-specific processing at an early stage of response inhibition (Study 1, Chapter 3) permits subgroup classification in a completely data-driven way (Study 3, Chapter 5). Subsequent unimodal ERP and fMRI analysis as well as conventional single-trial ERP/fMRI analysis revealed that the observed inter-individual differences in an electrophysiological correlate of response inhibition is associated with distinct neural activity. This may suggest the existence of electrophysiologically dissociable phenotypes of behavioral and neural motor response inhibition even in a group of healthy control subjects. It could also be hypothesized that the phenotype characterized by the existence of ICs related to early inhibitory processes may provide protection against impulsivity-related dysfunction. Using an approach sensitive to inter-individual varieties allows for subgroup classification and, hence, identification and characterization of neural correlates of inter-individual differences in response inhibition in healthy subjects. This in turn may provide important information for our understanding of deficits in response inhibition in heterogeneous psychiatric disorders such as ADHD or BPD.

Contents

List of Tables

List of Figures

List of abbreviations

AAL automated anatomical labeling

AAS average artifact substraction

ACC anterior cingulate cortex

ADHD Attention-Deficit/Hyperactivity Disorder

ANOVA analysis of variance

BCG ballistocardiographic

BDI Beck Depression Inventory

BIS-11 Barratt Impulsiveness Scale-11

BMBF Bundesministeriums für Bildung und Forschung

BOLD blood oxygenation level-dependent

BPD Borderline Personality Disorder

BPDSI Borderline Personality Disorder Severity Index

CAARS-S:L Conners' Adult ADHD Rating Scale

CoV coefficient of variability

DF degree of freedom

DSM Diagnostic and Statistical Manual of Mental Disorders

ECG electrocardiogram

EEG electroencephalography

EOG electrooculogram

EPI echo planar image

ERP event-related potential

fMRI functional magnetic resonance imaging

FOV field of view

FWE family-wise error

FWHM full-width at half maximum

GLM generalized linear model

HC healthy control

HRF hemodynamic response function

IC independent component

IC+ Nogo-IC-positive

IC− Nogo-IC-negative

ICA independent component analysis

ICD International Classification of Diseases

IFC inferior frontal cortex

IFG inferior frontal gyurs

IFJ inferior frontal junction

infomax information-maximization

IQR inter-quartile range

MADRS Montgomery Asberg Depression Scale

MCC middle cingulate cortex

MEG magnetoencephalography

MNI Montreal Neurological Institute

MPRAGE magnetization prepared, rapid acquisition gradient echo

MRI magnetic resonance imaging

MWT-B German multiple-choice vocabulary test

NIMH National Institute of Mental Health

PACE prospective acquisition correction

PCC posterior cingulate cortex

pre-SMA pre-supplementary motor area

PTSD post-traumatic stress disorder

RDoC Research Domain Criteria

RF radio frequency

ROI region of interest

RT Go response time

SCID I Structural Clinical Interviews for DSM-IV Axis I Disorders

SCID II Structural Clinical Interviews for DSM-IV Axis II Disorders

SMA supplementary motor area

SPM Statistical Parametric Mapping

SSS-V Sensation Seeking Scale

STN subthalamic nucleus

TE echo time

TR repetition time

UPPS UPPS Impulsive Behavior Scale

VEP visual-evoked potential

voxel volume element

WURS-k Wender Utah Rating Scale

1. Introduction

1.1. Impulse control

The ability to adapt or inhibit their own behavioral impulses in response to external influences is essential especially in a complex and rapidly changing environment. This flexible adaption of behaviors in interaction with changing situations or environments is mediated by higher order cognitive functions referred to as executive functions (Barkley, 1997; Diamond, 2013; Garavan, 2002; Logue and Gould, 2014).

Impulse control refers to the ability to refrain from actions which are not, or no longer, adequate to the current situation or even harmful for oneself or others. Impulse control is considered as a cold executive function that is related to a right-lateralized network of prefrontal cortex and basal ganglia (Aron, 2007, 2011; Garavan, 2002; Garavan et al., 2006; Munakata et al., 2011; Rubia, 2011; Schuch et al., 2015; Sebastian et al., 2015; Simmonds et al., 2008; Swick et al., 2011). Within the broad concept of impulse control (Aron, 2011; Simmonds et al., 2008; Swick et al., 2011), the component that controls motor responses and behavioral impulses on a late stage of output processing is referred to as response inhibition (Sebastian et al., 2013a; Stahl et al., 2014). The behavioral and neural correlates of inhibitory control over motor responses will be discussed in the following (cf. Section 1.1.1).

Impulsivity, i.e., the tendency towards impulsive (re-)actions and impulsive choices is viewed as a key element of a variety of psychiatric diseases such as Attention-Deficit/Hyperactivity Disorder (ADHD, cf. Section 1.1.2) and Borderline Personality Disorder (BPD, cf. Section 1.1.3) (American Psychiatric Association, 1994). This emphasizes the importance of impulse control for the individual's daily life and social functioning, and thus on the mental health (Chamberlain and Sahakian, 2007).

1.1.1. Response inhibition

Response inhibition refers to the ability to suppress inadequate but inadvertently activated prepotent or ongoing motor response tendencies (Barkley, 1997; Miyake, 2000; Stahl et al., 2014; Swick et al., 2011). This can be operationalized by a variety of paradigms such as Go/Nogo, Stop-Signal, Simon, Erikson flanker, Stroop, Continuous Performance and many others (Aron, 2011; Nee et al., 2007). It has been shown, that stopping motor responses is related neuroanatomically to right-lateralized prefrontal activation (Aron, 2011; Chambers et al., 2009) and electrophysiologically to the N2/P3 complex a characteristic sequence of a negative deflection at 150–400 ms and a positive deflection at 300–500 ms after stimulus onset (Falkenstein et al., 1999; Huster et al., 2013).

To assess the neural underpinnings of response inhibition in human beings, functional magnetic resonance imaging (fMRI or neuroimaging, cf. Section 1.2.1) and electroencephalography (EEG, cf. Section 1.2.2) are most often used. fMRI is a noninvasive technique that provides an indirect measurement of neural activity through the inherent coupling of slow metabolic and hemodynamic changes to local changes in neural activity (Ogawa et al., 1992). fMRI comes with low temporal resolution but with a high spatial resolution that enables to localize brain regions engaged during cognitive processes. As opposed to this, EEG is a direct measurement of neural brain activity mainly generated from cortical pyramidal cells (Bucci and Galderisi, 2011; Laufs, 2008; Woodman, 2010). As such it comes with significantly higher temporal resolution than fMRI measurement, but with substantially reduced spatial resolution. Amplitude and latency characteristics of event-related potentials (ERPs, i.e., EEG data averaged to a certain type of stimulus) are typically used to assess the temporal dynamics of large-scale neural activity in relation to a given stimulus or experimental condition.

1.1.1.1. Neuronal underpinnings of response inhibition

Neuroimaging studies showed that response inhibition as assessed by Stop-Signal and Go/Nogo paradigms is associated with activations in cortical and subcortical structures of a predominantly right hemispheric fronto-striatal network (Aron, 2011; Aron and Poldrack, 2006; Chambers et al., 2009). This network is composed of the right inferior frontal gyurs (IFG) stretching to anterior insula, the pre-supplementary and supplementary motor areas (pre-SMA, SMA), and the inferior parietal lobe, as well as striatum and the subthalamic nucleus (STN) (Aron et al., 2003a; Chambers et al., 2009; Chikazoe et al., 2009; Garavan et al., 2006; Jahfari et al., 2011; Konishi et al., 1998; Sebastian et al., 2013a, 2015; Sharp et al., 2010; Simmonds et al., 2008; Swick et al., 2011).

However, although there is evidence for overlapping activation in right ventrolateral prefrontal cortex, IFG, and pre-SMA, it has been repeatedly advocated that neither impulse control in general nor inhibitory control on the response level is an unitary construct (Aron, 2011; Chambers et al., 2009; Schachar et al., 2007; Sebastian et al., 2013a; Stahl et al., 2014). It seems plausible

that the process of withholding a prepotent motor response as assessed by the Go/Nogo task is closely related to, but different from, the process of canceling an already initiated motor response as assessed by the Stop-Signal task. This is supported by neuroimaging studies demonstrating that the neural networks as assessed by Stop-Signal and Go/Nogo tasks are associated with functionally distinct subcomponents of response inhibition (Aron, 2011; Dalley et al., 2011; Eagle and Baunez, 2010; Eagle et al., 2008; Rubia et al., 2001a; Sebastian et al., 2012, 2013a; Stahl et al., 2014; Swick et al., 2011). Thus, inconsistency in results as revealed by neuroimaging studies as well as by electrophysiological studies on response inhibition might be caused by the fact that these studies operationalized different subcomponents of response-related control.

1.1.1.2. Electrophysiological correlates of response inhibition

Electrophysiologically, the comparison between Go- and Nogo-related ERPs typically reveals robust task-dependent differences, mainly concerning the N2/P3 complex. This is a pronounced negative deflection at fronto-central electrodes (N2 or N200) followed by a late positive deflection over central electrodes (P3 or P300) which are both elicited stronger by Nogo stimuli relative to Go stimuli (Bokura et al., 2001; Falkenstein et al., 1999; Jodo and Kayama, 1992; Kopp et al., 1996; Ruchsow et al., 2008a; Simson et al., 1977). N2 is a negative deflection that typically appears at a latency of 150–400 ms with its largest deflection at the fronto-central electrode site Fz (Falkenstein et al., 1999). Nogo-N2 is assumed to reflect early, pre-motor processes of response inhibition (Beste et al., 2010; Falkenstein et al., 1999; Jodo and Kayama, 1992; Lavric et al., 2004). Nogo-P3 is a positivity deflection at the latency of 300–500 ms that reaches its maximum at central electrode sites Cz and Fz (Falkenstein et al., 1999). Nogo-P3 has been assumed to reflect the process of response inhibition (Beste et al., 2010; Falkenstein et al., 1999; Huster et al., 2013; Wessel and Aron, 2015). N2 and P3 together are also referred to as the N2/P3 complex.

Even though the N2/P3 complex has been associated with the inhibitory process (Falkenstein et al., 1999; Simson et al., 1977), there is also growing evidence that N2/P3 may reflect separable aspects of response inhibition, attentional processes and/or conflict and performance monitoring rather than response inhibition exclusively (Huster et al., 2013). Thus, although Nogo-N2 is assumed to reflect pre-motor processes either directly related to response inhibition (Beste et al., 2010; Falkenstein et al., 1999; Jodo and Kayama, 1992; Lavric et al., 2004), evidence is emerging that N2 may reflect rather other cognitive processes such as conflict monitoring or action updating (Donkers and van Boxtel, 2004; Huster et al., 2013; Nieuwenhuis et al., 2004). Likewise, the Nogo-P3 has also been assumed to reflect the process of response inhibition directly (Beste et al., 2010; Falkenstein et al., 1999; Huster et al., 2013; Wessel and Aron, 2015), but it has also been argued that the P3 do peak too late to reflect inhibitory processes (Dimoska et al., 2003; Huster et al., 2013; Naito and Matsumura, 1994) so that it has been claimed that P3 may reflect rather evaluative processes such as stimulus or performance evaluation (Friedman et al., 2001; Huster

et al., 2013; Liotti et al., 2005; Schmajuk et al., 2006; Wu and Zhou, 2009). Thus, it has been suggested that N2 and P3 may reflect task-independent stages of higher-level processing rather than modality specific components (Huster et al., 2013).

This view is supported by recent combined EEG/fMRI studies, demonstrating that N2 and P3 are most likely associated with anatomically and functionally distinguishable neural sources. Huster and colleagues for instance showed that neural generators of N2 and P3 can be clearly differentiated (Huster et al., 2010). Whereas the major generators of Nogo-N2 were predominantly located in the anterior part of the left middle cingulate cortex (MCC) and in the left IFG, the neural generators of Nogo-P3 were found primarily in the posterior part of right MCC as well as in middle frontal and precentral regions, and bilateral insula. Also supporting the notion that Nogo-N2 and Nogo-P3 are associated with different neural sources, a recently published EEG and fMRI study demonstrated that comparisons of task-conditions related to motor and cognitive (non-motor) inhibition revealed significant task-related effects only for Nogo-P3 but not for Nogo-N2 components (Smith et al., 2013b). The authors concluded that the Nogo-P3 is most likely related to movement-related negativity in the Go condition and not to inhibition related positivity in the Nogo condition. In contrast to this, however, pure ERP waveforms clearly demonstrate larger P3 in Nogo compared to Go (Beste et al., 2010; Falkenstein et al., 1999; Huster et al., 2013; Wessel and Aron, 2015). In the end the functional relevance of different ERP components to distinct cognitive processes remains unclear, so that it may be more reasonable to conceive these positive and negative deflections as indicative of task-independent sequential neural processing steps.

1.1.1.3. Spatio-temporal dynamics of response inhibition

Combined analysis of simultaneous EEG and fMRI data (cf. Section 1.2.3) can be used to disentangle neural responses related to different aspects and/or stages of information processing during response inhibition (Baumeister et al., 2014; Huster et al., 2011; Karch et al., 2008, 2014; Lavallee et al., 2014). This takes advantage of the fMRI's high spatial resolution and the EEG's high temporal resolution (Debener et al., 2005, 2006; Eichele et al., 2005; Huster et al., 2012). It has been demonstrated that correlating inhibition-related EEG features with fMRI blood oxygenation level-dependent (BOLD) signal can help to disentangle different stages of neural processing during response inhibition (Baumeister et al., 2014; Huster et al., 2011; Karch et al., 2008, 2014; Lavallee et al., 2014). However, as these few studies have employed very different paradigms and wide variety of analysis approaches they revealed largely deviant results.

Using a cued auditory Go/Nogo task and simultaneous EEG/fMRI, Karch and colleagues for example found correlations of fMRI BOLD signal in insula, right temporo-parietal and medial frontal cortex with fronto-central Nogo-P3 amplitude values (Karch et al., 2008). Combining Stop-Signal related EEG time-frequency values with fMRI signal, revealed an significant association

between fronto-central delta, theta and left motor high beta with increased right IFG and left middle frontal gyrus activity (Lavallee et al., 2014). Equally using a Stop-Signal paradigm, Huster et al. (Huster et al., 2011) demonstrated an association between Stop-Signal N2/P3 ERP values and fMRI activity in regions linked to response inhibition such as basal ganglia, anterior MCC and pre-SMA and the anterior insula. Using a combined Flanker and Go/Nogo task, Baumeister et al. (Baumeister et al., 2014) found that across conditions, N2 was correlated with deactivations in cingulate motor area and parts of the default mode network, while P3 was correlated with activations in left anterior insula, IFG and posterior cingulate cortex (PCC).

1.1.1.4. Neural underpinnings of response inhibition in personality trait of impulsivity

Even in a group of adult healthy subjects, the degree and effectiveness of inhibition in response inhibition paradigms varies across individuals. Thus, it seems reasonable to assume that such inter-individual differences constitute valuable information. However, the relationship between the personality trait of impulsivity and the neural underpinnings of response inhibition has not yet been investigated adequately. Only few neuroimaging (Asahi et al., 2004; Brown et al., 2015; Collins et al., 2012; Horn et al., 2003) and electrophysiological (Kam et al., 2012; Ruchsow et al., 2008a; Russo et al., 2008; Shen et al., 2014) studies exist on the subject of personality trait of impulsivity in healthy subjects. Moreover, potentially due to the multifaceted nature of impulsivity as well as the variety of employed task designs, these studies provided inhomogeneous results.

Some studies found negative correlations between high impulsive personality traits as assessed by the Barratt Impulsiveness Scale-11 (BIS-11, Patton et al., 1995) and reduced neural activity in prefrontal areas (Asahi et al., 2004) as well as significantly reduced P3 amplitudes (Kam et al., 2012; Russo et al., 2008; Shen et al., 2014). Positive correlations with BIS-11 subscale 'motor impulsiveness' but not with other BIS-11 subscales nor with total BIS-11 score might indicate a particular sensitivity of the right prefrontal cortex to motor impulsivity (Asahi et al., 2004). However, another study found an association between reduced prefrontal activity and higher risk tendency but not with higher BIS-11 scores (Brown et al., 2015). Using reaction time variability as a task-related measure of impulsivity instead of self-rated questionnaires, Ruchsow and colleagues (Ruchsow et al., 2008a) demonstrated that non-clinical high impulsive subjects compared to low impulsive subjects had significantly reduced Nogo-P3 amplitudes but no differences in Nogo-N2.

In contrast to this, there is also evidence for enhanced neural activity in subjects with a high impulsive personality. Several studies reported positive correlations between different impulsivity measures and enhanced neural activity in right prefrontal areas and left temporal gyrus (Horn et al., 2003), overall enhanced neural activity in Go condition (Collins et al., 2012), as well as significantly enhanced P3 amplitudes in high impulsive subjects (Kóbor et al., 2014). Positive correlations between Eysenck's Impulsivity Scale (Eysenck et al., 1985) and neural activity in right prefrontal

areas as well as positive correlations between BIS-11 and left temporal gyrus may indicate that subject with a higher impulsive personality trait needed to recruit more neuronal resources in order to attain an appropriate degree of response inhibition (Horn et al., 2003). In line with this, another study reported enhanced neural activity in Go condition but not in Nogo condition of an equal probability Go/Nogo task in subjects with a high sensation seeking profile (Collins et al., 2012). This may support the notion of additional, potentially overactive or overreactive recruitment of neural resources in subjects with a higher impulsive personality trait. Thus, despite of the mixed picture, these findings may indicate that potentially different dimensions of the personality trait of impulsivity are accompanied by altered neural network activity.

Assessing the correlation between impulsiveness and response inhibition functions in non-clinical populations, several ERP studies also demonstrated an association between personality traits of impulsivity and altered neural activity, as expressed in deviating Nogo-P3 amplitudes (Kam et al., 2012; Kóbor et al., 2014; Ruchsow et al., 2008a; Russo et al., 2008; Shen et al., 2014). Two studies demonstrated that high impulsive subjects compared to low impulsive subjects had significantly reduced Nogo-P3 amplitudes but no differences in Nogo-N2 amplitudes during response inhibition (Ruchsow et al., 2008a; Shen et al., 2014), while one study found enhanced P3 amplitudes during response interference in high impulsive subjects (Kóbor et al., 2014). However, response inhibition and response interference are related to different neural networks (Sebastian et al., 2013a; Stahl et al., 2014). Thus, enhanced P3 amplitudes in the context of response interference can be seen as reflecting enhanced attentional effort, while in the context of response inhibition reduced P3 amplitudes are thought to indicate less effective inhibitory processes (Beste et al., 2010; Falkenstein et al., 1999; Huster et al., 2013; Wessel and Aron, 2015).

Although counterintuitive at the first glance, these opposed alterations in P3 amplitudes in the context of response inhibition and response interference may indicate less effective neural processing in high impulsive subjects. In congruency with this, correlation analysis revealed significant negative correlations between P3 amplitudes and BIS-11 total scores in an oddball paradigm (Russo et al., 2008) as well as between P3 amplitudes and BIS-11 subscale 'motor impulsiveness' in a continuous performance task (Kam et al., 2012). As significant negative correlations were found regardless of task condition, the authors concluded that reduced P3 amplitudes in high impulsive subjects could reflect reduced efficiency in cognitive processing as well as in inhibiting task-irrelevant information (Kam et al., 2012; Russo et al., 2008). Further findings of positive correlations between P3 amplitudes and BIS-11 subscale 'non-planning' as well as no significant correlations between P3 amplitudes and BIS-11 subscale 'inattention' may indicate that this is specific for a certain subpopulation characterized by higher motor impulsiveness trait (Kam et al., 2012).

Together, although these studies provided inhomogeneous results, they seem to indicate that inter-individual differences in personality trait of impulsivity in healthy subjects may influence the

related neural activity which in turn may affect the results of group comparisons in clinical studies. This is of importance as a higher impulsive personality trait is also characteristic for psychiatric disorders. On the other hand, however, it has been shown that measures from self-reported questionnaires and behavioral tasks are only weakly correlated (Cyders and Coskunpinar, 2011; Jacob et al., 2010; Reynolds et al., 2006; Sebastian et al., 2013b; Stahl et al., 2014). Thus, to assess reliably inter-individual differences, and the subgroup classification associated therewith, more objective criteria are recommended. This may be differences in task-related behavioral measures, e.g., the individual RT as shown by Ruchsow and colleagues (Ruchsow et al., 2008a), or differences in electrophysiological parameters in the case of simultaneous EEG and fMRI data acquisition. At present, however, no combined EEG/fMRI study used this internally driven information for subgroup classification, although this may provide important information for our understanding of deficits in response inhibition in heterogeneous psychiatric disorders such as ADHD and BPD as they will be presented in the following two sections.

1.1.2. Attention-Deficit/Hyperactivity Disorder (ADHD)

Attention-Deficit/Hyperactivity Disorder (ADHD) is a neurodevelopmental disorder with onset in childhood. With a prevalence of 8–12 % it is one of the most frequent psychiatric disorders in school-aged children and adolescence (Faraone et al., 2003). Although recognized as a disorder of childhood and adolescence, symptoms can persist into adulthood (Davidson, 2007) with a prevalence of adult ADHD about 3–4 % (Faraone, 2005; Fayyad et al., 2007; Kessler et al., 2005; de Zwaan et al., 2012). ADHD is characterized by developmentally inappropriate levels of inattention, hyperactivity and impulsivity (American Psychiatric Association, 1994). Depending on the particular subtype of ADHD (i.e., primarily inattentive, primarily hyperactive-impulsive or combined) clinical symptoms are manifested in different ways (Barkley, 1998). Thus, ADHD is associated with a clinical picture of reduced concentration capacity and sustained attention, increased distractibility and emotional instability as well as enhanced impulsivity and hyperactivity as expressed in inner restlessness, motor hyperactivity and the tendency to act thoughtlessly (Arnsten, 2009; Barkley, 1998).

Although first mentions of ADHD-like symptoms in children can be traced back to early 1900 (Barkley, 1998), the pathophysiology of ADHD remains unclear. The absence of reliable biomarkers makes it necessary to relate the clinical diagnostics on subjective judgment. This, together with the disorder's clinical heterogeneity as well as with its unknown neurobiological underpinnings still causes controversial debates on the validity of ADHD as a psychiatric disorder diagnosis in the public area. At the same time, various studies based on neuroimaging and electrophysiology showed that cognitive impairments in ADHD are associated with structural and functional network anomalies. The most consistent functional deficits are found in fronto-striato-cerebellar and fronto-parietal circuits that mediate response inhibition and attention (Friedman and Rapoport, 2015; Hart et al., 2013; Konrad and Eickhoff, 2010; Sebastian et al., 2014). And also molecular genetic

analysis provided emerging evidence for a highly heritable disease of 70–80 % with a complex genetic architecture (Faraone and Mick, 2010; Faraone et al., 2005; Freitag et al., 2010).

1.1.2.1. Genetics and pathophysiology of ADHD

Meta-analyses of molecular genetic studies suggest a contribution of genes involved in the regulation of the neurotransmitter systems of dopamine, noradrenaline and serotonin in the pathogenesis of ADHD (Faraone et al., 2001; Gizer et al., 2009; Li et al., 2006; Schuch et al., 2015; Yang et al., 2007). However, up to date genome wide association studies revealed only marginal associations between allelic variants and ADHD pathophysiology (Doyle, 2015; Faraone and Mick, 2010; Scerif and Baker, 2015). This supports the idea of ADHD as a multifactorially determined neurobiological disease that is caused by a combination of environmental factors and multiple genes of small effects. Thus, molecular genetic studies may aim at reducing heterogeneity and thus enhance statistical power by taking into account the clinical phenomenology and complexity of ADHD (Faraone and Mick, 2010). This includes the known inter-individual differences and subtypes of ADHD, but also the existence of various comorbid psychopathology or cognitive impairments.

A more comprehensive understanding of the underlying pathophysiology may also be provided by studies which take the knowledge of neurophysiologically or neurofunctionally distinguishable endophenotypes into consideration (Castellanos and Tannock, 2002; Doyle et al., 2005). A major obstacle in studies on genetic and neurofunctional characteristics of ADHD may result from the traditional approach of separating patient groups categorically by means of diagnostic criteria irrespective of the underlying dimensional aspects. A better understanding of the pathophysiology underlying a specific psychiatric disorder may be provided by classifying patient groups based on dimensional measures such as behavior, neurobiology and genetics instead of, or in addition to, conventional categorical diagnostic criteria (i.e., Diagnostic and Statistical Manual of Mental Disorders (DSM), International Classification of Diseases (ICD)). Thus, the Research Domain Criteria (RDoC) was launched by the National Institute of Mental Health (NIMH) as a new framework that aims at classifying psychiatric disorders based on these observable measures rather than on categorical criteria (Insel et al., 2010). Although not established yet in European psychiatric research prospective studies may benefit from this approach by reducing variance.

1.1.2.2. Neuroanatomy and neurofunctionality in ADHD

Despite of considerable research activity, the neurodevelopmental pathways underpinning this disorder as well as the core neurophysiological dysfunction that substantially causes ADHD are still an open question. As potential causal processes underpinning ADHD the cognitive dysfunction model as well as the motivational dysfunction model are discussed (Barkley, 1997; Sonuga-Barke, 2005; Sonuga-Barke et al., 1994).

The motivational dysfunction model proposes that disturbances in ventral striatal-limbic circuits which are associated with bottom-up reward-related processing play a central role in ADHD pathophysiology. It is assumed that deficits in ventral striatal-limbic circuits lead to reduced influence of future rewards on the current behavior and thus the tendency to pursue immediate impulses regardless of the long-term consequences (Keune et al., 2015; Mitchell, 2010; Mitchell and Nelson-Gray, 2006; Sonuga-Barke et al., 1994). However, results from studies investigating reward-related processing in ADHD compared to healthy controls are inconsistent. The reward-related model is supported by a recent meta-analysis who demonstrated ventral-striatal hypoactivations in ADHD patients (Plichta and Scheres, 2014). However the authors also concluded that due to the small amount of data available, the result should be viewed with caution. Conversely, a meta-analysis of 55 fMRI-studies focusing on different cognitive domains found significant hypoactivations in the fronto-parietal network of executive functions and the ventral attentional network but failed to confirm an involvement of regions associated with motivational processing (Cortese et al., 2012).

The currently dominant model is the cognitive dysfunction model which considers deficient response inhibition as core element in ADHD neuropathophysiology. It is assumed that executive control dysfunctions of the frontal-striatal-cerebellar circuits lead to deficient response inhibition (Barkley, 1997; Boonstra et al., 2005; Doyle, 2006; Nigg, 2001; Nigg et al., 2005a; Willcutt et al., 2005). Executive functions are higher-order 'top-down' cognitive processes that facilitate goal directed behavior but also modify the behavior in accordance with the situation or cope with novel circumstances (Ardila, 2008; Miyake, 2000; Snyder et al., 2015). The cognitive dysfunction model is supported by two recent meta-analyses by Hart and colleagues who found reduced activation in ADHD in regions related to different domains of executive functions (Hart et al., 2012, 2013). A meta-analysis on timing-functions revealed in ADHD hypoactivations of left IFG, left inferior parietal lobe and right cerebellum (Hart et al., 2012). Meta-analyses on the attention and cognitive or motor inhibition revealed hypoactivations in the right hemispheric attention network (right dorsolateral prefrontal cortex, right inferior parietal cortex, caudal basal ganglia and thalamus) as well as in key regions of the impulse control network (right IFG, SMA, left striatum and right thalamus) (Hart et al., 2013). And also studies comparing ADHD with different psychiatric disorders (obsessive-compulsive disorder, conduct disorder and bipolar disorder) revealed significant hypoactivations in the IFG during tasks of cognitive flexibility (Rubia et al., 2010a), sustained attention (Rubia et al., 2009b), and response inhibition (Passarotti et al., 2010; Rubia et al., 2009c, 2010b).

In line with the cognitive dysfunction model, studies focusing on the neuroanatomical correlates of ADHD revealed structural alterations in regions mainly involved in the regulation of executive functions (Arnsten and Rubia, 2012; Friedman and Rapoport, 2015; Makris et al., 2007, 2008; Rubia et al., 2014a). Analyses of voxel based morphometry in ADHD patients compared to healthy controls revealed global gray matter reduction in cerebral volumes including prefrontal cortex

and parieto-temporal regions, basal ganglia as well as limbic regions such as anterior cingulate cortex (ACC), insula, amygdala and thalamus (Ellison-Wright et al., 2008; Frodl and Skokauskas, 2012; Greven et al., 2015; Ivanov et al., 2010; Maier et al., 2015; Tebartz van Elst et al., 2003; Valera et al., 2007; Villemonteix et al., 2015). It has also been shown that ADHD patients and their unaffected first-degree relatives share gray and white matter abnormalities. Although less pronounced than in ADHD patients, volumetric reduction in unaffected first-degree relatives confirms the notion that they are linked to a familial risk for ADHD (Durston et al., 2004; Greven et al., 2015; Pironti et al., 2014). This ties in with findings of delayed maturation in prefrontal cortex, caudate nucleus, and cerebellum in ADHD patients (Sharma and Couture, 2014). It has also been shown that decreased gray matter volume in right prefrontal cortex is positively correlated with deficits in motor response inhibition in adult ADHD patients (Depue et al., 2010). Together, structural and functional data indicate that dysfunction of the (inferior) prefrontal cortex may be disorder-specific to patients with ADHD.

1.1.2.3. Behavioral correlates of response inhibition in ADHD

Although impulsivity, i.e., the tendency towards impulsive (re-)actions and impulsive choices is viewed as a key element of ADHD (American Psychiatric Association, 1994), results are mixed regarding the behavioral correlates of response inhibition. A variety of behavioral measures has been reported with adult ADHD patients showing higher error rates together either with slower Go response times (RTs) (Morein-Zamir et al., 2014; Schneider et al., 2010) or without differences in RT (Dibbets et al., 2009; Karch et al., 2012; Sebastian et al., 2012; Woltering et al., 2013), but also slower RTs without enhanced error rates (Carmona et al., 2012; Kooistra et al., 2010; Wiersema et al., 2006a), or with no significant group differences at all (Dillo et al., 2010; Helenius et al., 2011; Köchel et al., 2012; Mulligan et al., 2011; Prox et al., 2007) were reported.

Interestingly, while increased commission errors are primarily linked to deficits in response inhibition, only few studies reported significantly enhanced commission error rates in adult ADHD (Morein-Zamir et al., 2014; Woltering et al., 2013). In contrast to this, most studies on response inhibition in adult ADHD reported increased omission error rates which are thought to be indicative of attentional deficits (Dibbets et al., 2009; Karch et al., 2014; Kenemans et al., 2005; Sebastian et al., 2012; Woltering et al., 2013). This may indicate that adult ADHD patients may have learned to cope with the impulsivity trait on motor level but not with attentional lapses. However, as opposed to this, deficient inhibitory control is seen as a key element of ADHD pathophysiology in adults as much as in younger ADHD patient groups. Nevertheless, the majority of studies provided evidence for behavioral deficits in adult ADHD being linked to dysfunctional activity on the neuronal level.

1.1.2.4. Neural correlates of response inhibition in ADHD

Neuroimaging studies on response inhibition in ADHD patients revealed functional underactivation in the fronto-striatal neural impulse control network. Particularly in children and adolescents with ADHD dysfunctions in fronto-striatal and fronto-parietal regions of the neural response inhibition network are often found (Dickstein et al., 2006; Durston et al., 2003; Hart et al., 2013; Rubia et al., 2001a, 2001b, 2005, 2009c, 2010b; Smith et al., 2006; Suskauer et al., 2007; Tamm et al., 2004; Vaidya et al., 2005). In contrast to this, to date studies on the neural correlates of response inhibition in adult ADHD have provided rather inconsistent findings (Congdon et al., 2014). A recent meta-analysis on neural correlates of response inhibition in ADHD patients of all ages found significantly decreased activation in the fronto-striatal network of response inhibition (Hart et al., 2013). However, if split into a pediatric group (14 studies) and an adult group (7 studies), the picture was changed substantially: Deficits in SMA/ACC and basal ganglia were only present in the child/adolescent group while the adult group was characterized by deficits in right IFG/insula and thalamus. The authors interpreted this finding as indicating that subcortical/basal ganglia deficits may be the primary cause of child ADHD pathology which normalizes with age, while frontal deficits become more prominent.

However, in contrast to this, studies focusing on response inhibition in adult ADHD did find reduced activity either in pre-frontal areas (Cubillo et al., 2010; Morein-Zamir et al., 2014; Mulligan et al., 2011) or in striatal regions (Schneider et al., 2010; Sebastian et al., 2012), while only one study found reduced activity in frontal and striatal regions at the same time (Epstein et al., 2007). Others also found increased cortical activity in ADHD patients (Dibbets et al., 2009; Dillo et al., 2010; Epstein et al., 2007), as well as no significant group differences at all (Carmona et al., 2012; Congdon et al., 2014; Karch et al., 2010). Taken together, neuroimaging studies provided evidence for deficits in key regions of response inhibition in adult ADHD, but these findings are inconsistent across studies. A possible reason could be the different paradigms and varying implementations thereof that have been employed in these studies. Thus, the differences in task demands might at least partly account for the variability in the results. But also the multifaceted nature and heterogeneity of ADHD as well as enhanced intra-individual variability in ADHD patients might contribute to this inconsistency.

1.1.2.5. Electrophysiological correlates of response inhibition in ADHD

Electrophysiological studies consistently reported reduced P3 amplitudes in children and adolescents with ADHD (Dimoska et al., 2003; Doehnert et al., 2010; Fallgatter et al., 2004; Gow et al., 2012; Liotti et al., 2010; Pliszka et al., 2000, 2007; Smith et al., 2004) as well as in adult ADHD patients (Dhar et al., 2010; Fallgatter et al., 2005; Fisher et al., 2011; Helenius et al., 2011; Köchel et al., 2012; Prox et al., 2007; Woltering et al., 2013). In addition, reduced N2 amplitudes are often

found in children and adolescents with ADHD (Dimoska et al., 2003; Gow et al., 2012; Liotti et al., 2010; Pliszka et al., 2000, 2007) but not in adult ADHD patients. This may be due to the fact that N2 is relatively small in amplitude and thus potentially more susceptible to artifacts or inter- and intra-individual variability. Nevertheless some studies also found differences in N2 amplitudes during response inhibition (Fisher et al., 2011; Prox et al., 2007; Woltering et al., 2013). However, reports of some electrophysiological (EEG) studies also seemed to emphasize that N2 alterations are associated with dysfunctional information processing in ADHD patients (Johnstone et al., 2013; Karch et al., 2014). Interestingly, it has been shown that abnormalities at the N2 latency in ADHD patients are associated with hypoactivation of the IFG (Fisher et al., 2011; Pliszka et al., 2000).

Since the IFG has been identified as one of the central regions in response inhibition (Aron, 2007; Sebastian et al., 2015), this may indicate a potential dysfunctional processing at an early stage of response inhibition. In line with this, a combined EEG/fMRI study investigating executive functions in adult ADHD found reduced fMRI correlations with N2 but not P3 amplitude values during voluntary decisions in ADHD patients (Karch et al., 2014). Using single-trial coupling of simultaneous EEG/fMRI data, the authors demonstrated that early (N2) but not later (P3) phases of information processing were affected in ADHD patients (Karch et al., 2014). Further evidence for altered early information processing stages in ADHD patients was also provided by other electrophysiological studies on motor preparatory processes (Banaschewski et al., 2003; Brandeis et al., 1998; Doehnert et al., 2010; van Leeuwen et al., 1998; McLoughlin et al., 2010). This may indicate that difficulties within the temporal dynamics or orchestration of neural processes underlying response inhibition are central in the pathophysiology of impulsivity in ADHD.

1.1.2.6. Spatio-temporal dynamics of response inhibition in ADHD

Increased intra-individual variability has been proposed as a candidate for an endophenotypic trait of ADHD (Noreika et al., 2013; Valera et al., 2010) and might contribute to inconsistency in conventional ERP and fMRI studies. Intra-individual variability can be accounted for by using single-trial correlations of EEG and fMRI data in addition to unimodal EEG and fMRI data analysis. Besides of incorporating trial-to-trial variability, combined analysis of simultaneous EEG and fMRI data also allows to disentangle neural responses related to different aspects and/or stages of information processing during response inhibition (Baumeister et al., 2014; Huster et al., 2011; Karch et al., 2008, 2014; Lavallee et al., 2014). Thus, single-trial EEG/fMRI enables to investigate the spatio-temporal dynamics of neural processes and therewith may contribute to a comprehensive understanding of neural pathophysiology in adult ADHD. However, up to date only one group used combined EEG/fMRI to investigate the spatio-temporal dynamics of neurocognitive processes in ADHD patients. Interestingly enough, neither unimodal ERP analysis nor unimodal fMRI analysis revealed any significant group differences during a voluntary motor response selection task (Karch et al., 2010). On the other hand, a single-trial analysis performed on the same data

revealed reduced fMRI correlations with N2 but not P3 ERPs in ADHD patients (Karch et al., 2014). This does not only indicate that dysfunctional early information processing may account for executive deficits in ADHD, but also emphasizes the potential power of combined EEG/fMRI analysis, especially if dealing with a patient group characterized by high intra- individual variability and inter-individual differences.

1.1.3. Borderline Personality Disorder (BPD)

Borderline Personality Disorder (BPD) is a severe disorder that is characterized by deficits in emotion regulation and impulse control as well as pervasive instability in interpersonal relationships and self-image (American Psychiatric Association, 1994). The prevalence of BPD in the general population is reported with 1.3 % (Coid et al., 2006) with a lifetime prevalence of 3–5.9 % (Grant et al., 2008; Trull et al., 2010). Among the variety of symptoms, impulsivity, i.e., inhibitory dysfunctions are regarded as a key element in BPD pathology (Lieb et al., 2004; Nigg et al., 2005b; Sebastian et al., 2013b). Clinically this is expressed as potentially self-damaging impulsive behaviors such as excessive spending, substance abuse, unsafe sex, binge eating, or physically self-harming acts (American Psychiatric Association, 2013). Recent data seem to suggest that in BPD patients impulsive behavior may arise from a negative interaction of emotional stress and impulse control, so that impulsive behavior will more likely occur under emotional distress than under emotionally neutral conditions (Domes et al., 2006; van Eijk et al., 2015; Jacob et al., 2013; Sebastian et al., 2013b; van Zutphen et al., 2015).

1.1.3.1. Genetics and pathophysiology of BPD

According to today's state of knowledge, the development of BPD can be explained best by a gene × environment interaction in which negative environmental (psychosocial) events through childhood play a central role (Leichsenring et al., 2011; Lieb et al., 2004; Paris, 2005). It seems conceivable that in individuals with a vulnerable phenotype the exposure to adverse childhood events may trigger a loop of neural network dysfunctions (impulsivity and emotional dysregulation) and behavioral deficits (dysfunctions in behavior and social interaction) which will reinforce each other (Lieb et al., 2004). Alternatively, it has been suggested that two distinct pathomechanisms may lead to the development of BPD pathology (Nigg et al., 2005b). According to this, the traumatic pathway is based on severe early caregiving disruption and/or chronic early traumatic experiences leading to a disturbed development of affect regulation which in turn results in an altered reactive affect system. While inhibitory dysfunctions play a minor part in this pathway, it is the central element in the second 'impulsivity' pathway. Nigg and colleagues suggested that this pathway is based on severe inhibitory deficits which cause dysfunctional impulsive and social behavior leading to a number of negative social experiences which in turn ultimately results in

interpersonal disturbances. In this pathway, it seems likely that other disorders such as ADHD or conduct disorder may play an important role.

Twin studies suggest a strong genetic background in the development in BPD with a estimated heritability ranging from 35 % to 60 % (Bornovalova et al., 2009; Kendler et al., 2008, 2011; Torgersen et al., 2000). Nonetheless, no specific gene has been identified yet to be causally related to the development of BPD pathology. Due to its association with impulsive aggression and self-destructive behavior the serotonergic system is considered as a potential candidate for a genetic link to BPD pathology (Leichsenring et al., 2011; Lis et al., 2007; Retz et al., 2004). Among women with bulimia spectrum syndromes carriers of a short allele variant of the serotine transporter promotor gene displayed significantly more behavioral impulsivity, affective instability and interpersonal insecurity as well as comorbid BPD (Steiger et al., 2005). Although this suggests a central role for the serotonergic system in the development of BPD pathology, it should be interpreted with caution, as data for the role genetic effects in BPD are sparse.

1.1.3.2. Neuroanatomy and neurofunctionality in BPD

Structural and functional neuroimaging studies revealed a dysfunctional fronto-limbic network in BPD (Berdahl, 2010; Brendel et al., 2005; Lieb et al., 2004; O'Neill and Frodl, 2012; Sebastian et al., 2014). This included ACC, orbitofrontal and dorsolateral prefrontal cortex as well as hippocampus and amygdala. Several studies reported reduced volumes in hippocampus and amygdala (Driessen et al., 2000; Nunes et al., 2009; O'Neill et al., 2013; Schmahl et al., 2009, 2003; Soloff et al., 2008; Tebartz van Elst et al., 2003; Weniger et al., 2009). Interestingly, two meta-analyses indicated that volume changes in hippocampus and amygdala may rely on different subtypes of BPD pathology and/or comorbid post-traumatic stress disorder (PTSD). While reduced amygdala volume seemed to be specific for BPD patients without comorbid PTSD (de-Almeida et al., 2012), reduced hippocampus volumes seemed to be related predominantly to comorbid PTSD (Rodrigues et al., 2011). The latter is supported by meta-analyses demonstrating reduced volumes in hippocampus but not in amygdala and hippocampus in PTSD patients (Kitayama et al., 2005; Woon and Hedges, 2009; Woon et al., 2010). Although this may suggest reduced hippocampus volume in BPD is caused by PTSD while reduced amygdala volume is specific for BPD, this is questioned by a another meta-analysis in which reduced volumes in hippocampus and amygdala were unrelated to comorbid PTSD symptoms (Ruocco et al., 2012). However, as pointed out by O'Neill and Frodl (2012) a conclusive statement on hippocampus and amygdala volume in BPD is compounded by the large heterogeneity in morphometric studies (O'Neill and Frodl, 2012). Additionally volume reductions in BPD were found in the gray matter of the ACC (Hazlett et al., 2005; Minzenberg et al., 2008; Soloff et al., 2008; Tebartz van Elst et al., 2003) and the orbitofrontal and dorsolateral prefrontal cortex (Brunner et al., 2010; O'Neill et al., 2013; Tebartz van Elst et al., 2003).

Fronto-limbic dysfunctions in BPD patients were demonstrated especially under negative emotional or stressful conditions. Most prominently, this included amygdala hyperactivity in BPD patients in response to emotional stimuli or negative emotional conditions (Donegan et al., 2003; Hazlett et al., 2012; Herpertz et al., 2001; Jacob et al., 2013; Krause-Utz et al., 2012; Silbersweig et al., 2007; Soloff et al., 2015). Additionally altered neural activity in ACC under emotionally and/or stressful conditions were often reported (Holtmann et al., 2013; Jacob et al., 2013; Silbersweig et al., 2007; Soloff et al., 2015, 2015; Wingenfeld et al., 2009a). In view of the orbitofrontal/dorsolateral volume reduction and the role of the interaction between orbitofrontal cortex and amygdala in affect regulation, it has been suggested that enhanced amygdala activity in BPD patients may arise from reduced prefrontal inhibitory control (Lieb et al., 2004; Tebartz van Elst et al., 2003). Further, it has been suggested that a fronto-limbic dual brain pathology, i.e., simultaneous volume reduction in amygdala/hippocampus and orbitofrontal cortex may be a neuropathological correlate of the hyperarousal-dyscontrol syndrome as it is present in BPD (Lieb et al., 2004; Tebartz van Elst et al., 2003).

1.1.3.3. Behavioral correlates of response inhibition in BPD

The failure to resist impulsive potentially harmful actions and choices, is viewed as a key element of BPD pathology (Lieb et al., 2004; Nigg et al., 2005b) as much as of ADHD pathology (Barkley, 1997; Nigg, 2010). This notion is supported by consistent findings of significantly higher scores in self-rating questionnaires regarding impulsivity in both patient groups (Sebastian et al., 2013b). However, most studies on response inhibition did not reveal significant differences between BPD patients and healthy control subjects on behavioral level (Cackowski et al., 2014; van Eijk et al., 2015; Hagenhoff et al., 2013; Jacob et al., 2013; Lampe et al., 2007; Ruchsow et al., 2008b; Völker et al., 2009). Although others also demonstrated enhanced omission error rates (Silbersweig et al., 2007) and enhanced commission error rates (Coffey et al., 2011; McCloskey et al., 2009; Rentrop et al., 2008), marginal group differences might be a confound of an (subclinical) ADHD-comorbidity in BPD patients (Cackowski et al., 2014; Lampe et al., 2007; Nigg et al., 2005b; (Cackowski et al., 2014; Lampe et al., 2007; Nigg et al., 2005b; Sebastian et al., 2013b) or due to emotional dysregulation in emotional impulse control tasks (Sebastian et al., 2013b; Silbersweig et al., 2007).

1.1.3.4. Neural correlates of response inhibition in BPD

In accordance with this, the few neuroimaging studies on response inhibition in BPD patients revealed a mixed picture (van Eijk et al., 2015; Jacob et al., 2013; Silbersweig et al., 2007; Wingenfeld et al., 2009b). Three of these studies investigated the neural underpinnings of response inhibition in BPD patients in the context of different emotional modulations (Jacob et al., 2013; Silbersweig et al., 2007; Wingenfeld et al., 2009b). They demonstrated that in BPD patients

compared to healthy controls the interaction between negative emotional modulation and response inhibition leads to decreased activation in subgenual ACC and medial orbitofrontal as well as in bilateral frontal, parietal and temporal areas (Silbersweig et al., 2007; Wingenfeld et al., 2009a). Significantly reduced activity in the left IFG as well as significantly enhanced activity in STN was also demonstrated in BPD patients during response inhibition after anger induction (Jacob et al., 2013). Interestingly, the same authors also reported that in emotionally neutral conditions the BPD patients did not differ from healthy controls, which may indicate that the disturbed prefrontal-limbic circuitry in BPD is compensated by a subcortical loop (Jacob et al., 2013).

Thus, while the response inhibition in the context of different emotional modulations was related to significant reduced activity in BPD patients, these differences were no longer detectable in emotionally neutral conditions (Sebastian et al., 2013b). In accordance with this, a recent study on pure response inhibition mechanisms in BPD patients demonstrated that the neural impulse control network of BPD patients is not impaired in emotionally neutral situations (van Eijk et al., 2015). Supporting the idea that the clinically relevant symptom of impulsivity in BPD patients may result from an interaction of emotional dysregulation and impulse control contrary to pure response inhibition deficits in ADHD patients (van Eijk et al., 2015; Lampe et al., 2007; Prada et al., 2014; Sebastian et al., 2013b, 2014; van Zutphen et al., 2015).

1.1.3.5. Electrophysiological correlates of response inhibition in BPD

On the subject of electrophysiological correlates of response inhibition in BPD only one ERP study exists (Ruchsow et al., 2008a). This study found no significant group differences for the Nogo-N2 components, but significantly reduced Nogo-P3 amplitudes in BPD patients compared to healthy control subjects, which was interpreted as evidence for impaired response inhibition in BPD. However, due to the lack of additional electrophysiological studies on response inhibition in BPD and the current debate on the association between Nogo-P3 and inhibitory control functions (Huster et al., 2013), this conclusion should be treated with caution. Nevertheless, studies on other neural processes also indicated abnormal P3 amplitudes in BPD (Meares et al., 2005, 2011). So it could be deduced, that this stage of information processing is affected, or at least altered, in BPD patients.

1.2. Analysis techniques

Electroencephalography (EEG) and functional magnetic resonance imaging (fMRI) are most widely used to investigate human brain functions non-invasively. However, as both techniques come with complementary strength and disadvantages, there is a growing interest in combining both modalities. This provides the possibility to benefit from their strengths and remediate their disadvantages. The following sections will focus on the methodological background of unimodal EEG and fMRI analysis, as well as combined EEG/fMRI analysis techniques.

Topic of Section 1.2.1 is the fMRI technology, a method that is based on the blood oxygenation level-dependent (BOLD) response, an indirect measure of neuronal activity as it is indicated by increased regional metabolism. fMRI provides a high spatial resolution which allows localizing brain regions engaged during cognitive processes with an accuracy of few millimeters. However, due to the temporal sluggishness of the measured hemodynamic responses, the temporal resolution is limited to the range of several seconds.

The next Section 1.2.2 will focus on EEG measurements which allow to assess the temporal dynamics of cognitive processes. The EEG is a direct recording of the summed electrical activity of the brain as a potential difference between a set of active electrodes and one reference electrode. According to nowadays understanding, the apical dendrites of pyramidal cells are the main contributors to the recorded EEG signal. While EEG recordings attain a temporal resolution at a sub-millisecond time range, its spatial resolution is limited to the range of centimeters. This is due to the volume conducting effect of the brain, which results in a spatially integrated signal.

The last Section 1.2.3 will focus on the combined analysis of EEG and fMRI data, which is supposed to circumvent the disadvantages of unimodal EEG and fMRI analysis and simultaneously benefit from their strengths. However, this technique comes with its own drawbacks and technical challenges mainly caused by the fact that the EEG recording system needs to be placed within the strong and changing magnetic field of the fMRI scanner. This section gives an overview of the main developments and achievements in the field of simultaneous EEG/fMRI measurements and the methodological challenges thereof.

1.2.1. Magnetic resonance imaging (MRI)

Magnetic resonance imaging (MRI) is a noninvasive technique not only used in medical diagnostics but also in research studies interested in brain structures. Functional magnetic resonance imaging (fMRI) is a special application of MRI that was designed to study brain functions, e.g., the neural correlates of cognitive processes such as response inhibition. The following section will summarize the principles of MRI and fMRI as they can be found in more detail in several textbooks (Buxton, 2009; Huettel et al., 2008; Lazar, 2008; Moore and Holland, 1980).

1.2.1.1. Principle of magnetic resonance imaging (MRI)

Magnetic resonance imaging MRI was developed in the early 1980's (Bailes et al., 1982; Bydder and Steiner, 1982; Doyle et al., 1981; Hawkes et al., 1980; Holland et al., 1980; Oldendorf, 1981; Young et al., 1981) and exploits the fact that the nuclei of certain nuclides resonate in a magnetic field, which is known as nuclear magnetic resonance (Bloch, 1946; Purcell et al., 1946). MRI is based on the principle that atomic nuclei with an uneven number of protons or neutrons possess a nuclear spin (i.e., spin angular momentum). Such nuclei naturally precess around a central axis and generate weak magnetic fields, which makes them responsive to external electromagnetic influences. When placed within a strong and static magnetic field, they precess with a characteristic frequency proportional to this external magnetic field. Simultaneously, they will also align with the direction of the static external magnetic field, causing the net magnetization to increase from the normal state of zero. A stronger external magnetic field will cause more nuclei to align in the parallel direction (i.e., lower energy) and thus result in a greater net magnetization.

3-dimensional images of the brain can be obtained by using a combination of the strong static magnetic field (1.5–4.0 Tesla), a short radio frequency (RF) pulse, and a set of additional gradient coils which will cause linear variations in the strength of the static magnetic field in one of the three dimensions. By applying a short RF pulse perpendicular to the external magnetic and tuned to the nuclei's resonance frequency (i.e., Larmor frequency), an excitation of the nuclear spins (i.e., the movement from the low energy state to the high energy state) can be induced. This causes the nuclei to realign in a uniform angle (i.e., flip angle) in direction of the RF field and to precess in phase in contrast to the former equilibrium state. In the following, the nuclei return to the former parallel alignment with the static magnetic field, while emitting the energy of the RF pulse. This in turn provides the so called spin echo signal that can be detected by an external receiver (i.e., radio-frequency) coil in the MRI scanner. Caused by two independent processes (i.e., longitudinal and transverse relaxation, each characterized by its own time constant T1 and T2), the emitted signal strength decays over time (Hendee and Morgan, 1984; Moore and Holland, 1980). As the nuclei's Lamor frequency depends on the strength of the external magnetic field, magnetic field inhomogeneities as caused by the magnetic field gradients will result in spatially varying Lamor frequencies which can be targeted precisely and thus allows to reconstruct 3D images with a spatial resolution of about 1 mm (Poustchi-Amin et al., 2001).

1.2.1.2. Principle of functional magnetic resonance imaging (fMRI)

Functional magnetic resonance imaging (fMRI) enables the investigation of brain functions as indirectly indicated by local changes in the brain's metabolic demand. It is assumed that local changes in neural activity are accompanied by regional changes in the cerebral blood flow, the

cerebral blood volume, and the cerebral metabolic rate of oxygen utilization (Ances, 2004; Bartels et al., 2008; Kim and Ogawa, 2012; Logothetis, 2002).

Neuronal activity is accompanied by complex cellular processes followed by metabolic and vascular processes. Energy demanding processes of neuronal activity such as membrane depolarization/repolarization and neurotransmitter synthesis/recycling consume energy in the form of adenosine triphosphate. This is mainly synthesized by the oxidative glucose metabolism and thus consumes glucose and oxygen which is provided by the brain's vascular system. Thus, the regional cerebral blood flow increases to comply with the increased neuronal metabolism and the correspondingly increased oxygen and glucose consumption. However, there is a mismatch between oxygenated cerebral blood flow and oxygen consumption (i.e., cerebral metabolic rate of oxygen) causing an oversupply with oxygenated blood in succession to an initial decrease of oxygenated blood due to metabolic activity. This excessive increase in oxygenated hemoglobin results in a strengthening of the measured fMRI signal as it reduces the local magnetic field inhomogeneities caused by the paramagnetic properties of deoxygenated hemoglobin (Hillman, 2014; Kim and Ogawa, 2012).

It is assumed that the vascular response is more closely related to local synaptic activity and transmission as reflected in local field potentials rather than to spiking neural activity, i.e., action potentials (Logothetis, 2002). In this connection, it is considered that the neurovascular coupling (i.e., the local interplay between neuronal activity and regional cerebral blood flow) is mediated via vasoactive agents who are either molecular by-products of the neuron's metabolic activity itself or molecules generated by glia cells involved in neurotransmitter recycling (Buxton, 2013; Hillman, 2014; Pasley and Freeman, 2008). In view of the metabolic-by-product hypothesis it is assumed that agents such as potassium, nitic oxides, adenosine, or carbon dioxide may act on the vascular smooth muscle and thus alter the diameter of the blood vessels. Alternatively, it was suggested that astrocytes may link neuronal activity to vascular responses. In this view it is suggested that in the process of glutamate recycling the astrocytes produce vasoactive agents (Attwell and Iadecola, 2002; Attwell et al., 2010; Howarth, 2014; Magistretti and Pellerin, 1999).

Physically, fMRI uses the so called BOLD effect, i.e., the intrinsic changes in the blood's concentration of deoxyhemoglobin as a naturally produced contrast agent (Ogawa et al., 1990). These changes in the ratio of deoxygenated (i.e., paramagnetic) and oxygenated (i.e., diamagnetic) blood as a consequence of neural activity changes the effective transverse relaxation times which can be measured by means of T2* weighted sequences (Kwong et al., 1992; Ogawa et al., 1992). The measured BOLD signal is characterized by a stereotyped temporal pattern: (1) initial dip of BOLD response, i.e., the signal's strength decreases after the stimulus due to the increased level of deoxygenated hemoglobin as a consequence of the increased oxygen consumption; (2) two seconds after stimulus onset the BOLD signal strengthens and reaches its maximum 6–8 seconds after stimulus onset, this is due to the subsequent oxygen oversupply and the inherent enrichment

of oxygenated hemoglobin in the specific area; (3) 10–12 seconds after stimulus onset the BOLD signal regains its initial strength. This relatively stereotyped temporal pattern of the stimulus induced BOLD response is described mathematically by the canonical hemodynamic response function (HRF) (Friston et al., 1994a).

1.2.1.3. Generalized linear model (GLM) and statistical analysis

As the stimulus induced alterations in the BOLD responses follow a stereotyped temporal pattern, the hemodynamic response to a certain type of stimulus can be predicted by a linear regression model (Boynton et al., 1996). Thus, using a generalized linear model (GLM) enables to assess which of the volume elements (voxels) show task-related changes in the detected BOLD signal (Huettel et al., 2008; Friston, 2007). To obtain an estimation of the expected event-related BOLD response (i.e., regressor-of-interest) for a specific task condition, the canonical HRF is convolved with the so called stimulus function. This stimulus function is derived from the temporal occurrence of the respective event type. Hence, it is typically a series of ones and zeros, with ones denoting each time point the event of interest occurred. This stimulus function is convolved with the HRF to take into account the delayed and blurred time course of the BOLD signal in response to the stimulus onset. Additional variance in the data, as for example caused by random movement of the subject, can be modeled by means of a second type of regressor (i.e., regressors-of-no-interest), e.g., using either movement parameters from the analysis software or if available additional physiological factors such as heart rate.

Both types of regressors are then included into the GLM in order to compare the expected BOLD responses with the empirically determined fMRI data of every single voxel independently (i.e., univariate analysis). If written in vector and matrix form, the GLM can be presented as follows (1.1):

$$Y = X \cdot \beta + \varepsilon \tag{1.1}$$

With Y beeing a $n \times m$ matrix representing the measured time-courses of the BOLD signal for each voxel (m) at every measured time point (n), which can be explained by a linear combination of several hypothetical time-series $x(n) \cdot \beta(n)$ along with the error term ε (i.e., the residual error). The term X denotes an $n \times p$ matrix (i.e, design matrix), which specifies the linear model and consists of p different explanatory variables (x), each of which represents a vector (i.e, regressor) of the length n (i.e., number of time points). For each voxel the related regression coefficients β (i.e., beta-weights, or model parameters) are estimated in order to achieve the best fit of the predicted model to the observed data, which is the smallest possible residual term.

After the beta weights have been estimated, specific predictions on the data can be tested using t or F statistics in order to identify a region with a significant experiment effect of interest. These statistics can be calculated using weighted combinations of beta values. Therefore a contrast vector is build in order to define how to weight the different columns (i.e., regressors) of the design matrix. To find brain regions active during a certain task condition, the related regressors are compared to an unmodeled baseline. Therefore, the regressor related to the event of interest is weighted with a +1, while every remaining regressor is zero-weighted. If for example the first regressor is weighted with +1 and the second regressor with −1, this will reveal brain regions more active in condition one compared to condition two. Running such a t- or F-contrast will create an image that contains the calculated contrast values which is used for subsequent statistical analyses on the group level (i.e., second level analysis).

1.2.2. Electroencephalography (EEG)

Electroencephalography (EEG) is one of the most often used non-invasive methods in cognitive neuroscience in addition to fMRI. While the fMRI's temporal resolution is high compared to anatomical MRI measurements, it is still limited by the relatively slow time course of the hemodynamic response. Thus, if interested in the temporal dynamics of neural processes in human beings, noninvasive electrophysiological measurements are the techniques of choice. The origins of EEG recording can be traced back to the research activities of Hans Berger who demonstrated first in 1924 that electrical potentials can be recorded by electrodes placed on the human scalp (Gloor, 1969). Although the recording techniques have continuously improved since then, it's basic principle of recording electronic potential differences between a set of electrodes and a reference electrode remained unchanged (Luck, 2005; Michel, 2009).

1.2.2.1. Principles of electroencephalography (EEG)

Through electrodes placed on the head surface, the EEG records the spontaneous electrical activity generated by the synchronized activity of large neuronal populations. It is thought, that the summed extracellular field generated by postsynaptic excitatory and inhibitory potentials of the pyramidal cells represent the most significant source of the recorded EEG signal (Bucci and Galderisi, 2011; Laufs, 2008; Woodman, 2010). While action potentials are too short-lasting events to contribute to the recorded electrical signal, the extracellular current flow caused by synaptic integration processes involves larger membrane surfaces and proceeds at a time range that facilitates temporal overlapping of several events (Bucci and Galderisi, 2011). However, in order to generate detectable potential differences on the head surface, large amounts of simultaneously excited and temporally synchronized neurons are required. Moreover, the detectability of the electrical potentials strongly depends on the neurons spatial arrangement. Thus, neuronal populations arranged in parallel to

one another and perpendicular to both cortical surface and scalp, as is the case in the cerebral cortex, can be optimally recorded (Bucci and Galderisi, 2011). In contrast to this, neuronal populations located in subcortical areas or arranged in a radial pattern or orthogonal to the scalp are less prominent in the recorded EEG signal.

While EEG recordings provide a temporal resolution within a time range of milliseconds, its spatial resolution is limited due to the volume conduction effect. This is that, if there is a conductive volume, the electrical currents will be transmitted throughout the entire volume (e.g., the whole brain) until it reaches a surface (Luck, 2005). Thus, the signal recorded by a particular electrode is not only generated by neuronal populations (sources) underneath this electrode but also by an unknown number of additional sources throughout the brain. Moreover, because of the different electrical conductivities of brain tissues, dura, skull, and skin, the EEG records a spatially blurred mixture of the underlying neural activity. The localization of the underlying neural sources requires the inverse reconstruction of the underlying neural activity. However, due to the unknown number of sources and the unknown proportion that each source contributes to the recorded signal, the inverse source reconstruction is mathematically an underdetermined problem. This can be solved by making assumptions about the total number of neural sources contributing to the recorded electrical signal, prior to the estimation of the signal's origin (Pascual-Marqui, 1999). Up to date different powerful algorithms are available to localize the sources within an accuracy of a few centimeters (Grech et al., 2008; Pascual-Marqui, 1999). Nevertheless, the strength of electrophysiological analysis lies in it's high temporal resolution. This allows to draw conclusions on the temporal dynamics of cognitive processes, for example by investigating the temporal characteristics of event-related potentials.

1.2.2.2. Event-related potentials (ERPs)

Event-related potentials (ERPs) are reflecting the electrical activity of the brain which is generated in response to an external stimulus. As they occur with a fixed temporal relationship to a certain experimental event but with relatively small amplitudes (1–30 µV) compared to the random background EEG activity, a signal-averaging procedure is used for evaluation of ERPs (Luck, 2004, 2005; Makeig and Onton, 2011; Picton et al., 2000). This assumes, that event-related brain responses are invariant over repeated stimulation (over 50–300 trials) and independent from spontaneously ongoing EEG activities. Thus by calculating averages over many trials of the same event type, the random brain activity will be averaged out while the ERP information remains, which improves the initially low signal-to-noise ratio. The resultant averaged ERPs can be depicted by plotting time in milliseconds [ms] on the x-axis against the electrode's averaged potential in microvolt [µV] on the y-axis. This results in a signal curve with a typical sequence of positive (P) and negative (N) deflections (peaks, waves or components) which are labeled P1, N2, P2, N2, and P3 accordingly to their sequential appearance (Key et al., 2005; Luck, 2005).

Latencies and amplitudes of these peaks vary depending on the employed experimental design. Thus, as discussed comprehensively in the work of Luck (2005), this sequence of peaks most probably reflects the information flow through the brain and is influenced by task and stimulus properties. The early components (N1 and P1) are thought to reflect task-independent responses to stimulus properties such as the luminance of visual stimuli in case of the P1 component. In contrast to this, the negative component N2 as well as the late positive component P3 presumably reflects task-dependent internal or cognitive processes which are entirely stimulus-independent (Enriquez-Geppert et al., 2010; Huster et al., 2013; Picton, 1992; Polich, 2007; Polich and Criado, 2006). Strongly depending on the employed paradigm, the N2 and P3 components were shown to be related to various aspects of executive functions. N2 has been associated with early 'pre-motor' stages of response inhibition (Beste et al., 2010; Falkenstein et al., 1999; Jodo and Kayama, 1992; Lavric et al., 2004; Rietdijk et al., 2014), as well as cognitive control, response selection, error detection or attention allocation (Donkers and van Boxtel, 2004; Huster et al., 2013; Nieuwenhuis et al., 2004; Rietdijk et al., 2014), while P3 was also associated with later stages of response inhibition, i.e., the actual inhibition of the motor response (Beste et al., 2010; Falkenstein et al., 1999; Huster et al., 2013; Rietdijk et al., 2014; Wessel and Aron, 2015) as well as performance monitoring, or updating of working memory (Friedman et al., 2001; Huster et al., 2013; Liotti et al., 2005; Schmajuk et al., 2006; Wu and Zhou, 2009).

1.2.3. Combined EEG/fMRI analysis

One major drawback of conventional ERP and conventional fMRI data analysis is the intrinsic assumption of stationary brain responses to repeated presentation of stimuli with the same physical and psychophysiological characteristics. This, however, is contrary to the observation that behaviorally the same stimulus elicits large response variability on trial-to-trial basis as it has been reported for behavioral performance such as reaction time (Kanai and Rees, 2011; MacDonald et al., 2006; Reed, 1998; Tamm et al., 2012). Based on these findings it could be assumed that intra-individually varying behavioral responses are possibly a manifestation of short-term changes in neural processes. In accordance with this, single-trial variations have been reported for amplitude and latency of evoked potentials (Kisley and Gerstein, 1999; Ledberg et al., 2012; Möcks et al., 1984, 1987; Rösler et al., 2008; Truccolo et al., 2002; Turetsky et al., 1989) as well as for the magnitude of fMRI BOLD signals (Aguirre et al., 1998; Bellgrove et al., 2004; Duann et al., 2002; Fox et al., 2005). Even on the level of single cell units, single-trial variability of evoked spiking activity can be observed (Arieli et al., 1996; Bollimunta et al., 2007; Carandini, 2004; Menzer et al., 2010; Reich et al., 1997).

Response variability of evoked cortical activity can be explained by a linear combination of random ongoing network activity and stationary stimulus-related responses (Arieli et al., 1996).

It can therefore be deduced that single-trial fluctuations of evoked responses reflect moment-to-moment fluctuations in the subject's cognitive state rather than random and irrelevant noise. This in turn could interact with task-relevant stages of information processing resulting in trial-to-trial variations of behavioral responses (Birn, 2007; Fontanini and Katz, 2008; Kelly et al., 2008; Ledberg et al., 2012; Lutz et al., 2002; van Maanen et al., 2011; Pessoa and Padmala, 2005; Saville et al., 2011a, 2011b). Single-trial analysis is one way of investigating task-related neural activity which take into account that task-related brain activity could differ from trial to trial (Jung et al., 2001; Lutz et al., 2002). This is one of the areas one could benefit from combined EEG/fMRI analyses in which regressors built from extracted single-trial information of the event-related EEG can be used as predictors of the BOLD responses (Bland et al., 2011; Debener et al., 2006; Huster et al., 2012). Intra-individual variability can be found even in healthy subjects, hwoever, this is particularly pronounced in elderly subjects or patients with neurological or psychiatric disorders (MacDonald et al., 2006), hence, combined EEG/fMRI studies may improve our understanding of neural processing in psychiatric disorders.

1.2.3.1. Concepts of combined EEG/fMRI

To circumvent the spatial and temporal disadvantages of unimodal EEG and fMRI analyses and benefit from their strengths on the same time, intense efforts have been undertaken to combine both modalities. Although combined EEG/fMRI provides higher spatial and temporal resolution as compared to unimodal EEG or fMRI, it comes along with its own drawbacks and technical challenges. These are mainly due to the placement of an EEG recording system within the magnetic field of the MRI scanner. This is a source of serious danger for every subject undertaking an fMRI scanning session while equipped with an EEG recording system. Thus, the first step in implementing simultaneous EEG/fMRI data acquisition had been the development of MRI-compatible EEG-recording systems and secure fMRI scanning sequences in the mid 1990s (Huang-Hellinger et al., 1995; Ives et al., 1993). After this, a variety of approaches and signal processing techniques have been developed in order to facilitate simultaneous EEG/fMRI recordings and the analysis thereof (Bland et al., 2011; Blinowska et al., 2009; Debener et al., 2006; Huster et al., 2012).

In clinical and scientific studies on epilepsy, EEG-triggered fMRI has been proven to be useful in localizing the neural generators of interictal epileptiform discharges (Aghakhani et al., 2015; Bagshaw et al., 2006; Bénar et al., 2003; Gotman et al., 2004; van Graan et al., 2015; Jacobs et al., 2009; Rathakrishnan et al., 2010). In cognitive neuroscience the fMRI information can be used to improve the spatial presumptions of EEG source reconstruction (Doñamayor et al., 2012; Esposito et al., 2009; Ou et al., 2010; Milner et al., 2014) or various parts of the EEG can be utilized to inform the fMRI data analysis. This could be either the EEG's spontaneous or task-related oscillatory activity (Becker et al., 2011; Feige et al., 2005; Goldman et al., 2002; Koch et al., 2009; Laufs, 2008; Laufs et al., 2003; Lavallee et al., 2014; Michels et al., 2012; Scheeringa et al., 2011a,

2011b) or the single-trial amplitudes of ERPs as it was introduced in mid 2000s (Bagshaw and Warbrick, 2007; Bénar et al., 2007; Debener et al., 2005, 2006; Eichele et al., 2005; Liebenthal et al., 2003; Mulert et al., 2004).

Single-trial coupling of event-related EEG features with fMRI data requires the identification and selection of ERPs which are small in amplitude compared to the fMRI-induced artifacts. To circumvent this, different approaches of simultaneous data acquisition as well as data analyses have been developed. In the initial years of simultaneous EEG/fMRI recordings, interleaved data acquisition was the recording technique of choice. This used alternating phases of scanning periods for fMRI data acquisition (with changing magnetic field) and interscan periods for EEG recording (with only the static magnetic), while the stimuli were presented in both periods (Bonmassar et al., 1999, 2001; Liebenthal et al., 2003; Mulert et al., 2004; Sommer et al., 2003). This approach avoided many of the MRI-related artifacts in the EEG and enabled data acquisition on the same circumstances, e.g., environment, conditions of stimulation, or subject state. However, it did not provide truly simultaneous data, which is the ultimate goal of combined EEG/fMRI data. This is that only continuously and simultaneously recorded EEG and fMRI data allow for the investigation of relationships between event-related potential variations of EEG data and BOLD response at the single-trial level. A step closer to this was the sparse sampling technique for EEG/fMRI data acquisition. By using a relatively long scan repetition time (TR) together with the acquisition of only few fMRI slices per volume this technique allowed for scan periods in which artifact-free EEG data can be recorded. Using this techniques, several researchers demonstrated that ERPs related to higher level cognitive processes can be identified and used to assess the spatio-temporal dynamics of neural processing (Debener et al., 2005; Eichele et al., 2005, 2008; Kruggel et al., 2000, 2001; Mulert et al., 2008). Although sparse sampling allowed for trial-to-trial coupling of single-trial EEG and fMRI data, it is limited due to the small number of slices.

In parallel to the development of advanced fMRI scanning sequences, many research activities concentrated on the improvement of specialized algorithms for artifact removal. In the end this allowed for uninterrupted and simultaneous acquisition of both EEG and fMRI data (Allen et al., 1998, 2000; Anami et al., 2003; Delorme et al., 2007; Negishi et al., 2007; Sijbers et al., 2000; Sun and Hinrichs, 2009). Becker and colleagues demonstrated that visual-evoked potentials (VEPs) from EEG data recorded during interscan periods did not differ significantly from those recorded during fMRI data acquisition if MRI-related artifacts were removed (Becker et al., 2005). Moreover, Bénar and colleagues demonstrated that single-trial amplitude and latency values extracted from EEG data recorded during continuous fMRI acquisition can be used to inform the fMRI data analysis on single-trial level (Bénar et al., 2007). Due to these powerful algorithms for reduction of MRI-related artifacts, nowadays it is standard practice to acquire simultaneous EEG/fMRI data continuously.

1.2.3.2. Single-trial coupling of simultaneous EEG/fMRI

Among a variety of different techniques, trial-by-trial coupling of simultaneous EEG/fMRI data is one of the most commonly applied methods for combining simultaneously acquired EEG and fMRI. This approach allows for assessing the spatio-temporal dynamics of neural networks related to cognitive processes (Debener et al., 2005; Eichele et al., 2005; Huster et al., 2012). As has been shown first in 2005 (Debener et al., 2005; Eichele et al., 2005), single-trial amplitude values of denoised EEG data can be used in order to model simultaneously acquired fMRI data (Bénar et al., 2007; Debener et al., 2005, 2006; Eichele et al., 2005). Since then, many studies have been published on the subject of trial-to-trial correlations of single-trial ERP amplitude values with fMRI BOLD responses (Baumeister et al., 2014; Goldman et al., 2009; Huster et al., 2011; Juckel et al., 2012; Karch et al., 2010, 2014; Mayhew et al., 2010; Mobascher et al., 2009; Mulert et al., 2008; Novitskiy et al., 2011; Sadeh et al., 2010; Scheibe et al., 2010; Warbrick et al., 2009).

The spatio-temporal dynamics of higher level cognitive processes such as response inhibition can be assessed by using electrophysiological values extracted from distinct latency ranges to predict BOLD responses at the single-trial level. In the context of response inhibition and executive functions, positive correlations between fronto-central Nogo-P3 amplitude values and fMRI BOLD signal in insula, right temporo-parietal and medial frontal cortex has been demonstrated (Karch et al., 2008). And also the sequential processes during response inhibition has been investigated by means of single-trial EEG/fMRI correlations (Baumeister et al., 2014). By using parametric modulation of fMRI BOLD signal with single-trial amplitude values derived from Cz at N2 and P3 latencies, the authors found an association of N2 with attentional processes while P3 was associated with inhibitory processes but also with memory recollection and internal reflection (Baumeister et al., 2014). Although this may indicate that Nogo-P3 is more specifically related to inhibitory processes, it is still not clear how specific variations of the N2/P3 complex are related to inhibition.

Besides of the possibility to investigate the spatiotemporal dynamics of neural processes, single-trial EEG/fMRI also enables to incorporate trial-to-trial variability as it is often seen on the behavioral level. As mentioned at the beginning of this section, behavioral variability such as the varying effectiveness of motor inhibition or trial-to-trial variations of reaction times can be linked to single-trial variabilities in neural processes (Fontanini and Katz, 2008; Ledberg et al., 2012; MacDonald et al., 2006). It has been shown that single-trial variability of evoked neural activity can be modeled by a combination of random ongoing network activity and stationary stimulus-related responses (Arieli et al., 1996). Therefore, single-trial fluctuations of evoked responses may contain aspects of moment-to-moment fluctuations in the subject's brain state rather than only representing noise (Kelly et al., 2008; Ledberg et al., 2012; Lutz et al., 2002). Single-trial EEG/fMRI data enables to relate single-trial ERPs with single-trial fMRI BOLD data in an attempt to map the short-term changes (i.e., trial-to-trial variations) in the subject's brain state to changes in metabolic

brain activity. This is based on the idea that single-trial fluctuations of ERP amplitudes are accompanied by systematic state variations which are reflected in trial-to-trial fluctuations of the fMRI BOLD responses. Under this precondition, trial-by-trial coupling of such ERP fluctuations with simultaneously recorded fMRI data should reveal those brain regions in which single-trial fMRI BOLD responses co-vary with the selected ERP amplitude variations.

1.2.3.3. Single-trial EEG feature extraction

The first step towards trial-to-trial coupling of event-related EEG and fMRI data is the extraction of the EEG features from each single trial of the artifact-cleaned EEG data. The resultant amplitude vectors are then convolved with HRF, leading to an internally driven model of the expected BOLD response. Similar to the stimulus derived regressors-of-interest, these EEG-regressors are included in the GLM of fMRI data analysis (Debener et al., 2005; Eichele et al., 2005; Huster et al., 2012). This allows relating single-trial event-related EEG to single-trial BOLD data in an attempt to map the changes in the subject's brain state, as mentioned above, to changes in metabolic brain activity. This approach is also designated 'integration-by-prediction' regarding that single-trial EEG/fMRI analyses usually employ EEG-derived regressors as predictors of the fMRI BOLD responses (Bland et al., 2011; Debener et al., 2006; Eichele et al., 2009; Huster et al., 2012). In the process of isolating task-related single-trial EEG activity, different routines have been used, i.e., single-trial EEG features were extracted from different electrophysiological sources: (1) from single independent components (ICs) reflecting best the EEG component of interest (Debener et al., 2005; Feige et al., 2005; Mobascher et al., 2009); (2) from artifact-cleaned EEG data using several electrodes (Eichele et al., 2005; Novitskiy et al., 2011); (3) or from single electrodes (Baumeister et al., 2014; Bénar et al., 2007; Juckel et al., 2012; Karch et al., 2010; Mulert et al., 2008; Scheibe et al., 2010; Warbrick et al., 2009). However, in the majority of studies components of interest were identified by visual inspection, which depends on subjective evaluation and can be biased by inter- and intra-individual variations of the evaluator.

Greater objectivity can instead be provided by data-driven approaches of component selection. Goldman and colleagues (2009) for example selected task-discriminating components in a completely data driven way. This was based on identifying components which are discriminating between two task-conditions in stimulus-locked and response-locked time windows. The authors demonstrated that trial-to-trial variations of these task-discriminating components correlated with fMRI BOLD responses could reveal a meaningful fMRI activation pattern that was different from those yielded by classical fMRI analyses (Goldman et al., 2009; Walz et al., 2013, 2014). Although this method allows for extracting task discriminating EEG components in a data driven way, an important limitation of this linear discrimination method is that the algorithm extracts only one EEG component for a given time window and thus could miss meaningful components. Also with the intent in providing more objectivity to the process of selecting meaningful EEG components, Wessel and Ullsperger

(2011) developed an algorithm (COMPASS) that automatically identifies ICs contributing to the ERP of interest by comparing each IC with a predefined ERP template. This approach however is limited by restricting the selection procedure to predefined ERP templates. Thus one central aspect of this thesis was the development and validation of a new analysis procedure that purely automatically identifies task-related ICs without using a priori defined ERP templates.

1.2.3.4. Artifact removal

The fundamental step towards trial-to-trial coupling of simultaneous EEG and fMRI data is the identification of that part of the EEG from which the single-trial information should be extracted. However, the selection of event-related EEG features from single-trial EEG data sets high standards for EEG data quality which is in conflict with simultaneous EEG and fMRI recording. As MRI-related artifacts as well as biologically caused artifacts are often characterized by high amplitudes they tend to superimpose that part of the signal that is truly related to neural activity. Hence, artifacts need to be identified and removed from the recordings prior to implementing further steps in the analysis. Although it has been demonstrated that filtering the EEG data at low frequencies improves the EEG data quality, so that amplitudes and latencies of the single-trial P3 deflections at a selected electrode site can be used for single-trial EEG/fMRI coupling (Bénar et al., 2007), this runs the risk of affecting or even removing event-related signals of interest (Sajda, 2009).

MRI-related artifacts: The crucial key towards single-trial EEG/fMRI analysis was the development of algorithms able to correct MRI-related artifacts such as gradient artifacts (Allen et al., 2000; Anami et al., 2003) or ballistocardiographic (BCG) artifact (Allen et al., 1998; Goldman et al., 2000; Ives et al., 1993).

The radio frequency (RF) artifact: This artifact is caused by the RF pulses which are applied perpendicular to the static magnetic field for fMRI data acquisition. RF artifacts are characterized by high frequencies and amplitudes that are 1000 times larger than the EEG signal related to neural activity. As the RF artifact appears in a frequency range that is higher than neural activity, it can be removed by applying an analog low-pass filter.

The gradient artifact: This artifact arises from the rapid switching of magnetic gradients used for spatial encoding in MRI data acquisition protocols. The gradient artifact arises from the physical principle of electromagnetic induction, which is the effect that a time varying magnetic field can induce a significant current flow in electrical wires. This current flow in the EEG's electrodes and/or wires results in the gradient artifact with amplitudes 10–100 times larger than the neural EEG data. In contrast to the RF artifact, the gradient artifact appears in a frequency range that

also includes frequencies of interest (< 100 Hz), so that filtering is an inappropriate method for gradient artifact removal (Allen et al., 2000). Instead, as for each EEG epoch recorded during the fMRI slice acquisition periods the waveform of gradient related artifacts remains almost identical, the average artifact substraction (AAS) method has been proven to be suitable for gradient artifact removal (Allen et al., 2000). This based on subtracting an averaged template of the gradient artifact from each single trial. In this context the synchronization of the EEG and fMRI hardware clocks turned out to be an useful tool in avoiding jitter-related variations of the gradient artifact, which will reduce the efficiency of the AAS method (Anami et al., 2003).

The ballistocardiographic (BCG) artifact: Similar to the gradient artifact, the BCG artifact arises from the physical principle of electromagnetic induction. While the gradient artifact grounds in the time varying external magnetic fields due to rapidly switching magnetic gradients, the BCG artifact is related to the effect that electromagnetic induction also arises from the movements of circuits formed by electrically conductive materials through a magnetic field. Thus, cardiac activity which results in a pulsatile movement of scalp and the attached EEG electrodes can produce the BCG artifact (Ives et al., 1993). As this heart beat related BCG artifact appears with a relatively constant waveform, a method based on the same concept as the abovementioned AAS method for gradient artifact removal can be used for removing BCG artifacts from EEG data (Allen et al., 1998). Therefore, an electrocardiographic (ECG) electrode is placed beneath the subject's scalpula to record the ECG relatively clean. Using the signal from this ECG electrode, the onset of each cardiac cycle can be identified and used to estimate a BCG artifact template for each EEG channel separately, which is then subtracted from the EEG in each cardiac cycle (Allen et al., 1998; Goldman et al., 2000).

Biological artifacts: Besides of MRI-related artifacts, EEG data may be compromised by a variety of artifacts regardless whether they were recorded simultaneously with fMRI data acquisition or in a shielded EEG recording room. While some artifacts arise from avoidable sources of error such as electrodes with poor conductive properties, electrical interference sources or defective electrodes or amplifiers, other artifacts derive from unavoidable biological sources such as muscle activity or eye movements.

In contrast to the abovementioned MRI-related artifacts, artifacts arising from biological sources are non-stationary over space and time, which makes it more challenging to detect and remove such artifacts. The most important source of such artifacts is related to the subject's eye movement which causes the electrooculographic (EOG) artifact that is characterized by high amplitudes (> 100 mV) and low frequencies (< 4 Hz). Due to the electrical potential differences between cornea and retina, every eye movement induces a change in the surrounding electric field which spread over the entire scalp. Importantly, as this artifact appears non-stationary, none of the

abovementioned methods are suitable for EOG artifact correction. It has also been claimed, that the ECG respectively BCG artifact which is the rhythmic artifactual EEG activity associated with the heart beats, are to some extent non-stationary as well (Srivastava et al., 2005). Thus, they suggested using the independent component analysis (ICA) technique instead of simple average removing methods.

1.2.3.5. Principles of independent component analysis (ICA)

In the context of biologically caused artifacts the independent component analysis (ICA) (Bell and Sejnowski, 1995; Lee et al., 1999; Makeig et al., 1999, 2002) has been proven to be a powerful approach in denoising the EEG data (Delorme et al., 2007; Hyvärinen and Oja, 2000; Jung et al., 2000; Lee et al., 2009, 1999; Makeig et al., 1996, 1996; Vigário et al., 2000). ICA is a signal processing technique that allows decomposing multichannel EEG data into temporally independent components (Makeig et al., 1996). This blind source separation technique is most frequently employed for correction of non-stationary artifacts, but has also been proven to be useful to reveal interesting information or to extract certain features of the EEG (Hyvärinen and Oja, 2000; Makeig and Onton, 2011). If applied to EEG data, the ICA is based on the assumption that the signals recorded by the electrodes are a linear mixture of superimposed activity of spatially distributed and thus spatially independent neural sources (Jung et al., 1998; Lee et al., 1999; Makeig et al., 1996).

ICA aims at the recovery of the sources, or ICs, contributing to an observed signal without knowledge about the quality of the underlying sources (Bell and Sejnowski, 1995). This refers to the source separation problem, also known as the 'cocktail party problem', which is generally associated with the occurrence of mixed signals or observations. To solve this problem, i.e., to blindly separate and deconvolve the statistically independent components of a given mixtures of observation, the information-maximization (infomax) algorithm was introduced (Bell and Sejnowski, 1995). The infomax ICA algorithm is an unsupervised learning algorithm for neural networks.

In the following years, it was demonstrated that through applying the infomax ICA algorithm to multichannel EEG data, the signal can be decomposed into spatially fixed and temporally independent components which allowed to separate EEG activity related to artifacts from those related to neural activity (Jung et al., 1998; Makeig et al., 1996). As the infomax ICA only separates super-gaussians data, an extended version of the infomax ICA algorithm that works for both sub- and super-Gaussians distributions was introduced (Lee et al., 1999). When the extended infomax ICA algorithm is applied to multichannel EEG data, the observed EEG signal is linearly transformed into time courses of activations, which are statistically as independent as possible.

By applying the ICA algorithm, the multichannel EEG data is linearly transformed from the original sensor space into the IC space. As the IC space is of the same size as the original EEG data,

the number of resultant ICs is equal to the original number of EEG channels. In matrix notation, the result of an ICA trained on multichannel EEG data yields a matrix (U) of the activation time courses of each IC, which is the matrix multiplication of the recorded EEG data (X) with the unmixing matrix (W), which is the square matrix of weights (1.2):

$$U = W \cdot X \tag{1.2}$$

With X being the recorded EEG data represented as a matrix of n numbers of channels (rows) and m time points (columns). W is a square matrix of weights with the size of the number of channels, which is estimated while the ICA is trained on the EEG data. Using the linear spatial filters given by the rows of W, the recorded EEG signal can be decomposed into maximally temporally independent components (U). By multiplying these independent components (U) with the inverse of W, i.e., the mixing matrix W^{-1}, the original EEG data can be reconstructed which is also referred to as the back-projection of the ICs into the sensor space (1.3):

$$X = W^{-1} \cdot U \tag{1.3}$$

With matrix U is reflecting the activation time courses of the ICs and the mixing matrix W^{-1} representing the corresponding topographical information.

In summary, each IC is characterized by its topographical information (i.e., the scalp map which is the spatial projection of the particular IC) and its time course (i.e., the temporally changing activity profile of the particular IC) (Hyvärinen and Oja, 2000; Makeig and Onton, 2011; Ullsperger and Debener, 2010). Thus, by multiplying the continuous EEG data (X) with the unmixing matrix (W), IC activations (U) can be computed for any EEG sample without repeating the ICA training. Although most frequently employed for artifact correction, the extended ICA algorithm can also be utilized to reveal interesting information or to extract certain features of the EEG (Hyvärinen and Oja, 2000; Makeig et al., 2002). In line with this, Debener and colleagues demonstrated that, besides artifact correction, ICA is also a practical solution to isolate task-related EEG activity on the single-trial level (Debener et al., 2005).

1.3. Motivation and outline

Response inhibition is the ability to suppress inadequate but prepotent or ongoing response tendencies. Between-subject differences in the intra-individual variability have been suggested to constitute a key to pathological processes underlying impulse control disorders. Single-trial electroencephalographic (EEG)/functional magnetic resonance imaging (fMRI) analysis allows to increase sensitivity for inter-individual differences by incorporating intra-individual variability and also allows to assess group differences in spatio-temporal dynamics of the neural impulse control network. Aim of this thesis was to assess comprehensively the spatio-temporal dynamics of the neural response inhibition network in healthy control (HC) subjects as well as in subjects characterized by non-clinical and clinical high impulsive personality traits like Attention-Deficit/Hyperactivity Disorder (ADHD) and Borderline Personality Disorder (BPD). This thesis is based on two manuscripts with first authorships and one hitherto unpublished study. One manuscript is published in an international peer-reviewed journal and one manuscript is submitted to an international peer-reviewed journal.

Chapter 3 [Study 1: Data-driven analysis of simultaneous EEG/fMRI using an ICA approach. Schmüser L, Sebastian A, Mobascher A, Lieb K, Tüscher O and Feige B (2014). Front. Neurosci. 8:175. doi: 10.3389/fnins.2014.00175.] introduces a newly developed analysis procedure that automatically selects task-specific electrophysiological independent components (ICs) which are reliably inhibition-related at different phases of motor response inhibition, i.e., before or around the individual median Go response time (RT). As the ICs were selected without using a priori defined event-related potential (ERP) components, this approach avoided the analytical bias of the human rater based assessment of EEG correlates of presumed task-related activity as measured by ERPs. This approach was essentially based on the intra-individual classification of ICs according to their relation to response inhibition. ICs which are identified as reliably inhibition-related (significantly larger in amplitude for Nogo than Go) within a predefined time window are combined into individual electrophysiological regressors and then included into fMRI first-level analysis. Single-trial correlations of fMRI blood oxygenation level-dependent (BOLD) signal with these electrophysiological regressors revealed fMRI BOLD responses in fronto-striatal regions which were more pronounced in an early compared to a late phase of task execution. This study also demonstrated that beyond detecting inhibition-related ICs the algorithm is able to detect ICs related to visual responses in the same data set. Moreover, a direct comparison with a more classical approach that uses N2/P3 amplitudes at specific electrodes as ERP-regressors, demonstrated that the IC-based approach is more specific for task-related neural activity.

In Chapter 4 [Study 2: Neural timing of response inhibition in Attention-Deficit/Hyperactivity Disorder (ADHD) and Borderline Personality Disorder (BPD), to be submitted] combined EEG/fMRI was used in addition to unimodal ERP and fMRI analyses to examine the temporal and spatial dynamics of neural processes underlying response inhibition in adult ADHD patients compared

to BPD and HC subjects. Using the novel single-trial EEG/fMRI analysis approach based on independent component analysis (ICA) from Study 1 allowed to specifically assess whether only certain, temporally distinct phases of neural processing are affected in adult ADHD patients and/or in adult BPD patients. In contrast to the usually marginal findings of unimodal fMRI analysis, this ICA-based single-trial EEG/fMRI analysis revealed significant group differences in key regions of the neural response inhibition network, especially in the early latency range of response inhibition in adult ADHD patients as compared to both HC and BPD patients. This finding of no substantial differences between BPD patients and HC subjects seems to point towards an almost intact neural response inhibition network in BPD patients. As opposed to this, the finding of deficient early activity in ADHD patients suggests that difficulties within the temporal dynamics or orchestration of neural processes underlying response inhibition are central in the pathophysiology of impulsivity in ADHD. This observation may shift our pathophysiological understanding of impulse dyscontrol from static to more dynamic models. This is the first multimodal study that demonstrated deficient neural processing at an early phase of response inhibition in adult ADHD patients.

Chapter 5 introduces Study 3 [Study 3: Data-driven analysis of simultaneous EEG/fMRI reveals neurophysiological phenotypes of impulse control. Schmüser L, Sebastian A, Mobascher A, Lieb K, Feige B and Tüscher O (2016). Hum. Brain Mapp.. doi: 10.1002/hbm.23230.] in which combined EEG/fMRI was employed to examine inter-individual differences in response inhibition in healthy subjects. Subgroups were defined on electrophysiological level using the existence or absence of specific ICs related to Nogo processing at an early stage of response inhibition as introduced in Study 1. To characterize these subgroups, behavioral, neuropsychiatric, unimodal ERP and fMRI measures, as well as single-trial ERP/fMRI correlations were used. It was demonstrated that the existence or absence of such early Nogo-related ICs is related to inter-individual differences in neural and behavioral correlates of responses inhibition. This is the first multimodal study that assessed inter-individual differences in response inhibition. Using automated selection of intra-individually classified Nogo-related ICs, distinct neurophysiological phenotypes of response inhibition were identified in a data-driven, unbiased way. Although further analyses are needed to differentiate whether inter-individual differences are state or trait related, the identification of these potential phenotypes already demonstrates the importance of inter-individual differences which may affect the results of group comparisons in clinical studies.

2. Material and Methods

2.1. Experimental design

2.1.1. Participants

All participants were selected from a larger data set that was acquired as part of a study founded by the Federal Ministry of Education and Research (Bundesministeriums für Bildung und Forschung (BMBF), Grant 01GW0730) on the subject *'Neural circuitry of impulse control: An integrative approach towards the understanding of normal and impaired impulse control in Humans'*. The study was approved by the Ethics Committee of the University of Freiburg Medical School. All participants were screened for factors contradicting magnetic resonance imaging (MRI) scanning and provided written informed consent prior to simultaneous electroencephalography (EEG) and functional MRI (fMRI) scanning. For the time spend for completing the questionnaires and experimental procedures, each participant received a financial compensation of 55 €.

Because of the necessity of good overall data quality for EEG and fMRI data, participants with non-existence data for one of the modalities (EEG or fMRI) as well as participants of whom the artifact correction of fMRI and/or EEG data did not achieve usable datasets were excluded from further analysis. Moreover, participant characterized by performance data or neuropsychometric values outside the normal range were excluded. All participants were right-handed as determined by the Edinburgh Handedness Inventory (Oldfield, 1971) and had normal or corrected-to-normal vision. All participants had no history of serious medical or neurological disease and were free of psychotropic medication.

Healthy control (HC) participants: Data of 39 participants (16 males; mean age: 38.85 ± 16.5) were included. Participants with a lifetime history of axis I or axis II disorder were excluded.

Attention-Deficit/Hyperactivity Disorder (ADHD) patients: Data of 19 adult ADHD patients (12 males; age: 35.84 ± 12.7) were included. All ADHD patients were recruited from a specialized outpatient clinic of the Department of Psychiatry and Psychotherapy of the University Medical Center Freiburg. To increase diagnostic validity, only ADHD patients who met the diagnostic criteria of ADHD for Diagnostic and Statistical Manual of Mental Disorders (DSM)-IV and International Classification of Diseases (ICD)-10 as assessed by a diagnostic interview

were included. Patients were medication naïve regarding methylphenidate and amphetamine compounds and had never taken long-term psychotropic medication. Further exclusion criteria were schizophrenia, bipolar disorder or current depressive episodes.

Borderline Personality Disorder (BPD) patients: Data of 19 adult female BPD patients (mean age: 23.63 ± 3.5) were included. Only BPD patients who met the diagnostic criteria of BPD according DSM-IV but had no lifetime diagnosis of ADHD were included. Further exclusion criteria were schizophrenia, bipolar disorder or current depressive episodes.

2.1.2. Questionnaires and diagnosis

As an approximate measure of intelligence quotient, the individual verbal intelligence was determined using the German multiple-choice vocabulary test (MWT-B), a verbal test with German norms (Lehrl, 1995). German versions of the Structural Clinical Interviews for DSM-IV Axis I and II Disorders were used by trained psychologists to assess current and lifetime psychiatric diagnoses of axis I or axis II disorders (SCID I: First et al., 1997, SCID I German version: Wittchen et al., 1997, SCID II: First et al., 1996, SCID II German version: Fydrich et al., 1997).

To assess self-rated impulsive personality traits, all participants were asked to complete the Barratt Impulsiveness Scale-11, (BIS-11, Patton et al., 1995), the Sensation Seeking Scale (SSS-V, Beauducel et al., 2003) and UPPS Impulsive Behavior Scale (UPPS, Whiteside and Lynam, 2001). As both, ADHD and BPD patients are often characterized by comorbid depressive symptoms, the current depressive mood was tested by the self-rating scale Beck Depression Inventory (BDI, Hautzinger et al., 1995) as well as by means of an independent rating by a trained psychologist (Montgomery Asberg Depression Scale (MADRS), (Montgomery and Asberg, 1979).

Clinical ratings regarding ADHD symptoms were assessed using the short version of the German validated Wender Utah Rating Scale (WURS-k, Retz-Junginger et al., 2003) for childhood ADHD symptoms and the Conners' Adult ADHD Rating Scale (CAARS-S:L, Christiansen et al., 2011, 2012) for current ADHD symptoms. Only ADHD patients with a total WURS-k score of > 30 and a total CAARS-S:L score of > 65 were included, while HC participants and BPD patients above WURS-k and CAARS-S:L cutoff were excluded. The Borderline Personality Disorder Severity Index (BPDSI, Arntz et al., 2003; Freese and Kröger, 1999) was used for clinical assessment of the frequency and severity of manifestations of BPD symptoms.

2.1.3. Paradigm

During simultaneous EEG/fMRI data acquisition all participants performed a visual Go/Nogo task (Figure 2.1). On the center of the screen, with visual angle of 3.5° vertically and 5.3° horizontally, a stream of in total 300 consonants was presented serially. Each consonant was shown for 0.5 s

followed by a black screen for the next 0.5 s. The consonants covered all consonants of the alphabet and were presented in a pseudo-randomized manner, with the restriction that the Nogo stimulus ('X') is presented with a mean probability of 29 % and each Nogo stimulus is followed by at least one Go stimulus (one of the remaining consonants). The participants were instructed to respond by pressing a mouse button with the right index finger to every Go stimulus and to withhold this response in case of the Nogo stimulus ('X'). In total, every participant completed two runs each consisting of 300 stimuli. Each run started and ended with a 16 s fixation phase in which a white cross was presented in the center of the screen against a black background to which participants were asked to fixate. Prior to the scanning session, every participant had received a brief training session on the task outside the scanner room. This paradigm was programmed using the software 'Presentation' (Neurobehavioral Systems, Version 11.1 http://www.neurobs.com/). Visual stimuli were projected on a screen at the head end of the scanner bore and viewed with the aid of a mirror mounted on the head coils.
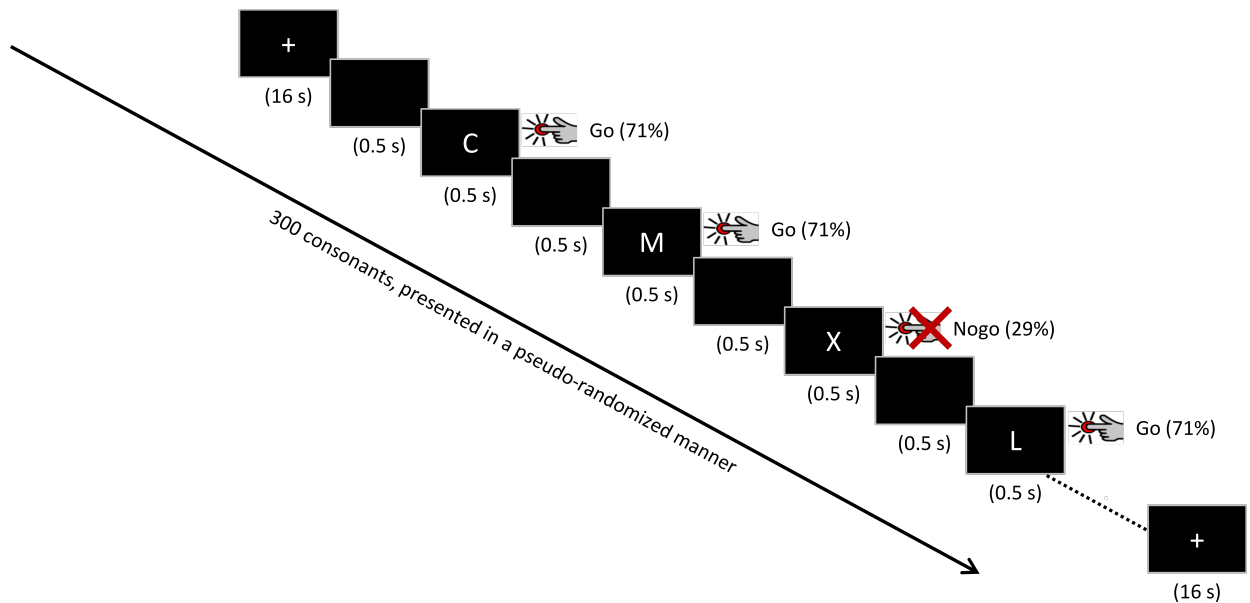
Figure 2.1. Schematic display of the Go/Nogo task. Participants were instructed to press a button for any letter (Go stimuli) except the 'X' (Nogo stimulus). Each letter was shown for 0.5 s followed by a black screen for the next 0.5 s.The task consisted of 2 runs with 300 stimuli per run and 29 % Nogo probability.Each run started and ended with a 16 s fixation phase: a white cross was presented in the center of the screen against a black background to which participants were asked to fixate. s: second.

2.2. Data acquisition

Data acquisition was performed at the University Hospital of Freiburg (Department of Radiology). For simultaneous EEG/fMRI data acquisition, fMRI and EEG data recordings were initiated manually while visual presentation was initiated by a trigger code sent from the MRI scanner to the presentation host. To allow for gradient artifact correction, the EEG-amplifier hardware clock was synchronized with the timing of gradient switching during fMRI measurements (SyncBox, Brain Products, Gilching, Germany). Furthermore, the onsets of echo planar image (EPI) scans, visual stimulation and the participant's response were registered on a trigger channel of the EEG acquisition system.

2.2.1. (functional) magnetic resonance imaging (MRI/fMRI)

MRI data was collected on a Magnetom 3T tim-TRIO scanner (Siemens Medical Systems, Erlangen) using a 12 channel head coil for signal reception. To limit head motion within the coil and thus reduce motion related artifacts, the participant's head was stabilized by means of foam padding. Ear plugs and headphones were used to reduce acoustical stress of the participant due to the scanner noise.

For fMRI blood oxygenation level-dependent (BOLD) imaging, T2*-weighted EPI volumes were acquired with repetition time (TR) = 2250 ms, echo time (TE) = 30 ms, flip angle = 90°, field of view (FOV) = 92 mm, voxel (volume element) size = 3 mm^3, and 36 interleaved slices. In each scanning session, movement and distortion correction were performed automatically by applying fully automated PACE (prospective acquisition correction) motion correction (Thesen et al., 2000) and distortion correction based on point spread function mapping (Zaitsev et al., 2004). A total of 157 complete brain volumes were acquired for each run.

Subsequent to simultaneous EEG/fMRI data acquisition, the EEG cap was removed. This allowed for acquisition of high resolution 3D MRI data for anatomical references by using a 3D magnetization prepared, rapid acquisition gradient echo (MPRAGE) sequence with TR = 2200 ms, TE = 4.11 ms, flip angle = 12°, FOV = 256 mm, voxel size = 1 mm^3.

2.2.2. Electroencephalography (EEG)

Simultaneously with fMRI data acquisition, continuous EEG data was recorded using a 64-channel EEG-system consisting of two 32-channel MRI-compatible EEG-amplifiers (BrainAmp MR plus, Brain Products) powered by a MRI-compatible rechargeable battery pack (PowerPack, Brain Products). To reduce potential scanner artifacts caused by wires moving inside the magnetic fields,

the EEG system was placed inside the scanner bore directly behind the head coil as this allowed for the use of short wires.

64-channel EEG-recording caps (Easycap, Falk Minow Services, Herrsching, Germany) compatible with 56 cm or 58 cm head size were used. A total of respectively 62 sintered Ag/AgCl ring electrodes were placed within the EEG-recording caps according to an extended international 10-20 system (Klem et al., 1999). Reference electrode was positioned at FCz and ground electrode was positioned at AFFz. An additional electrode was placed below the participant's left eye in order to monitor eye movements and eye blinks (electrooculogram (EOG)). To facilitate ballistocardiographic (BCG) artifact correction, another electrode was placed beneath the participant's left scapula in order to monitor the electrocardiogram (ECG). The electrodes were filled with an electrolyte gel, after cleaning the skin below the electrodes with a high-chloride abrasive electrolyte gel. This aims at optimizing the conductivity between skin and electrode. By means of this procedure, electrode-skin contact impedances were maintained below 10 kΩ.

The recorded analog EEG signal was filtered between DC and 1 kHz. To obtain a good sampling of the scanner artifacts, the analog EEG signal was digitized with a sampling frequency of 5 kHz. Furthermore, the EEG sampling was driven by the clock board of the MRI scanner (SyncBox, Brain Products) in order to facilitate the subtraction of the gradient artifact. The digitized EEG signal was then transmitted via fiber optic cables to the EEG acquisition host placed outside the scanner room. The Brain Vision Recorder software (Brain Products) was used to acquire, store and display EEG recordings online.

2.3. Data preprocessing

2.3.1. fMRI preprocessing

fMRI data preprocessing was performed using the Statistical Parametric Mapping (SPM) software (SPM5, released December 2005, Wellcome Trust Centre for Neuroimaging at UCL, London, UK; http://www.fil.ion.ucl.ac.uk/spm /software/spm5) running under Matlab 7.7.0 (The MathWorks Inc., Natick, Massachusetts, USA; http://www.mathworks.com). Prior to data analysis, images were screened for motion artifacts as caused by excessive head motion (> 2 mm). No participant had to be excluded because of such excessive head motion. In the next step, functional images were manually reoriented to the T1-template of SPM.

The first five volumes of each run were then discarded to allow for equilibrium effects. The remaining functional images of both runs were realigned to the first functional image of the first run using a six degree of freedom rigid body transformation and then coregistered to the individual anatomical T1 image. In the following step, this T1 image was spatially normalized to the reference system of the Montreal Neurological Institute's (MNI) reference brain using linear and nonlinear

transformation. Using the resultant normalizing parameters the functional images were spatially normalized to the standard MNI space, this allows for comparing functional images from different individuals. Finally, all functional images were smoothed by applying a 3D isotropic Gaussian kernel with 8 mm full-width at half maximum (FWHM).

2.3.2. EEG preprocessing

Continuous raw EEG data was processed offline using AvgQ (Feige, 1999; Freiburg, Germany; https://github.com/berndf/avg_q). This is an open source multichannel EEG/MEG (magnetoencephalography) data processor that is driven by Python scripts. Gradient artifact correction was performed by the template subtraction method of Allen and colleagues (average artifact substraction (AAS), Allen et al., 2000). To obtain an optimal estimate of the gradient artifact, one after another every EEG epoch was tested for the best overall correspondence with the other epochs. In the following step, all epochs that did not deviate too much from the epoch with the best overall fit were averaged together. This estimated gradient artifact was then subtracted from the continuous data. This approach ensures that non-representative epochs, e.g., compromised by large phasic artifacts, due to eye or head movements are excluded from the averaged template. The high sampling rate of 5 kHz provides a good temporal resolution of the artifact onset which facilitates a averaging as precise as possible. Moreover, as the EEG sampling was synchronized to the gradient clock (SyncBox, Brain Products), further data upsampling was not necessary.

Following the gradient artifact correction, the EEG data was then run through a bandpass filter (0.2–48 Hz) in order to remove residual scanner artifacts as well as low-frequency drifts. Subsequently, the data was down-sampled to 100 Hz. Using the extended information-maximization (infomax) independent component analysis (ICA) algorithm (Lee et al., 1999) an unmixing matrix was estimated for the artifact-cleaned EEG data of each participant and run separately. By multiplying the continuous EEG data with this unmixing matrix, independent component (IC) activations can be computed for any EEG sample without repeating the ICA training.

In the following, averages related to heart beat and eye blink were computed for BCG and EOG artifact correction. For detection of each single heart beat, the signal as recorded from the ECG channel was first convolved with a time-domain ECG template. Using these single heart beats as triggers, an individual BCG template was estimated by computing an ECG-triggered EEG average. Subsequently, ICs loading on this BCG average were identified and selected as artifact components. By removing these ICs, BCG artifact correction was performed. Similarly, EOG artifact detection and correction was performed on the BCG artifact corrected EEG data.

Importantly, in the context of the ICA-based approach of single-trial EEG/fMRI data analysis the electrophysiological information was extracted from the IC time courses themselves (cf. Section 2.4.1 *'Classification and selection of Nogo-related ICs'* and Section 2.4.2 *'Classification*

and selection of visual ICs'). Thus, simply excluding those ICs representing BCG/EOG artifacts was sufficient enough for avoiding BCG or EOG artifacts. This is different, however, for analyses based on EEG data instead of ICs (cf. Section 2.4.3 *'Classification and selection of N2/P3 ERPs'* and Section 2.5.4 *'Unimodal event-related potential (ERP) analysis'*). In this case the last step of BCG/EOG artifact correction (i.e., back-projection of every IC except those ICs loading on ECG and EOG artifacts) was necessary to obtain completely artifact-free EEG data.

2.4. Extraction of single-trial EEG information

2.4.1. Classification and selection of Nogo-related independent components (ICs)

After EEG data preprocessing was performed as described in Section 2.3.2 (*'EEG preprocessing'*), the 64 continuous IC time courses of each participant were segmented into epochs of 1200 ms length starting 200 ms prior to stimulus onset. All epochs were baseline corrected using the 200 ms prestimulus interval. Subsequently, epochs belonging to the same event type were averaged, resulting in event-related averages for correct Go, correct Nogo, omissions of Go trials and commission errors in Nogo trial, each consisting of 64 averaged ICs.

2.4.1.1. Reliability testing and thresholding

Within the process of averaging, the pointwise mean as well as the pointwise variance information for each time point was collected. These values were then used to compute pointwise t-tests on each IC time course and event type. Comparing the averaged IC time courses against baseline by means of one-sample t-tests yielded that part of the data that was reliably different from baseline at a specific time point. Secondly, comparing the Nogo and Go conditions by means of two-sample t-tests for independent groups allowed for assessing the latency ranges in which the IC is characterized by significantly larger in amplitude for Nogo than for Go trials. The pointwise t-values were then transformed into Z scores. This allowed to compare the results despite of a deviant number of trials in different conditions and participants, as caused by the individual error rate (2.1):

$$Z = t/N^2 \tag{2.1}$$

With Z being the ratio of two means (t) compared against the variability of the scores (N^2), a high Z score is indicative of a high signal-to-noise ratio. As high Z scores are indicative of high signal-to-noise ratios, only ICs with absolute Z scores crossing a predefined threshold entered further analysis steps.

2.4.1.2. IC classification

Thus determining whether an IC is reliably associated with the Nogo condition was based on the Z score differences between Nogo- and Go-related IC averages. This means, only ICs with absolute Z scores as obtained by the two-sample t-test comparing Nogo and Go conditions crossing a predefined threshold of 0.275 were selected. On the basis of 300 trials per block with maximally 90 Nogo trials, this Z score value of 0.275 corresponds to a two-sided p-value of 0.01 (two-sample t-test with a degree of freedom (DF) of 89). The DF was chosen conservatively from the condition with the smaller number of epochs, i.e., the Nogo condition. If the absolute value of this Z score differences exceeded this threshold of 0.275, the difference between Nogo and Go conditions within a certain IC was classified as sufficiently reliable. All latency ranges at which the threshold was crossed in positive and in negative direction were noted and used for selection of IC with activations within a specific time window. As the polarity of ICs in a given latency range is arbitrary, the polarity of the IC's maximal amplitude value during significant activation was noted. In the end, a list of Nogo-related ICs, latency ranges, and polarities was formed keeping only those ICs which were associated with larger absolute amplitudes in Nogo trials.

2.4.1.3. IC selection

One of the strengths of simultaneous EEG/fMRI is the possibility to bring higher temporal resolution in fMRI data analysis. Thus, in order to construct electrophysiological regressors representing different phases of the motor inhibition processes, ICs and latency ranges falling into different time windows were combined (Figure 2.2). Importantly, these time windows were not defined on the group level, as this is the case for classical ERPs such as N2 or P3 (cf. Section 2.4.3 *'Classification and selection of N2/P3 ERPs'*). Instead, they were defined for each participant individually by taking the stimulus onset and the individual's median correct Go response time (RT) as points of reference.

The first (early) time window aimed at capturing the neural correlates of an early stage of response inhibition or early stage of information processing associated with pre-motor response inhibition. To avoid including correlates of visual processing and object recognition (Johnson and Olshausen, 2003; Railo et al., 2011), this early time window started 200 ms after stimulus onset and ended with the individual median RT (Figure 2.2, yellow part). As the second (late) time window aimed at capturing the neural correlates of a later stage of response inhibition or later stage of information processing associated with response inhibition, it was located around the participant's individual median RT. To take into account that single trial RTs fluctuate from trial-to-trial around the individual median RT the late time window started 100 ms prior to the median RT and ended 300 ms after the median RT (Figure 2.2, red part).

These two time windows were chosen to have a 100 ms overlap in order to avoid the loss of too many meaningful activity candidates. Since both starting and ending point of each acceptable latency range as determined in the IC classification section (i.e., absolute Z score of Nogo$-$Go difference $|Z| > 0.275$) were strictly required to fall within the given time window, any acceptable activity not only has to be significant within the given time range but must also start (i.e., rise above Z threshold) after the beginning and end (i.e., fall under Z threshold) before the ending of the given time window.
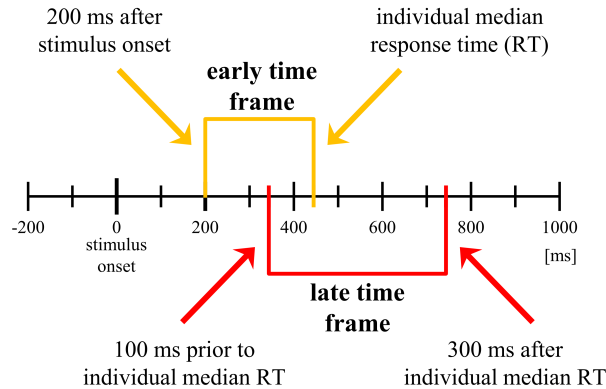
Figure 2.2. Visualization of the two predefined time windows in which the independent component's (IC) latency range of significant activation had to be confined. Starting point of the 'early' time frame (yellow brackets) is 200 ms after stimulus onset, ending point is the individual median correct Go response time (RT). The 'late' time frame (red brackets) starts 100 ms prior to RT and ends 300 ms after RT. To be selected, the IC's latency range of reliable activation must be wholly contained within one of the predefined time windows, i.e., the Nogo minus Go absolute Z score must arise above threshold ($|Z| > 0.275$) and must fall below threshold ($|Z| > 0.275$) within the time window. Black bars depicting 100 ms intervals. Adopted from (Schmüser et al., 2014).

2.4.1.4. Feature extraction

In the last step, the amplitude values of all single trials were extracted from every selected IC. This was done by extracting mean single-trial amplitude values from the latency range in which the respective IC was reliably larger during Nogo than during Go trials (Figure 2.3). Since the polarities of ICs are arbitrary, the polarity of the IC's maximal amplitude value during significant activation has been noted in the process of IC classification. Thus to ensure positive polarity with respect to the Nogo$-$Go difference, the amplitude values were inverted if necessary using the polarity noted above. For each participant, the resultant amplitude vectors of all ICs selected with respect to the same run and time window (early or late) were combined into a single amplitude vector by summation, resulting in two different amplitude vectors for each participant and run: early and late.
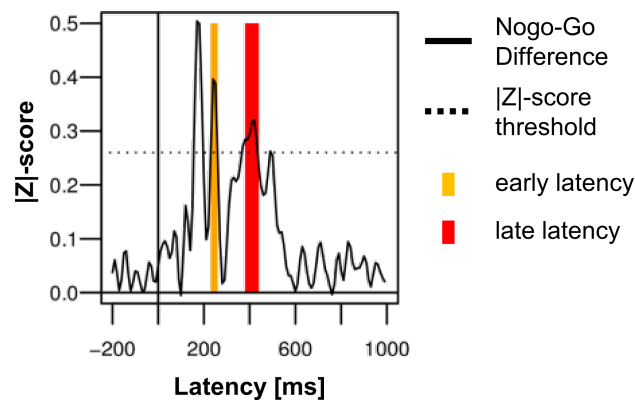
Figure 2.3. Visualization of independent component feature extraction from the two predefined time windows in which the IC's latency range of significant activation were identified. Shown is a single participant's $|Z|$-score average (stimulus locked) of an IC classified as reliable Nogo-related within the early (yellow) and late late (red) latency ranges. Early: starting 200 ms after stimulus onset and ending with the individual median Go response time (RT). Late: starting 100 ms prior to RT and ending 300 ms after RT. Colored bars depict the IC's specific latency range of reliable activation. Dotted line depicts the predefined threshold of $|Z| > 0.275$. Black bars are depicting 200 ms intervals. Adopted and modified from (Schmüser et al., 2014).

2.4.2. Classification and selection of independent components (ICs) related to early visual processing

2.4.2.1. IC classification

While the Nogo-related ICs were expected to have significantly larger amplitudes in Nogo trials compared to Go trials, it can be assumed that responses to visual Go and Nogo stimuli are similar. Thus, IC classification was not based on the Nogo−Go difference, but on IC averages and variances that were computed across Nogo and Go epochs against baseline. Similarly to the classification of Nogo-related ICs, the visual ICs were classified as sufficiently reliably activated if their absolute Z score exceeded a threshold of 0.275. Subsequently, a list of ICs, latency ranges, and polarities was formed for each participant and run.

2.4.2.2. IC selection

As visual processing is expected to be solely dependent on the time point of stimulus presentation, for each participant a stimulus-locked time window comparable to the latency range of the visual evoked P1 component was chosen. In conventional ERP analysis, the P1 is a positive deflection occurring shortly after 100 ms post-stimulus that has been associated with early conscious visual perception (Railo et al., 2011). In previous simultaneous EEG/fMRI studies, single-trial correlations of fMRI BOLD response with P1 amplitudes has been used for validation purposes as well (Di

Russo et al., 2002, 2005; Novitskiy et al., 2011; Warbrick et al., 2013).To construct a regressor associated with this early conscious visual processing, ICs and latency ranges falling into a time window starting 90 ms after stimulus onset and ending 140 ms after stimulus onset were selected. The size of this time windows is chosen in order to avoid losing too many meaningful activity candidates.

2.4.2.3. Feature extraction

Similarly as in the procedure of Nogo-related ICs, for every selected IC, mean amplitude values were extracted from each single trial at the latency range in which the respective IC had crossed the predefined Z threshold. Subsequently for each participant and run, the resultant amplitude vectors of the selected ICs were combined into a single amplitude vector by summation.

2.4.3. Classification and selection of N2/P3 event-related potentials (ERPs)

To obtain condition specific ERPs, the BCG/EOG artifact corrected EEG of each participant (cf. Section 2.3.2 *'EEG preprocessing'*) was re-referenced to the average of TP9 and TP10 and segmented into epochs of 1200 ms starting 200 ms prior to stimulus onset. The 200 ms pre-stimulus interval was used for baseline correction. Similarly, to the ICA-based approach (cf. Section 2.4.1 *'Classification and selection of Nogo-related ICs'*), epochs belonging to the same event type (correct Go, correct Nogo, omission of Go trials, and commission errors in Nogo trials) were averaged, resulting in four different event-related averages.

In the following, ERPs of the same event type were averaged over the entire group(s). These grand averages were then used to identify the electrode sites which demonstrated the most pronounced Nogo-N2/-P3 effects. Subsequently, the latency ranges which covered best the task-related N2 and P3 effects at the selected electrode site(s) on the group level were chosen (Figure 2.4).

In Study 1 (cf. Chapter 3) N2 and P3 single-trial amplitude values were selected from Cz, in line with a prior publication on single-trial analysis of simultaneous EEG/fMRI data (Baumeister et al., 2014). N2 was measured as the mean amplitude from a time window starting 280 ms after stimulus onset and ending 340 ms after stimulus onset. For the later P3-regressor, the mean amplitude was extracted from a time window starting 350 ms after stimulus onset and ending 580 ms after stimulus. In contrast to this, in Study 3 (cf. Chapter 5) the N2 effect was most pronounced at F4 from 240–350 ms while P3 was most pronounced at Cz from 350–580 ms. In each study, single-trial amplitude values were extracted from these specified electrode site(s) and latency ranges, resulting in two amplitude vectors for each participant.
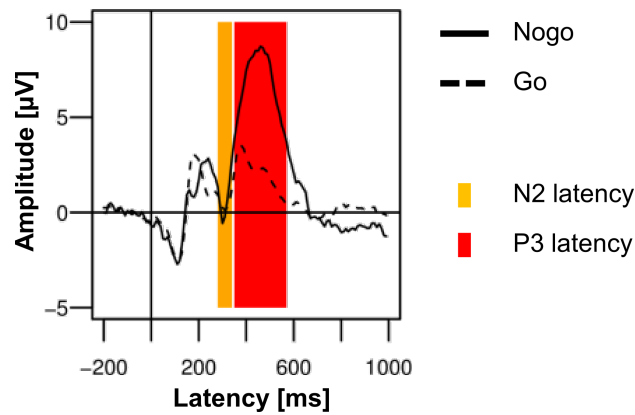
Figure 2.4. Visualization of the two time windows in which the most pronounced Nogo-related N2/P3 effects were found. Shown is the a grand average of Go- and Nogo-related event-related potentials (ERPs) at Cz where the Nogo-N2 and Nogo-P3 effect was most pronounced in a group of 22 healthy participants. Black lines display grand averages of Go (dotted line) and Nogo (solid line) ERPs at Cz electrode. The yellow bar indicates the N2 time window. The red bar indicates the P3 time window.

2.4.4. EEG-derived regressors

As described in the prior sections, single-trial amplitude values of the selected electrophysiological components—either Nogo-related ICs, or visual ICs, or ERPs from Cz (Study 1, cf. Chapter 3), or from F4 and Cz (Study 3, cf. Chapter 5)—were combined into individual electrophysiological amplitude vectors. While amplitude values are available for each trial ($f = 1$ Hz), not every trial was sampled by fMRI data acquisition ($f = 1/2.25$ Hz).

Thus to compensate for these deviant sampling frequencies, each electrophysiological amplitude vector was first interpolated over time by using a cubic smoothing spline function and then re-sampled at the time points of fMRI data acquisition. This down-sampled time course was then normalized to inter-quartile range (IQR $= 1$) and convolved with a canonical hemodynamic response function (HRF).

To test for effects only driven by the electrophysiological regressors, except of visual IC-derived regressors, each EEG-derived regressor (early and late ICs, N2 and P3 ERPs) was also orthogonalized with respect to classical onset regressors (Go, Nogo, Errors). This resulted in orthogonalized and non-orthogonalized versions of the task-related electrophysiological regressors (Nogo-related ICs and N2/P3 ERPs).

2.5. Data analysis

2.5.1. Statistical analysis of behavioral data

To characterize the groups on behavioral level, measures of interest were mean response time on correct Go trials (= RT), percentage of commission errors on Nogo trials and omission errors on Go trials. To assess intra-individual RT variability the coefficient of variability (CoV) was computed by dividing the standard deviation of RT by the mean RT (Stuss, 2003). Statistical analysis was performed using the package 'stats' (R Core Team, 2014) from the open-source statistical computing software 'R' (http://cran.r-project.org/).

2.5.2. First-level unimodal fMRI analysis: Single-subject analysis of fMRI data

Statistical analysis of fMRI data was performed using SPM8 (released April 2009, Wellcome Trust Centre for Neuroimaging at UCL, London, UK, http://www.fil.ion.ucl.ac.uk/spm/software/spm8) running under Matlab 7.7.0 (The MathWorks Inc.). For each participant the first-level generalized linear model (GLM) consisted of two onset regressors which corresponded to the correct and incorrect Nogo conditions. As the frequent Go stimuli were presented in a frequency that is beyond the fMRI's temporal resolution, the Go stimuli were not modeled by onset regressors but instead used as an active baseline (Sebastian et al., 2012, 2013a, 2013c). Using Go as an active baseline allowed comparing Nogo vs. Go (active baseline) implicitly. The time courses of regressors and functional data were then run through a high-pass filter (128 second cut-off) in order to remove artifacts resulting from low-frequency temporal variations.

2.5.3. First-level single-trial EEG/fMRI analysis: single-subject analysis of multimodal fMRI data

Statistical analysis of fMRI data was performed using SPM8 (Wellcome Trust Centre for Neuroimaging at UCL) running under Matlab 7.7.0 (The MathWorks Inc.). GLMs were fitted for each participant, each run, and each EEG-derived regressor separately to the fMRI data. Besides the three onset regressors Go, Nogo and errors, the design matrix of each GLM contained one EEG regressor derived from either early or late ICs, N2 or P3 ERPs, or visual ICs. Depending on the main research question, the task-related electrophysiological regressors were orthogonalized or non-orthogonalized to the onset regressors, whereas the non-task-related visual regressor was not orthogonalized. The regressors were orthogonalized if the analysis aimed at revealing exclusively the additional information provided by the electrophysiological regressors (Study 1 in Chapter 3). However, if the analysis aimed at assessing comprehensively the spatio-temporal dynamics of the neural impulse network, the electrophysiological regressor were non-orthogonalized to the

electrophysiological regressors (Study 2 in Chapter 4 and Study 3 in Chapter 5). To remove artifacts resulting from low frequency temporal variations, the time courses of regressors and functional data were run through a high-pass filter with a 128 second cut-off.

As the ICA was applied to each run independently, every step required for the selection of the task-related ICs of interest was performed on the runs independently resulting in two EEG-derived regressors per participant. For the sake of consistency, N2/P3-derived regressors were also based on the two runs independently. Thus, in the end, for each type of EEG-derived regressor, the first-level analysis could result in two corresponding contrast images for each participant. However, in some cases reliably task-related ICs were only obtained for one of the two runs. To obtain a single beta image per participant for second-level analyses, the two contrast images belonging to the same participant and time window were averaged prior to group analysis resulting in one contrast image per participant and electrophysiological component, i.e., early, late, N2, and P3.

2.5.4. Unimodal ERP analysis

To obtain condition specific ERPs, the artifact-free continuous EEG signal (cf. Section 2.3.2 *'EEG preprocessing'*) was re-referenced to the average of TP9 and TP10 and segmented into epochs of 1200 ms starting 200 ms prior to onset. The 200 ms pre-stimulus interval was used for baseline correction. Epochs belonging to the same event type (correct Go, correct Nogo, omission of Go trials, and commission errors in Nogo trials) were then averaged, resulting in four different event-related averages. Due to the overall low error rate, ERPs corresponding to incorrect behavioral responses (i.e., omissions of Go trials and commissions of Nogo trials) were statistically not analyzable and therefore discarded from further analyses.

For evaluation of Go and Nogo-related effects, N2 and P3 amplitudes were measured as the mean amplitude relative to baseline in the time windows 240–350 ms (N2), and 350–580 ms (P3) after stimulus onset. Following Ruchsow and colleagues (Ruchsow et al., 2008c) ERP values were extracted from a 3 by 3 electrode array: frontal-left (F3), frontal-midline (Fz), frontal-right (F4), central-left (C3), central-midline (Cz), central-right (C4), parietal-left (P3), parietal-midline (Pz), and parietal-right (P4). The latency ranges were chosen—similarly to ERP-based single-trial EEG/fMRI data analysis (cf. Section 2.4.3 *'Classification and selection of N2/P3 ERPs'*)—to cover best the task-related N2 and P3 effects at the selected electrode sites as determined based on visual inspection of the grand-averaged waveforms across all participants.

3. Study 1: Data-driven analysis of simultaneous EEG/fMRI using an ICA approach (Schmüser et al., 2014, published)

This chapter presents a new method developed for the automated selection of task-related independent components (ICs). This approach aimed at automatically selecting ICs with significantly increased amplitudes in Nogo trials compared to Go trials within predefined time windows located prior and around the individual's median Go response time (RT). Importantly, as the existence of such Nogo-related ICs was verified intra-individually, one advantage of this approach is that it allows accounting for individual differences in the electroencephalographic (EEG) data, which may arise from different electrode placement, head shapes, or anatomical differences at the brain level. A second analysis aimed at selecting ICs related to early visual components in order to test whether IC selection can be done on early visual responses in the same data. Finally, the new automated independent component analysis (ICA) approach is contrasted with a more classical approach that uses single-trial amplitudes of N2/P3 event-related potentials (ERPs) at specific electrodes as regressors.

Single-trial correlations of functional magnetic resonance imaging (fMRI) blood oxygenation level-dependent (BOLD) responses with IC-regressors revealed an activation pattern related to inhibitory control (i.e., positive correlations in right inferior frontal cortex (IFC), pre-supplementary motor area (pre-SMA) and basal ganglia). The activation pattern revealed by single-trial correlation with N2/P3 ERP-regressors, resembled a mixture of the impulse control network and networks related to attentional processing and response monitoring (i.e., pre-SMA, middle frontal gyrus and basal ganglia but also precuneus and superior medial cortex). This may indicate that the IC-based approach is more specific for task-related neural activity. This study was published in 2014 in a peer-reviewed journal paper in order to show the general feasibility and validity of the selection procedure (Schmüser et al., 2014).

3.1. Material and methods

This study was designed to examine the BOLD correlates of variations in electrophysiological (EEG) inhibition-related components in a data-driven approach. While previous studies used fixed latency windows and distinct EEG channels to derive regressors from the EEG, relying upon data from other EEG studies or own grand averages for their choice, we automatically selected IC components reliably associated with response inhibition for each single participant. We ensured to use only ICs which had reliably larger amplitude in Nogo than in Go trials securing the specificity of EEG components for neural activity of response inhibition. Therefore the present study introduces a newly developed data-driven analysis procedure that automatically selects participant-specific electrophysiological ICs which are reliably and specifically Nogo-related at an early or late stage of response inhibition to inform fMRI data analysis. To assess and validate the performance and outcome of our automated procedure in the context of combined EEG/fMRI analysis procedures, the automated IC-based approach was compared to an approach based on selecting single-trial amplitude values from predefined ERP components (see Figure 3.1 for a graphical overview). Thus, in line with Baumeister et al. (2014) for each participant the mean amplitude values of N2 (280–340 ms post-stimulus) and P3 (350–570 ms post-stimulus) were extracted from the Cz site.

Second, to illustrate the utility of the method beyond detecting Nogo-related components, the same data-driven analysis procedure was used for detecting visual responses in the same dataset. Visual components are well suited for validation purpose, as consistent results have been found in previous EEG/fMRI studies with different task settings (Di Russo et al., 2002, 2005; Novitskiy et al., 2011; Warbrick et al., 2013). Using separate EEG and fMRI data acquisition, Di Russo et al. (2005, 2002) showed that the P1 and N1 subcomponents can be accounted for by dipoles localized to middle occipital gyrus, fusiform gyrus and parietal lobe. More recently Novitskiy et al. (2011) and Warbrick et al. (2013) found positive single-trial correlations of visual components with fMRI BOLD signal in regions of the visual dorsal stream but also in medial frontal and precentral gyri.

3.1.1. Participants

39 participants (16 males; mean age: 38.85 ± 16.5) were included in this analysis (cf. Section 2.1.1 *'Participants'* for a detailed information on participant samples).

3.1.2. Data analysis

3.1.2.1. Extraction of electrophysiological single-trial amplitude values

Classification and selection of Nogo-related independent components (ICs): As described in Section 2.4.1 (*'Classification and selection of Nogo-related ICs'*), for each participant, EEG data

were decomposed into temporally ICs which were then intra-individually classified according to their relation to response inhibition (i.e., significantly larger in amplitude for Nogo than for Go). ICs identified as reliably Nogo-related within a predefined time window (early or late, cf. Figure 2.2 on page 43) were combined into individual electrophysiological regressors and then included into fMRI first-level analysis (cf. Figure 3.1.D.2).

Thus, ICA was employed in order to selectively extract time series related to different phases of task execution of a visual Go/Nogo task. This takes advantage of the fact that ICA can be used to isolate task-related components (Bagshaw and Warbrick, 2007; Debener et al., 2005). Importantly, the algorithm was not designed to identify ICs associated with classical event-related components such as N2 and P3, but to automatically select ICs with significantly increased amplitudes in Nogo trials compared to Go trials within predefined time windows located prior and around the individual's median RT. Nogo-related ICs for both latency ranges were identified in 22 participants (7 males; mean age: 34.41 ± 14.1), out of initially 39 participants.

Classification and selection of visual independent components (ICs): As presented in Section 2.4.2 (*'Classification and selection of visual ICs'*), the automated IC selection procedure was modified so that visual ICs can be detected. This aimed at testing whether component selection can be done on other electrophysiological ICs beyond the Nogo-related components it was designed for. This was applied to the same dataset of the visual Go/Nogo task as the automated classification and selection of Nogo-related ICs.

Two participants failed to display visual ICs on the chosen absolute Z score level ($|Z| > 0.275$), any further analyses were performed on the remaining 37 participants (15 males; mean age: 38.27 ± 16.1). These two participants did not belong to the subsample of 22 participants, for which Nogo-related ICs could be identified.

Classification and selection of N2/P3 event-related potential (ERP): To compare the automated IC-based approach to a more classical approach based on selecting single-trial amplitude values from predefined ERP components, the mean N2/P3 amplitude values were extracted. To achieve improved comparability, single-trial EEG/fMRI analysis of N2/P3 amplitudes was computed for the same 22 participants as the single-trial EEG/fMRI analysis of Nogo-related ICs.

As described in Section 2.4.3 (*'Classification and selection of N2/P3 ERPs'*), for each participant, single-trial amplitude values were extracted from Cz where the Nogo-N2/P3 effects were most pronounced in the grand average. N2 was measured as the mean amplitude in the time window 280–340 ms after stimulus onset, whereas P3 was measured as the mean amplitude between 350 and 570 ms after stimulus. These latency ranges were chosen to cover best the task-related N2 and P3 effects on group level (Figure 3.1.D.1) Mean amplitudes of each single trial were extracted from the N2 and P3 latency ranges at Cz, resulting in two amplitude vectors for each participant.
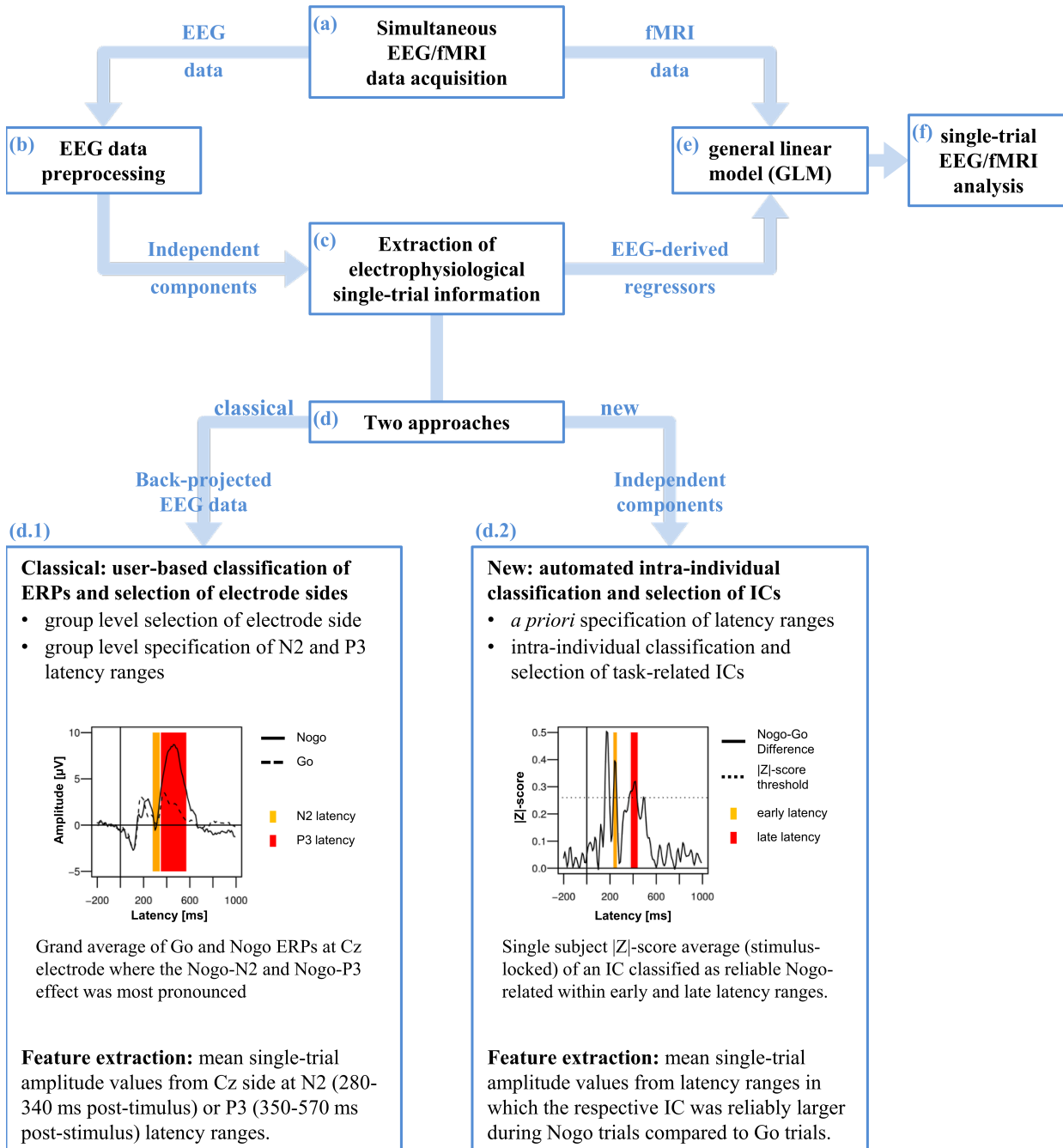
Figure 3.1 *(previous page)* Graphical representation of single-trial EEG/fMRI analysis. After simultaneous EEG/fMRI data acquisition (A) the EEG data is preprocessed and corrected for fMRI artifacts (B) using independent component analysis (ICA). Subsequently the electrophysiological single-trial values can be extracted (C) using different approaches (D). Classically (D1), single-trial amplitude values are extracted from predefined ERP components. This is based on a chosen electrode site where the ERP component of interest (Nogo-N2 and Nogo-P3) is most pronounced in the grand mean average. Followed by the specification of N2 (280–340 ms, yellow) and P3 (350–570 ms, red) latency ranges which cover best the task-related ERP effects on group level at the selected electrode site (Cz). For each participant the mean single-trial values are extracted from these predefined latency ranges. Alternatively (D2), our approach allows to extract single-trial values from independent components (ICs) which are intra-individually classified and selected in an automated procedure. This is based on a priori specification of latency ranges of interest, in this case located prior (early, yellow) and around (late, red) the individual's median response time (RT). ICs are intra-individually classified according their association with the Nogo condition (significantly increased amplitudes in Nogo trials compared to Go trials). For each participant the mean single-trial values are extracted from latency ranges in which the respective IC was reliably larger during Nogo. In both approaches the resulting electrophysiological regressors are included in the general linear model of fMRI data analysis (E) in order to perform the single-trial EEG/fMRI data analysis (F). Adopted from (Schmüser et al., 2014).

3.1.2.2. fMRI regressors and first level analysis

As described in Section 2.4.4 (*'EEG-derived regressors'*), each amplitude vector was interpolated over time, re-sampled at the time points of fMRI data acquisition, normalized to inter-quartile range (IQR = 1) and convolved with a canonical hemodynamic response function (HRF). In a second step, the task-related electrophysiological regressors (i.e., derived from Nogo-related ICs and N2/P3 ERPs) were orthogonalized with respect to classical onset regressors (Go, Nogo, Errors).

For each participant ($N = 37$ in case of visual components and $N = 22$ in all other cases) different generalized linear models (GLMs) were fitted separately to the fMRI data (cf. Section 2.5.3, *'First-level single-trial EEG/fMRI analysis'*). The design matrix of each GLM contained four regressors of interest: three onset regressors (Go, Nogo, and Errors) and one EEG regressor derived from either early or late ICs, N2 or P3 ERPs, or visual ICs. A single beta image per participant was computed for second-level analyses by averaging the two contrast images belonging to the same participant and time window.

3.1.2.3. Group analysis

The first level analysis results of task-related regressors (i.e., early/late and N2/P3) were subjected to paired *t*-tests with either early/late or N2/P3 as paired observations. The first level analysis results of EEG regressors derived from visual components were subjected to a one-sample *t*-test. For whole brain analysis the statistic images were assessed for cluster-wise significance by using a cluster-defining height threshold of $p_{(\mathrm{FWE})} < .05$ (family-wise error (FWE) correction for multiple comparisons).

In the case of region of interest (ROI) analyses, clusters were assessed for peak-wise significance by using a height threshold of $p_{(\mathrm{FWE})} < .05$ (FWE corrected). Following Sebastian et al. (2013a), small volume correction was computed for the following predefined ROIs as derived from the automated anatomical labeling (AAL) atlas: lateral inferior frontal gyurs (IFG); derived from a combination of pars opercularis and pars triangularis); middle frontal gyrus; pre-SMA; derived from the supplementary motor area (SMA) region with $y > 0$); caudate nucleus; putamen and pallidum. Additionally small volume correction was computed for the subthalamic nucleus (STN), consisting of two boxes of respectively 10 mm^3 in size and localized at the Montreal Neurological Institute (MNI) coordinates $-10, -15, -5$ (left STN) and $+10, -15, -5$ (right STN) (Aron and Poldrack, 2006). For visual components, bilateral inferior occipital cortex, bilateral middle occipital cortex and bilateral superior occipital cortex were additionally included.

3.2. Results

3.2.1. EEG/fMRI single-trial analysis of Nogo-related ICs

Positive correlations of the fMRI BOLD signal with EEG regressors derived from ICs related to task processing at an early (200 ms after stimulus onset until individual median RT) and later (100 ms prior to median RT until 300 ms after median RT) stage of response inhibition are listed in Table 3.1. Due to orthogonalization, these regressors revealed those parts of the trial-to-trial fluctuation that are not captured by the onset regressors. As shown in Figure 3.2.B, EEG-derived regressors correlated positively with fMRI BOLD signal in cortical and subcortical regions associated with response inhibition. Although no significant differences between early and late were found at the level of $p < .05$ (FWE corrected), it can be seen that correlations with early and late EEG-derived regressors revealed overlapping but also different areas of activation in regions associated with response inhibition.

The early regressor but not the late regressors correlated positively with fMRI BOLD signal in bilateral frontal regions such as right posterior IFG (pars opercularis), right insula/IFG (pars orbitalis), bilateral superior frontal gyrus and left precentral gyrus (adjacent to inferior frontal junction (IFJ)) as well as bilateral insula lobe. Subcortically positive correlations between fMRI BOLD signal and early regressor were found in right putamen, bilateral caudate nucleus and bilateral pallidum, whereas the late regressor correlated positively with left putamen. Positive correlations with both regressors but with reduced cluster size in correlations with late regressor were found in pre-SMA, bilateral dorso-lateral prefrontal cortex and right supramarginal gyrus/temporo-parietal junctions. Further positive correlations between fMRI BOLD signal and both EEG-derived regressors were found in left superior temporal gyrus, right precuneus, bilateral occipital regions, left hippocampus and bilateral insula lobe/amygdala.

Table 3.1. Positive correlations of fMRI BOLD signal with orthogonalized EEG-derived regressors early (time window starting 200 ms after stimulus onset and ending with the individual median Go response time (RT)) and late (time window starting 100 ms prior to RT and ending 300 ms after RT).

Region		Early: positive correlations						Late: positive correlations					
		x	y	z	k	Z	p	x	y	z	k	Z	p
Frontal Lobe													
IFG (pars Opercularis)	R	54	18	27	36	3.84	.045	-	-	-	-	-	-
IFG (pars Orbitalis)	R	51	21	-3	516	4.20	.013*	-	-	-	-	-	-
Middle Frontal Gyrus	R	24	51	33	821	4.18	.020*	27	36	24	213	4.49	.005*
Middle Frontal Gyrus	L	-39	45	15	187	4.55	<.001	-27	42	36	225	4.01	.038*
Superior Frontal Gyrus	R	24	54	33	92	4.42	<.001	-	-	-	-	-	-
Superior Frontal Gyrus	L	-21	-3	57	636	5.37	<.001	-	-	-	-	-	-
pre-SMA	C	-9	3	48	449	4.46	.002*	12	15	66	132	4.63	.001*
Precentral Gyrus	L	-36	3	39	101	4.28	<.001	-	-	-	-	-	-
Temporal Lobe													
Superior Temporal Gyrus	L	-63	-27	42	86	4.01	.001	-51	-33	9	54	4.60	.008
Temporal Pole/Insula Lobe	R	-	-	-	-	-	-	36	12	0	59	4.07	.005
Middle Temporal Gyrus	R	51	-72	18	44	4.06	.020	-	-	-	-	-	-
Supramarginal Gyrus	R	66	-39	24	317	5.15	<.001	66	-21	18	48	4.29	.014
Insula Lobe	L	-39	-6	-6	57	4.49	.006	-	-	-	-	-	-
Insula Lobe/Amygdala	R	42	-3	-27	58	4.24	.005	-	-	-	-	-	-
Insula Lobe/Amygdala	L	-	-	-	-	-	-	-27	6	-15	56	4.68	.007
Hippocampus	L	-24	-18	-9	57	4.93	.006	-27	-15	-12	53	5.24	.009
Parietal Lobe													
Precuneus	R	9	-42	54	128	4.68	<.001	15	-54	60	65	4.70	.003
Occipital Lobe													
Middle Occipital Gyrus	R	33	-78	27	146	4.93	<.001	-	-	-	-	-	-
Middle Occipital Gyrus	L	-	-	-	-	-	-	-39	-63	0	57	4.79	.006
Superior Occipital Gyrus	L	-18	-78	27	217	4.76	<.001	-24	-66	21	88	4.68	<.001
Lingual Gyrus	L	-	-	-	-	-	-	-3	-72	0	36	4.57	.045
Subcortical Areas													
Putamen	R	18	15	-3	45	3.87	.018	-	-	-	-	-	-
Putamen	L	-	-	-	-	-	-	-27	6	-9	86	3.84	.017*
Caudate Nucleus	R	15	15	-3	154	3.85	.015*	-	-	-	-	-	-
Caudate Nucleus	L	-9	12	9	103	3.53	.045*	-	-	-	-	-	-
Pallidum	R	15	9	-3	*	3.74	.004*	-	-	-	-	-	-
Pallidum	L	-21	0	6	20	3.21	.023*	-	-	-	-	-	-

Note: The region in which the cluster's local maximum is located in hemispheres right (R), left (L), or central (C); the peak location in Montreal Neurological Institute (MNI) coordinates (x, y, z); cluster extend in number of voxels (k); maximum Z score; and FWE-corrected p-values (cluster level corrected, * small volume corrected) are reported for each significantly activated cluster separately. FWE: family-wise error. IFG: inferior frontal gyurs. pre-SMA: pre-supplementary motor area.

3.2.2. EEG/fMRI single-trial analysis of N2/P3

Positive and negative correlations of the fMRI BOLD signal with EEG regressors derived from Cz electrode at the latency ranges N2 (280–340 ms post-stimulus) and P3 (350–570 ms post-stimulus) are listed in Table 3.2 and Table 3.4. As these regressors were orthogonalized to onset regressors, correlations of these EEG-derived regressors with fMRI BOLD signal only revealed that part of the trial-to-trial fluctuation that is not captured by the onset regressors. As shown in Figure 3.3.B, the N2/P3 EEG-derived regressors correlated positively with fMRI BOLD signal in cortical and subcortical regions associated with response inhibition. Despite significant differences (P3 > N2) in left postcentral gyrus, left STN/thalamus and a large area stretching from cerebellar vermis/lingual gyrus to cuneus/precuneus (Table 3.3), it can be seen that correlations with N2 and P3 EEG-derived regressors revealed overlapping but also different areas of activation in regions associated with response inhibition.

The N2 regressor but not the P3 regressors correlated positively with fMRI BOLD signal in right posterior IFG (pars opercularis), right superior temporal gyrus and left caudate nucleus. The P3 regressor but not the N2 regressors correlated positively with fMRI BOLD signal in left anterior IFG (pars triangularis), right precentral gyrus, left middle cingulate cortex (MCC), right middle and inferior temporal regions, bilateral occipital areas and subcortical regions such as left putamen, left STN and bilateral thalamus/hippocampus. Positive correlations with both regressors but with reduced cluster size in correlations with P3 regressor were found in right insula/IFG (pars orbitalis) and right precuneus/inferior parietal lobule. Reduced cluster size in correlations with N2 regressor compared to P3 regressor was found in left dorso-lateral prefrontal cortex, right pre-SMA and left superior temporal gyrus. The N2 regressor but not the P3 regressors correlated negatively with fMRI BOLD signal in a cluster located at the superior medial frontal gyrus and a large area stretching from central lingual gyrus and cerebellum to precuneus and calcarine gyrus, but also in smaller cortical and subcortical clusters located in pre-SMA, left middle frontal gyrus, bilateral fusiform gyri, left STN, and right Pallidum and caudate nucleus (Table 3.4).

Supplementary Table 3.6 contains a side-by-side comparison of positive fMRI BOLD correlations obtained using the new method (early/late regressors, Section EEG/fMRI single-trial analysis of Nogo-related ICs) and the classical method (current section).

Table 3.2. Positive correlations of fMRI BOLD signal with orthogonalized EEG-derived regressors N2 (280–340 ms after stimulus onset), and P3 (350–570 ms after stimulus onset).

Region		N2: positive correlations						P3: positive correlations					
		x	y	z	k	Z	p	x	y	z	k	Z	p
Frontal Lobe													
IFG (pars Opercularis)	R	51	15	27	35	4.24	.036	-	-	-	-	-	-
IFG (pars Orbitalis)	R	51	12	-3	218	4.60	.002*	51	12	-3	53	4.49	.004*
IFG (pars Triangularis)	L	-	-	-	-	-	-	-45	45	9	48	4.32	.009
Middle Frontal Gyrus	R	-	-	-	-	-	-	27	3	51	215	4.23	.016*
Middle Frontal Gyrus	L	-30	48	33	117	4.71	.002*	-33	27	45	412	4.74	.001*
pre-SMA	C	6	18	63	101	4.38	.004*	6	18	63	157	4.71	.001*
Precentral Gyrus	R	-	-	-	-	-	-	27	-9	48	59	4.65	.003
Middle Cingulate Cortex	L	-	-	-	-	-	-	-9	-33	45	41	4.68	.019
Temporal Lobe													
Superior Temporal Gyrus/Insula Lobe	R	54	-3	-3	99	5.27	<.001	-	-	-	-	-	-
Superior Temporal Gyrus/Insula Lobe	L	-39	-12	-6	76	5.08	.001	-39	-12	-6	183	5.93	<.001
Superior Temporal Gyrus	L	-42	-27	12	36	5.51	.032	-42	-27	12	35	5.38	.036
Superior Temporal Gyrus	L	-63	-39	12	76	5.20	.001	-63	-33	15	48	5.78	.009
Middle/Inferior Temporal Gyrus	R	-	-	-	-	-	-	57	-66	0	44	4.97	.014
Supramarginal Gyrus	R	-	-	-	-	-	-	54	-21	18	42	4.49	.017
Fusiform Gyrus	R	-	-	-	-	-	-	33	-39	-15	74	5.31	.001
Temporal Pole/Insula Lobe	R	-	-	-	-	-	-	60	3	-9	148	5.41	<.001
Parietal Lobe													
Postcentral Gyrus	R	-	-	-	-	-	-	51	-30	51	94	5.48	<.001
Inferior Parietal Lobule	L	-39	-51	54	80	4.95	<.001	-42	-51	54	631	5.05	<.001
Precuneus	R	9	-45	60	63	4.93	.002	18	-42	57	49	4.45	.008
Occipital Lobe													
Middle Occipital Gyrus	R	-	-	-	-	-	-	36	-75	6	46	4.35	.011
Middle Occipital Gyrus	L	-	-	-	-	-	-	-27	-69	30	68	4.36	.001
Lingual Gyrus	R	-	-	-	-	-	-	12	-54	-3	33	4.17	.045
Lingual Gyrus	L	-27	-48	-3	43	5.08	.015	-18	-66	-9	676	5.31	<.001
Cuneus/Precuneus	R	-	-	-	-	-	-	24	-54	30	148	4.97	<.001

Note: The region in which the cluster's local maximum is located in hemispheres right (R), left (L), or central (C); peak location in Montreal Neurological Institute (MNI) coordinates (x, y, z); cluster extend in number of voxels (k); the maximum Z score; and FWE-corrected p-values (cluster level corrected, * small volume corrected) are reported for each significantly activated cluster separately. FWE: family-wise error. IFG: inferior frontal gyurs. pre-SMA: pre-supplementary motor area.

Table 3.2. Continuation: Positive correlations of fMRI BOLD signal with orthogonalized EEG-derived regressors N2 (280–340 ms after stimulus onset), and P3 (350–570 ms after stimulus onset).

Region		N2: positive correlations						P3: positive correlations					
		x	y	z	k	Z	p	x	y	z	k	Z	p
Subcortical Areas													
Caudate Nucleus	L	-18	-15	24	14	3.95	.010*	-	-	-	-	-	-
Putamen	L	-	-	-	-	-	-	-33	-15	-6	14	3.65	.035*
Subthalamic Nucleus	L	-	-	-	-	-	-	-12	-18	-6	5	2.92	.047*
Thalamus	R	-	-	-	-	-	-	21	-27	-3	79	4.61	<.001
Thalamus/Hippocampus	L	-	-	-	-	-	-	-21	-24	-6	138	5.50	<.001

Note: The region in which the cluster's local maximum is located in hemispheres right (R), left (L), or central (C); peak location in Montreal Neurological Institute (MNI) coordinates (x, y, z); cluster extend in number of voxels (k); the maximum Z score; and FWE-corrected p-values (cluster level corrected, * small volume corrected) are reported for each significantly activated cluster separately. FWE: family-wise error. IFG: inferior frontal gyurs. pre-SMA: pre-supplementary motor area.

Table 3.3. Brain regions significantly stronger correlated with P3 single-trial amplitude values (350–570 ms after stimulus onset) than with N2 single-trial amplitude values (280–340 ms after stimulus onset).

Region		P3 > N2					
		x	y	z	k	Z	p
Parietal Lobe							
Postcentral Gyrus	L	-39	-24	54	91	3.45	.029
Occipital Lobe							
Lingual/Calcarine Gyrus	C	0	-63	12	414	4.53	<.001
Subcortical Areas							
Subthalamic Nucleus	L	-12	-18	-6	11	3.49	.006*
Thalamus	L	-18	-24	-6	88	3.61	.034

Note: The region in which the cluster's local maximum is located in hemispheres left (L) or central (C); peak location in Montreal Neurological Institute (MNI) coordinates (x, y, z); cluster extend in number of voxels (k); maximum Z score; and FWE-corrected p-values (cluster level corrected, * small volume corrected) are reported for each significantly activated cluster separately. FWE: family-wise error.

Table 3.4. Negative correlations of fMRI BOLD signal with orthogonalized EEG-derived regressor N2 (280–340 ms after stimulus onset).

Region		x	y	z	k	Z	p
		N2: negative correlations					
Frontal Lobe							
Superior Medial Gyrus	L	-6	60	3	121	5.00	<.001
Middle Frontal Gyrus	L	-27	54	9	48	4.26	.013*
pre-SMA	C	0	18	54	73	3.99	.020*
Temporal Lobe							
Fusiform Gyrus	R	27	-42	-12	88	5.21	<.001
Fusiform Gyrus	L	-24	-45	-15	47	5.17	.010
Angular Gyrus	L	-42	-75	39	48	4.22	.009
Occipital Lobe							
Lingual Gyrus/Cerebellum	R	9	-54	-15	156	4.52	<.001
Subcortical Areas							
Caudate Nucleus	R	12	-3	18	31	3.60	.041*
Pallidum	R	15	3	3	10	3.68	.005*
Subthalamic Nucleus	L	-12	-18	-9	8	3.16	.021*

Note: The region in which the cluster's local maximum is located in hemispheres right (R), left (L), or central (C); peak location in Montreal Neurological Institute (MNI) coordinates (x, y, z); cluster extend in number of voxels (k); the maximum Z score; and FWE-corrected p-values (cluster level corrected, * small volume corrected) are reported for each significantly activated cluster separately. FWE: family-wise error. pre-SMA: pre-supplementary motor area.

A)

B)
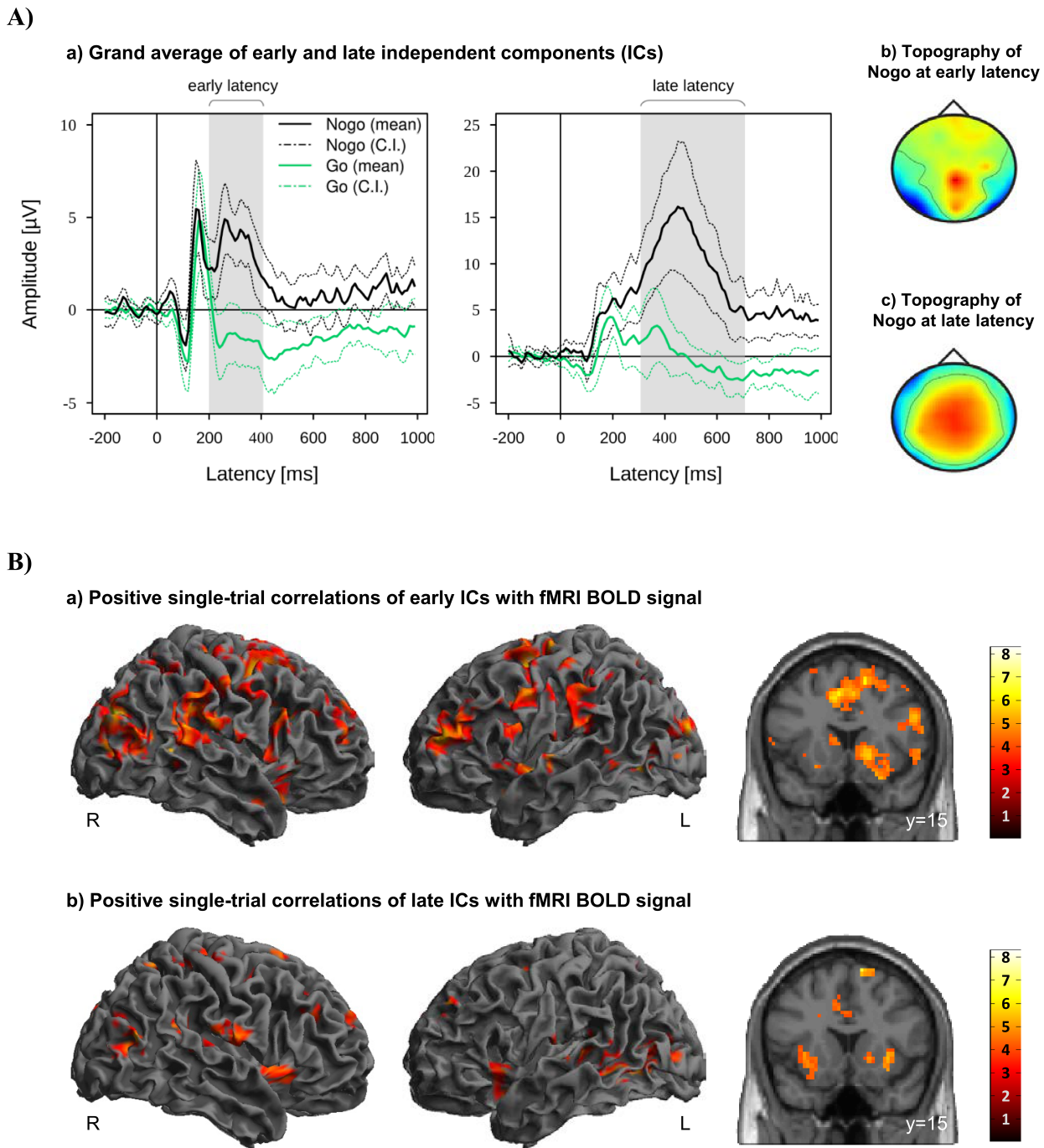
Figure 3.2. (A) independent component (IC) activation grand averages (a) and grand mean topographies (b, c) of all participants ICs which were classified as reliably Nogo-related within the early latency range or late latency range. Mean and 95 % confidence interval (C.I.) of Nogo (black lines) and Go (green lines) are displayed in solid and dotted lines, respectively; gray bars indicate the early and late latency ranges on the group level. (B) Activation maps displaying the main effects of positive correlations with EEG-derived early (a; time window starting 200 ms after stimulus onset and ending with the RT) and late (b; time window starting 100 ms prior to RT and ending 300 ms after RT) regressors. These regressors were orthogonalized to onset regressors. Images are displayed in neurological order (L: Left; R: Right), with $p < .005$ (uncorrected) and $k = 20$. RT: individual median Go response time. Adopted from (Schmüser et al., 2014).

A)

a) Grand average at Cz electrode

b) Topography of Nogo at N2

c) Topography of Nogo at P3

B)

a) Positive single-trial correlations of N2 at Cz with fMRI BOLD signal

b) Positive single-trial correlations of P3 at Cz with fMRI BOLD signal
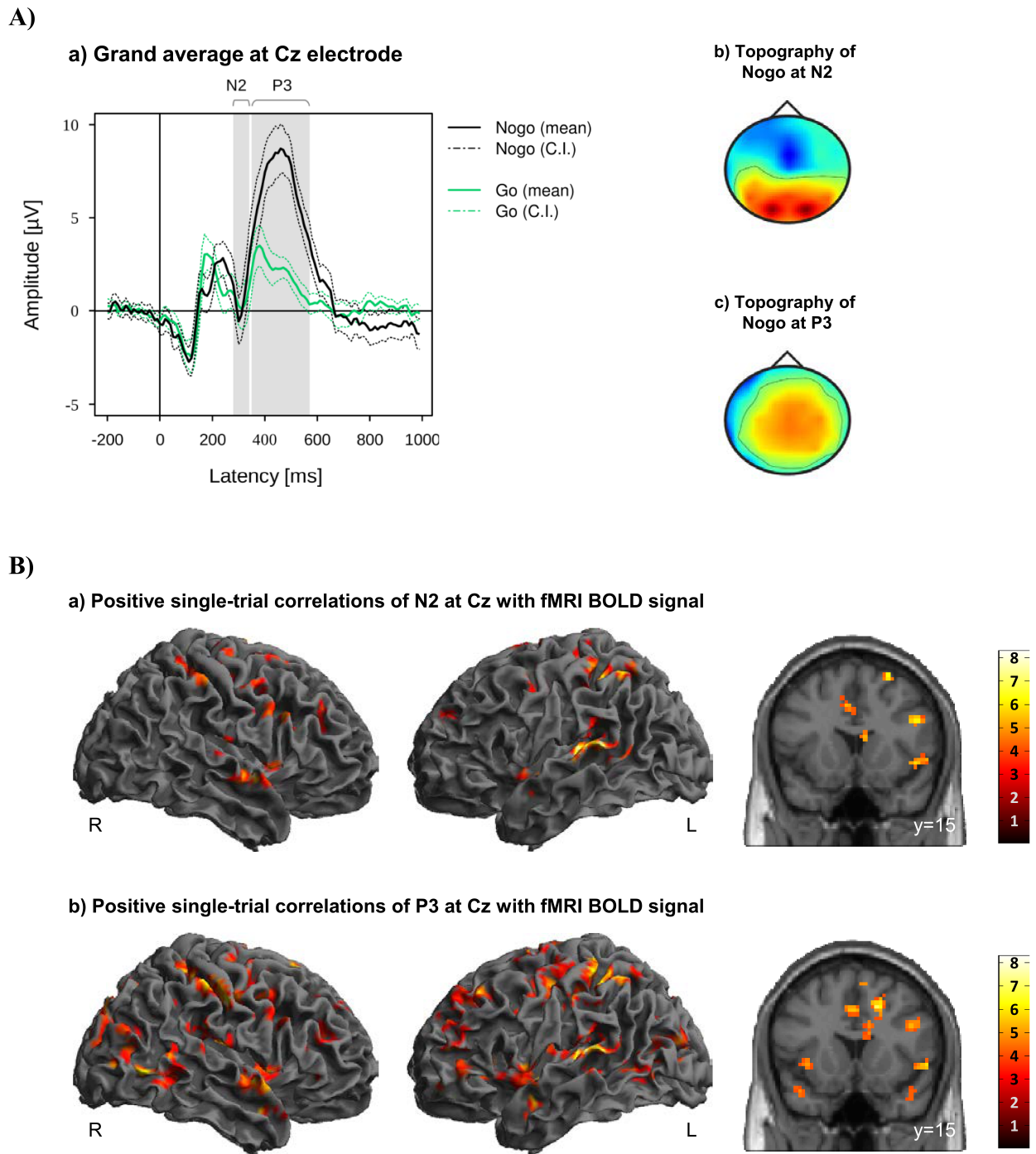
Figure 3.3. (A) Grand average (a) and grand mean topographies at N2 latency range (b) and P3 latency range (c). Mean and 95 % confidence interval (C.I.) of Nogo (black lines) and Go (green lines) are displayed in solid and dotted lines; gray bars indicate the early and late latency ranges on the group level (a). (B) Activation maps displaying the main effects of positive correlations with EEG-derived N2 (a; time window 280–340 ms after stimulus onset) and P3 (b; time window 350–570 ms after stimulus onset) regressors. These regressors were orthogonalized to onset regressors. Images are displayed in neurological order (L: Left; R: Right), with $p < .005$ (uncorrected) and $k = 20$. RT: individual median Go response time. Adopted from (Schmüser et al., 2014).

3.2.3. EEG/fMRI single-trial analysis of visual ICs

Positive correlations of the fMRI BOLD signal with EEG regressors derived from ICs related to visual processing (ICs with $|Z| > 0.275$ within the latency ranges of 90–140 ms post-stimulus) are listed in Table 3.5. Correlations of fMRI BOLD signal with EEG regressor derived from single-trial amplitudes of visual components yielded activations primarily in visual areas but also in the left premotor cortex (Figure 3.4.B). However, significant positive correlations at the level of $p < .05$ (FWE corrected) were found exclusively in visual areas (bilateral middle and superior occipital gyri) but not in premotor areas.

Table 3.5. Positive correlations of fMRI BOLD signal EEG-regressor derived from visual response (time window starting 90 ms after stimulus onset and ending 140 ms after stimulus onset).

Region		x	y	z	k	Z	p
Occipital Lobe							
Superior Occipital Gyrus	R	24	-93	12	42	3.65	.037*
Superior Occipital Gyrus	L	-15	-93	12	70	4.22	.003*
Middle Occipital Gyrus	R	33	-87	15	114	3.88	.021*
Middle Occipital Gyrus	L	-21	-93	9	55	5.25	.019
Middle Occipital Gyrus	L	-42	-69	3	59	4.69	.014

(table header spanning "visual components" over x, y, z, k, Z, p)

Note: The region in which the cluster's local maximum is located in hemispheres right (R) or left (L); peak location in Montreal Neurological Institute (MNI) coordinates (x, y, z); cluster extend in number of voxels (k); maximum Z score; and FWE-corrected p-values (cluster level corrected, * small volume corrected) are reported for each significantly activated cluster separately. FWE: family-wise error.

A)

a) Grand average of visual independent components (ICs)

b) Topography of Nogo at 120 ms

c) Topography of Go at 120 ms

B)

a) Positive single-trial correlations of visual ICs with fMRI BOLD signal
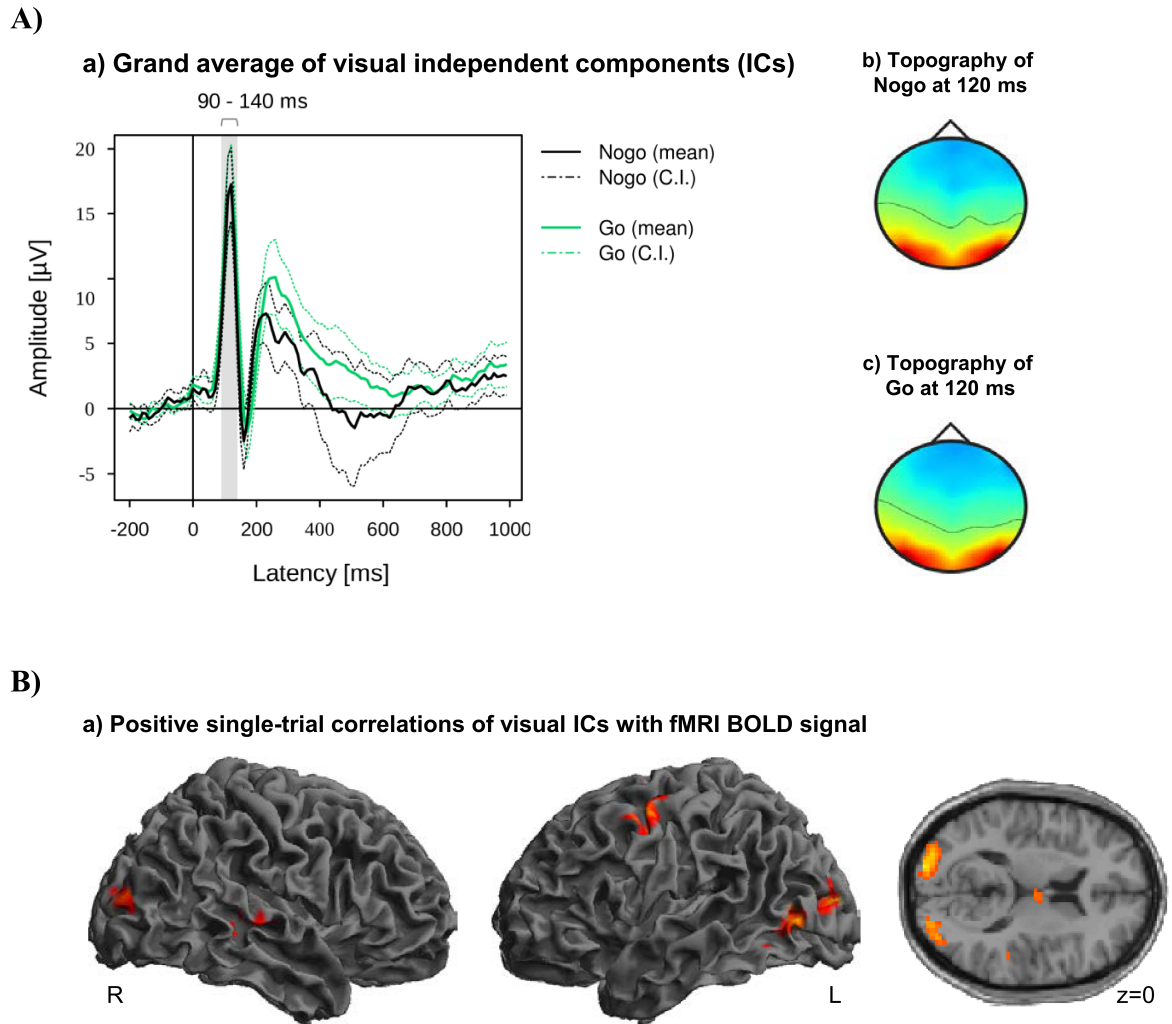
Figure 3.4. (A) Grand averages (a) and grand mean independent component (IC) topography (b) of all participants' ICs which were classified as reliable related to visual processing within the latency range of 90–140 ms. Mean and 95 % confidence interval (C.I.) of Nogo (black lines) and Go (green lines) are displayed in solid and dotted lines; the gray bar indicates the latency range of 90–140 ms (a). (B) Positive correlations of fMRI BOLD signal with EEG regressor derived from visual components (90–140 ms after stimulus onset). Images are displayed in neurological order (L: Left; R: Right), with $p < .005$ (uncorrected) and $k = 20$. Adopted from (Schmüser et al., 2014).

3.3. Discussion

The current study aimed at a data-driven identification of correlates of trial-to-trial variability in inhibition specific neurophysiological activity in simultaneously acquired EEG and fMRI. Using data of 39 healthy participants in a visual Go/Nogo task, single trial EEG/fMRI analysis was performed based on the automated identification of inhibition-related electrophysiological ICs. This identification was done for each participant in a completely data driven way using an extended ICA (Bell and Sejnowski, 1995; Lee et al., 1999; Makeig et al., 1999, 2002). Specifically Nogo-related ICs (i.e. Nogo minus Go) were identified by Z scores of stimulus-locked averages above a predefined threshold within one of two time windows.

3.3.1. Single-trial EEG/fMRI analysis of Nogo-related ICs and N2/P3 ERPs

In those participants showing reliable inhibition-related components, we were able to analyze the relationship between trial-to-trial variations in these ICs and fMRI brain activity. Due to the high temporal resolution of the EEG, we could specifically assess inhibition-related EEG activity occurring clearly before the typical RT (early time window) and inhibition-related EEG activity occurring around the typical RT (later time window; Figure 3.2.A). The corresponding EEG-derived regressors were orthogonalized to the classical paradigm-derived onset regressors to reveal only those brain regions in which the BOLD signal is attributed genuinely to trial-to-trial fluctuations of inhibition-related ICs rather than to condition effects.

Both, early and late EEG-derived regressors correlated positively with fronto-striatal regions (right IFC, pre-SMA and basal ganglia) associated with response inhibition (Aron, 2011; Chambers et al., 2009). Although there were no significant differences between early and late, in most areas including right insula/IFC, right posterior IFC, premotor areas and basal ganglia, correlations of fMRI BOLD signal with the early EEG regressor were stronger than with the late EEG regressor. This indicates that the strength of positive correlations is decreasing from early to late stages of response inhibition. However, when interpreting results of single-trial EEG/fMRI analysis it should be considered that although the EEG's high temporal resolution allows extracting electrophysiological activity clearly related to different stages of neural processing, the fMRI BOLD signal's temporal resolution remains low. Accordingly, we are able to correlate electrophysiological signals generated by the brain at different stages of neural processing with the fMRI BOLD signal but we are not able to distinguish whether there is a causal relationship between a certain region and the Nogo-related activity or whether the activity of the regions are just statistically more likely to be preceded, accompanied, or followed by Nogo-related activity without a causal relationship.

Single-trial correlation of N2/P3 amplitude values with fMRI BOLD signal was computed for the same 22 participants as the single-trial EEG/fMRI analysis of Nogo-related ICs. The

N2-derived EEG regressor correlated negatively with regions associated with the default mode network (precuneus and superior medial cortex) (Buckner et al., 2008; Raichle et al., 2001) but also with areas in pre-SMA, middle frontal gyrus and basal ganglia. To some degree, these results are consistent with Baumeister et al. (2014), who found negative correlations of increased N2 amplitudes in right middle frontal gyrus, bilateral middle temporal and fusiform gyri but also in regions associated with the default mode network (right precuneus, bilateral superior temporal gyrus and right medial frontal gyrus). As discussed by Baumeister et al. (2014), this might indicate an association between increasing N2 amplitudes and deactivation of the default mode network.

Both, N2- and P3-derived EEG regressors correlated positively with fMRI BOLD signal in fronto-striatal regions associated with response inhibition (right IFC, pre-SMA and basal ganglia), but also in distributed areas located in temporal and parietal lobule. Except for right IFC the degree of positive correlations with N2/P3-derived EEG regressors increased from N2 to P3, whereas in IC-based EEG/fMRI analysis fewer regions were positively correlated with the late EEG regressor relative to the early EEG regressor. The latter may indicate that regions relevant for a successful response inhibition are up-regulated at an early stage of response inhibition but not at the later stage of response inhibition. This seems to be reasonable as it could be expected that regions essential for withholding a prepotent motor response are activated prior to the time point when the Go response would be executed. In contrast to this, N2/P3 single-trial amplitude values seem to correlate with a mixture of network parts associated with response inhibition, attentional processing or response monitoring.

When comparing both approaches (i.e., early/late vs. N2/P3) it can be seen that the activation pattern yielded by the early EEG regressor and the N2 EEG regressor are largely deviating. This might be related to fundamental differences in both approaches. While the early and late EEG regressors were constructed exclusively of participant-specific components which are reliably differentiating between different task conditions at the respective latency range, the N2/P3 ERPs were defined on the group level at the latency ranges and EEG site with the most pronounced Nogo effect. Repeated measure analysis of variance (ANOVA) with the factors condition (Go and Nogo) and ERP (N2 and P3) revealed a significant condition $\times$ ERP interaction [$F(1, 21) = 61.516$, $p < .001$] on mean amplitude values. However, post hoc test revealed that mean amplitudes of P3 but not of N2 were significantly different between Go and Nogo which is in line with Baumeister et al. (2014), who also reported significant differences for P3 amplitude values but not for N2 amplitude values. The prominent difference between correlations of the fMRI BOLD signal with the early EEG regressor or the N2 EEG regressor might be related to the fact that the early ICs are reliably task-discriminating at the respective latency range and thus more sensitive to the Nogo condition, while the N2 seems to be less specific to the task condition.

In conclusion, the deviating results between ERP-based N2/P3 and IC-based early/late single-trial correlations are probably related to the fundamentally different approaches of selecting the

EEG features used for single-trial correlations. Following Baumeister et al. (2014), for each participant the mean single-trial amplitude values of N2 and P3 were extracted from Cz electrode at the latency ranges 280–340 and 350–570 ms after stimulus onset. These time windows were chosen as they reflected best the Nogo-N2 and Nogo-P3 effects for the entire group (Figure 3.3.A). However, these fixed time windows were determined on the group level which is insensitive to inter-individual variability as they were observable for example in the participant's median RT (ranging from 322.81 to 487.94 ms). As it is known that such phenotypes exist even for simple reaction time paradigms, inter-individual differences constitute valuable information when analyzing more complex cognitive functions (Kanai and Rees, 2011). Thus, inter-individual differences make it necessary to verify intra-individually the presence of certain components prior to including them into group-level analyses. Therefore, we developed an analysis procedure that does not build exclusively on N2/P3 effects, but classifies and selects task- and participant-specific electrophysiological components in a completely data driven manner. For every single participant, the algorithm identifies those participant-specific components which are differentiating best between the different task conditions at the specific latency range (Figure 3.2.A). Thus, in contrast to N2/P3 ERPs which were defined on the group level (Figure 3.3.A), early and late regressors were constructed of functionally characterized ICs.

3.3.2. EEG/fMRI single-trial analysis of visual ICs

We introduced an algorithm that allows for selecting Nogo-related ICs in an automated procedure; however, the fact that the algorithm could identify Nogo-related ICs only in about half of the participants may question the validity of the algorithm. Thus, to test whether our IC selection method is generalizable and usable beyond Nogo-related IC detection, we modified the algorithm so that ICs associated with the visual responses can be detected. Single-trial amplitudes of ICs related to visual processing (i.e., $|Z| > 0.275$ within the latency ranges of 90–140 ms post-stimulus) correlated positively with fMRI BOLD signal in left inferior occipital gyrus as well as bilateral middle and superior occipital gyri.

The results are consistent with Fuglø et al. (2012) who found positive correlations of visual components with fMRI BOLD responses in primary visual cortex and middle occipital gyrus. However, Fuglø et al. (2012) employed a block design with checkerboard stimulus blocks alternating with blocks without stimuli, while continuously estimating visual-evoked potential (VEP) amplitudes. Therefore, the resulting regressor necessarily follows the stimulation design to a larger degree. EEG-fMRI correlations from experiments in which either a constant stimulus is repeated or stimuli matched for physical properties such as size, complexity and luminance are presented must be viewed from a different perspective. Variability observed across such stimuli may either reflect early discriminative activity for different stimuli or spontaneous fluctuations in brain state. A study following a spontaneous fluctuation design (visual oddball with motor responses) comparable

to the current one revealed positive correlations of visual components with fMRI BOLD signal not only in regions of the visual dorsal stream but also in medial frontal and precentral gyri (Warbrick et al., 2013). In addition to visual cortex activity our approach also revealed medial frontal precentral activity patterns comparable to Warbrick et al. (2013). Thus, despite of different task settings and the fact that Warbrick et al. (2013) used a selection procedure based on *a priori* defined ERP components (P1 and N1), whereas we selected ICs related to visual processing in a purely data-driven approach, the resultant correlations between EEG-derived regressors and fMRI BOLD responses are quite similar. This illustrates that beyond of detecting Nogo-related ICs our algorithm is also able to detect ICs related to visual responses in the same data set.

3.3.3. Limitations

As a result of IC selection only about half of participants could be included into the single-trial EEG/fMRI data analysis. As such these results of temporal signal evolution in response inhibition may not be generalizable. Moreover, the fact that Nogo-related ICs were not identified in one half of the participants suggests that correlations using these restrictive IC selection criteria can only be determined for part of the initial population of a study. On the other hand, the same algorithm was able to detect ICs related to visual responses in 37 of 39 participants, which argues against a principal failure of the algorithm. Thus, the finding that certain Nogo-related components are not present in every participant may give an indication of substantial inter-individual differences as state or trait related differences in cognitive strategy when performing the task, illustrating the sensitivity and specificity of the algorithm for detection of different event related responses.

3.3.4. Conclusion

Using EEG-derived regressors based on single-trial amplitude variability of Nogo-related ICs selected with respect to different time windows allows visualizing the evolution of brain processes during motor inhibition. Furthermore, by classifying and selecting ICs intra-individually our approach takes account of known inter-individual differences in neural processing. In line with existing automated approaches (Goldman et al., 2009; Wessel and Ullsperger, 2011) we used an algorithm that allows for selecting task-related ICs in an automated procedure. As is the case in the COMPASS-approach (Wessel and Ullsperger, 2011), our approach uses an automated IC selection procedure but is independent of ERP templates, which was one of the major drawbacks of COMPASS. This can be achieved by using an algorithm that automatically selects inhibition-specific ICs with significantly increased amplitude during Nogo trials relative to Go trials. Additionally, these ICs were automatically classified depending on whether the latency range of reliably Nogo-related activity occurred early or late relative to median correct Go RT. This is partially comparable to the approach of Goldman et al. (2009) but without the drawback of just being able to extract

one component per time window. As our method is independent of *a priori* defined ERPs, we suggest that this approach of using functionally defined components could be used for EEG features other than event-related transient responses. Although not tested yet, one possible application would be to use it in the context of background rhythms. In this case, one could selectively use those components that are characterized by increased spectral power in one condition relative to another condition.

Table 3.6. Side-by-side comparison of positive correlations of fMRI BOLD signal with orthogonalized EEG-derived regressors early (time window starting 200 ms after stimulus onset and ending with the individual median Go response time (RT)) and late (time window starting 100 ms prior to RT and ending 300 ms after RT), as well as with orthogonalized EEG-derived regressors N2 (280–340 ms after stimulus onset) and P3 (350–570 ms after stimulus onset).

Region		early ICs						late ICs						N2 ERPs						P3 ERPs					
		x	y	z	k	Z	p	x	y	z	k	Z	p	x	y	z	k	Z	p	x	y	z	k	Z	p
Frontal Lobe																									
IFG (pars Opercularis)	R	54	18	27	36	3.84	.045	-	-	-	-	-	-	51	15	27	35	4.24	.036	-	-	-	-	-	-
IFG (pars Orbitalis)	R	51	21	-3	516	4.20	.013*	-	-	-	-	-	-	51	12	-3	218	4.60	.002*	51	12	-3	53	4.49	.004*
IFG (pars Triangularis)	L	-	-	-	-	-	-	-	-	-	-	-	-	-	-	-	-	-	-	-45	45	9	48	4.32	.009
Middle Frontal Gyrus	R	24	51	33	821	4.18	.020*	27	36	24	213	4.49	.005*	-	-	-	-	-	-	27	3	51	215	4.23	.016*
Middle Frontal Gyrus	L	-39	45	15	187	4.55	<.001	-27	42	36	225	4.01	.038*	-30	48	33	117	4.71	.002*	-33	27	45	412	4.74	.001*
Superior Frontal Gyrus	R	24	54	33	92	4.42	<.001	-	-	-	-	-	-	-	-	-	-	-	-	-	-	-	-	-	-
Superior Frontal Gyrus	L	-21	-3	57	636	5.37	<.001	-	-	-	-	-	-	-	-	-	-	-	-	-	-	-	-	-	-
pre-SMA	C	-9	3	48	449	4.46	.002*	12	15	66	132	4.63	.001*	6	18	63	101	4.38	.004*	6	18	63	157	4.71	.001*
Precentral Gyrus	L	-36	3	39	101	4.28	<.001	-	-	-	-	-	-	-	-	-	-	-	-	27	-9	48	59	4.65	.003
Middle Cingulate Cortex	L	-	-	-	-	-	-	-	-	-	-	-	-	-	-	-	-	-	-	-9	-33	45	41	4.68	.019
Temporal Lobe																									
Superior Temporal Gyrus	L	-63	-27	42	86	4.01	.001	-51	-33	9	54	4.60	.008	-63	-39	12	76	5.20	.001	-63	-33	15	48	5.78	.009
Superior Temporal Gyrus	L	-	-	-	-	-	-	-	-	-	-	-	-	-42	-27	12	36	5.51	.032	-42	-27	12	35	5.38	.036
Middle/Inferior Temporal Gyrus	R	-	-	-	-	-	-	-	-	-	-	-	-	-	-	-	-	-	-	57	-66	0	44	4.97	.014

Note: The region in which the cluster's local maximum is located in hemispheres right (R), left (L), or central (C); the peak location in MNI coordinates (x, y, z); cluster extend in number of voxels (k); maximum Z score; and FWE-corrected p-values (cluster level corrected, * small volume corrected) are reported for each significantly activated cluster separately. ICs: independent components. ERPs: event-related potentials. MNI: Montreal Neurological Institute. FWE: family-wise error. IFG: inferior frontal gyurs. pre-SMA: pre-supplementary motor area.

Table 3.6. Continuation: Side-by-side comparison of positive correlations of fMRI BOLD signal with orthogonalized EEG-derived regressors early and late, as well as with orthogonalized EEG-derived regressors N2 and P3.

Region		early ICs						late ICs						N2 ERPs						P3 ERPs					
		x	y	z	k	Z	p	x	y	z	k	Z	p	x	y	z	k	Z	p	x	y	z	k	Z	p
Temporal Pole/Insula Lobe	R	-	-	-	-	-	-	36	12	0	59	4.07	.005	-	-	-	-	-	-	60	3	-9	148	5.41	<.001
Middle Temporal Gyrus	R	51	-72	18	44	4.06	.020	-	-	-	-	-	-	-	-	-	-	-	-	-	-	-	-	-	-
Fusiform Gyrus	R													-	-	-	-	-	-	33	-39	-15	74	5.31	.001
Supramarginal Gyrus	R	66	-39	24	317	5.15	<.001	66	-21	18	48	4.29	.014	-	-	-	-	-	-	54	-21	18	42	4.49	.017
Insula Lobe	L	-39	-6	-6	57	4.49	.006	-	-	-	-	-	-	-	-	-	-	-	-	-	-	-	-	-	-
Superior Temporal Gyrus/Insula Lobe	R	-	-	-	-	-	-	-	-	-	-	-	-	54	-3	-3	99	5.27	<.001	-	-	-	-	-	-
Superior Temporal Gyrus/Insula Lobe	L	-	-	-	-	-	-	-	-	-	-	-	-	-39	-12	-6	76	5.08	.001	-39	-12	-6	183	5.93	<.001
Insula Lobe/Amygdala	R	42	-3	-27	58	4.24	.005	-	-	-	-	-	-	-	-	-	-	-	-	-	-	-	-	-	-
Insula Lobe/Amygdala	L	-	-	-	-	-	-	-27	6	-15	56	4.68	.007	-	-	-	-	-	-	-	-	-	-	-	-
Hippocampus	L	-24	-18	-9	57	4.93	.006	-27	-15	-12	53	5.24	.009	-	-	-	-	-	-	-	-	-	-	-	-
Parietal Lobe																									
Postcentral Gyrus	R	-	-	-	-	-	-	-	-	-	-	-	-	-	-	-	-	-	-	51	-30	51	94	5.48	<.001
Inferior Parietal Lobule	L	-	-	-	-	-	-	-	-	-	-	-	-	-39	-51	54	80	4.95	<.001	-42	-51	54	631	5.05	<.001
Precuneus	R	9	-42	54	128	4.68	<.001	15	-54	60	65	4.70	.003	9	-45	60	63	4.93	.002	18	-42	57	49	4.45	.008

Note: The region in which the cluster's local maximum is located in hemispheres right (R), left (L), or central (C); the peak location in MNI coordinates (x, y, z); cluster extend in number of voxels (k); maximum Z score; and FWE-corrected p-values (cluster level corrected, * small volume corrected) are reported for each significantly activated cluster separately. ICs: independent components. ERPs: event-related potentials. MNI: Montreal Neurological Institute. FWE: family-wise error. IFG: inferior frontal gyurs. pre-SMA: pre-supplementary motor area.

Table 3.6. Continuation: Side-by-side comparison of positive correlations of fMRI BOLD signal with orthogonalized EEG-derived regressors early and late, as well as with orthogonalized EEG-derived regressors N2 and P3.

Region		early ICs						late ICs						N2 ERPs						P3 ERPs					
		x	y	z	k	Z	p	x	y	z	k	Z	p	x	y	z	k	Z	p	x	y	z	k	Z	p
Occipital Lobe																									
Middle Occipital Gyrus	R	33	-78	27	146	4.93	<.001	-	-	-	-	-	-	-	-	-	-	-	-	36	-75	6	46	4.35	.011
Middle Occipital Gyrus	L	-	-	-	-	-	-	-39	-63	0	57	4.79	.006	-	-	-	-	-	-	-27	-69	30	68	4.36	.001
Superior Occipital Gyrus	L	-18	-78	27	217	4.76	<.001	-24	-66	21	88	4.68	<.001	-	-	-	-	-	-	-	-	-	-	-	-
Lingual Gyrus	R	-	-	-	-	-	-	-	-	-	-	-	-	-	-	-	-	-	-	12	-54	-3	33	4.17	.045
Lingual Gyrus	L	-	-	-	-	-	-	-3	-72	0	36	4.57	.045	-27	-48	-3	43	5.08	.015	-18	-66	-9	676	5.31	<.001
Cuneus/Precuneus	R	-	-	-	-	-	-	-	-	-	-	-	-	-	-	-	-	-	-	24	-54	30	148	4.97	<.001
Subcortical Areas																									
Putamen	R	18	15	-3	45	3.87	.018	-	-	-	-	-	-	-	-	-	-	-	-	-	-	-	-	-	-
Putamen	L	-	-	-	-	-	-	-27	6	-9	86	3.84	.017*	-	-	-	-	-	-	-33	-15	-6	14	3.65	.035*
Caudate Nucleus	R	15	15	-3	154	3.85	.015*	-	-	-	-	-	-	-	-	-	-	-	-	-	-	-	-	-	-
Caudate Nucleus	L	-9	12	9	103	3.53	.045*	-	-	-	-	-	-	-18	-15	24	14	3.95	.010*	-	-	-	-	-	-
Pallidum	R	15	9	-3	*	3.74	.004*	-	-	-	-	-	-	-	-	-	-	-	-	-	-	-	-	-	-
Pallidum	L	-21	0	6	20	3.21	.023*	-	-	-	-	-	-	-	-	-	-	-	-	-	-	-	-	-	-
Subthalamic Nucleus	L	-	-	-	-	-	-	-	-	-	-	-	-	-	-	-	-	-	-	-12	-18	-6	5	2.92	.047*
Thalamus	R	-	-	-	-	-	-	-	-	-	-	-	-	-	-	-	-	-	-	21	-27	-3	79	4.61	<.001
Thalamus/Hippocampus	L	-	-	-	-	-	-	-	-	-	-	-	-	-	-	-	-	-	-	-21	-24	-6	138	5.50	<.001

The region in which the cluster's local maximum is located in hemispheres right (R), left (L), or central (C); the peak location in MNI coordinates (x, y, z); cluster extend in number of voxels (k); maximum *Z* score; and FWE-corrected *p*-values (cluster level corrected, * small volume corrected) are reported for each significantly activated cluster separately. ICs: independent components. ERPs: event-related potentials. MNI: Montreal Neurological Institute. FWE: family-wise error. IFG: inferior frontal gyurs. pre-SMA: pre-supplementary motor area.

4. Study 2: Neural timing of the response inhibition network in Attention-Deficit/Hyperactivity Disorder (ADHD) and Borderline Personality Disorder (BPD)

Impulsivity is central to Attention-Deficit/Hyperactivity Disorder (ADHD) and Borderline Personality Disorder (BPD). Especially in ADHD, increased intra-individual variability in response inhibition has been suggested to constitute a key pathophysiological process of impulsivity. To comprehensively characterize group differences in response inhibition, the novel independent component analysis (ICA)-based single-trial electroencephalographic (EEG)/functional magnetic resonance imaging (fMRI) analysis was conducted as presented in Study 1 (cf. Chapter 3) in addition to common unimodal event-related potential (ERP) or fMRI analyses. This allows assessing group differences in neural timing of response inhibition as well as incorporating intra-individual signal variability thereby increasing sensitivity for inter-individual differences in comparison to control subjects. 19 adult ADHD patients, 19 adult female BPD patients, and 31 adult healthy control (HC) subjects were included in this study.

Both patient groups showed significantly enhanced Go response time (RT) variability and reduced Nogo-P3 amplitudes in comparison to HC subjects. Unimodal fMRI analysis revealed a hypoactivation of striatal regions in ADHD compared to HC, but no differences between BPD and HC. Single-trial EEG/fMRI unveiled significantly reduced activity in frontal-striatal regions in ADHD in comparison to both BPD and HC, but only marginal differences between HC and BPD. This may indicated that deficient neural processing at an early phase of response inhibition may be a specific pathophysiological hallmark of ADHD. Hence, response inhibition deficits in ADHD may be due to dysfunctions in neural timing of inhibitory control networks opposed to static regional neural activity deficits. In contrast, neural networks of response inhibition in BPD were only mildly affected complementing current evidence of largely unaffected impulse control in BPD. These observations may shift our pathophysiological understanding of impulsivity in ADHD and BPD.

4.1. Material and methods

4.1.1. Participants

Data from 31 adult healthy control (HC) subjects (13 males; mean age: 35.65 ± 14.7), 19 adult Attention-Deficit/Hyperactivity Disorder (ADHD) patients (12 males; mean age: 35.84 ± 12.7) and 19 adult female Borderline Personality Disorder (BPD) patients (mean age: 23.63 ± 3.5) were included in the following analyses (cf. Section 2.1.1 *'Participants'* for a detailed information on participant samples).

As age and gender were substantially different between the groups, age and gender were included as a covariate of no interest in all subsequent analyses in order to prevent any age- or gender-dependent effects from affecting the results. Nogo-related independent components (ICs) were only detectable in a subsample of the whole groups (21 HC subjects: 7 males; mean age: 35.00 ± 14.6, 12 ADHD patients: 8 males; mean age: 36.75 ± 14.5, 11 female BPD patients: mean age: 24.27 ± 3.7). Hence, unimodal ERP and fMRI analysis were preformed on the whole groups, while single-trial EEG/fMRI analysis was performed on the subgroups.

4.1.2. Data analysis

4.1.2.1. ERP analysis

Mean amplitudes were measured in the predefined time windows 240–350 ms (N2), and 350–580 ms (P3) after stimulus onset at nine selected electrode sites: F3, Fz, F4, C3, Cz, C4, P3, Pz, and P4. To assess group differences in Go- and Nogo-related effects, N2 and P3 amplitudes were subjected to separate repeated measures analysis of variance (ANOVA) including within-subject factors Condition (correct Go, correct Nogo), Anteriorization (frontal (F3, Fz, F4), central (C3, Cz, C4), parietal (P3, Pz, P4)), and Laterality (left (F3, C3, P3), midline (Fz, Cz, Pz), right (F4, C4, P4)) as well as between-subject factor Group (HC ($N = 31$), ADHD ($N = 19$), BPD ($N = 19$)). In case of nonsphericity as indicated by a significant Mauchly test the corrected p-values and degree of freedom (DF)-values (Greenhouse-Geisser epsilon correction) are reported.

As the study was focused on group differences, only significant main effects as well as significant two-way interactions effects including Group as factor were further assessed with post hoc t-tests (Tukey multiple comparisons of means with 95 % family-wise confidence level). All three-way significant effects involving the factor Group were analyzed post-hoc by applying second ANOVA models and post hoc t-tests. Statistical analysis was performed using the packages 'stats' (R Core Team, 2014) and 'ez' (Lawrence, 2013) from the open-source statistical computing software 'R' (http://CRAN.R-project.org/).

4.1.2.2. Unimodal fMRI analysis

As described in Section 2.5.2 (*'First-level unimodal fMRI analysis'*), for each subject the unimodal fMRI first-level generalized linear model (GLM) consisted of two onset regressors corresponding to the correct and incorrect Nogo conditions. Go was used as an active baseline which allowed comparing Nogo vs. Go (active baseline) implicitly.

Unimodal fMRI first-level GLMs were computed for 31 HC subjects (13 males; mean age: 35.65 ± 14.7), 19 ADHD patients (12 males; mean age: 35.84 ± 12.7) and 19 female BPD patients (mean age: 23.63 ± 3.5)

4.1.2.3. Multimodal fMRI analysis

As described in Section 2.5.3 (*'First-level single-trial EEG/fMRI analysis'*), ICs intra-individually identified as reliably related to Nogo processing (Nogo > Go) with respect to the same latency range were used for single-trial EEG/fMRI analysis. Predefined time windows are referred to as 'early' (200 ms after stimulus onset until the individual's median RT) and 'late' (100 ms before RT until 300 ms after RT).

Only subjects characterized by the existence of Nogo-related ICs at these specific latency ranges were included to the single-trial EEG/fMRI analysis: 21 HC subjects (7 males; mean age: 35.00 ± 14.6), 12 ADHD patients (8 males; mean age: 36.75 ± 14.5), and 11 female BPD patients (mean age: 24.27 ± 3.7). ICs classified as Nogo-related with respect to the early or late latency were combined into individual IC-regressors and included into fMRI first-level analysis.

4.1.2.4. Group analysis of unimodal and multimodal fMRI data

Beta images corresponding to the 'correct Nogo−Go' contrasts were subjected to a full-factorial model with Group (HC, ADHD, BPD) as between-subject factor. Beta images corresponding to single-trial EEG/fMRI correlations with either early or late IC-regressors were subjected to a full-factorial repeated measures model with within-subject factor Latency (early, late) and between-subject factor Group (HC, ADHD, BPD).

Multiple comparisons correction was based on cluster-extent based thresholding (Friston et al., 1994b; Woo et al., 2014) using a primary voxel-level threshold of $p < .001$ and a minimum cluster-extend level of $k = 10$ continuous voxels. These thresholded data were assessed for cluster-wise significance by using a cluster-defining height threshold of $p_{(\mathrm{FWE})} < .05$ (family-wise error (FWE) correction for multiple comparisons).

Small volume correction was used for the following regions of interest (ROIs) as derived from the automated anatomical labeling (AAL) atlas: pars opercularis of inferior frontal gyurs (IFG); pre-supplementary motor area (pre-SMA) derived from the supplementary motor area (SMA); caudate nucleus; putamen; pallidum; subthalamic nucleus (STN) consisting of two boxes of respectively 10 mm^3 box at MNI (Montreal Neurological Institute) coordinates $-/+10, -15, -5$; inferior and superior parietal lobule (Sebastian et al., 2013a) and anterior cingulate cortex (ACC). Clusters were assessed for peak-wise significance by using a height threshold of $p_{(\text{FWE})} < .05$ (FWE corrected) after using a primary voxel-level threshold of $p < .05$ and no minimum cluster-extend level.

Group analysis of unimodal fMRI data: To assess group-specific effects of task-related activity, for each group beta images corresponding to the 'correct Nogo$-$Go' contrast were subjected to one-sample t-tests. To test for group differences, beta images corresponding to the 'correct Nogo$-$Go' contrast were further subjected to full-factorial models with between-subject factor Group (HC ($N = 31$), ADHD ($N = 19$), BPD ($N = 19$)).

Multiple comparisons correction of the statistical maps was based on cluster-extent based thresholding (Friston et al., 1994b; Woo et al., 2014) using a primary voxel-level threshold of $p < .001$ ($p < .005$ in case of an interaction effect) and a minimum cluster-extend level of $k = 10$ continuous voxels. Thereafter, the thresholded data were assessed for cluster-wise significance by using a cluster-defining height threshold of $p_{(\text{FWE})} < .05$ (FWE correction for multiple comparisons).

The small volume correction was computed for the following *a priori* defined ROIs: pars opercularis of the lateral IFG, pre-SMA derived from the SMA region with $y > 0$), caudate nucleus, putamen and pallidum, STN consisting of two boxes of respectively 10 mm^3 box at MNI coordinates $-/+10, -15, -5$, inferior parietal lobule and superior parietal lobule. Clusters were assessed for peak-wise significance by using a height threshold of $p_{(\text{FWE})} < .05$ (FWE corrected) after using a primary voxel-level threshold of $p < .05$ and no minimum cluster-extend level.

Group analysis of single-trial EEG/fMRI data: From the initial groups of 19 ADHD patients, 19 BPD patients and 31 HC subjects, 7 ADHD patients, 8 BPD patients and 17 HC subjects did not displayed Nogo-specific ICs on the chosen absolute Z score level (Nogo$-$Go difference: $|Z| > 0.275$) for either early or late time window. Thus, while unimodal fMRI and ERP analysis were computed for the larger group of 19 ADHD patients, 19 BPD patients and 31 HC subjects, single-trial correlations of fMRI blood oxygenation level-dependent (BOLD) signals with Nogo-IC derived regressors were computed for the intersection of 21 HC subjects, 12 ADHD patients, and 11 BPD patients.

Single-trial correlations of fMRI BOLD responses with the Nogo-IC derived electrophysiological regressors were tested for significance using full-factorial repeated measures models with within-subject factor Latency (early, late) and between-subject factor Group (HC ($N = 21$), ADHD

($N = 12$), BPD ($N = 11$)). As this study aimed at testing for functional group differences in neural activity related to different phases of response inhibition, non-orthogonalized IC-regressors were used (cf. Section 2.4.4 *'EEG-derived regressors'*).

Similar to the group unimodal fMRI analysis, whole brain results were corrected at the cluster level using a height threshold of $p_{\text{(FWE)}} < .05$ (FWE corrected) using a primary voxel-level threshold of $p < .001$ ($p < .005$ in case of an interaction effect) and a minimum cluster-extend level of $k = 10$ continuous voxels. Small volume correction was computed for the same predefined ROIs as for unimodal fMRI group analysis and were assessed for peak-wise significance by using a height threshold of $p_{\text{(FWE)}} < .05$ based on a primary voxel-level threshold of $p < .05$ and no minimum cluster-extend level.

4.2. Results

4.2.1. Demographics and task performance

Demographic data: ADHD and HC subjects did not differ significantly with respect to age, gender or verbal intelligence, neither in the whole groups for unimodal analyses nor in the subgroups for combined EEG/fMRI (Table 4.1.A). In contrast to this, age and gender of the BPD whole group and subgroup differed significantly from both ADHD groups and from both HC groups. Thus to prevent age- or gender-dependent effects from affecting the results, age and gender were included as a covariate of no interest in all subsequent analyses.

Performance data: Behaviorally (Table 4.1.B), both ADHD and both BPD groups were characterized by significantly higher intra-individual RT variability, i.e., higher coefficient of variability (CoV) compared to both HC groups, which was driven by higher CoV values in patient groups in comparison to HC groups. Additionally, the subgroups differed significantly in the omission error rate, which was driven by significantly higher omission error rates in ADHD compared to both HC and BPD.

Table 4.1. Group comparison of demographic and performance data in whole groups and subgroups.

	HC		ADHD		BPD		Group comp.		HC vs. ADHD	HC vs. BPD	BPD vs. ADHD
	mean	SD	mean	SD	mean	SD	t	p	p	p	p
A) Demographic											
Gender (male/N)											
Whole group	13/31		12/19		0/19		-	-	-	-	-	-
Subgroup	7/21		8/12		0/11		-	-	-	-	-	-
Age											
Whole group	35.65	14.7	35.84	12.7	23.63	3.5	6.83	.002	n.s.	.003	.008
Subgroup	35.00	14.6	36.75	14.5	24.27	3.7	3.27	.048	n.s.	n.s.	n.s.
MWT-B											
Whole group	31.13	3.5	31.06	4.3	28.72	4.2	2.27	n.s.	n.s.	n.s.	n.s.
Subgroup	30.71	3.5	32.64	4.3	29.80	3.9	1.81	n.s.	n.s.	n.s.	n.s.
B) Performance											
RT [ms]											
Whole group	415.53	59.6	399.90	30.9	399.42	54.3	1.02	n.s.	n.s.	n.s.	n.s.
Subgroup	408.24	45.2	397.57	33.5	389.20	54.4	0.71	n.s.	n.s.	n.s.	n.s.
CoV											
Whole group	0.21	0.04	0.26	0.05	0.25	0.04	12.84	<.001	<.001	.002	n.s.
Subgroup	0.195	0.04	0.261	0.05	0.236	0.04	9.58	<.001	<.001	.040	n.s.
Commission [%]											
Whole group	11.44	9.6	16.75	7.7	17.72	9.3	3.23	n.s.	n.s.	n.s.	n.s.
Subgroup	10.19	8.2	15.34	7.2	15.10	10.8	1.76	n.s.	n.s.	n.s.	n.s.
Omission [%]											
Whole group	0.32	0.5	1.37	1.5	1.85	4.2	1.74	n.s.	n.s.	n.s.	n.s.
Subgroup	0.19	0.3	1.19	1.2	0.45	0.5	7.52	.002	.001	n.s.	.047

Note: (A) Demographic data regarding age in years, intelligence as measured with German multiple-choice vocabulary test (MWT-B) and gender (male/N: ratio of number of males and sample size). (B) Behavioral data regarding mean Go response time (RT) on Go trials in milliseconds (ms), coefficient of variability (CoV) of RTs, mean percentage [%] omission errors of Go trials and mean percentage [%] of commission errors of Nogo trials. CoV is estimated by dividing SD of RT by mean RT. Percentage error is estimated by dividing the number of incorrect trials (Go for omission error and Nogo for commission error) by the total number of each trial type. Whole group: HC ($N = 31$), ADHD ($N = 19$), BPD ($N = 19$). Subgroup: HC ($N = 21$), ADHD ($N = 12$), BPD ($N = 11$). HC: healthy control. ADHD: Attention-Deficit/Hyperactivity Disorder. BPD: Borderline Personality Disorder. SD: standard deviation. n.s.: not significant ($p > .05$).

4.2.2. Psychometrics

As depicted in Table 4.2, group comparisons of psychometric data revealed significant interaction effects in most subscales of almost all questionnaires and items in the whole groups (HC: $N = 31$, ADHD: $N = 19$, BPD: $N = 19$) as well as in the smaller subgroups (HC: $N = 21$, ADHD: $N = 12$, BPD: $N = 11$).

In comparison to HC, both ADHD and BPD scored significantly higher on all subscales of the Barratt Impulsiveness Scale-11 (BIS-11) and UPPS Impulsive Behavior Scale (UPPS) (except for the UPPS subscale 'sensation seeking' in the subgroup), and on the Sensation Seeking Scale (SSS-V) subscales 'thrill and adventure seeking' (only the whole groups) and 'boredom susceptibility', with higher scores in the ADHD groups. Post-hoc comparisons of HC and ADHD groups revealed significantly higher scores in all subscales of BIS-11 and UPPS except for the UPPS subscale 'sensation seeking' and higher scores on the SSS-V subscale 'boredom susceptibility' but not on the SSS-V subscale 'thrill and adventure seeking'. Post-hoc comparison of HC and BPD revealed, that similarly to ADHD patients, BPD patients were characterized by significantly higher scores on all BIS-11 subscales, on all UPPS subscales except for 'sensation seeking' in the whole group, and on SSS-V subscales 'boredom susceptibility' and 'thrill/adventure seeking' (only the whole group of BPD patients). Post-hoc group comparisons of both ADHD and BPD groups revealed significant differences on the UPPS subscales 'premeditation' and 'perseverance', with higher scores in the ADHD group, but neither differences on the other UPPS subscales nor on SSS-V or BIS-11 subscales.

Regarding the clinical assessment of childhood and current ADHD symptoms, significant interaction effects were found on all subscales with ADHD patients displaying higher scores on the Wender Utah Rating Scale (WURS-k) and on all Conners' Adult ADHD Rating Scale (CAARS-S:L) subscales in comparison to both HC and BPD. Post-hoc comparison of both ADHD and HC groups revealed significantly higher scores on the WURS-k and on all CAARS-S:L subscales in ADHD. Despite having no lifetime diagnosis of ADHD, BPD patients had elevated scores on the WURS-k and most subscales of the CAARS-S:L except the subscale 'hyperactivity/restlessness' as compared to HC and did not differ significantly from ADHD patients on the subscales 'impulsivity/emotional lability' and 'problems with self-concept'.

Although below cut off, ADHD patients in comparison to HC subjects were also characterized by higher scores on the clinical assessments of BPD symptoms (Borderline Personality Disorder Severity Index (BPDSI)) and the current depressive mood (Beck Depression Inventory (BDI), Montgomery Asberg Depression Scale (MADRS)). In contrast to this, BPD patients were clearly above cut-off and significantly different from both HC groups and both ADHD groups regarding the clinical assessments of BPD symptoms (BPDSI) and the current depressive mood (BDI, MADRS).

Table 4.2. Group comparison of psychometric data in the whole groups and subgroups.

	HC		ADHD		BPD		Group comp.		HC vs. ADHD	HC vs. BPD	BPD vs. ADHD
	mean	SD	mean	SD	mean	SD	t	p	p	p	p
BIS-11											
Attentional impulsiveness											
Whole group	13.48	2.7	20.42	4.1	19.47	3.4	37.79	<.001	<.001	<.001	n.s.
Subgroup	13.24	3.0	19.83	3.6	20.43	3.8	19.97	<.001	<.001	<.001	n.s.
Motor impulsiveness											
Whole group	20.97	4.1	25.89	5.5	25.20	5.5	7.23	.003	.005	.028	n.s.
Subgroup	20.19	3.0	26.75	4.9	25.57	7.1	9.34	.001	.001	.026	n.s.
Non-planning impulsiveness											
Whole group	22.10	4.0	30.32	4.8	27.53	5.5	16.02	<.001	<.001	.008	n.s.
Subgroup	21.14	3.9	31.42	4.8	28.14	6.9	18.97	<.001	<.001	.007	n.s.
UPPS											
Premeditation											
Whole group	23.23	4.2	28.37	5.3	24.25	5.4	7.59	.002	.002	n.s.	.034
Subgroup	22.57	4.0	28.92	5.1	23.38	5.6	8.00	.001	.001	n.s.	.027
Urgency											
Whole group	37.90	3.9	24.74	4.8	22.50	5.1	97.48	<.001	<.001	<.001	n.s.
Subgroup	37.90	4.0	25.75	3.1	22.37	5.4	55.17	<.001	<.001	<.001	n.s.
Sensation seeking											
Whole group	27.61	6.1	28.53	8.8	33.50	8.0	3.82	.033	n.s.	.029	n.s.
Subgroup	28.38	6.2	27.58	7.5	32.25	9.4	1.35	n.s.	n.s.	n.s.	n.s.
Perseverance											
Whole group	16.58	3.4	28.21	4.8	22.69	6.0	46.74	<.001	<.001	<.001	.001
Subgroup	16.33	3.6	29.25	4.5	22.38	8.1	26.13	<.001	<.001	.016	.012
SSS-V											
Thrill and adventure seeking											
Whole group	6.55	2.4	5.95	3.3	3.75	3.2	5.21	.011	n.s.	.009	n.s.
Subgroup	6.24	2.6	6.42	2.9	4.63	3.2	1.30	n.s.	n.s.	n.s.	n.s.

Note: Whole group: HC ($N = 31$), ADHD ($N = 19$), BPD ($N = 19$). Subgroup: HC ($N = 21$), ADHD ($N = 12$), BPD ($N = 11$). HC: healthy control. ADHD: Attention-Deficit/Hyperactivity Disorder. BPD: Borderline Personality Disorder. SD: standard deviation. n.s.: not significant ($p > .05$).

Table 4.2. Continuation: Group comparison of psychometric data in the whole groups and subgroups.

	HC		ADHD		BPD		Group comp.		HC vs. ADHD	HC vs. BPD	BPD vs. ADHD
	mean	SD	mean	SD	mean	SD	t	*p*	*p*	*p*	*p*
Disinhibition											
Whole group	3.29	2.2	4.53	3.0	4.75	2.7	2.69	n.s.	n.s.	n.s.	n.s.
Subgroup	2.81	2.1	3.58	2.7	4.88	3.4	2.41	n.s.	n.s.	n.s.	n.s.
Experience seeking											
Whole group	6.42	1.9	6.68	1.7	6.56	2.2	0.10	n.s.	n.s.	n.s.	n.s.
Subgroup	5.86	1.8	6.67	1.7	6.38	2.4	0.73	n.s.	n.s.	n.s.	n.s.
Boredom susceptibility											
Whole group	2.26	1.8	4.05	1.8	4.75	2.3	9.85	.001	.011	.001	n.s.
Subgroup	1.57	1.2	4.08	2.1	5.75	2.2	19.02	<.001	.001	<.001	n.s.
CAARS:S-L											
Inattention/memory problems											
Whole group	42.58	6.4	67.53	11.1	54.53	10.6	37.49	<.001	<.001	.001	.001
Subgroup	42.00	6.5	68.92	9.5	54.91	13.1	34.07	<.001	<.001	.001	.002
Hyperactivity/ restlessness											
Whole group	43.45	6.6	56.21	9.9	47.74	10.2	11.22	<.001	<.001	n.s.	.021
Subgroup	42.14	5.7	55.33	10.3	49.09	10.7	9.11	.001	<.001	n.s.	n.s.
Impulsivity/emotional lability											
Whole group	40.90	5.0	65.32	8.3	61.11	8.9	69.86	<.001	<.001	<.001	n.s.
Subgroup	40.10	4.8	67.75	8.7	60.82	9.0	65.27	<.001	<.001	<.001	n.s.
Problems with self-concept											
Whole group	41.94	3.7	60.11	10.8	64.05	8.6	73.88	<.001	<.001	<.001	n.s.
Subgroup	41.67	3.8	58.33	11.5	65.45	8.1	40.47	<.001	<.001	<.001	n.s.
DSM-IV inattentive symptoms											
Whole group	41.87	7.3	79.58	10.3	54.74	11.5	94.00	<.001	<.001	<.001	<.001
Subgroup	40.86	7.5	83.58	8.1	55.18	13.9	76.60	<.001	<.001	.001	<.001

Note: Whole group: HC ($N = 31$), ADHD ($N = 19$), BPD ($N = 19$). Subgroup: HC ($N = 21$), ADHD ($N = 12$), BPD ($N = 11$). HC: healthy control. ADHD: Attention-Deficit/Hyperactivity Disorder. BPD: Borderline Personality Disorder. SD: standard deviation. n.s.: not significant ($p > .05$).

Table 4.2. Continuation: Group comparison of psychometric data in the whole groups and subgroups.

	HC		ADHD		BPD		Group comp.		HC vs. ADHD	HC vs. BPD	BPD vs. ADHD
	mean	SD	mean	SD	mean	SD	t	p	p	p	p
DSM-IV hyperactive-impulsive symptoms											
Whole group	38.61	6.7	58.95	10.9	47.74	11.3	27.28	<.001	<.001	.006	.003
Subgroup	37.19	4.7	59.83	12.0	48.00	11.7	24.90	<.001	<.001	.007	.008
DSM-IV ADHD symptoms total											
Whole group	39.03	7.3	73.47	10.2	52.00	10.9	75.69	<.001	<.001	<.001	<.001
Subgroup	37.43	6.4	76.42	9.0	52.27	12.3	75.08	<.001	<.001	<.001	<.001
ADHD index											
Whole group	40.03	6.1	68.26	9.8	59.68	9.3	85.42	<.001	<.001	<.001	.005
Subgroup	39.48	6.2	70.50	10.2	60.64	9.8	60.47	<.001	<.001	<.001	.017
WURS-k											
Whole group	10.00	7.5	42.68	11.3	30.89	13.8	61.50	<.001	<.001	<.001	.004
Subgroup	7.21	5.0	41.92	11.8	29.18	11.6	52.52	<.001	<.001	<.001	.007
BPDSI											
Whole group	0.69	0.7	9.07	7.6	26.53	8.8	87.11	<.001	.001	<.001	<.001
Subgroup	0.66	0.7	6.33	4.0	26.74	9.7	82.70	<.001	.024	<.001	<.001
MADRS											
Whole group	0.10	0.4	5.67	4.2	12.00	5.7	50.49	<.001	<.001	<.001	<.001
Subgroup	0.15	0.5	5.73	3.9	12.09	6.0	37.60	<.001	.001	<.001	.001
BDI											
Whole group	0.86	1.6	7.94	7.9	21.58	8.6	79.65	<.001	.001	<.001	<.001
Subgroup	1.22	1.9	6.55	6.3	20.73	9.5	34.88	<.001	.074	<.001	<.001

Note: Neuropsychological data with self-ratings regarding impulsivity (Barratt Impulsiveness Scale-11 (BIS-11), UPPS Impulsive Behavior Scale (UPPS), Sensation Seeking Scale (SSS-V)). Clinical ratings regarding ADHD symptoms in childhood (Wender Utah Rating Scale (WURS-k) [total score]) and adulthood (Conners' Adult ADHD Rating Scale (CAARS-S:L), [t-value])), clinical assessment of BPD symptoms (Borderline Personality Disorder Severity Index (BPDSI)), and clinical rating (Montgomery Asberg Depression Scale (MADRS)) and self-rating (Beck Depression Inventory (BDI)) of current depressive mood. Whole group: HC ($N = 31$), ADHD ($N = 19$), BPD ($N = 19$). Subgroup: HC ($N = 21$), ADHD ($N = 12$), BPD ($N = 11$). HC: healthy control. ADHD: Attention-Deficit/Hyperactivity Disorder. BPD: Borderline Personality Disorder. SD: standard deviation. n.s.: not significant ($p > .05$).

4.2.3. Unimodal ERP analysis

Grand averages at two representative electrodes and topographical maps plotted from 150–800 ms post-stimulus are shown in Figure 4.1 (Nogo-related ERPs) and Figure 4.2 (Go-related ERPs). Table 4.3 presents the results of repeated measures ANOVA on amplitudes of N2 and P3 measured at nine electrodes (F3, Fz, F4, C3, Cz, C4, P3, Pz, and P4) with between-subject factor Group and within-subject factors Anteriorization, Lateralization and Condition.

N2 (240–350 ms): The N2 amplitude showed the strongest negativity at frontal and central electrodes as compared to parietal electrodes ($F(1.30, 85.74) = 57.41$, $p < .001$) and was larger in Nogo compared to Go condition ($F(1, 66) = 9.79$, $p = .003$). Post-hoc Tukey tests on the significant interaction effect between group and task condition of N2 amplitude values ($F(2, 66) = 6.19$, $p = .003$) revealed significant within-group differences only in HC ($p < .001$), while between-group differences were mainly driven by significantly lower Nogo-N2 amplitudes in ADHD compared to BPD ($p < .001$) and HC ($p < .001$) as well as significantly larger Go-N2 amplitudes in BPD compared to ADHD ($p = .009$) and HC ($p < .001$).

P3 (350–580 ms): P3 amplitudes were significantly more pronounced at central and parietal electrodes as compared to frontal electrodes ($F(1.14, 75.27) = 9.41$, $p = .002$) and larger in Nogo compared to Go conditions ($F(1, 66) = 176.02$, $p < .001$). Post-hoc analysis of a significant interaction effect between group and task condition of P3 amplitude values ($F(2, 66) = 6.55$, $p = .003$) revealed significantly higher amplitudes in Nogo condition compared to Go condition in all groups ($p_{(HC)} < .001$, $p_{(BPD)} < .001$, $p_{(ADHD)} < .001$), with the smallest differences between Nogo-P3 and Go-P3 in ADHD, but also higher Nogo-P3 amplitude values in HC compared to both ADHD ($p < .001$) and BPD ($p = .006$).

A.1) Nogo related grand mean ERPs at F4

A.2) Nogo related grand mean ERPs at Cz
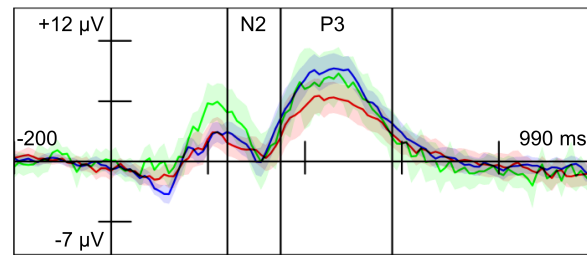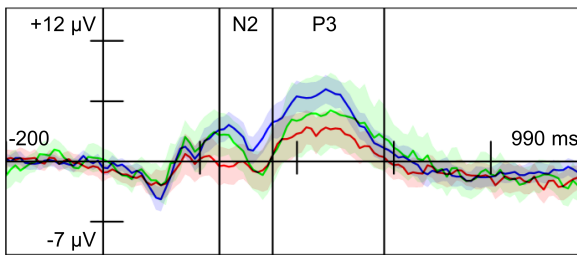
B1) Nogo related topographies (150 – 800 ms post stimulus) in HC (N = 31)
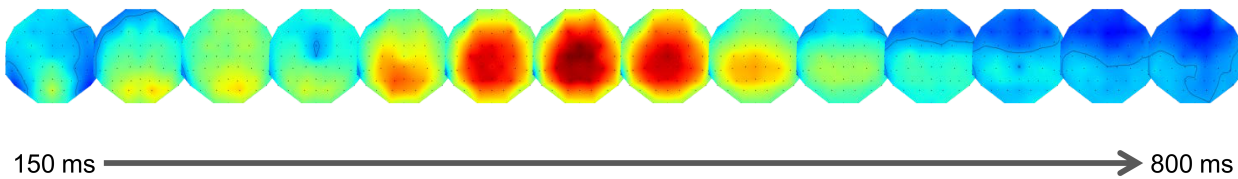
150 ms ⟶ 800 ms

B2) Nogo related topographies (150 – 800 ms post stimulus) in ADHD (N = 19)
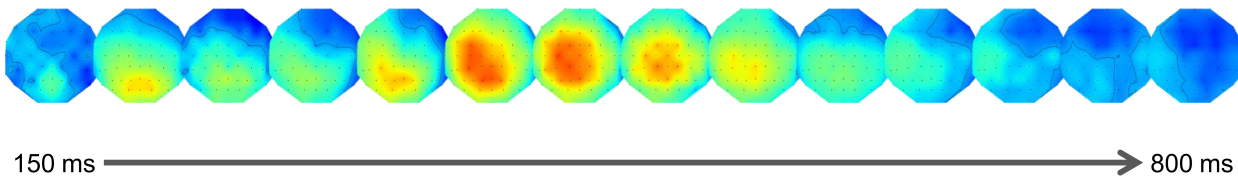
150 ms ⟶ 800 ms

B3) Nogo related topographies (150 – 800 ms post stimulus) in BPD (N = 19)

150 ms ⟶ 800 ms

C) Legend

HC: mean	ADHD: mean	BPD: mean	
HC: 95% C.I.	ADHD: 95% C.I.	BPD: 95% C.I.	-3.07 µV +7.63 µV
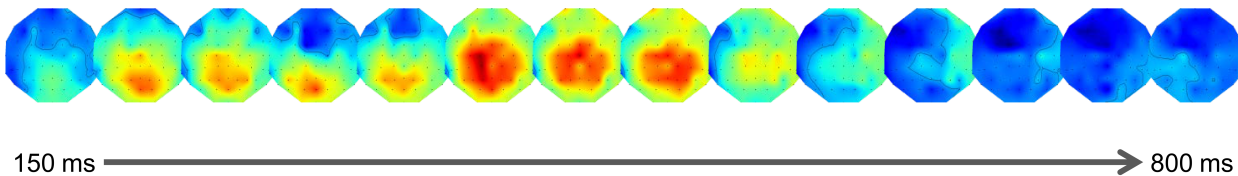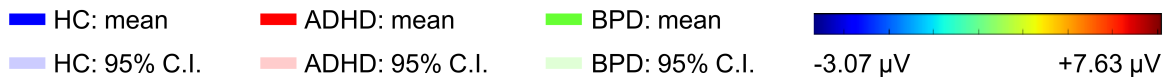
Figure 4.1. Nogo related grand mean event-related potentials (ERPs) at two representative electrodes (F4 and Cz) and topographic map series from 150–800 ms after stimulus onset, averaged from Nogo stimulus onsets in the whole groups of healthy control (HC) subjects (blue), Attention-Deficit/Hyperactivity Disorder (ADHD) patients (red), and Borderline Personality Disorder (BPD) patients (green). A) Shows the time courses (Mean as solid lines; 95 % confidence interval as shaded areas) of Nogo related ERPs at right-frontal electrode (F4) and at central electrode (Cz). B) Shows series of topographical maps related to Nogo condition in HC subjects (B.1), ADHD patients (B.2), and BPD patients (B.3), plotted every 50 ms from 150 ms to 800 ms after stimulus onset. In A): Vertical black lines indicate the N2 latency at 240–350 ms after stimulus onset and P3 latency at 350–580 ms after stimulus onset. In B): Black lines demark the zero line; black dots demark the positions of 62 scalp-electrodes.

A.1) Go related grand mean ERPs at F4
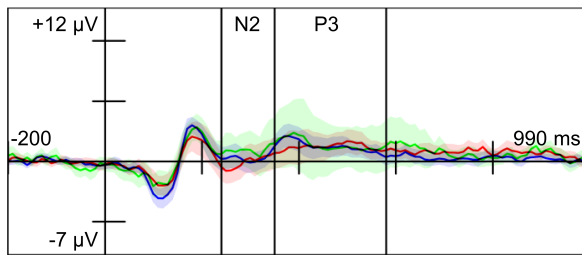
A.2) Go related grand mean ERPs at Cz
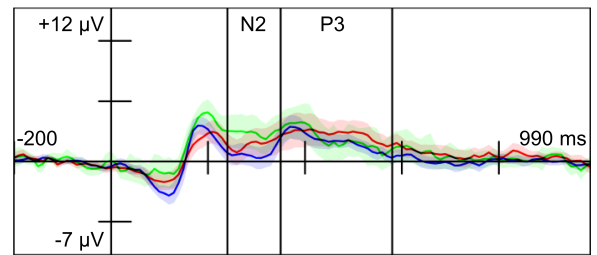
B1) Go related topographies (150 – 800 ms post stimulus) in HC (N = 31)
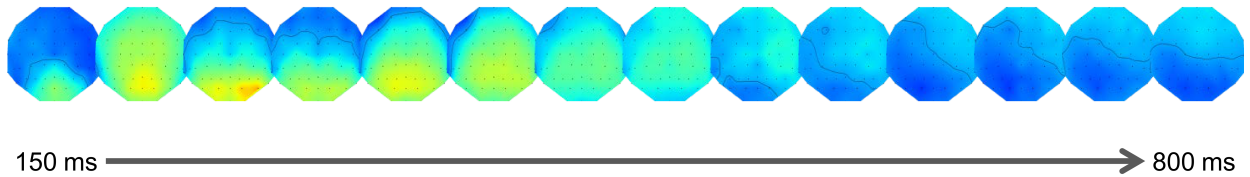
150 ms → 800 ms

B2) Go related topographies (150 – 800 ms post stimulus) in ADHD (N = 19)

150 ms → 800 ms

B3) Go related topographies (150 – 800 ms post stimulus) in BPD (N = 19)

150 ms → 800 ms

C) Legend

HC: mean   ADHD: mean   BPD: mean

HC: 95% C.I.   ADHD: 95% C.I.   BPD: 95% C.I.   -3.07 µV   +7.63 µV
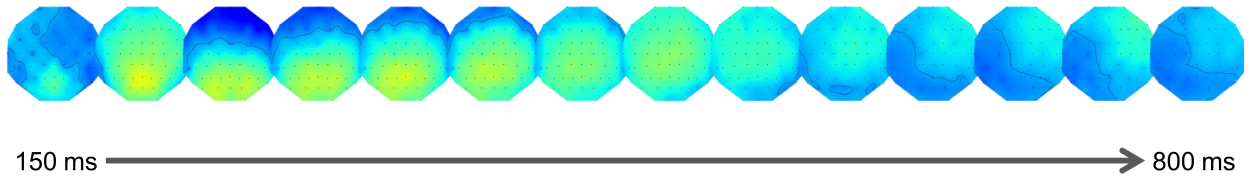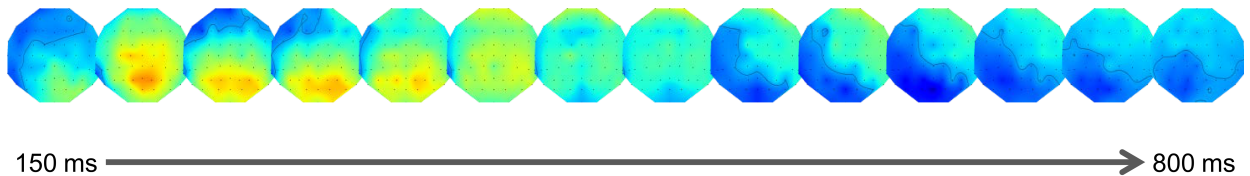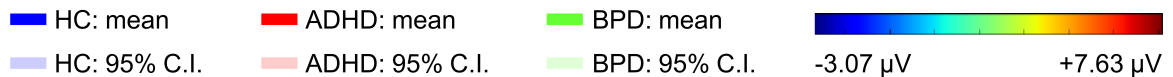
Figure 4.2. Go related grand mean event-related potentials (ERPs) at two representative electrodes (F4 and Cz) and topographic map series from 150–800 ms after stimulus onset, averaged from Go stimulus onsets in the whole groups of healthy control (HC) subjects (blue), Attention-Deficit/Hyperactivity Disorder (ADHD) patients (red), and Borderline Personality Disorder (BPD) patients (green). A) Shows the time courses (Mean as solid lines; 95 % confidence interval as shaded areas) of Go related ERPs at right-frontal electrode (F4) and at central electrode (Cz). B) Shows series of topographical maps related to Go condition in HC subjects (B.1), ADHD patients (B.2), and BPD patients (B.3), plotted every 50 ms from 150 ms to 800 ms after stimulus onset. In A): Vertical black lines indicate the N2 latency at 240–350 ms after stimulus onset and P3 latency at 350–580 ms after stimulus onset. In B): Black lines demark the zero line; black dots demark the positions of 62 scalp-electrodes.

Table 4.3. Results of separate repeated measures ANOVAs on N2 and P3 amplitudes in the whole groups.

Effect	N2 amplitude				P3 amplitude			
	DF	MT	F	p	DF	MT	F	p
Group	2, 66	-	0.18	n.s.	2, 66	-	0.08	n.s.
Condition	1, 66	-	9.79	.003	1, 66	-	176.02	<.001
Anteriorization	1.30, 85.74	*	57.41	<.001	1.14, 75.27	*	9.41	.002
Laterality	1.38, 91.36	*	1.07	n.s.	1.43, 94.59	*	1.27	n.s.
Group × Condition	2, 66	-	6.19	.003	2, 66	-	6.55	.003
Group × Anteriorization	2.60, 85.74	*	2.14	n.s.	2.28, 75.27	*	0.10	n.s.
Group × Laterality	2.77, 91.36	*	0.63	n.s.	2.87, 94.59	*	2.02	n.s.
Condition × Anteriorization	1.35, 89.43	*	1.87	n.s.	1.23, 81.27	*	10.66	.001
Condition × Laterality	1.22, 80.49	*	2.99	n.s.	1.41, 93.22	*	6.97	.004
Anteriorization × Laterality	3.46, 228.45	*	4.27	.004	3.27, 215.77	*	1.44	n.s.
Group × Condition × Anteriorization	2.71, 89.43	*	2.44	n.s.	2.46, 81.27	*	0.86	n.s.
Group × Condition × Laterality	2.44, 80.49	*	1.37	n.s.	2.82, 93.22	*	0.85	n.s.
Group × Anteriorization × Laterality	6.92, 228.45	*	0.67	n.s.	6.54, 215.77	*	0.98	n.s.
Condition × Anteriorization × Laterality	3.12, 205.92	*	7.40	<.001	3.35, 220.95	*	2.90	.031
Group:Condition × Anteriorization × Laterality	6.24, 205.92	*	0.80	n.s.	6.70, 220.95	*	1.28	n.s.

Note: Main and interaction effects of separate repeated measures analysis of variance (ANOVA) on N2 and P3 amplitudes and latency values with within-subject factors Condition (correct Go, correct Nogo), Anteriorization (frontal (F3, Fz, F4), central (C3, Cz, C4), parietal (P3, Pz, P4)), and Laterality (left (F3, C3, P3), midline (Fz, Cz, Pz), right (F4, C4, P4)) and between-subject factor Group (healthy control (HC): $N = 31$, Attention-Deficit/Hyperactivity Disorder (ADHD): $N = 19$, Borderline Personality Disorder (BPD): $N = 19$). In case of a significant Mauchly test (MT = *) the corrected p-values and degree of freedom (DF)-values (Greenhouse-Geisser epsilon correction) are reported. MT: Mauchly Test. n.s.: not significant ($p > .05$).

4.2.4. Unimodal fMRI data analysis: Within-group task related activation

Side-by-side comparison of the contrast 'correct Nogo−Go' revealed overlapping but also different regions of task-related activation in HC, ADHD and BPD (Figure 4.3, Table 4.4). In HC and ADHD significant task-related activity was concordantly found in pre-SMA and right precentral gyrus, stretching in HC from precentral gyrus to right superior frontal gyrus and in ADHD from precentral gyrus to right middle frontal gyrus. Additionally, in HC but not in ADHD nor in BPD, task-related activity was also located in ACC, in right middle frontal gyrus and in a large cluster stretching from bilateral posterior-medial frontal cortex to left middle/superior frontal gyri, left precentral gyrus and middle cingulate cortex (MCC). Task-related activity in right posterior IFG/insula was only detected in BPD, while task-related activity in left precentral/middle frontal gyrus was only detectable in ADHD.

HC subjects and ADHD patients but not BPD patients displayed further concurrent activity in right middle/superior temporal gyrus and in a cluster enclosing left middle occipital gyrus and left calcarine gyrus. HC subjects and BPD patients but not ADHD patients showed significant task related activity in another cluster enclosing right superior parietal lobule and right angular gyrus. Additionally, HC subjects showed task-related activity in a cluster enclosing right temporal and occipital areas (middle temporal gyrus, right middle/superior occipital gyri, right fusiform gyrus), while only ADHD patients showed additional activity in right inferior/middle temporal gyrus and only BPD patients showed activity in left superior parietal lobule. Subcortically, in HC significant task-related activation was found in bilateral putamen and caudate nucleus, and right pallidum, while neither ADHD patients nor BPD patients showed any significant subcortical activity.

Table 4.4.   Results of unimodal fMRI analysis in healthy control (HC) subjects, Attention-Deficit/Hyperactivity Disorder (ADHD) patients, and Borderline Personality Disorder (BPD) patients: Side-by-side comparison of task-related activation in the whole groups.

Region	HC						ADHD						BPD					
	k	p	Z	x	y	z	k	p	Z	x	y	z	k	p	Z	x	y	z
Frontal																		
R Mid. Frontal G.	65	.019	4.41	36	39	27	-	-	-	-	-	-	-	-	-	-	-	-
R IFG (pars Opercularis)	-	-	-	-	-	-	-	-	-	-	-	-	204*	.017*	3,35	57	15	-3
pre-SMA	299*	<.001*	5.84	-6	3	57	246*	.003*	4.42	0	6	51	-	-	-	-	-	-
R/L post.-medial frontal; L Precentral G.; R MCC; L Mid. /Sup. Frontal G.	745	<.001	5.98	6	0	63	-	-	-	-	-	-	-	-	-	-	-	-
HC: R Precentral G.; R Sup. Frontal G.	-	-	-	-	-	-	-	-	-	-	-	-	-	-	-	-	-	-
ADHD: R Precentral G.; R Mid. Frontal G.	199	<.001	4.63	45	-3	48	64	.008	3.89	27	-3	48	-	-	-	-	-	-
L Precentral G.; L Mid. Frontal G.	-	-	-	-	-	-	156	<.001	4.39	-39	-6	51	-	-	-	-	-	-

Note: The region in which the cluster's local maximum is located in Montreal Neurological Institute (MNI) coordinates (x, y, z) for the contrast 'correct Nogo−Go' with associated Z score ($p_{(FWE)}$ < .05, cluster level corrected; *small volume corrected, $p_{(FWE)}$ < .05) and cluster extend in number of voxels (k). R: right. L: left. IFG: inferior frontal gyurs. ACC: anterior cingulate cortex. MCC: middle cingulate cortex. Sup: superior. Mid: middle. Inf: inferior. G: gyrus. Lob: lobule. HC: healthy control ($N = 31$). ADHD: Attention-Deficit/Hyperactivity Disorder ($N = 19$). BPD: Borderline Personality Disorder ($N = 19$).

Table 4.4. Continuation: Side-by-side comparison of task-related activation in the whole groups of HC, ADHD and BPD.

	HC						ADHD						BPD					
Region	k	p	Z	x	y	z	k	p	Z	x	y	z	k	p	Z	x	y	z
Cingulum	-	-	-	-	-	-	-	-	-	-	-	-	-	-	-	-	-	-
R ACC; L ACC	126	.001	3.82	3	45	0	-	-	-	-	-	-	-	-	-	-	-	-
C ACC	498*	.032*	3.81	0	45	0	-	-	-	-	-	-	-	-	-	-	-	-
Subcortical																		
R Caudate Nucleus	225*	.010*	3.90	9	21	0	-	-	-	-	-	-	-	-	-	-	-	-
L Caudate Nucleus	243*	.017*	3.72	-15	3	12	-	-	-	-	-	-	-	-	-	-	-	-
L Putamen; L Thalamus; L Caudate Nucleus	143	<.001	4.73	-24	9	6	-	-	-	-	-	-	-	-	-	-	-	-
R Putamen; R Caudate Nucleus; R Insula Lob.	199	<.001	4.36	21	3	9	-	-	-	-	-	-	-	-	-	-	-	-
R Pallidum	22*	.004*	3.76	18	3	6	-	-	-	-	-	-	-	-	-	-	-	-
Temporal																		
R Sup. Temporal G.; R Mid. Temporal G.	319	<.001	4.87	54	-24	-3	42	.045	4.25	57	-36	18	-	-	-	-	-	-
R Inf. Temporal G.; R Mid. Temporal G.							76	.003	4.43	42	-66	-3	-	-	-	-	-	-
R Mid. Temporal G.; R Sup./Mid. Occipital G.; R Fusiform G.	215	<.001	6.00	48	-72	0	-	-	-	-	-	-	-	-	-	-	-	-
Parietal																		
R Sup. Parietal Lob.; R Angular G.	92	.004	3.90	33	-63	54	-	-	-	-	-	-	186*	.038*	3,17	42	-48	60
L Sup. Parietal Lob.	-	-	-	-	-	-	-	-	-	-	-	-	221*	.005*	3,8	-33	-54	63
Occipital																		
L Mid. Occipital G.; L Calcarine G.	239	<.001	5.68	-42	-81	0	132	<.001	4.26	-39	-63	3	-	-	-	-	-	-

Note: The region in which the cluster's local maximum is located in Montreal Neurological Institute (MNI) coordinates (x, y, z) for the contrast 'correct Nogo−Go' with associated Z score ($p_{(FWE)} < .05$, cluster level corrected; *small volume corrected, $p_{(FWE)} < .05$) and cluster extend in number of voxels (k). R: right. L: left. IFG: inferior frontal gyrus. ACC: anterior cingulate cortex. MCC: middle cingulate cortex. Sup: superior. Mid: middle. Inf: inferior. G: gyrus. Lob: lobule. HC: healthy control ($N = 31$). ADHD: Attention-Deficit/Hyperactivity Disorder ($N = 19$). BPD: Borderline Personality Disorder ($N = 19$).

A) Task-related activity in HC (N = 31, *p*<.001)

B) Task-related activity in ADHD (N = 19, *p*<.001)

C) Task-related activity in BPD (N = 19, *p*<.001)

Figure 4.3. Activation maps displaying task-related activity during 'correct Nogo−Go' as assessed by unimodal fMRI analysis in the whole groups. (A) Activation patterns in healthy control(HC, $N = 31$) subjects. (B) Activation patterns in patients with Attention-Deficit/Hyperactivity Disorder (ADHD, $N = 19$). (C) Activation patterns in patients with Borderline Personality Disorder (BPD, $N = 19$). Images are displayed with $p < .001$ (uncorrected) and $k = 10$ for display purposes. Images are displayed in neurological order. The color bar indicates *t*-scores (0–6.77).

4.2.5. Group comparisons of unimodal fMRI and single-trial EEG/fMRI analyses

4.2.5.1. Healthy controls vs. Attention-Deficit/Hyperactivity Disorder

Unimodal fMRI group comparison of task-related activity revealed significantly reduced activity in ADHD in bilateral caudate nuclei, left putamen and bilateral pallidum as compared to HC subjects (Figure 4.4.B, Table 4.6). Multimodal EEG/fMRI group comparisons in the subgroups yielded significantly reduced correlations at the early latency in ADHD in bilateral fronto-striatal regions associated with response inhibition (IFG/insula, pre-SMA, superior/medial frontal areas, striatum and right pallidum) and parietal areas. Additionally, reduced correlations at the early latency were found in ACC and right thalamus/insula (Figure 4.4.A.1 and Figure 4.4.A.2, Table 4.5.A). Reduced correlations at the late latency were found exclusively in bilateral caudate nuclei and bilateral pallidum. A significant group by latency (early/late) related interaction was identified in bilateral IFG/insula regions (significant in left IFG and trend in right IFG) showing a relative activity decrease from early to late in HC in contrast to a relative activity increase from early to late in ADHD (Figure 4.4.A.3, Table 4.5.B).

Figure 4.4 *(next page)* Activation maps displaying results of group comparisons of healthy control (HC) vs. Attention-Deficit/Hyperactivity Disorder (ADHD) as assessed by single-trial EEG/fMRI analysis in the subgroups (HC ($N = 21$) > ADHD ($N = 12$)) and unimodal fMRI analysis in the whole group (HC ($N = 31$) > ADHD ($N = 19$)). (A) Group differences (HC > ADHD) in the strength of single-trial EEG/fMRI correlations at (A.1) early latency and (A.2) late latency. (A.3) Positive interaction effect between factors Group (HC, ADHD) and Latency (early, late), and contrast estimates with 90 % confidence intervals at left (L) insula/IFG and right (R) IFG. (B) Group differences (HC > ADHD) in task-related activity during 'correct Nogo−Go' as assessed by unimodal fMRI analysis. Images A.1 and B are displayed with uncorrected $p < .001$ and $k = 10$, images A.2 and A.3 are displayed with uncorrected $p < .005$ and $k = 10$ for display purposes. Images are displayed in neurological order. The color bar indicates t-scores (0–5.46). IFG: inferior frontal gyurs (IFG)

A) Single-trial EEG/fMRI: Group comparison (HC (N = 21) > ADHD (N = 12))

A.1) Early latency ($p<.001$)

Early latency: 200 ms after stimulus onset until individual median Go RT

late latency: 100 ms prior to individual median Go RT until 300 ms after individual median Go RT
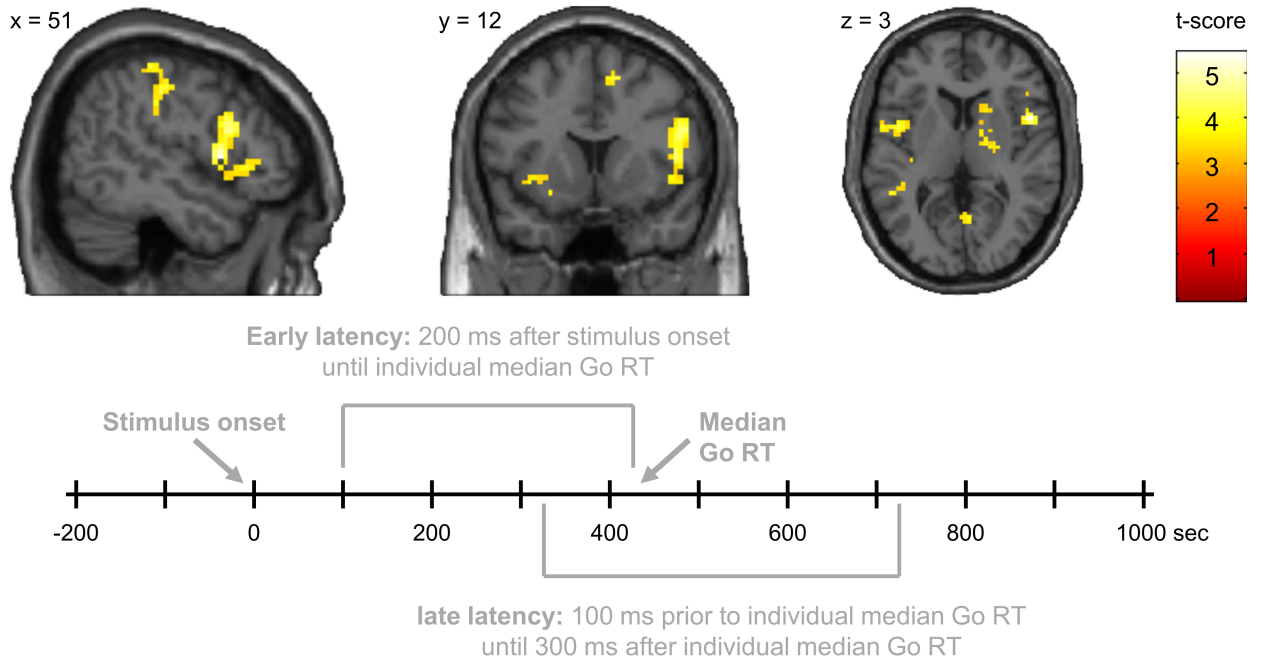
A.2) Late latency ($p<.005$)

Á.3) Group (HC/ADHD) by time (early/late) interaction ($p<.005$) and contrast estimates
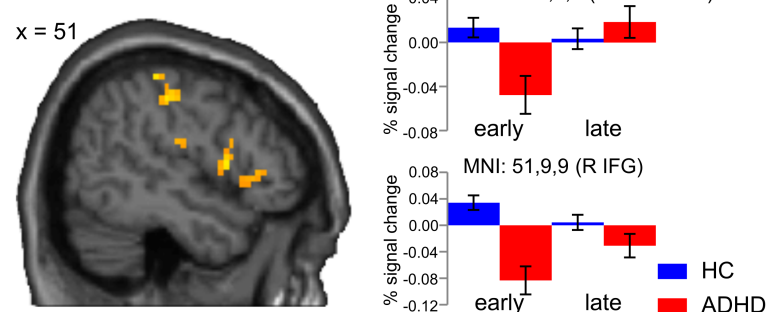
B) Unimodal fMRI: Group comparison HC (N = 31) > ADHD (N = 19) $p<.001$)
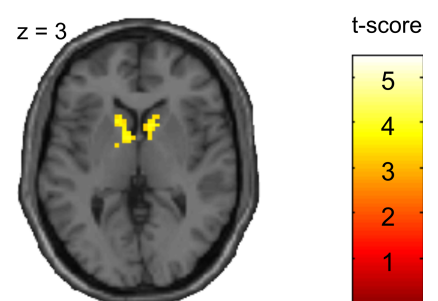
Table 4.5. Results of multimodal fMRI analysis in healthy control (HC) subjects and Attention-Deficit/Hyperactivity Disorder (ADHD) patients: Between group comparisons and Group (HC, ADHD) by Latency (early, late) interaction effect of correlations of fMRI signal with early and late IC-regressors.

A) HC > ADHD	early						late					
Region	k	p	Z	x	y	z	k	p	Z	x	y	z
Frontal												
L IFG (pars Triangularis)	54	.028	4.78	-48	42	12	-	-	-	-	-	-
R pre-SMA	288*	.022*	3.85	12	12	54	-	-	-	-	-	-
R IFG (pars Opercularis; pars Triangularis); R Insula	141	<.001	5.02	51	9	6	-	-	-	-	-	-
L IFG (pars Opercularis)	207*	.022*	3.68	-45	6	9	-	-	-	-	-	-
L Sup. Frontal G.	127	<.001	4.96	-21	-3	57	-	-	-	-	-	-
R post.-medial frontal; R MCC	49	.040	3.9	3	-21	51	-	-	-	-	-	-
Cingulum												
R ACC	329*	.030*	3.83	9	27	27	-	-	-	-	R	-
Subcortical												
R Thalamus; R Insula L.; R Rolandic Operculum	50	.038	4.15	21	21	-3	-	-	-	-	-	-
R Caudate Nucleus	182*	.025*	3.62	12	18	3	90*	.017*	3.74	24	6	12
L Caudate Nucleus	161*	.023*	3.65	-12	9	12	133*	.047*	3.41	-9	12	9
R Putamen; R Caudate Nucleus	89	.003	4.14	24	-18	15	-	-	-	-	-	-
L Putamen	15*	.020*	3.68	-33	-18	-6	-	-	-	-	-	-
R Pallidum	29*	.003*	3.83	15	3	3	-	-	-	-	-	-
L Pallidum	-	-	-	-	-	-	1*	.007*	3.52	-12	-3	0
Parietal												
R Postcentral G.; R Supramarginal G.	83	.004	4.15	57	-24	45	-	-	-	-	-	-
L Supramarginal G.; L Inf. Parietal Lob.	75	.007	4.24	-54	-27	33	-	-	-	-	-	-
B) Interaction effect	Group × Latency						late					
Frontal												
L IFG (pars Opercularis)	75*	.017*	3.76	-42	6	9	-	-	-	-	-	-

Note: The region in which the cluster's local maximum is located in Montreal Neurological Institute (MNI) coordinates (x, y, z) for early (time window starting 200 ms after stimulus onset and ending with the individual median Go response time (RT)) and late (time window starting 100 ms prior to RT and ending 300 ms after RT), and the positive interaction effect of Group (HC vs. ADHD) × Latency (early, late) with associated Z score ($p_{(FWE)} < .05$, cluster level corrected; *small volume corrected, $p_{(FWE)} < .05$) and cluster extend in number of voxels (k). FWE: family-wise error. R: right. L: left. IFG: inferior frontal gyurs. pre-SMA: pre-supplementary motor area. ACC: anterior cingulate cortex. MCC: middle cingulate cortex. Sup: superior. Mid: middle. Inf: inferior. G: gyrus. Lob: lobule. HC: healthy control ($N = 21$). ADHD: Attention-Deficit/Hyperactivity Disorder ($N = 12$).

4.2.5.2. Healthy controls vs. Borderline Personality Disorder

Unimodal fMRI group comparison of task-related activity revealed no significant differences. Multimodal EEG/fMRI group comparisons in the subgroups revealed significantly stronger correlations of the late IC-regressor in pregenual ACC in BPD compared to HC (Figure 4.5.B, Table 4.7) but no differences at the early latency (Figure 4.5.A).

A) Single-trial EEG/fMRI: Group comparison (BPD (N = 11) > HC (N = 21))
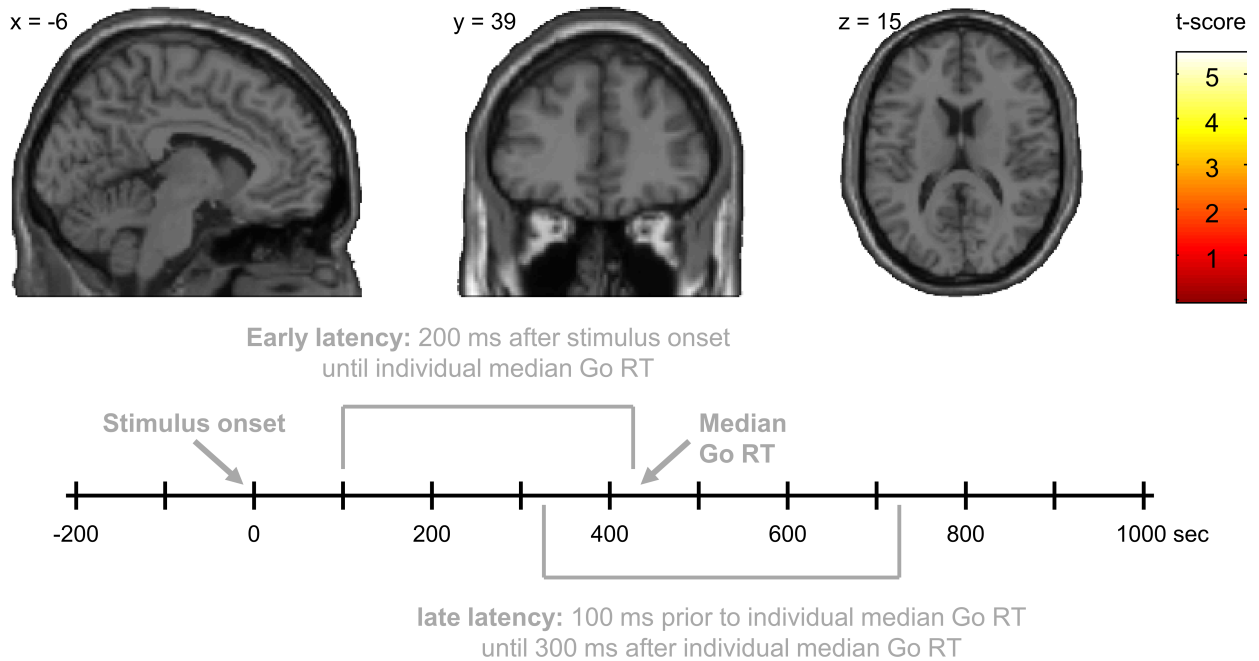
A.1) Early latency ($p<.001$)
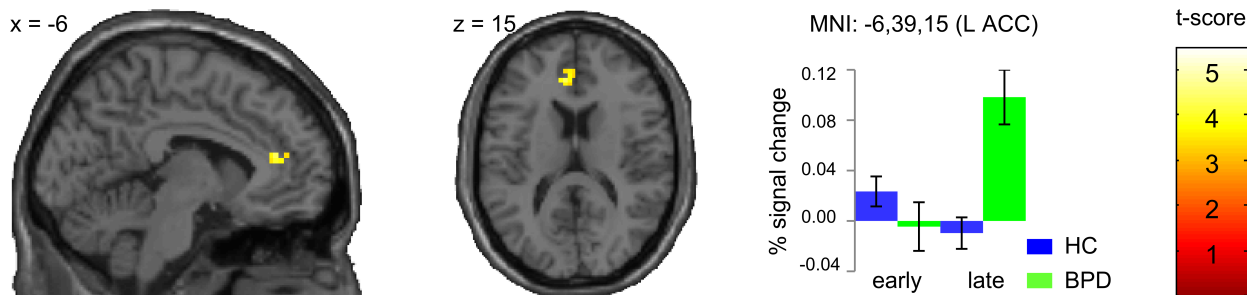
Figure 4.5. Activation maps displaying results of group comparisons of Borderline Personality Disorder (BPD) vs. healthy control (HC) as assessed by single-trial EEG/fMRI analysis in the subgroups (HC: $N = 21$; BPD: $N = 11$). (A) Group differences (BPD > HC) in the strength of single-trial EEG/fMRI correlations at (A.1) early latency and (A.2) late latency and contrast estimates with 90 % confidence intervals at left (L) ACC. Images are displayed with uncorrected $p < .001$ and $k = 10$ for display purposes. Images are displayed in neurological order. The color bar indicates t-scores (0–5.46). anterior cingulate cortex: ACC
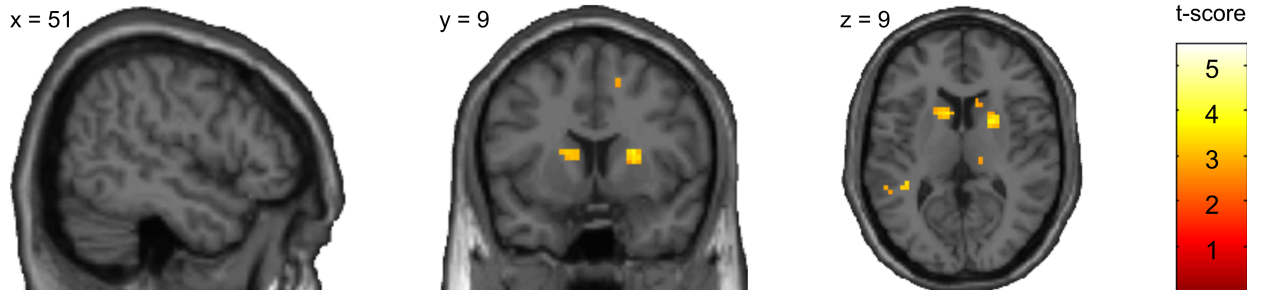
4.2.5.3. Borderline Personality Disorder vs. Attention-Deficit/Hyperactivity Disorder

Unimodal fMRI group comparison (BPD > ADHD) of task-related activity revealed significantly reduced cortical activity in ADHD in ACC (Figure 4.6.B; Table 4.6.B). Multimodal EEG/fMRI group comparison in the subgroups revealed significantly stronger correlations of both IC-regressors in fronto-subcortical (ACC, IFG/insula, caudate nuclei, putamen and left pallidum) regions of inhibitory control in BPD (Table 4.8). At the early latency, stronger correlations in BPD were found in left frontal areas (IFG/insula, superior frontal/medial gyrus) and temporo-parietal regions (Figure 4.6.A.1) while at the late latency stronger correlations were found in pre-SMA (Figure 4.6.A.2).

4.2.6. Time-window shifts around the early latency range

To test whether early processing of response inhibition is affected in ADHD patients or whether it is just temporally shifted and thus not detected by our regressors, we shifted the early latency range in steps of 20 ms from 120 ms to 280 ms as starting points and $RT - 80$ ms to $RT + 80$ ms as ending points (Figure 4.7). Grand average topographies of ICs selected from these different time-windows pointed towards altered early information processing in ADHD patients rather than towards information processing shifted in time.

Figure 4.6 *(next page)* Activation maps displaying results of group comparisons of Borderline Personality Disorder (BPD) vs.Attention-Deficit/Hyperactivity Disorder (ADHD) as assessed by single-trial EEG/fMRI analysis in the subgroups (BPD: $N = 11$; ADHD: $N = 12$) and unimodal fMRI analysis in the whole group (BPD: $N = 19$; ADHD: $N = 19$). (A) Group differences (BPD > ADHD) in the strength of single-trial EEG/fMRI correlations at (A.1) early latency and (A.2) late latency. (B) Group differences (BPD > ADHD) in task-related activity during 'correct Nogo−Go' as assessed by unimodal fMRI analysis. Images are displayed with uncorrected $p < .001$ and $k = 10$ for display purposes. Images are displayed in neurological order. The color bar indicates t-scores (0–5.46).

A) Single-trial EEG/fMRI: Group comparison (BPD (N = 11) > ADHD (N = 12))

A.1) Early latency (*p*<.001)
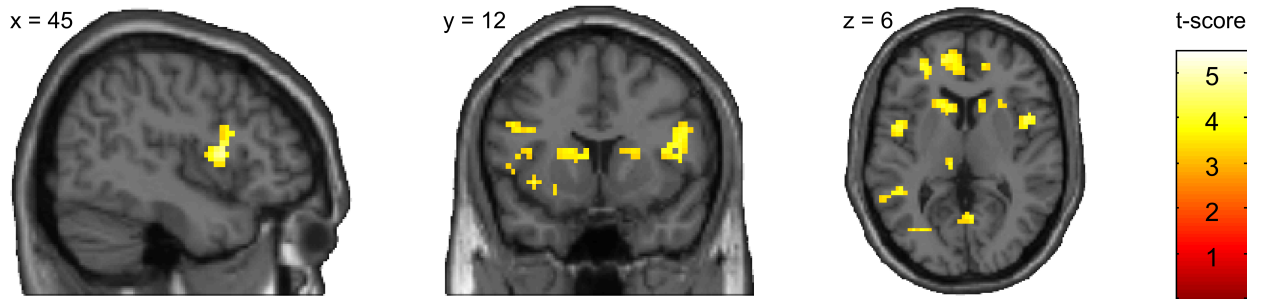
Early latency: 200 ms after stimulus onset
until individual median Go RT
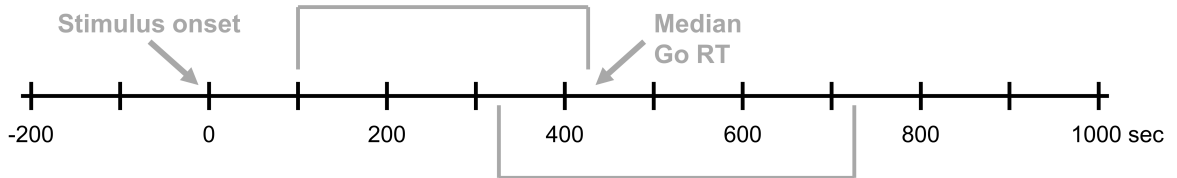
late latency: 100 ms prior to individual median Go RT
until 300 ms after individual median Go RT

A.2) Late latency (*p*<.001)
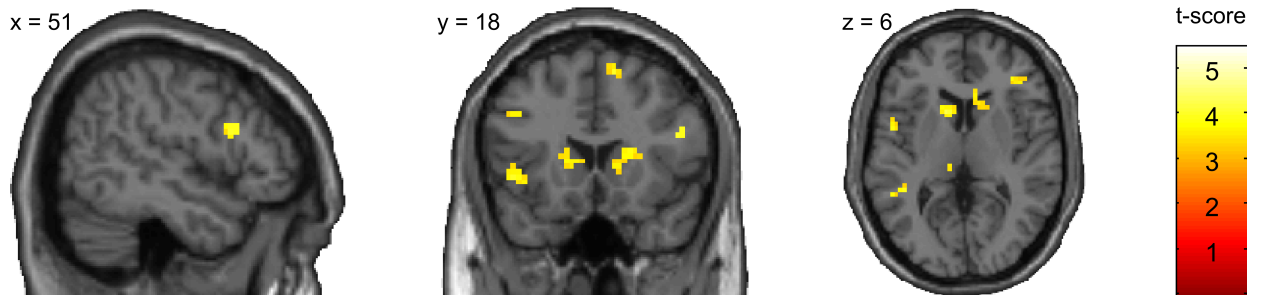
B) Unimodal fMRI: Group comparison (BPD (N = 19) > ADHD (N = 19), *p*<.001)
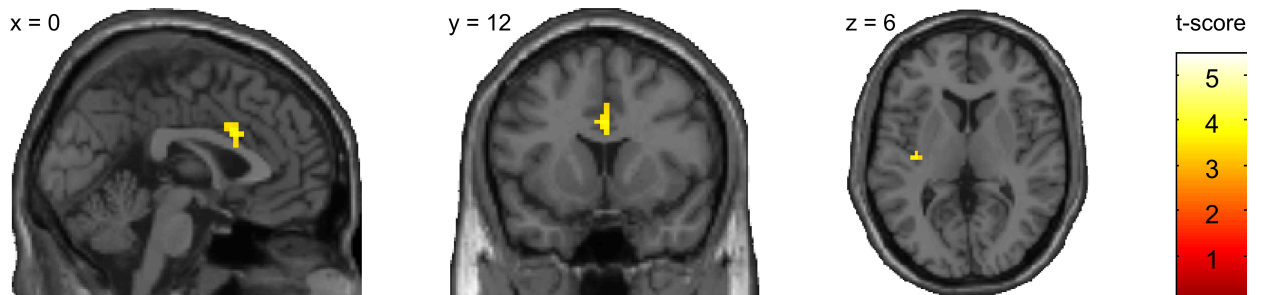
Table 4.6. Results of unimodal fMRI analysis in healthy control (HC) subjects, Attention-Deficit/Hyperactivity Disorder (ADHD) patients, and Borderline Personality Disorder (BPD) patients: Between group comparison of task-related activity in the whole groups.

Region	k	p	Z	x	y	z
A) HC > ADHD						
R Caudate Nucleus	192*	.005*	3,90	12	15	0
L Caudate Nucleus	161*	.007*	3,81	-9	3	6
L Putamen	75*	.017*	3,56	-15	12	-3
R Pallidum	23*	.028*	3,03	21	0	3
L Pallidum	10*	.011*	3,37	-18	-3	6
B) BPD > ADHD						
Anterior Cingulate Cortex (ACC)	733*	.040*	3,54	0	12	30

Note: The region in which the cluster's local maximum is located in Montreal Neurological Institute (MNI) coordinates (x, y, z) for the contrast 'correct Nogo−Go' with associated z-score ($p_{(FWE)} < .05$, cluster level corrected; *small volume corrected, $p_{(FWE)} < .05$) and cluster extend in number of voxels (k). FWE: family-wise error. R: right. L: left. C: central. ACC: anterior cingulate cortex HC: healthy control ($N = 31$). ADHD: Attention-Deficit/Hyperactivity Disorder ($N = 19$). BPD: Borderline Personality Disorder ($N = 19$).

Table 4.7. Results of multimodal fMRI analysis in healthy control (HC) subjects and Borderline Personality Disorder (BPD) patients: Between group comparisons of correlations of fMRI signal with early and late IC-regressors.

BPD > HC	early						Late					
Region	k	p	Z	x	y	z	k	p	Z	x	y	z
Cingulum												
L anterior cingulate cortex (ACC)	-	-	-	-	-	-	447*	.014*	4.04	-6	39	15

Note: The region in which the cluster's local maximum is located in Montreal Neurological Institute (MNI) coordinates (x, y, z) for early (time window starting 200 ms after stimulus onset and ending with the individual median Go response time (RT)) and late (time window starting 100 ms prior to RT and ending 300 ms after RT) with associated Z score ($p_{(FWE)} < .05$, cluster level corrected; *small volume corrected, $p_{(FWE)} < .05$) and cluster extend in number of voxels (k). FWE: family-wise error. L: left. ACC: anterior cingulate cortex. HC: healthy control ($N = 21$). BPD: Borderline Personality Disorder ($N = 11$).

Table 4.8. Results of multimodal fMRI analysis in Borderline Personality Disorder (BPD) patients and Attention-Deficit/Hyperactivity Disorder (ADHD) patients): Between group comparisons of correlations of fMRI signal with early and late IC-regressors.

BPD > ADHD	early						Late					
Region	k	p	Z	x	y	z	k	p	Z	x	y	z
Frontal												
L Mid. Frontal G.; L Sup. Medial G.; L/R ACC	203	<.001	4.14	-27	42	9	-	-	-	-	-	-
L IFG (pars Orbitalis; pars Opercularis); L Rolandic Operculum; L Insula	154	<.001	5.00	-24	18	-9	-	-	-	-	-	-
R IFG (pars Opercularis; pars Triangularis); R Caudate Nucleus; R Putamen	164	<.001	4.51	48	9	9	187*	.044*	3.55	51	12	24
L IFG (pars Opercularis)	196*	.011*	3.88	-48	3	6	161*	.014*	3.82	-51	6	9
L IFG (pars Opercularis)							11*	.044*	3.47	-45	18	33
L Sup. Frontal G.	63	.015	4.22	-18	-6	57						
R Pre-SMA	-	-	-	-	-	-	161*	.033*	3.73	12	18	57
Cingulum												
L/R ACC	590*	.012*	4.09	-6	39	15	487*	.037*	3.77	6	27	27
Subcortical												
R Caudate Nucleus	168*	.020*	3.69	12	18	3	182*	.017*	3.75	21	15	12
L Caudate Nucleus	48	.044	4.00	-9	15	9	57	.023	4.12	-9	12	9
R Putamen; L Caudate Nucleus	178*	.024*	3.64	24	9	12	52	.033	4	24	9	12
L Putamen	156*	.002*	4.36	-21	18	-9	101*	.042*	3.45	-33	0	-6
L Pallidum	1*	.021*	3.21	-12	-3	0	1*	.001*	4.06	-12	-3	0
Temporal												
L Mid. Temporal G.; L Sup. Temporal G.	49	.040	3.76	-45	-42	9	-	-	-	-	-	-
Parietal												
L PCC; L Precuneus	55	.026	4.19	-3	-42	18	-	-	-	-	-	-
Occipital												
R Linual G.; L Calcarine G.	57	.023	3.84	6	-63	3	-	-	-	-	-	-

Note: The region in which the cluster's local maximum is located in Montreal Neurological Institute (MNI) coordinates (x, y, z) for early (time window starting 200 ms after stimulus onset and ending with the individual median Go response time (RT)) and late (time window starting 100 ms prior to RT and ending 300 ms after RT) with associated Z score ($p_{(\text{FWE})} < .05$, cluster level corrected; *small volume corrected, $p_{(\text{FWE})} < .05$) and cluster extend in number of voxels (k). FWE: family-wise error. R: right. L: left. IFG: inferior frontal gyurs. pre-SMA: pre-supplementary motor area. ACC: anterior cingulate cortex. PCC: posterior cingulate cortex. Sup: superior. Mid: middle. Inf: inferior. G: gyrus. ADHD: Attention-Deficit/Hyperactivity Disorder ($N = 12$). BPD: Borderline Personality Disorder ($N = 11$).
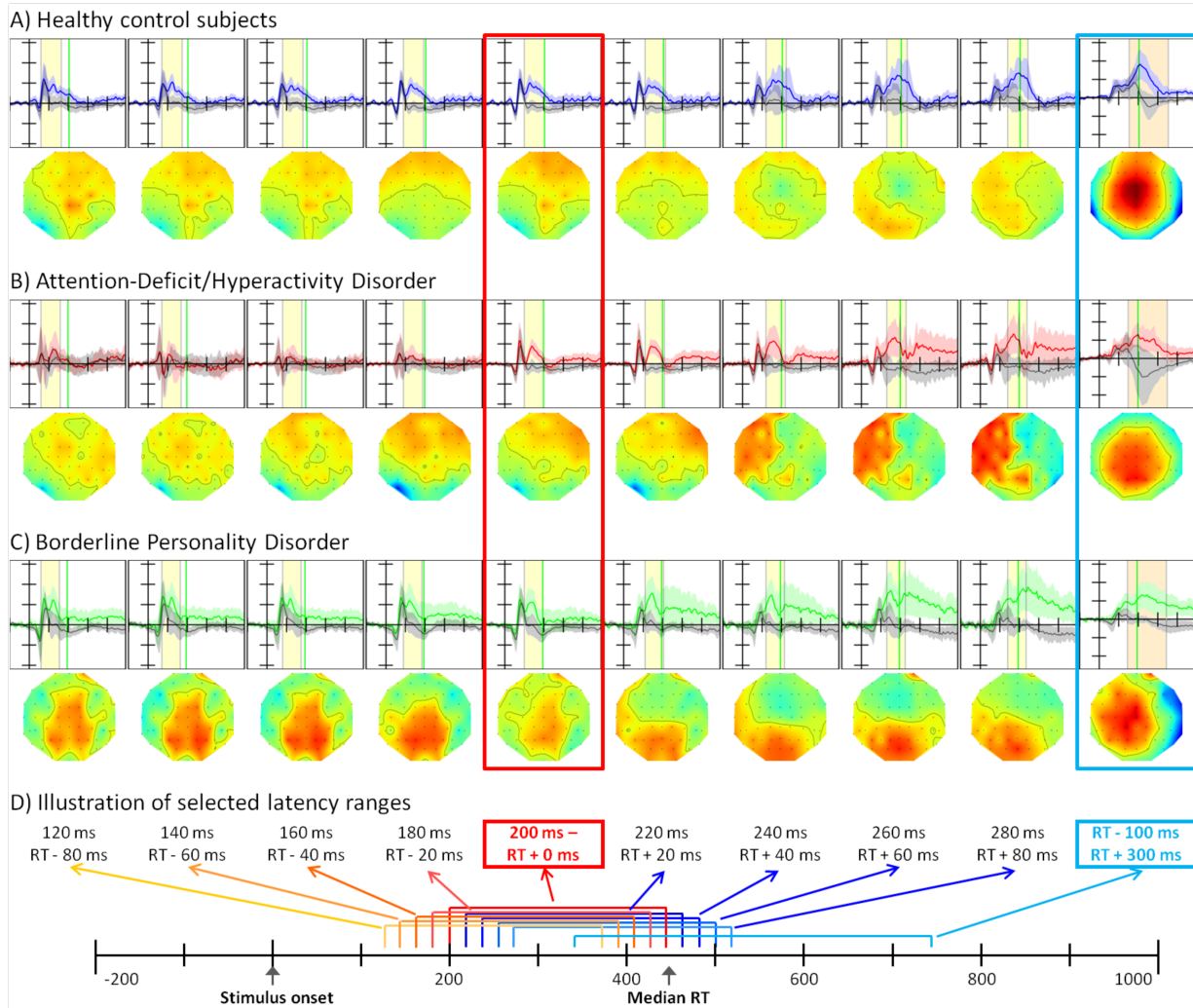
Figure 4.7. Independent component (IC) activation grand averages and related grand mean topographies of all subjects' ICs which were classified as reliably Nogo-related within ten different latency ranges. The first nine time windows were defined according to the early latency range (starting 200 ms after stimulus onset and ending with individual's median Go response time (RT), marked by the red box), but with borders shifted for −80 ms, −60 ms, −40 ms, −20 ms, 0 ms, +20 ms, +40 ms, +60 ms, and +80 ms; the last time window (starting 100 ms prior to the individual's median RT and ending 300 ms after the individual's median Go response time (RT), marked by the blue box) corresponds to the late latency range. (A) Healthy controls (HC, $N = 21$). (B) Attention-Deficit/Hyperactivity Disorder (ADHD, $N = 12$). (C) Borderline Personality Disorder (BPD, $N = 11$).

4.3. Discussion

In contrast to usually marginal findings of unimodal fMRI analysis, multimodal single-trial EEG/fMRI analysis revealed reduced activity in ADHD but not in BPD in the fronto-striatal response inhibition network. Group differences between ADHD and HC were strongest at an early stage of response inhibition, suggesting that critical regions of the cortical neural response inhibition network in adult ADHD are not locally impaired, but that the timing of the neural network is hindered.

ADHD but not BPD patients made significantly more omission errors, which corresponds with often reported enhanced omission error rates in adult ADHD (Dibbets et al., 2009; Morein-Zamir et al., 2014; Sebastian et al., 2012; Woltering et al., 2013) but not in adult BPD (Sebastian et al., 2013b). Increased intra-individual RT variability as it was found in both groups has been proposed as a candidate for an endophenotypic trait of ADHD (Noreika et al., 2013; Valera et al., 2010) and might be related to subclinical ADHD symptoms in BPD patients or indicative of a shared impulsivity trait. Although striatal hypoactivation in ADHD as assessed by unimodal fMRI is consistent with previous studies, it does not tie in with expectations of concurrent dysfunctions in frontal areas as it is known from children and adolescents with ADHD (Hart et al., 2013).

On the other hand, our combined EEG/fMRI analysis along with Karch and colleagues (Karch et al., 2014) indicated that regional frontal cortical dysfunction in childhood ADHD may convert to deficits in temporal orchestration of the neural response inhibition network in adult ADHD. Intriguingly, results of a group by latency range interaction indicated that HC subjects showed an expected relative activity decrease from early to late inhibition stages in bilateral IFG/insula, whereas ADHD patients had a delayed relative activity increase. Between-group comparisons revealed reduced correlations in the fronto-striatal impulse control network in ADHD especially at the early latency. This suggests that early cortical processing of response inhibition is impaired in ADHD, resulting in an overall reduced activity in basal ganglia as it can be detected by unimodal fMRI data analysis.

In contrast to this, unimodal fMRI analysis revealed no differences between BPD and HC, while multimodal analysis revealed stronger correlation only in left ACC in BPD at the later latency, supporting the growing evidence for a, if at all, mildly affected neural impulse control network in BPD (van Eijk et al., 2015; Krause-Utz et al., 2014; Sebastian et al., 2013b). While comparisons of both patient groups on unimodal fMRI level revealed enhanced activity in ACC in BPD, multimodal group comparison yielded significantly stronger correlations at both latencies in fronto-striatal regions in BPD compared to ADHD. Taken together this may indicate that specifically early processing of response inhibition is impaired in ADHD, while in BPD the network seems to be activated in a slightly exaggerated manner.

Reduced Nogo-P3 amplitudes in both patient groups compared to HC as well as the lack of significant differences between Go-N2 and Nogo-N2 in ADHD and BPD hints at globally, though potentially not inhibition specific, altered neural processing in both groups. In line with the suggestion that N2 and P3 might reflect task-independent higher-level processing stages (Huster et al., 2013), reduced P3 amplitudes might result from deficits at earlier processing stages. Our multimodal fMRI analysis as well as a recent study on voluntary decisions in ADHD (Karch et al., 2014) thus indicate that in ADHD, deficits in executive functioning are caused by dysfunctions in neural timing of inhibitory control networks.

In addition, grand average topographies of ICs selected from time-window shifts around the early latency range pointed toward disturbed or altered information processing in ADHD patients in the early but not the late latency. This is another observation which indicates that response inhibition deficits in ADHD are rather due to dysfunctions in neural timing of inhibitory control networks than due to static focal or regional neural activity deficits. Deficits in the temporal domain of neural processing in ADHD have been described recently for other cognitive functions (Karch et al., 2014). Similarly, it has already been suggested that inhibitory control deficits may be caused by sensorimotor timing disturbances in ADHD (Noreika et al., 2013; Rubia et al., 2009a; Valera et al., 2010) and that deficits in inhibitory control and behavioral temporal processing are both related to dopamine dysregulation (Aron et al., 2003b; Brown et al., 2009; Rubia et al., 2014b). In line with this, we suggest that the observed timing deficits on the neuronal level of inhibitory control in ADHD are strongly related to neurocognitive timing deficits, possibly caused by imprecise neural synchronization on the striatal level and by dopaminergic imbalances.

Limitations: Findings of multimodal analysis may be limited to subpopulations, characterized by the existence of Nogo-related ICs detectable at the chosen threshold. However, the same algorithm is able to detect ICs related to visual processing (as demonstrated in Study 1, Chapter 3, Schmüser et al., 2014), which argues against a principal failure of the algorithm. Thus, since there are equal distributions of Nogo-related ICs detectability present across ADHD, BPD and HC, the finding that certain Nogo-related ICs are not present in every subject may give an indication of substantial inter-individual trait differences in neurocognitive strategy while performing the task. This emphasizes that both, EEG and fMRI data analysis should take into account that both intra-individual variability and inter-individual differences may have an impact on group analyses across modalities.

Conclusion: To the best of our knowledge this is the first multimodal study assessing the temporal evolution of the neural impulse control network in ADHD compared to another impulsive patient population (i.e., the BPD group) as well as compared to HC subjects. Multimodal analysis allowed specifically assessing whether only certain temporally distinct phases of neural processing are affected in a patient group. While the results of unimodal and multimodal analyses in BPD

patients compared to HC subjects support the notion of a largely unaffected neural impulse control network in BPD patients, this was not true for ADHD patients.

Employing automated, inhibitory control specific single-trial analysis we were able to reveal that in ADHD key regions of the neural impulse control network are not activated on time. With respect to the known behavioral deficits in the temporal domain which have been linked to the impulsivity trait in ADHD (Noreika et al., 2013; Rubia et al., 2009a; Valera et al., 2010), the present data suggest that this is also reflected on the neural level in terms of neural timing deficits. This may provide a new route into the pathomechanism of inhibitory control deficits in ADHD.

5. Study 3: Data-driven analysis of simultaneous EEG/fMRI reveals neurophysiological phenotypes of impulse control (Schmüser et al., 2016, published)

As demonstrated in Study 1 (cf. Chapter 3), the spatio-temporal dynamics of the neural underpinnings of response inhibition can be assessed by using single-trial correlations of inhibition-related electrophysiological (EEG) independent components (ICs) with functional magnetic resonance imaging (fMRI) blood oxygenation level-dependent (BOLD) responses. Furthermore, as demonstrated in Study 2 (cf. Chapter 4), applying single-trial EEG/fMRI analysis allows to increase sensitivity for inter-individual differences by incorporating intra-individual variability. This allowed to assess the neural processing at distinct phases of response inhibition in adult Attention-Deficit/Hyperactivity Disorder (ADHD) patients and Borderline Personality Disorder (BPD) patients compared to healthy control (HC) subjects.

Thus, incorporating EEG data into fMRI data analysis allows the analysis of trial-to-trial neural variability. Based on that, it also allows for detailed inter-individual difference analysis, which can be used to classify neurocognitive differences in inter-individual neural variability. E.g., across all investigated groups the required reliability of inhibition-related ICs was attained only in about half of the subjects confirming inter-individual difference in an electrophysiological correlate of response inhibition based on intra-individual variability. Thus, as this finding was stable irrespective of the groups' background—HC subjects, ADHD patients, or BPD patients—this may suggest the existence of electrophysiologically dissociable phenotypes of behavioral and neural motor response inhibition. Thus, in this study these potential phenotypic groups in HC subjects are further characterized and compared using behavioral and neuropsychiatric measures as well as unimodal and multimodal event-related potential (ERP)/fMRI data (Schmüser et al., 2016).

Importantly, using an approach sensitive to inter-individual differences allows for subgroup classification and hence to identify and characterize the neural correlates of inter-individual differences in response inhibition in healthy individuals. This in turn may provide important information for our understanding of deficits in response inhibition in heterogeneous psychiatric disorders such as ADHD or BPD.

5.1. Material and methods

5.1.1. Participants

38 healthy subjects (15 males; mean age: 37.34 ± 16.0) were included in this analysis (Figure 5.1). Subjects were recruited from a larger sample (cf. Section 2.1.1 *'Participants'* for a detailed information on participant samples) on the basis of good overall data quality for EEG and fMRI.
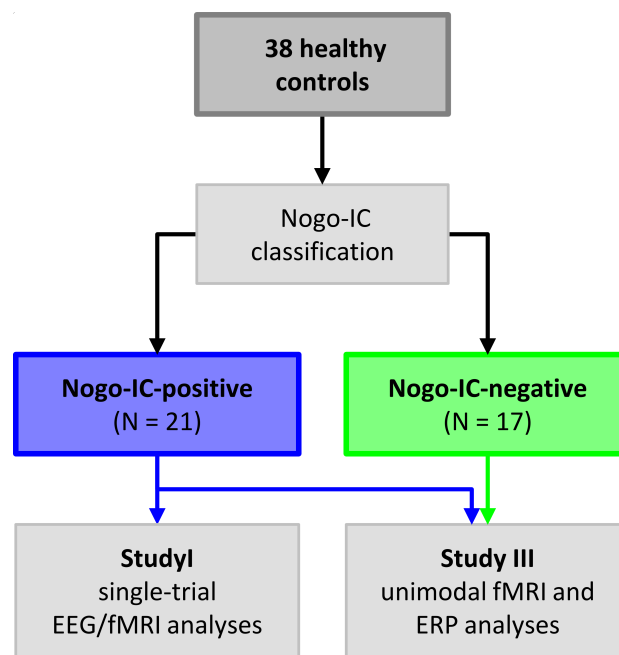
Figure 5.1. Group selection in healthy control subjects.

5.1.1.1. Group selection:

Based on automated IC-classification (cf. Section 2.4.1, *'Classification and selection of Nogo-related ICs'*) the initial group of 38 subjects was split into two subgroups: Nogo-IC-positive (in short: IC+, $N = 21$, 7 males, mean age: 35.00 ± 14.6) and Nogo-IC-negative (in short: IC−, $N = 17$, 8+males, mean age: 40.24 ± 17.6). Subgroups were defined on electrophysiological level using the existence or absence of specific ICs related to Nogo processing at an early latency located prior to the individual's median Go response time (RT) as group separator.

5.1.2. Data analysis

5.1.2.1. Unimodal fMRI group analysis

Beta images corresponding to the correct Nogo vs. Go contrast (correct Nogo−Go) were subjected to a two-sample t-test for independent groups comparing IC+ subjects against IC− subjects. Task-related brain activation as well as differential brain activation between groups (IC+ vs. IC−) was initially examined with a whole brain analysis. This allows to assess global brain activations irrespective of *a priori* defined regions of interest (ROIs).

For whole brain analysis, multiple comparisons correction of the statistical maps was based on cluster-extent based thresholding (Friston et al., 1994b; Woo et al., 2014) using a primary voxel-level threshold of $p < .001$ and an minimum cluster-extend level of $k = 10$ continuous voxels. This yielded a cluster-level corrected significance of $p_{(FWE)} < .05$ (family-wise error (FWE) correction for multiple comparisons). We chose a minimum cluster-extend level of 10 continuous voxels to avoid false positives by small but high peak voxel activity.

In addition to this whole brain analysis, small volume correction was performed in *a priori* predefined ROIs in order to test specifically for brain activity in areas associated with response inhibition (Aron, 2007; Aron and Poldrack, 2006; Sebastian et al., 2013a). In this context, voxel-wise test of significance was performed using the small volume correction toolbox within SPM8 which allows accounting for the multiple comparison problem within the selected ROI. Peak-wise significance was assessed by using a height threshold of $p_{(FWE)} < .05$ (FWE corrected) after using a primary voxel-level threshold of $p < .05$ and no minimum cluster-extend level.

The following ROIs were defined based on atlas-based masks as derived from the automated anatomical labeling (AAL) atlas: pars opercularis of the lateral inferior frontal gyurs (IFG), pre-supplementary motor area (pre-SMA) (derived from the supplementary motor area (SMA) region with $y > 0$), caudate nucleus, putamen and pallidum, subthalamic nucleus (STN) consisting of two boxes of respectively 10 mm^3 box at Montreal Neurological Institute (MNI) coordinates $-/+10, -15, -5$, inferior parietal lobule and superior parietal lobule (Sebastian et al., 2013a).

5.1.2.2. Unimodal ERP analysis

N2 and P3 amplitudes were measured as the mean amplitude in the time windows 240–350 ms (N2), and 350–580 ms (P3) after stimulus onset at nine selected electrode sites: F3, Fz, F4, C3, Cz, C4, P3, Pz, and P4. To assess group differences in Go and Nogo-related effects, N2 and P3 amplitude and latency values were subjected to separate repeated measures analysis of variance (ANOVA) including within-subject factors Condition (correct Go, correct Nogo), Anteriorization (frontal (F3, Fz, F4), central (C3, Cz, C4), parietal (P3, Pz, P4)), and Laterality (left (F3, C3, P3), midline

(Fz, Cz, Pz), right (F4, C4, P4)) as well as between-subject factor Group (IC+, IC−). In case of nonsphericity as indicated by a significant Mauchly test the corrected p-values and degree of freedom (DF)-values (Greenhouse-Geisser epsilon correction) are reported.

As the study was focused on group differences, only significant main effects as well as significant two-way interactions effects including Group as factor were further assessed with post hoc t-tests (Tukey multiple comparisons of means with 95 % family-wise confidence level). All three-way significant effects involving the factor Group were analyzed post-hoc by applying second ANOVA models and post-hoc t-tests. Statistical analysis was performed using the packages 'stats' (R Core Team, 2014) and 'ez' (Lawrence, 2013) from the open-source statistical computing software 'R' (http://CRAN.R-project.org/).

5.1.2.3. Single-trial EEG/fMRI analysis

Extraction of N2/P3 single-trial information: As described in Section 2.4.3 (*'Classification and selection of N2/P3 ERPs'*), for each subject, the N2 and P3 ERP components were quantified at the same latency ranges as it was used for unimodal ERP statistic (N2: 240–350 ms after stimulus onset. P3: 350–580 ms after stimulus onset). N2 was measured from electrode F4 while P3 was quantified at electrode Cz where the most pronounced Nogo-N2/-P3 effects across all subjects were expected. Visual inspection of grand averages as well as statistical comparisons based on an omnibus ANOVA (calculated separately on the amplitude values of N2 and P3 extracted from the nine electrode sites used for unimodal ERP analysis) confirmed that Nogo amplitudes where significantly different from Go amplitudes in the grand averages at these electrode sites. However, while the largest Nogo−Go differences at the N2 latency was clearly allocated to F4, at the P3 latency Nogo−Go differences were present at all electrode sites (cf. Table 5.1).

Thus, P3 was quantified at a fronto-central electrode site in accordance with most EEG literature (Baumeister et al., 2014; Huster et al., 2013; Karch et al., 2014; Wessel and Aron, 2015). This is also in compliance with findings from neuroimaging and some electrophysiological studies which suggest to expect a lateral right inferior prefrontal cortical source for the inhibition-related N2 component in contrast to a more central cortical source for the P3 component (Aron, 2007; Aron and Poldrack, 2006; Bokura et al., 2001; Fisher et al., 2011; Lavric et al., 2004; Sebastian et al., 2013a, 2015).

Thus, N2 was measured as the mean amplitude in the time window 240–350 ms after stimulus onset at the frontal-lateral electrode F4, whereas P3 was measured as the mean amplitude between 350 and 580 ms after stimulus at the central electrode Cz. Mean amplitudes of each single trial were extracted from the N2 and P3 latency ranges, combined into individual regressors and included into fMRI first-level analysis. For each subject and time window (i.e., ERP component N2 or P3)

the two contrast images belonging to the first and the second run of the task were averaged prior to group analysis resulting in one contrast image per subject and ERP component, i.e., N2 and P3.

Table 5.1. Results of ANOVAs on the main effect of task condition (Go and Nogo) on event-related potential (ERP) amplitudes at 9 selected electrode site: computed separately for amplitudes of N2 and P3 ERPs across Nogo-IC-positive and Nogo-IC-negative subjects.

Electrode site	N2 amplitude			P3 amplitudes		
	Std.Error	*t*-value	*p*-value	Std.Error	*t*-value	*p*-value
F4	0.82	-2.186	**.032**	0.71	-4.348	**<.001**
Fz	0.87	-1.717	.090	0.78	-5.145	**<.001**
F3	0.93	-1.998	.050	0.80	-4.748	**<.001**
C4	0.80	-1.154	.252	0.86	-3.863	**<.001**
Cz	0.95	-0.863	.391	0.79	-6.169	**<.001**
C3	0.88	-1.680	.097	0.74	-6.853	**<.001**
P4	0.81	-0.574	.568	0.67	-5.438	**<.001**
Pz	0.93	-1.003	.319	0.77	-6.429	**<.001**
P3	0.88	-0.520	.605	0.68	-6.635	**<.001**

Note: Main effect of Condition (correct Go, correct Nogo) on N2 amplitudes and P3 amplitudes across all subjects as assessed by separate measures analysis of variance (ANOVA). With within-subject factor Condition (correct Go, correct Nogo) and between-subject factor Group (Nogo-IC-positive (IC+), Nogo-IC-negative (IC−)). Std. Error: standard error. N2: 240–350 ms after stimulus onset. P3: 350–580 ms after stimulus onset.

Single-trial EEG/fMRI group analysis: Single trial correlations of fMRI BOLD responses with electrophysiological regressors derived from N2 and P3 ERP single-trial amplitude values were tested for group-specific significance using paired *t*-test for each group independently. To test for group differences, beta images corresponding to single-trial EEG/fMRI correlations with either N2 or P3 regressors were subjected to a full-factorial repeated measures model with within-subject factor Latency (N2, P3) and between-subject factor Group (IC+, IC−). As this study aimed at testing for functional group differences in neural activity related to different phases of response inhibition and not in the effects exclusively driven by the electrophysiological regressors, the full factorial model was fitted with ERP-regressors, which were non-orthogonalized with respect to classical onset regressors (Go, Nogo, Errors).

Similar to the group unimodal fMRI analysis, whole brain analysis was used to examine global brain activations irrespective of *a priori* defined ROIs. Whole brain results were corrected at the cluster level using a height threshold of $p < .05$ (FWE corrected) using a primary voxel-level threshold of $p < .001$ and a minimum cluster-extend level of $k = 10$ continuous voxels. Additionally, small-volume correction was performed for *a priori* defined ROIs located in brain areas associated with response inhibition (Aron, 2007; Aron and Poldrack, 2006; Sebastian et al., 2013a). Thus

small volume correction was used for the same predefined ROIs as described in the section of unimodal fMRI group analysis and assessed for peak-wise significance by using a height threshold of $p_{(\text{FWE})} < .05$ based on a primary voxel-level threshold of $p < .05$ and no minimum cluster-extend level.

5.2. Results

5.2.1. Demographics and Task Performance

Both groups did not differ significantly with respect to age, gender and verbal intelligence as measured by the German multiple-choice vocabulary test (MWT-B) (Table 5.2). The IC+ group was characterized by a shorter RT, lower coefficient of variability (CoV), i.e., intra-individual variability of RT as well as by reduced error rates (commission error and omission error). However, group differences were only statistically significant regarding the CoV rate of RT and reached trend level for the omission error rate (Table 5.2).

Table 5.2. Group comparison of demographic and performance data in Nogo-IC-positive and Nogo-IC-negative subjects.

	IC+		IC−		Group comp.	
	mean	SD	mean	SD	t	p
Demographic						
Age	35.00	14.6	40.24	17.6	1.00	n.s.
MWT-B	30.71	3.5	30.76	3.8	0.00	n.s.
Gender	7/21		8/17			
Performance						
RT [ms]	408.24	45.2	431.24	66.0	1.62	n.s.
Commission errors [%]	10.19	8.2	12.19	10.0	0.46	n.s.
Omission errors [%]	0.19	0.3	1.21	2.5	3.56	.067
CoV	0.195	0.04	0.224	0.05	4.16	.049

Note: Demographic data regarding age in years and intelligence as measured with German multiple-choice vocabulary test (MWT-B, sum score). Behavioral data regarding mean Go response time (RT) in milliseconds (ms), coefficient of variability (CoV) of RTs, mean percentage [%] omission errors of Go trials and mean percentage [%] of commission errors of Nogo trials. CoV is estimated by dividing SD of RT by mean RT. Percentage error is estimated by dividing the number of incorrect trials (Go for omission error and Nogo for commission error) by the total number of each trial type. Gender (male/N): ratio of number of males and sample size. IC+: Nogo-IC-positive. IC−: Nogo-IC-negative. SD: standard deviation. n.s.: not significant ($p > .1$).

5.2.2. Psychometrics

As depicted in Table 5.3, group differences were significant or reached a trend level of significance on the subscales of questionnaires on self-rated impulsive personality traits, i.e., Barratt Impulsiveness Scale-11 (BIS-11) and Sensation Seeking Scale (SSS-V) as well as on the questionnaires used for clinical ratings regarding ADHD symptoms in childhood, i.e., Wender Utah Rating Scale (WURS-k), and ADHD symptoms in adulthood, i.e., Conners' Adult ADHD Rating Scale (CAARS-S:L). The IC− group was characterized by enhanced ratings on the subscales assessing motor impulsivity and hyperactivity (BIS-11 subscales: 'motor impulsiveness' and 'non-planning impulsiveness'; CAARS-S:L subscales: 'hyperactivity/restlessness', 'impulsivity/emotional lability', and 'DSM-IV hyperactive-impulsive symptoms') but also by higher rating on the boredom/sensation seeking domain (SSS-V subscales: 'experience seeking', and 'boredom susceptibility') and enhanced ratings on retrospective and current ADHD symptoms (CAARS-S:L: 'DSM-IV ADHD symptoms total', and WURS-k).

Table 5.3. Group comparison of psychometric data in Nogo-IC-positive and Nogo-IC-negative subjects.

	IC+		IC−		Group comp.	
	mean	SD	mean	SD	t	p
BIS-11						
Attentional impulsiveness	13.24	3.0	13.75	1.8	0.35	n.s.
Motor impulsiveness	20.19	3.0	22.75	4.9	3.87	.057
Non-planning impulsiveness	21.14	3.9	23.50	3.8	3.39	.074
UPPS						
Premeditation	22.57	4.0	23.56	4.4	0.51	n.s.
Urgency	37.90	4.0	37.50	4.6	0.08	n.s.
Sensation seeking	28.38	6.2	26.88	6.4	0.52	n.s.
Perseverance	16.33	3.6	16.63	3.6	0.06	n.s.
SSS-V						
Thrill and adventure seeking	6.24	2.6	6.56	2.7	0.13	n.s.
Disinhibition	2.81	2.1	3.69	2.1	1.63	n.s.
Experience seeking	5.86	1.8	7.19	1.9	4.65	.038
Boredom susceptibility	1.57	1.2	3.56	2.2	12.47	.001

Note: Neuropsychological data with self-ratings regarding impulsivity (BIS-11: Barratt Impulsiveness Scale-11, UPPS: UPPS Impulsive Behavior Scale, SSS-V: Sensation Seeking Scale). Gender (male/N): ratio of number of males and sample size. IC+: Nogo-IC-positive. IC−: Nogo-IC-negative. SD: standard deviation. n.s.: not significant ($p > .1$).

Table 5.3. Continuation: Group comparison of psychometric data in the whole groups and subgroups.

	IC+		IC−		Group comp.	
	mean	SD	mean	SD	t	p
CAARS-S:L						
Inattention/memory problems	42.00	6.5	45.06	5.6	2.33	n.s.
Hyperactivity/restlessness	42.14	5.7	46.41	7.6	3.97	.054
Impulsivity/emotional lability	40.10	4.8	42.94	5.0	3.13	.085
Problems with self-concept	41.67	3.8	43.35	3.3	2.06	n.s.
DSM-IV inattentive symptoms	40.86	7.5	45.12	7.7	2.98	.093
DSM-IV hyperactive-impulsive symptoms	37.19	4.7	42.06	9.5	4.27	.046
DSM-IV ADHD symptoms total	37.43	6.4	43.12	8.7	5.43	.026
ADHD index	39.48	6.2	42.82	7.3	2.35	n.s.
WURS-k						
WURS	7.21	5.0	11.44	8.9	3.15	.085
BPDSI						
BPDSI	0.66	0.7	0.68	0.6	0.00	n.s.
BDI						
BDI	1.22	1.9	1.88	3.6	0.46	n.s.
MADRS						
MADRS	0.15	0.5	0.41	1.0	1.07	n.s.

Note: Neuropsychological data with self-ratings regarding impulsivity (BIS-11: Barratt Impulsiveness Scale-11, UPPS: UPPS Impulsive Behavior Scale, SSS-V: Sensation Seeking Scale), clinical ratings regarding childhood ADHD symptoms (WURS-k: Wender Utah Rating Scale, [total score]) and current ADHD symptoms (CAARS-S:L: Conners' Adult ADHD Rating Scale, [t-value])), clinical assessment of the frequency and severity of manifestations of BPD (BPDSI: Borderline Personality Disorder Severity Index), and the clinical rating (MADRS: Montgomery Asberg Depression Scale) and self-rating (BDI: Beck Depression Inventory) of current depressive mood. Gender (male/N): ratio of number of males and sample size. IC+: Nogo-IC-positive. IC−: Nogo-IC-negative. ADHD: Attention-Deficit/Hyperactivity Disorder. BPD: Borderline Personality Disorder. SD: standard deviation. n.s.: not significant ($p > .1$).

5.2.3. Unimodal fMRI analysis

Group specific task related activation in IC+ and IC− groups are shown in Figure 5.2 rows A and B. Between group comparison of task related activation is shown in Figure 5.2 row C.

5.2.3.1. Unimodal fMRI: Group specific task related activation

Side-by-side comparison revealed overlapping but also different regions of task-related activation in both groups (Table 5.4). However, in the IC− group the activated network appeared to be extended. Significant task-related activation was found in both groups in frontal areas including SMA/pre-SMA, a cluster stretching from left precentral gyrus to left superior and middle frontal gyrus, and in bilateral posterior medial frontal cortex. Further congruent cortical activity was found in right middle temporal gyrus, right superior parietal lobule and left middle occipital gyrus.

Subcortically, both groups displayed task-related activity in a cluster in left putamen, which was in IC− subjects extended to the pars opercularis of left posterior IFG. In IC− subjects only, significant task-related cortical activation was found in bilateral posterior IFG (pars opercularis)/insula, a cluster enclosing right superior/middle temporal gyrus and right supramarginal gyrus, and clusters in left inferior and superior parietal lobule. Subcortically, IC− subjects also displayed significant task-related activity in right caudate nucleus, right pallidum and right putamen extended to right posterior IFG (pars opercularis)/insula.

5.2.3.2. Unimodal fMRI: Between group comparison of task related activation

Between group comparisons as revealed by t-tests for independent samples are listed in Table 5.5. Group comparison of the contrast 'correct Nogo−Go' revealed significantly more activation in posterior IFG (pars opercularis)/insula (significant in left IFG and on trend level in right IFG) and left putamen/insula in IC− subjects compared to IC+ subjects at the predefined threshold of $p < .05$ (FWE corrected).
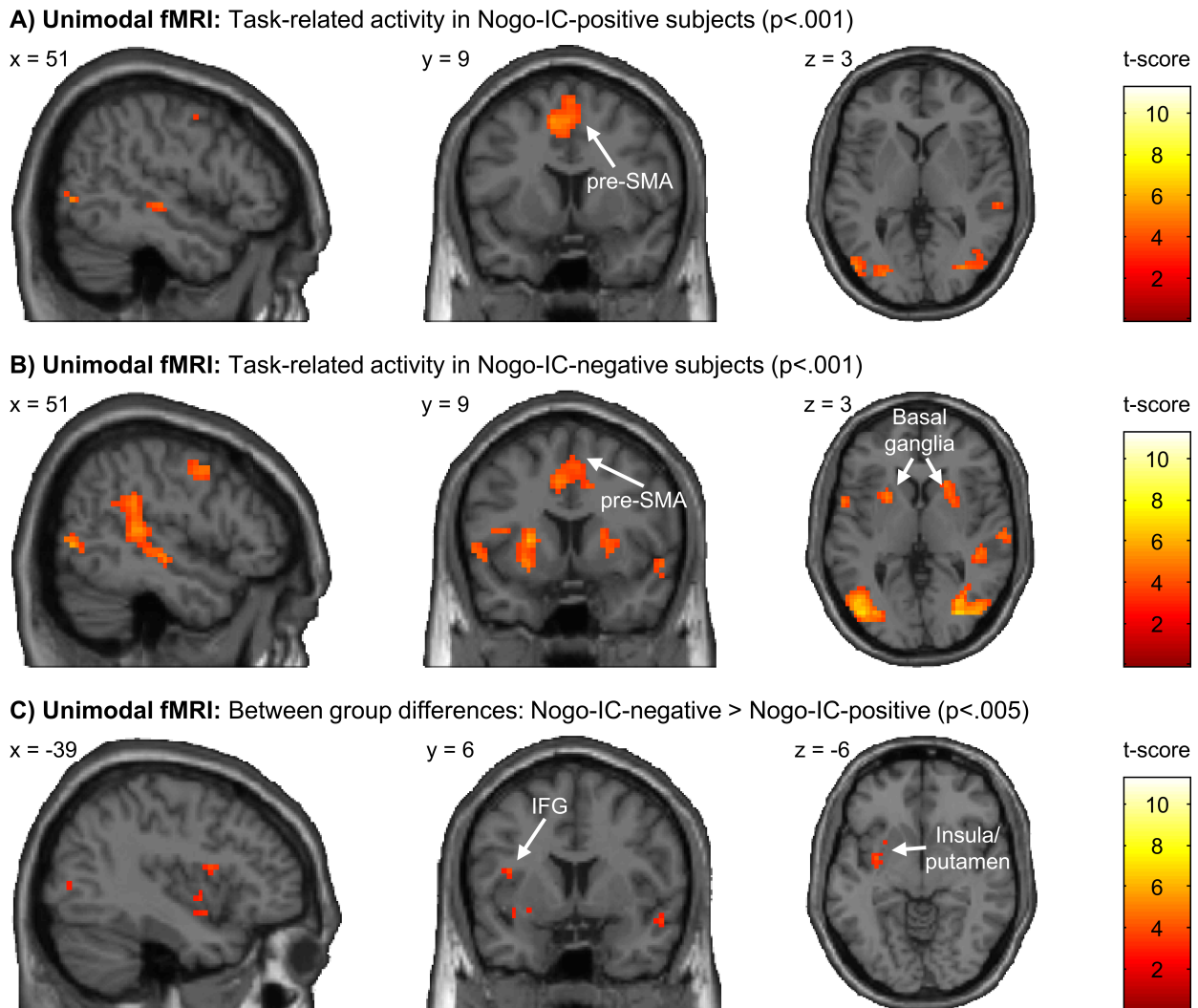
Figure 5.2. Unimodal fMRI: Activation maps displaying task-related activity during 'correct Nogo−Go' as assessed by unimodal fMRI analysis. A) Task-related activity in Nogo-IC-positive (IC+) subjects. B) Task-related activity in Nogo-IC-negative (IC−) subjects. C) Results of between group differences (IC− > IC+). Images of task-related activity are displayed at $p < .001$ (uncorrected) and $k = 10$ for display purposes. Images of between group comparisons are displayed at $p < .005$ (uncorrected) and $k = 10$ for display purposes. The color bar indicates t-scores (0–11.24). IFG: inferior frontal gyurs. pre-SMA: pre-supplementary motor area. Adopted from (Schmüser et al., 2016).

Table 5.4. Unimodal fMRI: Task-related activity in Nogo-IC-positive and Nogo-IC-negative subjects.

Region	Nogo-IC-positive (IC+)						Nogo-IC-negative (IC−)					
	k	p	Z	x	y	z	k	p	Z	x	y	z
Frontal												
R IFG (pars Opercularis)	-	-	-	-	-	-	94*	.018*	3.81	39	15	12
L IFG (pars Opercularis)	-	-	-	-	-	-	76*	.027*	3.61	-39	9	12
pre-SMA	259*	<.001*	4.80	-6	3	57	235*	<.001*	4.95	6	3	63
IC+: L/R Post.-medial frontal/**IC−:** L/R Post.-medial frontal; R Mid./Sup. Frontal G.; R Precentral G.; L MCC	285	<.001	5.46	6	0	66	502	<.001	5.27	6	0	63
IC+: L Precentral G.; L Sup. Frontal G.; L Mid. Frontal G./**IC−:** L Precentral G.; L Mid. Frontal G.	78	.008	4.24	-42	-3	51	138	<.001	4.85	-42	-3	48
Subcortical												
R Caudate Nucleus	-	-	-	-	-	-	119*	.009*	3.92	21	21	3
R Putamen; R IFG (pars Opercularis)	-	-	-	-	-	-	121	.001	4.06	21	18	3
R Putamen	-	-	-	-	-	-	182*	.010*	3.90	24	15	0
IC+: L Putamen/**IC−:** L Putamen; L IFG (pars Opercularis)	87*	.029*	3.56	-24	9	6	112	.001	5.02	-24	9	6
R Pallidum	-	-	-	-	-	-	13*	.034*	2.99	21	0	6
Temporal												
R Sup. Temporal G.; R Mid. Temporal G.; R Supramarginal G.	-	-	-	-	-	-	342	<.001	4.55	51	-36	9
IC+: R Mid. Temporal G.; R Sup. Occipital G.; R Mid. Occipital G./**IC−:** R Mid. Temporal G.; R Mid. Occipital G.; R Cuneus	107	.002	5.27	48	-72	0	274	<.001	5.69	48	-72	0
Parietal												
L Inf. Parietal Lob.	-	-	-	-	-	-	110*	.042*	3.69	-27	-51	54
L Sup. Parietal Lob.; L Inf. Parietal Lob.	-	-	-	-	-	-	50	.047	3.96	-21	-60	51
R Sup. Parietal Lob.	111*	.012*	3.86	33	-63	54	151*	.006*	4.01	21	-63	57
Occipital												
L Mid. Occipital G.	61	.023	4.79	-24	-87	6	224	<.001	5.59	-42	-78	0

Note: The region in which the cluster's local maximum is located in Montreal Neurological Institute (MNI) coordinates (x, y, z) for the contrast 'correct Nogo−Go' with associated Z score ($p_{(FWE)} < .05$, cluster level corrected; * small volume corrected, $p_{(FWE)} < .05$) and cluster extend in number of voxels (k). FWE: family-wise error. IFG: inferior frontal gyurs. ACC: anterior cingulate cortex. MCC: middle cingulate cortex. Sup: superior. Mid: Middle. Inf: Inferior. Post: Posterior. G: Gyrus. Lob.: Lobule. R: right. L: left.

Table 5.5. Unimodal fMRI: Between group comparison of task-related activity in Nogo-IC-positive subjects compared to Nogo-IC-negative subjects

	IC+ vs. IC−						IC− vs. IC+					
Region	k	p	Z	x	y	z	k	p	Z	x	y	z
Frontal												
L IFG (pars Opercularis)	-	-	-	-	-	-	42*	.049*	3.41	-39	6	15
Subcortical												
L Putamen/Insula	-	-	-	-	-	-	80*	.024*	3.62	-33	-3	-6

Note: The region in which the cluster's local maximum is located in Montreal Neurological Institute (MNI) coordinates (x, y, z) for the contrast 'correct Nogo−Go' with associated Z score ($p_{(FWE)} < .05$, cluster level corrected; * small volume corrected, $p_{(FWE)} < .05$) and cluster extend in number of voxels (k). IC+: Nogo-IC-positive. IC−: Nogo-IC-negative. FWE: family-wise error. IFG: inferior frontal gyurs. R: right. L: left.

5.2.4. Unimodal ERP Analysis

Figure 5.3 shows grand averages at two selected electrode sites and series of topographical maps plotted from 200–600 ms post-stimulus of Nogo- and Go-related ERPs. Table 5.6 and Table 5.7 present results of repeated measures ANOVA on amplitudes and latencies of N2 and P3 as extracted from nine electrode sites (F3, Fz, F4, C3, Cz, C4, P3, Pz, P4) with within subject factors Condition (correct Go, correct Nogo), Anteriorization (frontal (F3, Fz, F4), central (C3, Cz, C4), parietal (P3, Pz, P4)), and Laterality (left (F3, C3, P3), midline (Fz, Cz, Pz), right (F4, C4, P4)) as well as between-subject factor Group (IC+, IC−).

Figure 5.3 *(next page)* Nogo- and Go-related grand mean event-related potentials (ERPs) and topographic map series from 200–600 ms after stimulus onset, averaged from stimulus onsets in 21 Nogo-IC-positive subjects (IC+, blue) and 17 Nogo-IC-negative subjects (IC−, green). (A.1, A.2) show the time courses of Nogo-related ERPs at F4 (A.1) and at Cz (A.2). (A.3, A.4) show series of topographical maps related to Nogo condition in IC+ (A.3) and IC− (A.4) subjects, plotted every 50 ms from 200–600 ms after stimulus onset. (B.1, B.2) show the time courses of Go-related ERPs at F4 (B.1) and at Cz (B.2). (B.3, B.4) show series of topographical maps related to Go condition in IC+ (B.3) and IC− (B.4) subjects, plotted every 50 ms from 200–600 ms after stimulus onset. In A.1, A.2, B.1, and B.2: Mean (solid lines) and 95 % confidence interval (C.I., shaded areas) of IC+ (blue) and IC− (green) related waveforms; the black lines indicate the N2 latency at 240–350 ms after stimulus onset and P3 latency at 350–580 ms after stimulus onset. In A.3, A.4, B.3, and B.4: Black lines demark the zero line; black dots demark the positions of 62 scalp-electrodes. Adopted from (Schmüser et al., 2016).

A) Nogo-related potentials in Nogo-IC-positive (IC+) and Nogo-IC-negative (IC-) subjects

A.1) Grand averages at F4

A.3) Topographies (200 – 600 ms) in IC+ subjects

200 ms ⟶ 600 ms

A.2) Grand averages at Cz

A.4) Topographies (200–600ms) in IC- subjects

200 ms ⟶ 600 ms

IC+: mean   IC-: mean

IC+: 95% C.I.   IC-: 95% C.I.   -2.67 µV   +9.24 µV

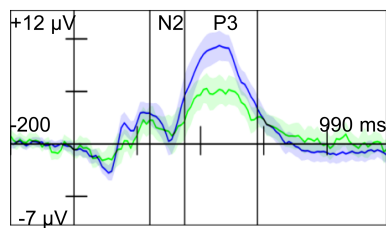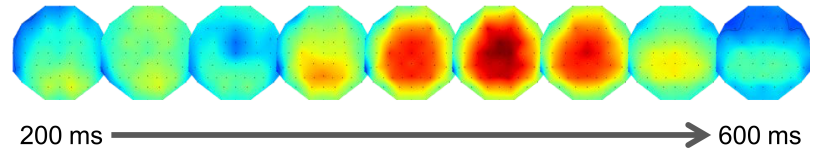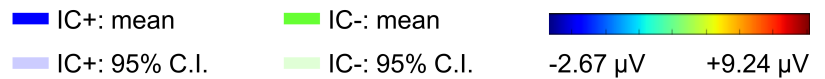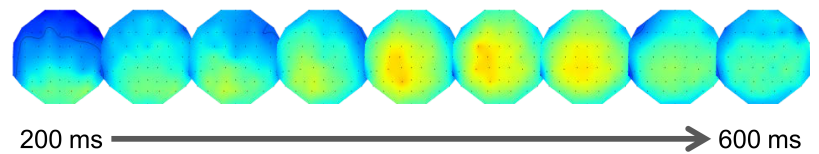## B) Go-related potentials in Nogo-IC-positive (IC+) and Nogo-IC-negative (IC-) subjects

B.1) Grand averages at F4

B.3) Topographies (200 – 600 ms) in IC+ subjects

200 ms ⟶ 600 ms
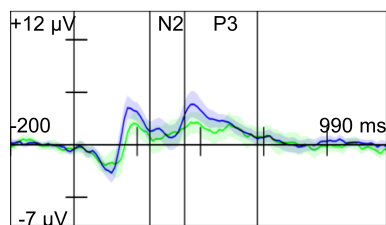
B.2) Grand averages at Cz

B.4) Topographies (200 – 600 ms) in IC- subjects

200 ms ⟶ 860 ms

IC+: mean   IC-: mean

IC+: 95% C.I.   IC-: 95% C.I.   -2.67 µV   +9.24 µV
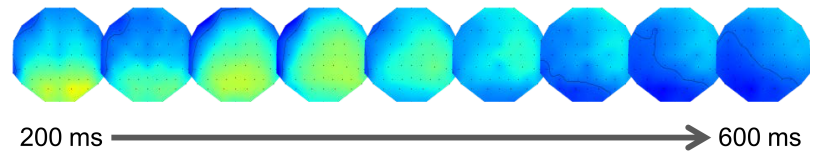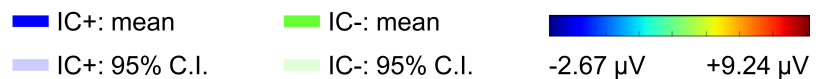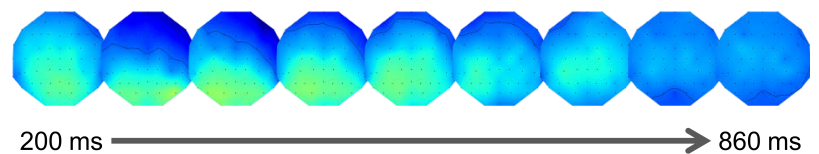
5.2.4.1. N2 (240–350 ms) amplitude and latency:

Significant main effects of condition but not of group was found for N2 amplitudes and latencies indicated that across both groups and all electrode sites, the N2 peaked later (Nogo−Go = 2.28 ms, $p = .001$) and with larger amplitudes (Nogo−Go = 1.08 µV, $p < .001$) in Nogo compared to Go condition ($F_{(amp)}(1, 36) = 19.96$, $p < .001$ and $F_{(lat)}(1, 36) = 5.76$, $p = .022$). Additionally, a significant main effect of anteriorization ($F(1.29, 46.30) = 18.10$, $p < .001$) indicated that across all groups and task conditions, the N2 amplitude was significantly more pronounced, i.e., showed the strongest negativity at frontal (1.20 µV) and central (1.81 µV) as compared to parietal (3.23 µV) electrode sites (frontal−parietal = −2.04 µV, $p < .001$; central−parietal = −1.43 µV, $p < .001$). There was no significant interaction effect involving the factor Group.

5.2.4.2. P3 (350–580 ms) amplitude and latency:

Significant main effects of condition but not of group on P3 amplitude and latency showed that across both groups and all electrode sites, the P3 peaked later (Nogo−Go = 7.23 ms, $p < .001$) and with larger amplitudes (Nogo−Go = 3.39 µV, $p < .001$) in Nogo compared to Go condition ($F_{(amp)}(1, 36) = 136.26$, $p < .001$ and $F_{(lat)}(1, 36) = 8.40$, $p = .006$).

Furthermore, a significant main effect of anteriorization on P3 amplitudes ($F(1.34, 48.09) = 8.44$, $p = .003$) and P3 latencies ($F(1.48, 53.11) = 7.30$, $p = .004$) indicated that across both groups and task conditions, the P3 amplitude was significantly more pronounced at central (3.61 µV) and parietal (3.71 µV) as compared to frontal (2.57 µV) electrode sites (frontal−central = −1.04 µV, $p < .001$; frontal−parietal = −1.14 µV, $p < .001$), and peaked significantly earlier at parietal electrodes (451.63 ms) compared to frontal (456.98 ms) electrode sites (frontal−parietal = 5.35 ms, $p = .005$). There was a significant interaction effect between group and task condition of P3 amplitude values ($F(1, 36) = 8.33$, $p = .007$). Post-hoc analysis of the interaction effect revealed significantly higher amplitudes in Nogo condition compared to Go condition in both groups (IC+: Nogo−Go = 4.14 µV, $p < .001$; IC−: Nogo−Go = 2.46 µV, $p < .001$) as well as significantly higher Nogo-P3 amplitudes in IC+ subjects compared to IC− subjects (Nogo-P3$_{IC+}$−Nogo-P3$_{IC-}$ = 2.29 µV, $p < .001$) and higher Nogo-P3 amplitudes in both groups compared to Go-P3 amplitudes in the other group (Nogo-P3$_{IC+}$−Go-P3$_{IC-}$ = 4.74 µV, $p < .001$; Nogo-P3$_{IC-}$−Go-P3$_{IC+}$ = 1.85 µV, $p < .001$). There was no further significant interaction effect involving the factor Group.

Table 5.6. Results of separate repeated measures ANOVAs on amplitudes and latencies of N2 (240–350 ms) ERPs in Nogo-IC-positive and Nogo-IC-negative subjects.

Effect	N2 Amplitude				N2 Latency			
	DF	MT	F	p	DF	MT	F	p
Group	1, 36	-	1.10	n.s.	1, 36	-	0.04	n.s.
Condition	1, 36	-	19.96	$<.001$	1, 36	-	5.76	.022
Anteriorization	1.29, 46.30	*	18.10	$<.001$	1.57, 56.63	*	2.81	.081
Laterality	1.44, 51.73	*	0.81	n.s.	1.66, 59.74	*	0.20	n.s.
Group × Condition	1, 36	-	0.06	n.s.	1, 36	-	0.64	n.s.
Group × Anteriorization	1.29, 46.30	*	0.58	n.s.	1.57, 56.63	*	0.23	n.s.
Group × Laterality	1.44, 51.73	*	2.56	n.s.	1.66, 59.74	*	0.80	n.s.
Condition × Anteriorization	1.22, 43.85	*	10.96	.001	1.61, 57.98	*	1.04	n.s.
Condition × Laterality	1.33, 47.89	*	0.59	n.s.	2, 72	-	1.87	n.s.
Anteriorization × Laterality	4, 144	-	4.12	.003	3.24, 116.55	*	2.51	.058
Group × Condition × Anteriorization	1.22, 43.85	*	0.11	n.s.	1.61, 57.98	*	0.52	n.s.
Group × Condition × Laterality	1.33, 47.89	*	0.08	n.s.	2, 72	-	0.90	n.s.
Group × Anteriorization × Laterality	4, 144	-	1.03	n.s.	3.24, 116.55	*	0.79	n.s.
Condition × Anteriorization × Laterality	3.22, 115.91	*	6.77	$<.001$	4, 144	-	2.14	.079
Group × Condition × Anteriorization × Laterality	3.22, 115.91	*	0.78	n.s.	4, 144	-	0.86	n.s.

Note: Main and interaction effects of separate repeated measures analysis of variance (ANOVA) on N2 amplitudes and latency values with within-subject factors Condition (correct Go, correct Nogo), Anteriorization (frontal (F3, Fz, F4), central (C3, Cz, C4), parietal (P3, Pz, P4)), and Laterality (left (F3, C3, P3), midline (Fz, Cz, Pz), right (F4, C4, P4)) and between-subject factor Group (Nogo-IC-positive, Nogo-IC-negative). In case of nonsphericity as indicated by a significant Mauchly test (MT: *) the corrected p-values and DF-values (Greenhouse-Geisser epsilon correction) are reported. MT: Mauchly Test. * significant Mauchly Test. n.s.: not significant ($p > .1$). N2: 240–350 ms after stimulus onset.

Table 5.7. Results of separate repeated measures ANOVAs on amplitudes and latencies of P3 ERPs in Nogo-IC-positive and Nogo-IC-negative subjects.

Effect	P3 Amplitude				P3 Latency			
	DF	MT	*F*	*p*	DF	MT	*F*	*p*
Group	1, 36	-	7.44	.010	1, 36	-	0.83	n.s.
Condition	1, 36	-	136.26	<.001	1, 36	-	8.40	.006
Anteriorization	1.34, 48.09	*	8.44	.003	1.48, 53.11	*	7.30	.004
Laterality	1.43, 51.56	*	1.62	n.s.	1.48, 53.36	*	0.02	n.s.
Group × Condition	1, 36	-	8.33	.007	1, 36	-	1.36	n.s.
Group × Anteriorization	1.34, 48.09	*	0.09	n.s.	1.48, 53.11	*	1.91	n.s.
Group × Laterality	1.43, 51.56	*	2.15	n.s.	1.48, 53.36	*	0.73	n.s.
Condition × Anteriorization	1.15, 41.52	*	1.52	n.s.	1.50, 54.06	*	9.77	.001
Condition × Laterality	1.57, 56.53	*	8.68	.001	1.36, 49.12	*	0.57	n.s.
Anteriorization × Laterality	2.91, 104.74	*	2.99	.036	3.05, 109.79	*	1.03	n.s.
Group × Condition × Anteriorization	1.15, 41.52	*	0.76	n.s.	1.50, 54.06	*	0.12	n.s.
Group × Condition × Laterality	1.57, 56.53	*	1.16	n.s.	1.36, 49.12	*	1.63	n.s.
Group × Anteriorization × Laterality	2.91, 104.74	*	0.16	n.s.	3.05, 109.79	*	1.06	n.s.
Condition × Anteriorization × Laterality	4, 144	-	3.33	.012	4, 144	-	0.53	n.s.
Group × Condition × Anteriorization × Laterality	4, 144	-	1.43	n.s.	4, 144	-	0.99	n.s.

Note: Main and interaction effects of separate repeated measures analysis of variance (ANOVA) on P3 amplitudes and latency values with within-subject factors Condition (correct Go, correct Nogo), Anteriorization (frontal (F3, Fz, F4), central (C3, Cz, C4), parietal (P3, Pz, P4)), and Laterality (left (F3, C3, P3), midline (Fz, Cz, Pz), right (F4, C4, P4)) and between-subject factor Group (Nogo-IC-positive, Nogo-IC-negative). In case of nonsphericity as indicated by a significant Mauchly test (MT: *) the corrected *p*-values and DF-values (Greenhouse-Geisser epsilon correction) are reported. MT: Mauchly Test. * significant Mauchly Test. n.s.: not significant ($p > .1$). P3: 350–580 ms after stimulus onset.

5.2.5. N2/P3-ERP Single-trial EEG/fMRI analysis

5.2.5.1. Group specific correlations with ERP-regressors

Results of group specific correlations with ERP-regressors as revealed by within-group paired t-tests are listed in Table 5.8 (IC−) and in Table 5.9 (IC+). Single-trial fluctuations of electrophysiological activity as derived from the latency ranges N2 (240–350 ms post-stimulus) at F4 site and P3 (350–580 ms post-stimulus) at Cz site correlated positively with several cortical and subcortical regions in both groups (Figure 5.4).

Single-trial correlations with ERP-regressors revealed widespread activity in cortical and subcortical regions, especially at the N2 latency range in IC+ subjects. Correlations exclusively with the N2 regressor were found in IC+ subjects in bilateral frontal areas (including left posterior IFG/insula, anterior cingulate cortex (ACC), bilateral dorsolateral and ventrolateral prefrontal cortices), bilateral putamen, bilateral temporal and parietal areas (Table 5.9), while in IC− subjects (Table 5.8) positive correlations exclusively with the N2 regressor were found in left temporal gyrus and right parietal lobule. Significant positive correlations with both ERP-regressors were found in both groups in pre-SMA, and left caudate nucleus. Additionally, in IC− subjects both ERP-regressors correlated positively with left medial frontal cortex, bilateral ACC, and left middle temporal gyrus, while in IC+ subjects further correlations with both ERP-regressors were found in right basal ganglia (putamen and caudate nucleus), right posterior IFG (pars opercularis)/insula, and bilateral parietal lobule.

Furthermore, correlations with the P3 but not the N2 ERP-regressor were found in IC+ subjects in right IFG (pars triangularis and pars opercularis), bilateral posterior-medial frontal cortex, left middle cingulate cortex (MCC) as well as left temporal and parietal areas, and bilateral middle occipital areas. While the strength of positive correlations is decreasing from N2- to P3-associated neural activity in IC+ subjects, more positive correlations with P3 compared to the N2 regressor was found in IC− subjects. This included frontal areas such as bilateral posterior IFG (pars opercularis)/insula, bilateral superior medial gyrus and a cluster enclosing left superior frontal/medial gyrus, right middle orbital gyrus and ACC as well as temporal areas (left hippocampus, left parahippocampus and right fusiform gyrus), left parietal areas enclosing precuneus, linual gyrus and inferior occipital gyrus, as well as bilateral occipital gyrus. Subcortically, the P3 but not the N2 regressor correlated positively with the fMRI BOLD signal in right caudate nucleus and bilateral putamen in IC− subjects.

Table 5.9. Multimodal fMRI: Correlations of fMRI BOLD signal with ERP-regressors at N2 and P3 latency in Nogo-IC-positive subjects.

Region	N2 regressor						P3 regressor					
	k	p	Z	x	y	z	k	p	Z	x	y	z
Frontal												
L Sup. Frontal G.	41	.018	4.79	-18	63	21	-	-	-	-	-	-
R Mid. Frontal G.; R Sup. Frontal G.	42	.016	4.87	33	57	27	-	-	-	-	-	-
R Sup. Medial G.	32	.049	3.95	9	51	24	-	-	-	-	-	-
Pre-SMA	351*	<.001*	5.08	0	9	54	197*	.004*	4.38	-3	6	51
L IFG (pars Opercularis)	115*	<.001*	4.73	-33	6	27	-	-	-	-	-	-
R IFG (pars Opercularis)	253*	.001*	4.55	42	6	24	123*	.003*	4.32	45	9	27
R IFG (pars Triangularis); R IFG (pars Opercularis)	-	-	-	-	-	-	311	<.001	5.09	21	-30	30
L post.-medial frontal; R post.-medial frontal	-	-	-	-	-	-	54	.005	4.47	51	-63	-9
L Insula Lob.; L Putamen; L ACC	201	<.001	4.93	-9	24	3	-	-	-	-	-	-
Cingulum												
R ACC	667*	.008*	4.28	9	30	27	-	-	-	-	-	-
R MCC; R/L Mid. Frontal G.; R IFG (pars Triangularis); L IFG (pars Opercularis); L post.-medial frontal	1581	<.001	5.19	9	15	30	-	-	-	-	-	-
L MCC	-	-	-	-	-	-	36	.031	4.26	63	-27	15
Subcortical												
L Caudate Nucleus	34*	.003*	4.21	-12	24	3	-	-	-	-	-	-
R Putamen; R Insula Lob.; R Pallidum	32	.049	4.04	33	6	0	-	-	-	-	-	-
R Putamen	128*	.008*	4.04	33	6	0	94*	.005*	4.16	27	-12	3
R Caudate Nucleus	48*	.009*	3.99	18	3	18	9*	.029*	3.69	18	-15	21
L Caudate Nucleus	95*	<.001*	4.86	-21	-24	21	54*	<.001*	5.66	-21	-21	24
L STN	7*	.032*	3.02	-12	-12	-9	-	-	-	-	-	-

Note: IFG: inferior frontal gyurs. pre-SMA: pre-supplementary motor area. ACC: anterior cingulate cortex. MCC: middle cingulate cortex. Sup: superior. Mid: Middle. Inf: Inferior. Post: Posterior. G: Gyrus. Lob.: Lobule. R: right. L: left.

Table 5.9. Continuation: Correlations of fMRI BOLD signal with ERP-regressors at N2 and P3 latency in Nogo-IC-positive subjects.

Region	N2 regressor						P3 regressor					
	k	p	Z	x	y	z	k	p	Z	x	y	z
Temporal												
L Sup. Temporal G.; L Mid. Temporal G.	40	.020	4.35	-54	-24	9	-	-	-	-	-	-
R Sup. Temporal G.; R Postcentral G.; R Supramarginal G.	133	<.001	4.64	63	-27	15	-	-	-	-	-	-
L Fusiform G.; L Hippocampus	59	.003	4.49	-30	-39	-15	-	-	-	-	-	-
R Mid. Temporal G.; R Inf. Temporal G.	104	<.001	4.47	48	-42	-3	-	-	-	-	-	-
L Mid. Temporal G.	32	.049	4.24	-60	-54	0	-	-	-	-	-	-
R Inf. Temporal G.	-	-	-	-	-	-	123	<.001	4.72	57	27	18
R Sup. Temporal G.	-	-	-	-	-	-	80	<.001	4.38	-3	6	51
Parietal												
L Inf. Parietal Lob.	383*	<.001*	5.39	-45	-33	39	395*	<.001*	5.35	-45	-33	39
R Inf. Parietal Lob.	173*	.048*	3.63	27	-57	54	-	-	-	-	-	-
L Sup. Parietal Lob.	283*	.001*	4.68	-21	-63	42	235*	<.001*	5.39	-21	-63	42
R Sup. Parietal Lob.	130*	.003*	4.26	15	-72	51	153*	<.001*	4.78	27	-60	57
L Sup. Parietal Lob.; L Inf. Parietal Lob.; L Supramarginal G.	-	-	-	-	-	-	154	<.001	6.28	-15	-24	30
Occipital												
L Calcarine G.; L Postcentral G.; L Inf. Parietal Lob.; R Precuneus; L Sup./ Mid. Occipital G.; R Linual G.	1975	<.001	6.44	-15	-81	9	-	-	-	-	-	-
R Mid./Sup. Occipital G.; R Sup. Parietal Lob.; R Cuneus; R Mid. Temporal G.	-	-	-	-	-	-	38	.025	5.26	-6	27	0
L Mid./Sup. Occipital G.; R Linual G.; R Cuneus; R Calcarine G.; L Mid. Temporal G.	-	-	-	-	-	-	373	<.001	5.39	-21	-63	42

Note: The region in which the cluster's local maximum is located in Montreal Neurological Institute (MNI) coordinates (x, y, z) for N2 (240–350 ms after stimulus onset at F4 electrode site) and P3 (350–580 ms after stimulus onset at Cz electrode site) with associated Z score ($p_{(FWE)} < .05$, cluster level corrected; * small volume corrected, $p_{(FWE)} < .05$) and cluster extend in number of voxels (k). FWE: family-wise error. IFG: inferior frontal gyurs. pre-SMA: pre-supplementary motor area. ACC: anterior cingulate cortex. MCC: middle cingulate cortex. Sup: superior. Mid: Middle. Inf: Inferior. Post: Posterior. G: Gyrus. R: right. L: left.

A) Multimodal fMRI (N2 regressor): Positive correlations in Nogo-IC-positive subjects (p<.001)

B) Multimodal fMRI (N2 regressor): Positive correlations in Nogo-IC-negative subjects (p<.001)

C) Multimodal fMRI (P3 regressor): Positive correlations in Nogo-IC-positive subjects (p<.001)

D) Multimodal fMRI (P3 regressor): Positive correlations in Nogo-IC-negative subjects (p<.001)

Figure 5.4. Multimodal fMRI: Activation maps displaying the main effects of positive correlations with N2/P3 regressors in Nogo-IC-positive (IC+) (A.1 and A.2C) and in Nogo-IC-negative (IC−) subjects (B.1 and B.2D). Correlations with N2 single-trial amplitude values as derived from F4 at 280–340 ms after stimulus onset are shown in rows A.1 and B.1. Correlations with P3 single-trial amplitude values as derived from Cz at 350–580 ms after stimulus onset are shown in rows A.2C and B.2D. Images are displayed with $p < .001$ (uncorrected) and $k = 10$ for display purposes. The color bar indicates t-scores (0–11.24). Adopted from (Schmüser et al., 2016)

Table 5.8. Multimodal fMRI: Correlations of fMRI BOLD signal with ERP-regressors at N2 and P3 latency in Nogo-IC-negative subjects.

Region	N2 regressor						P3 regressor					
	k	p	Z	x	y	z	k	p	Z	x	y	z
Frontal												
L/R Sup. Medial G.	-	-	-	-	-	-	97	<.001	4.84	0	51	39
L Mid. Frontal G.; L Sup. Frontal G.	65	.001	4.27	-9	42	3	41	.016	4.39	-24	51	15
L Sup. Frontal G.; L Sup. Medial G.; L ACC; R Mid Orbital G.	-	-	-	-	-	-	209	<.001	4.96	-15	45	-6
Pre-SMA	25*	.028*	3.86	-12	18	63	176*	.001*	4.57	-6	15	63
R IFG (pars Opercularis)	-	-	-	-	-	-	39*	.025*	3.82	45	15	0
L IFG (pars Opercularis)	-	-	-	-	-	-	134*	.007*	3.99	-57	6	9
Cingulum												
R ACC	38	.022	4.05	21	36	9	58	.003	4.34	3	27	18
L ACC	353*	.008*	4.27	-9	42	3	376*	<.001*	4.96	-15	45	-6
L ACC	70	.001	4.95	-21	24	3	-	-	-	-	-	-
Subcortical												
L Caudate Nucleus	154*	.025*	3.73	-12	18	-6	97*	.002*	4.34	-18	9	18
R Caudate Nucleus	-	-	-	-	-	-	67*	.002*	4.33	21	6	21
R Putamen	-	-	-	-	-	-	73*	.028*	3.72	24	3	9
L Putamen	-	-	-	-	-	-	53*	.012*	3.91	-24	3	-9
Temporal												
L Hippocampus	-	-	-	-	-	-	127	<.001	4.59	-24	-15	-6
L Parahippocampal G.	-	-	-	-	-	-	37	.025	4.34	-18	-36	-12
L Medial Temporal Pole; L Mid. Temporal G.	52	.005	4.85	-45	9	-33	-	-	-	-	-	-
L Mid. Temporal G.	104	<.001	4.70	-57	-51	9	65	.001	4.92	-57	-51	9
R Fusiform G.	-	-	-	-	-	-	64	.001	4.90	30	-63	0
Parietal												
R Precuneus; R PCC; R Linual G.	36	.028	4.01	21	-42	0	-	-	-	-	-	-
L Precuneus; L Linual G.; L Inf. Occipital G.	-	-	-	-	-	-	294	<.001	5.10	-30	-69	21
Occipital												
L/R Calcarine G.; L Cuneus	-	-	-	-	-	-	47	.008	4.37	-3	-72	15
R Cuneus; R Sup. Occipital G.	-	-	-	-	-	-	69	.001	4.83	21	-90	9

Note: The region in which the cluster's local maximum is located in Montreal Neurological Institute (MNI) coordinates (x, y, z) for N2 (240–350 ms after stimulus onset at F4 electrode site) and P3 (350–580 ms after stimulus onset at Cz electrode site) with associated Z score ($p_{(FWE)} < .05$, cluster level corrected; * small volume corrected, $p_{(FWE)} < .05$) and cluster extend in number of voxels (k). FWE: family-wise error. IFG: inferior frontal gyurs. pre-SMA: pre-supplementary motor area. ACC: anterior cingulate cortex. MCC: middle cingulate cortex. Sup: superior. Mid: Middle. Inf: Inferior. Post: Posterior. G: Gyrus. R: right. L: left.
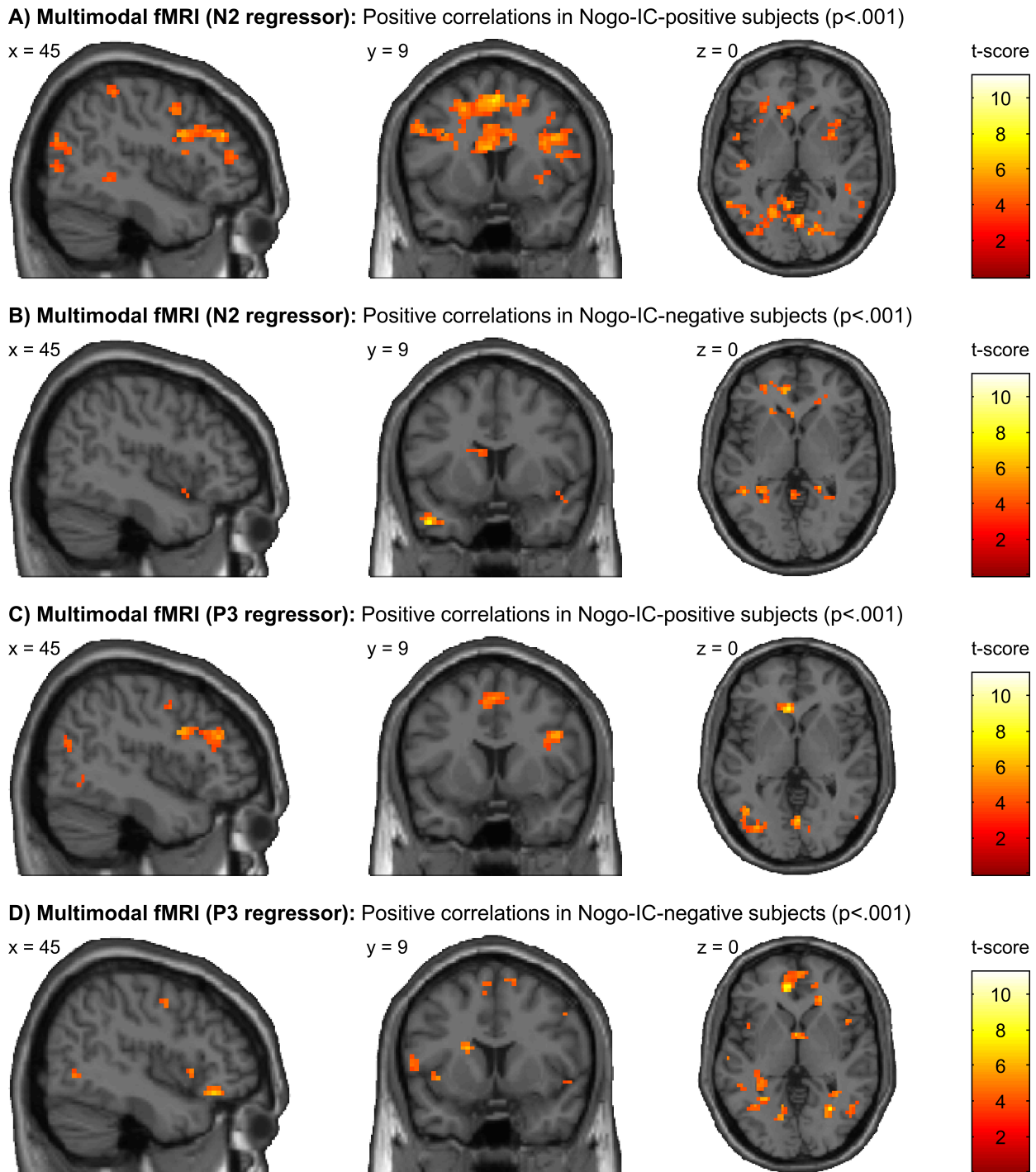
5.2.5.2. Between group comparisons of correlations with ERP-regressors

Results of between group comparisons as revealed by full factorial design are shown in Figure 5.5. As listed in Table 5.10, group comparison of full factorial single-trial correlations with N2/P3 ERP-regressors revealed significant group differences at the N2 and P3 latency. In IC+ subjects compared to IC− subjects, the N2 regressor correlated significantly stronger with right pre-SMA while the P3 regressor correlated significantly stronger with fMRI BOLD signal in right posterior IFG (pars opercularis)/insula. The inverse comparison (IC− > IC+) revealed no significant differences at the N2-latency and significantly stronger correlations of P3 regressor with the fMRI BOLD signal in a cluster located in pregenual ACC/left superior medial gyrus.

Table 5.10. Multimodal fMRI: Between group comparisons of correlations of fMRI BOLD signal with ERP-regressors at N2 and P3 latency in Nogo-IC-positive (IC+) subjects compared to Nogo-IC-negative (IC−) subjects.

Region	N2 regressor						P3 regressor					
	k	p	Z	x	y	z	k	p	Z	x	y	z
A) Nogo-IC-positive > Nogo-IC-negative												
Frontal												
R Pre-SMA	193*	.035*	3.72	3	9	51	-	-	-	-	-	-
R IFG (pars Opercularis)	-	-	-	-	-	-	65*	.028*	3.70	42	9	27
B) Nogo-IC-negative > Nogo-IC-positive												
Frontal												
L Sup. Medial G.; L pregenual ACC	-	-	-	-	-	-	61	.015	4.01	-6	57	9

Note: The region in which the cluster's local maximum is located in Montreal Neurological Institute (MNI) coordinates (x, y, z) for N2 (240–350 ms after stimulus onset at F4 electrode site) > P3 (350–580 ms after stimulus onset at Cz electrode site) and vice versa with associated Z score ($p_{(FWE)} < .05$, cluster level corrected; * small volume corrected, $p_{(FWE)} < .05$) and cluster extend in number of voxels (k). FWE: family-wise error. IFG: inferior frontal gyurs. pre-SMA: pre-supplementary motor area. ACC: anterior cingulate cortex. Sup: superior. G: Gyrus. R: right. L: left.
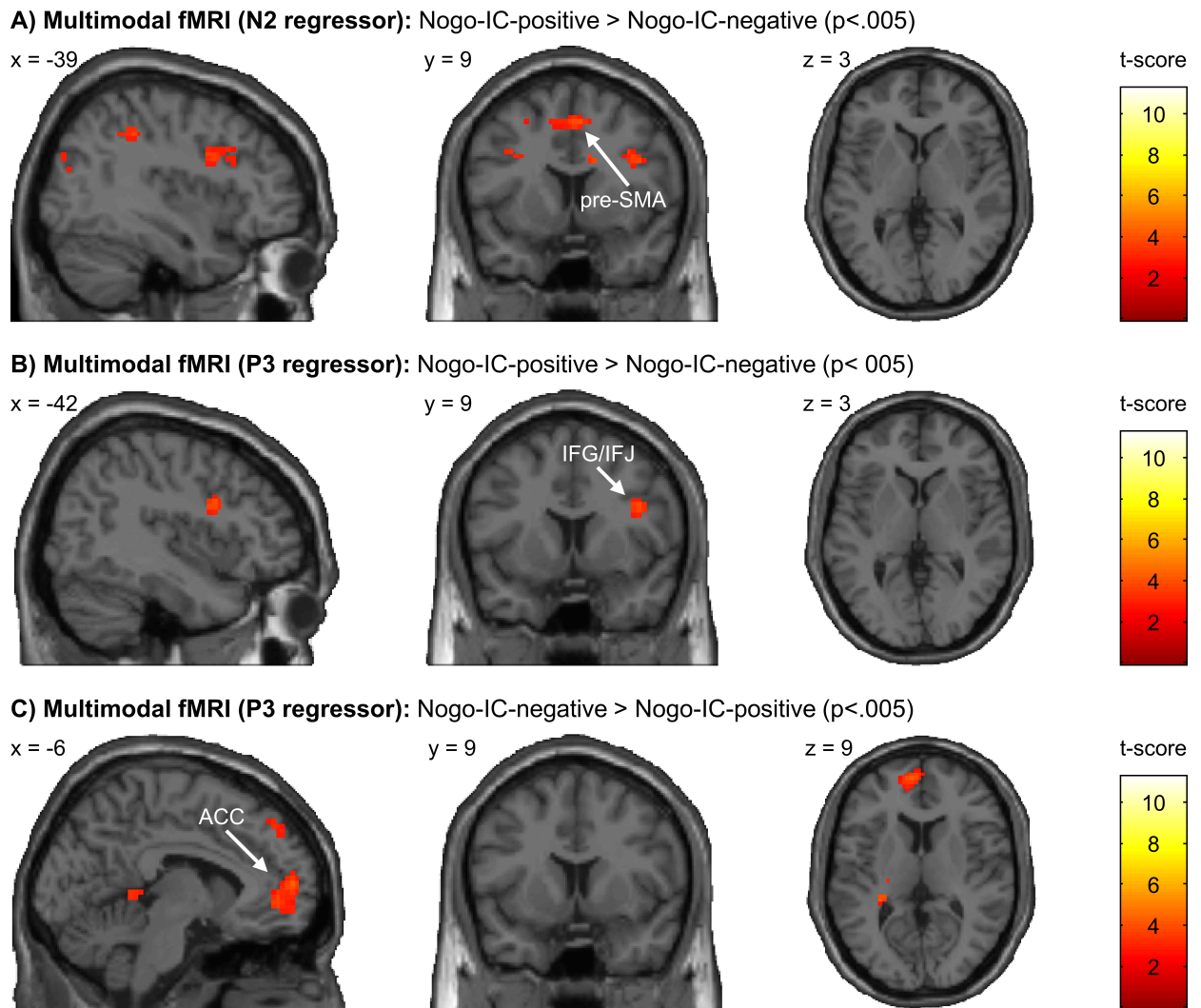
Figure 5.5. Multimodal fMRI: Activation maps displaying the results of comparing effects of positive correlations with N2/P3 regressors in Nogo-IC-positive (IC+) and in Nogo-IC-negative (IC−) subjects. A) Stronger correlations with N2 single-trial amplitude values (from F4 at 280–340 ms) in IC+ subjects relative to IC−. B) Stronger correlations with P3 single-trial amplitude values (from Cz at 350–580 ms) in IC+ subjects relative to IC−. C) Stronger correlations with N2 single-trial amplitude values (from F4 at 280–340 ms) in IC− subjects relative to IC+. Please note that the threshold for visualization is set at $p < .005$ ($k = 10$) level uncorrected for multiple comparisons for the purpose of presentation only. This may lead to the depiction of clusters that does not reach corrected significance levels, e.g., IFG/IFJ activity in (A) is in difference to (B) just not significant for multiple comparisons. The color bar indicates t-scores (0–11.24). ACC: anterior cingulate cortex. IFG: inferior frontal gyurs. IFJ: inferior frontal junction. pre-SMA: pre-supplementary motor area. Adopted from (Schmüser et al., 2016).

5.3. Discussion

In a group of 38 subjects, 21 subjects (Nogo-IC-positive, in short: IC+) were characterized by the existence of ICs related to Nogo in a latency range located prior to the individuals median Go response time (RT) whereas 17 subjects (Nogo-IC-negative, in short: IC−) were characterized by the absence of such early Nogo-related ICs. Although groups did not differ with respect to demographic characteristics, group comparisons revealed important differences on psychometric, behavioral and neurophysiological levels. This suggests the existence of electrophysiologically dissociable phenotypes of behavioral and neural motor response inhibition.

Psychometric and behavioral characteristics of IC− subjects indicate an impulsive personality trait that is to some degree comparable to adult ADHD. Findings of higher scores on subscales addressing motor impulsivity/hyperactivity and impulsive/non-planning characteristics as well as ADHD traits in IC− subjects but not on any other questionnaires complete the picture of a group of healthy subjects that is characterized by a more impulsive personality trait. In line with this, the IC− group was behaviorally also characterized by significant higher intra-individual CoV of RT and a trend towards higher omission error rates. This is strikingly similar to comparisons of adult ADHD patients with healthy control subjects, with increased intra-individual RT variability being hypothesized as a candidate for an intermediate endophenotypic trait of ADHD (e.g. Albrecht et al., 2013; Carmona et al., 2012; Epstein et al., 2011; Feige et al., 2013; Klein et al., 2006; Sebastian et al., 2012; Vaurio et al., 2009; for a review see Tamm et al., 2012).

In unimodal fMRI analysis, both groups displayed significant activations in typical regions of response inhibition network, though to different extents. These regions were the medial prefrontal areas (SMA/pre-SMA, posterior-medial gyrus, and precentral gyrus), left basal ganglia (putamen), and tempo-parietal regions (middle/superior temporal gyri and right superior parietal lobule). In the IC+ group significant activations were restricted to these regions, while the IC− group showed a more distributed network with additional significant clusters of activation in bilateral posterior IFG (pars opercularis)/insula and right basal ganglia (caudate nucleus, putamen, and pallidum). These group differences were further supported by significant between-group differences (IC− > IC+) in left IFG and left putamen/insula in ROI analysis, suggesting that IC− subjects might have additionally recruited these regions to successfully solve the Go/Nogo task. Thus, together with the differences in RT and error rates, these results suggest that both groups used a neural response inhibition network differing mainly in activation extent which may be due to increased behavioral (here increased CoV) and thus neural variance in responses. Increased extent in activation in IC− subjects could then be necessary compensatory activity to maintain a comparable level of inhibitory control compared to IC+ subjects. As others also found additional or potentially overactive recruitment of neural resources in more impulsive subjects compared to less impulsive subjects (Chester and DeWall, 2014; Collins et al., 2012; Horn et al., 2003), our finding of increased extent in activation of left IFG and left putamen/insula regions in higher impulsive

(= IC−) subjects may hint as well to an overactive (Chester and DeWall, 2014) or compensatory (Collins et al., 2012) neural activity in left hemispheric fronto-striatal regions while less impulsive subjects (= IC+) have access to an effective impulse control network that is well orchestrated and thus requires less neural sources.

In accordance with this assumption, single-trial correlations with N2/P3 regressors revealed stronger activations in response inhibition and attention network in the low impulsive group. In contrast to this, the high impulsive group was characterized by enhanced activity in the more affective, pregenual ACC possibly indicating overactivity or compensatory activity in IC− subjects. The activation pattern revealed by single-trial correlation with N2/P3 ERP-regressors in IC+ subjects resembled a mixture of networks related to response inhibition and the ventral attention system, which is in line with the notion that in addition to inhibitory control mechanisms the Go/Nogo task might also trigger processes related to response selection and selective attention (Mostofsky and Simmonds, 2008; Stahl et al., 2014). In contrast to this the activation pattern in the IC− group seems to be a mixture of inhibitory control and medial prefrontal evaluative and limbic system. Medial prefrontal activity in higher impulsive subjects during inhibitory control paradigms have been linked to an interaction of motivational aspects and cognitive processing (Horn et al., 2003). When comparing results of single-trial ERP/fMRI data analysis in both groups, two essential regions of inhibitory control were significantly stronger correlated with N2 (pre-SMA) and P3 (right posterior IFG/insula) regressors in IC+ subjects, whereas in IC− subjects the P3 regressor was significantly stronger correlated with the left pregenual ACC/superior medial gyrus a region associated with several processes such as emotion regulation, working memory, attention, and response selection (Bush et al., 2000; Criaud and Boulinguez, 2013; Drevets et al., 2008; Simmonds et al., 2007). This might indicate a central role of the more affective, pregenual ACC in higher impulsive subjects, although it is not clear if this activity is an overactivity or compensatory activity (Chester and DeWall, 2014; Collins et al., 2012) leading either to an interference or maintenance, respectively, of an appropriate level of synchronized neural activity in regions necessary for inhibitory control.

Results of the ERP analysis also support this finding of an overall intact inhibitory control network in high impulsive subjects, but also the assumption of a less effective network functioning in these subjects. Within-group post-hoc comparisons of Nogo-P3 and Go-P3 amplitudes revealed significantly higher Nogo amplitudes in both groups, potentially indicating an overall intact inhibitory control network in both groups. However, post-hoc analyses of the robust main effect of group as well as a significant interaction between group and task condition revealed that this difference was more pronounced in IC+ subjects relative to IC− subjects, as IC+ subjects were characterized by significantly higher Nogo-P3 amplitudes but not Go-P3 amplitudes. Furthermore, reduced Nogo-P3 amplitudes in the high impulsive group, i.e., IC− subjects is also consistent with findings from other ERP studies who demonstrated significantly reduced Nogo-P3 amplitudes but no differences in Nogo-N2 amplitudes in non-clinical high impulsive subjects compared to

low impulsive subjects (Kam et al., 2012; Ruchsow et al., 2008a; Russo et al., 2008; Shen et al., 2014). Moreover, this is also strikingly similar to the finding of significantly reduced Nogo-P3 amplitudes in psychiatric diseases such as ADHD (Fisher et al., 2011; Helenius et al., 2011; Prox et al., 2007; Wiersema et al., 2006b; Woltering et al., 2013). This may point towards that shared differences in Nogo-related neural processing in ADHD and IC− subjects potentially are related to the enhanced higher impulsivity trait in these groups compared to IC+ subjects. Thus these data-drivenly identified electrophysiological phenotypes point towards important inter-individual differences in inhibitory control.

Although reduced Nogo-P3 amplitudes in IC− subjects seem to indicate disturbed or altered neural processing during response inhibition, it is important to see this finding in the context of the ongoing debate on which neurocognitive subprocesses of response inhibition are reflected in the N2 and P3 components. Thus, despite that the N2/P3 complex has been associated with the inhibitory process there is evidence that N2/P3 may reflect separable aspects of response inhibition, attentional processes and/or conflict and performance monitoring rather than response inhibition only (Huster et al., 2013). As the Nogo-N2 is typically observed in a latency range clearly located prior to the individual Go response, it has been suggested to reflect early pre-motor processes either directly related to response inhibition (Beste et al., 2010; Falkenstein et al., 1999; Jodo and Kayama, 1992; Lavric et al., 2004) or related to cognitive processes such as conflict monitoring or action updating potentially (Donkers and van Boxtel, 2004; Huster et al., 2013; Nieuwenhuis et al., 2004). Regarding P3, it has been argued that the P3 do peak too late to reflect inhibitory processes (Dimoska et al., 2003; Huster et al., 2013; Naito and Matsumura, 1994); therefore it was claimed that P3 may reflect rather evaluative processes such as stimulus or performance evaluation after response inhibition proper (Friedman et al., 2001; Huster et al., 2013; Liotti et al., 2005; Schmajuk et al., 2006; Wu and Zhou, 2009). Others, however, suggested that the Nogo-P3 reflects the process of response inhibition itself (Beste et al., 2010; Falkenstein et al., 1999; Huster et al., 2013, 2014; Wessel and Aron, 2015).

The results of the current study add multiple multimodal evidence to this discussion. Our unimodal ERP results of reduced Nogo-P3 amplitudes in the high impulsive group (i.e., IC−) but no group differences in N2 amplitudes may support the notion that Nogo-P3 may reflect motor response inhibition rather than Nogo-N2, since this seems to be unaffected in high impulsive subjects. This is also in line with findings from other ERP studies which demonstrated significantly reduced Nogo-P3 amplitudes but no differences in Nogo-N2 amplitudes in non-clinical high impulsive subjects compared to low impulsive subjects (Kam et al., 2012; Ruchsow et al., 2008a; Russo et al., 2008; Shen et al., 2014). However, if we use the multimodal information (i.e., ERP correlated fMRI) we do see pronounced response inhibition network differences speaking to the point of N2 group differences beyond insignificant unimodal ERP amplitude differences. Significant pre-SMA difference between IC+ and IC− (Figure 5.5.A) implies differences already at an early stage of processing in response inhibition proper. This is supported by the single-trial correlation with the

N2 component revealing a neural network clearly related to response inhibition in IC+ subjects but not in IC− subjects (Figure 5.4). Regarding P3 our finding of stronger posterior IFG in IC+ subjects (Figure 5.5.B) may point at P3 being also involved in response inhibition itself. However, data of our recent study dissecting response inhibition proper from its attentional components (Sebastian et al., 2015) show that this very region as an attentional area possibly is monitoring the response inhibition process. Our results of greater P3-related ACC activity in lower performing IC− subjects (Figure 5.5.C) may actually speak to the role of P3 in performance evaluation (error monitoring).

Since the specificity of N2 (and P3) for inhibition associated neurocognitive processes is still not clear, group selection here was deliberately data-driven. Thus, group selection was based on the existence of specific ICs with significantly Nogo vs. Go-related activity occurring within a latency range located clearly before the subject's typical Go RT. In line with the ongoing debate on functional associations of N2 with response inhibition, it could be argued that, N2 indeed reflects other cognitive processes but not response inhibition or, at least, not response inhibition only. Since single-trial correlation with the N2 component revealed a neural network clearly related to response inhibition in IC+ subjects but not in IC− subjects, it could also be argued that Nogo-N2 reflects an early stage of response inhibition which is less effectively activated in high impulsive subjects.

There is an alternative interpretation of the current results coming with a motor control rather than inhibitory control view of the neurocognitive processes underlying Go/Nogo paradigms. The observed group differences reflect important differences in the Go rather than stopping behavior. Indeed as already implied in our own component analysis of the response inhibition tasks especially the Go/Nogo task entails both response selection (selecting go vs. stopping behavior) as well as response inhibition (withholding a prepotent action) components (Stahl et al., 2014). Since response selection and monitoring is often associated with neural activity in the pre-SMA and the ACC, respectively, our current finding could point towards a behavioral and neural difference in response selection rather than response inhibition proper. This will also fit to our finding of prominent differences in P3 rather than in N2 ERP amplitudes. In this view our finding of neural based behavioral differences (IC+ vs. IC−) can be interpreted as a primary Go selection, hence motor control finding. Interestingly, in adult ADHD patients behavioral differences are found mainly in CoV and omission error rates but not in the commission error rates, supporting this view from a disease model (Fisher et al., 2011; Helenius et al., 2011; Prox et al., 2007; Wiersema et al., 2006b; Woltering et al., 2013). On the neural level this view is supported by our finding that IC+ more than IC− show pre-SMA activity (response selection) related to N2. In addition, we find IFG activity for IC+ more than IC− during both phases of response inhibition (N2 and P3; see Figure 5.5; significant in P3). Interestingly, this particular subregion of the IFG, which is the inferior frontal junction (IFJ), has been shown to handle primarily attentional information during response inhibition (Sebastian et al., 2015). Hence activity in this region during both phases of

response inhibition may represent enhanced attentional monitoring of response inhibition in IC+ subjects. Lastly pregenual ACC overactivity in IC− compared to IC+ subjects could mean greater error monitoring in subjects with lesser 'motor' (behavioral) control. However, this attractive alternative interpretation of our findings is challenged by the fact that our basic, data-driven neural contrast identifies neural activity which is greater during Nogo, hence response inhibition proper (stopping/withholding an action), than during Go (motor behavior/control). However, if there is a difference on the neurocognitive level between what we call motor control on the one hand and response inhibition/inhibitory control on the other hand might rather be a semantic than a biological question.

In conclusion, our data suggests the existence of electrophysiologically dissociable phenotypes of behavioral and neural motor response inhibition. Group comparisons performed on behavioral data revealed significantly higher intra-individual variability of RT and enhanced omission errors in IC− subjects. In line with this, results of unimodal fMRI analysis revealed differently recruited neural networks with additional activation of left IFG/insula and left putamen in IC− subjects. This may indicate that subjects with lower trait impulsivity have access to a more effective impulse control network. Thus, the recruitment of only few key areas of inhibitory control in fMRI may be the result of an effective and well-orchestrated (as indicated by higher P3 amplitudes) network performance. Alternatively, additional activations may be the cause of higher intra-individual variability in performance and more impulsive traits. Therefore, the presence or absence of identifiable Nogo-related ICs may represent different neurophysiological phenotypes of response inhibition. Although we cannot unambiguously distinguish between different mechanisms in terms of state (short term strategy adaptation) vs. trait (static individual neurobiologically determined differences), the behavioral data together with psychological data support a trait hypothesis of different neurophysiological phenotypes of response inhibition.

6. Discussion

6.1. General Discussion

Response inhibition is the ability to suppress inadequate but prepotent or ongoing response tendencies. A network of right lateral inferior frontal gyurs (IFG), pre-supplementary motor area (pre-SMA) and basal ganglia is involved in these processes (Aron, 2007; Aron and Poldrack, 2006; Sebastian et al., 2013a; Swick et al., 2011). Taking advantage of the electroencephalographic's (EEG) high temporal resolution and the functional magnetic resonance imaging's (fMRI) high spatial resolution, single-trial analysis of simultaneous EEG and fMRI data can be used to disentangle the spatio-temporal dynamics of neural responses (Debener et al., 2005, 2006; Eichele et al., 2005; Huster et al., 2012). Recent studies demonstrated that single-trial correlations of inhibition-related event-related potential (ERP) with fMRI blood oxygenation level-dependent (BOLD) signal can help to disentangle neural responses related to different stages of information processing during response inhibition (Baumeister et al., 2014; Huster et al., 2011; Karch et al., 2014; Lavallee et al., 2014; Mulert et al., 2008). However, most approaches for EEG/fMRI coupling are based on the correlation of the time series from known ERP components with the fMRI BOLD signal. While measuring known ERP components is a valuable first step, it cannot guarantee specificity for the targeted neurophysiological process, i.e., response inhibition proper versus, e.g., attention or task monitoring, on the group and single subject level. Thus, although single-trial ERP/fMRI data analysis enables to assess the spatio-temporal dynamics of task-related neural activity, it also comes with a high influenceability by the user-based selection of the ERP component of interest and also a reduced sensitivity to condition-specific processes. Together this emphasizes the need for a more objective method that allows for a subject and condition specific classification and selection of electrophysiological components.

Thus, in Study 1 (cf. Chapter 3, Schmüser et al., 2014) I introduced a new algorithm for selecting Nogo-related independent components (ICs) in an automated, ERP-independent procedure complementing existing automated approaches (Goldman et al., 2009; Wessel and Ullsperger, 2011). This approach aimed at automatically selecting task-related ICs with significantly increased amplitudes in Nogo trials compared to Go trials within predefined time windows 'early' and 'late' located prior and around the individual's median Go response time (RT). Importantly, as the existence of such Nogo-related ICs is verified intra-individually, one advantage of this approach is

that it allows accounting for individual differences in the EEG data, as it may arise from different electrode placements, head shapes, or anatomical differences at the brain level.

This new automated independent component analysis (ICA)-based approach was applied to the simultaneous EEG/fMRI data of 39 healthy subjects who had performed a visual Go/Nogo task. It was demonstrated that early and late IC-regressors correlated positively with fronto-striatal and parietal regions of the response inhibition network (Aron, 2011; Chambers et al., 2009; Chikazoe, 2010; Jahfari et al., 2011; Sebastian et al., 2013a; Swick et al., 2011). Although comparison of correlations with early and late IC-regressors revealed no significant differences, in most of these areas the strength and extent of positive correlations was decreasing from early to late stages of response inhibition. Thus, single-trial correlations with early and late IC-regressors go along with the expectation that regions relevant for motor control are active prior to the time of motor execution. This demonstrates that integration of EEG single-trial information, extracted from automatically selected ICs, into fMRI data analysis can be used to assess the temporal evolution of the neural impulse control network. By using the same analysis procedure for selecting ICs related to visual processing, which was successful in 37 of 39 subjects, Study 1 also demonstrated the utility of this method beyond detecting Nogo-related components.

Additionally, the new automated ICA-based approach was also contrasted with a more classical approach that uses N2/P3 amplitudes at specific electrodes as ERP-regressors. This combined ERP/fMRI analysis was performed on the same data to assess and validate the outcome of this automated ICA-based approach in the context of combined EEG/fMRI analysis procedures (cf. Figure 3.1 in Chapter 3 for a graphical overview). In line with a previous 'ERP-informed fMRI analyses' of response inhibition (Baumeister et al., 2014), the mean single-trial amplitude values were extracted from latency ranges which covered best the task-related N2 and P3 effects as determined based on visual inspection of the grand-averaged waveforms across all subjects. Based on this, mean N2/P3 amplitude values were extracted from the Cz site at the latency ranges 280–340 ms post-stimulus (N2) and 350–570 ms post-stimulus (P3).

While single-trial correlations with IC-regressors revealed an activation pattern clearly related to known neural inhibitory control networks (Aron, 2011; Chambers et al., 2009; Chikazoe, 2010; Jahfari et al., 2011; Sebastian et al., 2013a), the activation pattern revealed by single-trial correlation with N2/P3 ERP-regressors, resembled a mixture of the impulse control network and networks related to attentional processing and response monitoring. Thus, in comparison to the ICA-based single-trial EEG/fMRI analysis, correlations of N2/P3 single-trail amplitude values with fMRI BOLD responses lack of specificity to inhibitory processes. Nevertheless, it also shows that N2/P3-based single-trial EEG/fMRI data analysis does provide additional information on differences in spatio-temporal processing in inhibitory control. Since the automated IC-selection procedure restricts the ICA-based single-trial EEG/fMRI analysis to a certain subgroup, in some cases N2/P3-based single-trial EEG/fMRI analysis together with unimodal EEG and fMRI analysis

may also provide valuable information as also demonstrated in Study 3 (cf. Chapter 5, Schmüser et al., 2016).

The main criticism and limitation of Study 1 is that due to the restrictive IC selection criteria only a certain part of subjects could be included into the task-related single-trial EEG/fMRI data analysis. As such the demonstrated temporal signal evolution in central region of response inhibition as detected by the ICA-based approach may not be generalizable, but be specific for a subpopulation only. Moreover, the fact that Nogo-related ICs were not identified in one half of the subjects may also question the usability and validity of the IC-selection procedure in general. However, this is contrasted by the finding that the same algorithm was able to detect ICs related to visual processing in 37 of 39 subjects, which may argue against a principal failure of the algorithm. And also the fact that across all investigated groups (cf. Studies 1 and 2, Chapters 3 and 4) the required reliability of inhibition-related ICs was attained only in about half of the subjects argues against a technical issue. Thus, as this finding was stable irrespective of the groups' background (i.e., healthy control (HC) subjects, Attention-Deficit/Hyperactivity Disorder (ADHD) patients or Borderline Personality Disorder (BPD) patients) this may rather point towards inter-individual difference in an electrophysiological correlate of response inhibition based on intra-individual variability which in turn may suggest the existence of electrophysiologically dissociable phenotypes of behavioral and neural motor response inhibition.

In Study 3 it was tested whether the finding that certain Nogo-related components are not present in every subject is related to the existence of substantial inter-individual differences, i.e., electrophysiologically dissociable phenotypes. 21 subjects showed ICs reliable related to early Nogo processes (Nogo-IC-positive; in short IC+), whereas 17 subjects did not show these early Nogo-related ICs (Nogo-IC-negative; in short IC−) on the chosen level of significance. These potential phenotypic groups in healthy individuals were further characterized and compared using behavioral, neuropsychiatric as well as unimodal and multimodal ERP and fMRI measures. Finally we demonstrated that using the data-driven approach for IC selection and the resulting presence or absence of Nogo-specific ICs as criterion for group selection could reveal group differences at behavioral and neurophysiological levels. Interestingly, the IC− group (i.e., the group characterized by the absence of early Nogo-related ICs) was characterized by higher scores on self-rated impulsivity measures, i.e., experience seeking and boredom susceptibility on the sensation seeking questionnaire Sensation Seeking Scale (SSS-V) and motor and non-planning impulsiveness on the impulsivity questionnaire Barratt Impulsiveness Scale-11 (BIS-11).

The picture of a group of healthy subjects that is characterized by a more impulsive personality trait is completed by the significantly higher scores on subscales addressing motor impulsivity/hyperactivity and impulsive/non-planning characteristics as well as ADHD traits in IC− subjects. Thus, already based on psychometric data it seems plausible that IC+ and IC− subjects are psychologically distinguishable and suggest a trait character of the electrophysiological

phenotype. This notion was supported by behavioral data showing differences in intra-individual coefficient of variability (CoV) of RT and omission error rates but not in mean RTs or commission error rates. This finding of enhanced omission error rates and higher CoV values is strikingly similar to comparisons of adult ADHD patients with HC subjects (cf. Study 2, Chapter 4), with increased intra-individual RT variability being hypothesized as a candidate for an intermediate endophenotypic trait of ADHD (Tamm et al., 2012). Although it cannot unambiguously be distinguished whether these performance differences are related to state (short term adaptation in task strategy) or trait (static individual neurobiologically determined differences), the behavioral data together with psychological data seem to support a trait hypothesis.

The relationship between the personality trait impulsivity and the neural underpinnings of inhibitory control has been investigated by several neuroimaging studies (Asahi et al., 2004; Brown et al., 2015; Collins et al., 2012; Horn et al., 2003; Ruchsow et al., 2008a). Although these studies provided inhomogeneous results, potentially due to the multifaceted nature of impulsivity (Caswell et al., 2015; Cyders and Coskunpinar, 2011; Sebastian et al., 2013b; Stahl et al., 2014), they do point towards altered, either reduced or overactive or compensatory, neural activity in high impulsive subjects compared to low impulsive subjects. Thus, our finding of completive activation of left IFG and left putamen/insula regions in higher impulsive subjects (IC−) may hint to a compensatory neural activity in left hemispheric fronto-striatal regions while less impulsive subjects (IC+) have access to an effective impulse control network that is well orchestrated (i.e., higher P3 amplitudes) and thus requires less neural sources (regional neural activity).

This notion of a less effective core network functioning in IC− subjects is also supported by unimodal ERP analysis, as indicated by a robust main effect of group as well as a significant interaction between group and task condition on the dependent variable P3 amplitude. However, since groups were selected based on electrophysiological characteristics, results of unimodal ERP analysis should be regarded with care and not succumb to a circular argument. Nevertheless, as group selection was based on EEG components related to *early* inhibitory processes, *later* ERP components may remain independent from this and thus provide meaningful information. The finding of significantly reduced Nogo-P3 amplitudes in IC− but no differences in Go-P3 amplitudes is strikingly similar to the finding of group comparisons in Study 2 (cf. Chapter 4): significantly reduced Nogo-P3 amplitudes in ADHD compared to BPD and HC as well as in BPD compared to HC. This may point towards shared differences in Nogo-related neural processing potentially related to the enhanced higher impulsivity trait in these groups compared to IC+ subjects.

Although Study 1 (cf. Chapter 3) demonstrated that correlations of N2/P3 single-trail amplitude values with fMRI BOLD responses lack specificity to inhibitory processes, it has also been shown to provide additional information on differences in spatio-temporal processing in inhibitory control tasks (Baumeister et al., 2014; Karch et al., 2010; Schmüser et al., 2014). Thus to further characterize the neural differences between IC+ and IC− subjects, single-trial amplitudes

from N2 and P3 ERPs were correlated with fMRI BOLD signal. While in IC+ subjects the resultant activation pattern was a mixture of the response inhibition and the ventral attention system, in IC− subjects the activation patterns resembled more a mixture of response inhibition and medial prefrontal evaluative and limbic systems. The activation pattern in IC+ subjects goes along with the assumption that in addition to inhibitory control mechanisms the Go/Nogo task might also trigger processes related to response selection and selective attention (Mostofsky and Simmonds, 2008; Stahl et al., 2014), while medial prefrontal activity in higher impulsive subjects have been linked to an interaction of motivational aspects and cognitive processing (Horn et al., 2003).

In line with this, group comparisons revealed significantly stronger correlations in pre-SMA (N2) and right posterior IFG/insula (P3) in IC+ subjects, whereas in IC− subjects the P3 regressor was significantly stronger correlated only with the left pregenual anterior cingulate cortex (ACC)/superior medial gyrus. Interestingly enough, this region is not only associated with several processes such as emotion regulation, working memory, attention, and response selection (Bush et al., 2000; Criaud and Boulinguez, 2013; Drevets et al., 2008; Simmonds et al., 2007), it was also the only region in which the late IC-regressor correlated stronger with the fMRI BOLD signal in BPD patients compared to HC subjects in Study 2 (cf. Chapter 4). This might indicate a central role of pregenual ACC in higher impulsive subjects, potentially pertaining to the maintenance of an appropriate level of synchronized neural activity in regions necessary for inhibitory control. Although it is not clear whether it is an overactivity or compensatory activity (Chester and DeWall, 2014; Collins et al., 2012) that is potentially leading either to an interference or maintenance, respectively, of an appropriate level of synchronized neural activity in regions necessary for inhibitory control. In congruency with the maintenance hypothesis, the absence of enhanced activity in pregenual ACC in ADHD patients might explain why ADHD patients failed to activate the neural impulse control network, whereas BPD patients seem to fail to activate the network only under emotional stress. Alternatively, hyperactivations in ACC as it was found in BPD and IC− subjects may indicate overactive neural activity leading to the personality trait of impulsivity (Stone, 2013).

Taken together, Study 3 demonstrated that between-subject differences in Nogo-related electrophysiological components are related to distinct neurophysiological phenotypes of response inhibition. These results emphasize the importance of intra-individual variability (i.e., trial-to-trial fluctuations) as well as inter-individual differences (i.e., neurophysiological phenotypes) which may have an impact on the results and should be accounted for whenever comparing neurocognitive processes regardless of the methods of measurement, e.g., unimodal ERP, unimodal EEG, or combined EEG/fMRI data. Hence, based on the automated selection of intra-individually classified Nogo-related ICs, electrophysiological phenotypes of impulse control were identified in a data-driven, unbiased way. Although further analyses are needed to differentiate whether differences in cognitive

strategy when performing the task are state or trait related, the identification of these potential phenotypes already demonstrates importance of intra- and inter-individual differences.

Between-subject differences in the intra-individual variability have been suggested to constitute a key to pathological processes in impulsivity which in turn is viewed as a central element of ADHD and BPD pathophysiology (Lieb et al., 2004; Nigg et al., 2005b; Sebastian et al., 2013b). Although this is supported by consistent findings of significantly higher scores in self-rating questionnaires regarding impulsivity in BPD and ADHD patients (Sebastian et al., 2013b), current electrophysiological and neuroimaging studies provided mixed results. To increase sensitivity for inter-individual differences the ICA-based single-trial EEG/fMRI analysis (cf. Study 1, Chapter 3, Schmüser et al., 2014) was used to examine the neural processing at distinct phases of response inhibition in adult ADHD patients and BPD patients compared to HC subjects. As demonstrated in Study 1 (cf. Chapter 3), this approach allows for increasing sensitivity for inter-individual differences by incorporating intra-individual variability. Additionally, this approach also takes into account inter-individual differences potentially related to different substantial phenotypes as demonstrated in Study 3 (cf. Chapter 5). Moreover, by using electrophysiological components related to different phases of task execution, this approach also enables to assess group differences in spatio-temporal dynamics of the neural impulse control network. Thus, to examine the temporal and spatial dynamics of neural processes underlying response inhibition in adult ADHD patients in comparison to BPD patients and HC, ICA-based single-trial EEG/fMRI analysis was used in addition to conventional unimodal ERP and fMRI data analyses.

Interestingly, in contrast to the usually marginal findings of unimodal fMRI analysis, the ICA-based single-trial EEG/fMRI analysis revealed significant group differences between ADHD and HC as well as between ADHD and BPD but not between BPD and HC in the neural response inhibition network. Differences between ADHD and the two other groups were found in key regions of the neural response inhibition network, especially in the early stage of response inhibition. This provided initial evidence that critical regions of the cortical neural response inhibition network in adult ADHD patients are not locally impaired but that the timing of the neural network is hindered. As the timing of the inhibitory control network was not affected in BPD patients, this timing deficit may indicate an ADHD-specific pathomechanism.

As expected from ADHD and BPD pathophysiology, compared to HC subjects both patient groups showed significantly higher scores of self-rated impulsivity scores which is in line with previous studies on impulsivity in ADHD and BPD (Lampe et al., 2007; Prada et al., 2014). Behaviorally, both patient groups were characterized by significantly enhanced CoV values, i.e., the intra-individual variance of RT. This supports the notion of intra-individual variability of RTs being a key element in ADHD pathology and might also co-occur in BPD-patients with a subclinical ADHD comorbidity. Increased intra-individual RT variability in ADHD patients has been reported across studies using a variety of paradigms (Tamm et al., 2012) and has been proposed

as a candidate for an intermediate endophenotypic trait of ADHD and is potentially mirrored by intra-individual variability assessed by our ICA-based single-trial EEG/fMRI analysis.

Behavioral and psychometric data of Study 2 (cf. Chapter 4) and Study 3 (cf. Chapter 5) seem to suggest shared differences in Nogo-related neural processing potentially related to the enhanced higher impulsivity trait in these different groups compared to low impulsive subjects. However, comparisons of the neuroimaging data might question this assumption. Conventional fMRI analysis revealed in IC+ and IC− subjects significant activations in medial prefrontal areas including pre-SMA/SMA, left basal ganglia, and tempo-parietal regions. In the IC+ group significant activations were restricted to these regions, while the IC− group showed a more distributed network with additional significant clusters of positive correlations in bilateral posterior IFG/insula and right basal ganglia (caudate nucleus, putamen, and pallidum). These conspicuous group differences were further supported by significant between-group differences (IC− > IC+) in left IFG and left putamen/insula, suggesting an additional potentially compensatory recruitment of these regions in subjects with a higher impulsive personality trait. In contrast to this, conventional fMRI data analysis in adult ADHD patients revealed task-related fMRI BOLD responses in pre-frontal areas such as the pre-SMA, while the basal ganglia were not significantly activated. Moreover, direct group comparison (HC > ADHD) revealed significantly decreased activity in bilateral caudate nucleus/pallidum and left putamen, but no differences in pre-frontal areas and no compensatory or overactive activity in ADHD patients, which largely differs from group comparison in Study 3 (IC+ vs. IC−). Thus, it could be argued that the additional, potentially compensatory, recruitment of left hemispheric fronto-striatal areas differentiates non-clinical impulsive subjects from clinical patients with ADHD. As group comparison of BPD patients and HC subjects revealed no significant differences, this seems to support the idea that the clinical relevant symptom of impulsivity in BPD patients may result from an interaction of emotional dysregulation and impulse control (van Eijk et al., 2015; Lampe et al., 2007; Prada et al., 2014; Sebastian et al., 2013b, 2014; van Zutphen et al., 2015). This is contrary to the rather pure inhibitory control deficits in ADHD patients. On the other hand, unimodal fMRI analysis revealed that BPD patients also did not differ significantly from ADHD patients in regions central to inhibitory control, which might indicate a mildly impacted neural impulse control network in BPD patients. Thus, it could be hypothesized that impulsivity in BPD patients might result from an intermediate network functionality that is more prone to emotional influences.

In contrast to this rather divergent neuroimaging results, electrophysiological data seem to corroborate the hypothesis of shared neural characteristics in these high impulsive groups compared to low impulsive subjects. Although within-group post-hoc comparisons of Nogo-P3 and Go-P3 amplitudes revealed significantly higher amplitudes for Nogo than for Go in all groups, this difference was more pronounced in IC+ subjects relative to IC− subjects as well as in HC (= IC+) subjects compared to ADHD and BPD patients. In accordance with this, between-group comparison in Study 3 revealed significantly higher Nogo-P3 amplitudes in IC+ subjects relative

to IC− subjects, while Go-P3 amplitudes did not differ significantly between groups. Likewise, in Study 2 post-hoc analysis of the group and condition interaction effect revealed significantly reduced Nogo-P3 amplitudes in ADHD and BPD patients compared with HC, but no differences in Go condition. As this late EEG component is thought to reflect inhibitory processes and/or performance monitoring (Bruin et al., 2001; Enriquez-Geppert et al., 2010; Smith et al., 2008), reduced amplitude values might indicate deficient inhibitory processing in both patient groups as well as in the high impulsive IC− group.

However, since the P3 peaks on average after the mean Go RT, it has been claimed that P3 rather reflects evaluative processes such as stimulus evaluation (Friedman et al., 2001) or performance evaluation (Huster et al., 2013; Liotti et al., 2005; Schmajuk et al., 2006; Wu and Zhou, 2009). Thus, findings of reduced Nogo-P3 amplitudes in both patient groups as well as in the high impulsive IC− group seems to be indicative of disturbed Nogo-related neural processing at this latency, but it could not be disentangled whether this is related to impaired inhibitory processes itself or rather impairments in evaluative processes or even a result of deficits at earlier processing stages. Hence, it is conceivable that late processing deficits as reflected by reduced P3 amplitudes might simply be caused by deficits at earlier processing stages. In line with this, the findings of abnormalities at the N2 latency (Fisher et al., 2011; Pliszka et al., 2000), as well as findings of reduced fMRI correlations with N2 but not P3 ERPs during voluntary decisions in ADHD patients (Karch et al., 2014) can be interpreted as indicating that—at least in ADHD patients—deficits in executive functioning might be caused by dysfunctions in early stages of processing.

This is also supported by results of Study 2 in which single-trial correlation of fMRI BOLD response with Nogo-related EEG activity occurring clearly before (early) or around (late) the typical RT revealed significant group differences between HC and ADHD in key regions of the neural impulse control network. Interestingly enough, ADHD patients displayed significantly reduced correlations in the entire fronto-striatal network of impulse control especially at the early stage of response inhibition and in striatal regions also at the later stage of inhibitory control. In contrast to this, significantly stronger correlations of late IC-regressor with fMRI BOLD signal in left ACC regions in BPD patients was the only difference between BPD patients and HC subjects. Additionally, comparison of both patient groups yielded significantly stronger correlations of both IC-regressors with fMRI BOLD signal in bilateral IFG and striatal key regions of inhibitory control in BPD patients compared to ADHD patients. This suggests that especially the early processing of response inhibition is impaired in ADHD patients (temporal and, to a lesser extent, spatial aberrations), while in BPD patients the network seems to be activated in a slightly exaggerated manner (minimal, mainly spatial aberrations).

Moreover, the results of unimodal and multimodal analyses in BPD patients compared to HC subjects support the notion of a largely unaltered neural impulse control network in BPD patients. Concerning unimodal data analysis, the functionality of the neural impulse control network seems

to be located between ADHD patients and HC subjects, though much closer to the healthy side. Similarly, multimodal data analysis demonstrated significant differences in neural regions relevant for inhibitory control between BPD and ADHD patients but not between BPD and HC. At the late latency these differences were even more pronounced than in the contrast HC vs. ADHD, which may indicate a longer lasting overactive activity of the neural network in BPD patients.

The idea of deficient early processing of response inhibition in ADHD patients is supported by findings of a significant interaction effect between group (HC, ADHD) and latency range (early, late) showing that key regions of the cortical neural response inhibition network, i.e., posterior IFG/insula regions (significant in left pars opercularis and trend in right pars opercularis) are not activated within the early latency range in ADHD patients. Intriguingly, this indicated that in bilateral posterior IFG (pars opercularis)/insula controls showed an expected relative activity decrease from early to late inhibition stages whereas ADHD patients had only a delayed relative activity increase from early to late inhibition stages. This corresponds to findings of Karch and colleagues who demonstrated that during voluntary motor decisions especially the early phase of information processing was affected in ADHD patients (Karch et al., 2014). To further test whether early processing of response inhibition is affected in ADHD or whether it is just temporally shifted and thus not detected by the early IC-regressors, we shifted the early latency range in steps of 20 ms from 120 ms to 280 ms as starting points and $RT - 80$ ms to $RT + 80$ ms as ending points. As depicted in Figure 4.7 (Section 4.2.6 *'Time-window shifts around the early latency range'*), grand average topographies of ICs selected from time-window shifts around the early latency range pointed toward disturbed or altered information processing in ADHD patients but not in BPD patients at the early latency. This is another observation which indicates that response inhibition deficits in ADHD are rather due to dysfunctions in neural timing of inhibitory control networks than due to static focal or regional neural activity deficits.

Deficits in the temporal domain of neural processing in ADHD patients have been described recently for other cognitive functions (Karch et al., 2014). Neurocognitive dysfunctions in temporal processes are mirrored by behavioral deficits, i.e., in motor timing, perceptual timing and temporal foresight typically found in ADHD patients (Hart et al., 2012; Noreika et al., 2013; Rubia et al., 2009a). In view of the similarities between the neural correlates of deficits in inhibitory control and behavioral temporal processing in ADHD patients, it has been suggested that inhibitory control deficits may be caused by timing disturbances in ADHD patients (Noreika et al., 2013; Rubia et al., 2009a). It has been assumed that deficits in both domains, i.e., inhibitory control and behavioral temporal processing, are related to dopamine dysregulation since there is evidence for normalization by administration of dopamine reuptake inhibitors such as methylphenidate (Aron et al., 2003b; Coghill et al., 2014; Cubillo et al., 2014; Nandam et al., 2014; Rubia et al., 2011; Smith et al., 2013a; Vaidya et al., 1998) which acts on striatal dopamine receptors (Rosa-Neto et al., 2005; Vaidya et al., 1998; Volkow et al., 1998).

Recently, it has also been proposed that treatment effects of methylphenidate in ADHD patients may be related to overall normalization of functional interaction in neural networks (Cooper et al., 2014), indicating an association between dopaminergic dysregulation and neural synchronization. The importance of the striatal dopaminergic system in the context of inhibitory control is supported by findings that even slight striatal dysfunctions in premanifest Huntington's disease gene carriers can cause a reduced precision of neural synchronization processes in the fronto-striatal network which in turn affects the early phases of response inhibition, i.e., pre-motor inhibition processes (Beste et al., 2011). In line with this, it has been shown that methylphenidate treatment leads to a normalization in amplitudes and latencies of Nogo-related N2 in ADHD patients (Pliszka et al., 2007). As it has been suggested that rhythmic motor abnormalities in ADHD patients may be related to an oscillatory pathology in the fronto-striatal network (Ben-Pazi et al., 2006), our data suggest that the observed timing deficits on the neuronal level of inhibitory control are strongly related to neurocognitive timing deficits, possibly caused by imprecise neural synchronization on the striatal level and by dopaminergic imbalances.

6.2. Conclusion

Study 1 (cf. Chapter 3) demonstrated that single-trial correlation of automatically selected inhibition-related ICs with fMRI BOLD response allows to assess the spatio-temporal dynamics of the neural underpinnings of response inhibition. This study introduced a newly developed analysis procedure that automatically selects task-specific electrophysiological ICs which are reliably inhibition-related at different phases of motor response inhibition (i.e., before or around the individual median Go response time). As these ICs were selected without using a priori defined ERP components, in contrast to conventional combined EEG/fMRI data analyses, it avoids the analytical bias of the human rater based assessment of EEG correlates of presumed task-related activity as measured by ERPs. To increase sensitivity to inter-individual differences, this approach is essentially based on the intra-individual classification of ICs according to their relation to response inhibition under consideration of the subject's individual median RT. ICs which are identified as reliably inhibition-related, i.e., significantly larger in amplitude for Nogo than Go trials, within a predefined time window (early or late) are then combined into individual electrophysiological regressors and then included into fMRI first-level analysis. Single-trial correlations of fMRI BOLD signal with these electrophysiological regressors revealed fMRI BOLD responses in fronto-striatal regions which were clearly more pronounced in the early compared to the late phase of task execution.

Study 2 (cf. Chapter 4) demonstrated that integration of EEG single-trial information, extracted from automatically selected Nogo-related ICs, into fMRI analysis allows to assess the neural processing at distinct phases of response inhibition in adult ADHD patients and BPD

patients compared to HC subjects. This allows to assess whether only certain, temporally distinct phases of neural processing are affected specifically in a certain patient group. This is the first combined EEG/fMRI study that demonstrated deficient neural processing at an early phase of response inhibition in adult ADHD patients compared to HC and BPD patients. Inhibitory control specific single-trial analysis revealed that fronto-striatal key regions of the neural impulse control network are not activated on time in ADHD patients, while BPD patients were almost indistinguishable from HC subjects. This finding may link the known behavioral deficits in the temporal domain, e.g., temporal perception and discrimination, or motor timing of ADHD patients (Noreika et al., 2013; Rubia et al., 2009a) to deficiency on the neural level in terms of neural timing deficits. This may provide a new route into the pathomechanism of inhibitory control deficits in ADHD.

However, a certain proportion of subjects (17 from 38 HC, 7 from 19 ADHD patients, and 8 from 19 BPD patients) did not show early Nogo-related ICs on the chosen level of significance (Nogo−Go difference: $|Z| > 0.275$). Thus, as a result of IC selection, a certain percentage of subjects had to be excluded from the ICA-based combined EEG/fMRI analysis. As such, these findings may be limited to specific subpopulations, characterized by the existence of Nogo-related ICs detectable at the chosen threshold. However, as demonstrated in Study 1 (cf. Chapter 3) the same algorithm was able to detect ICs related to early visual responses, which argues against a principal failure of the algorithm. Thus, the finding that certain Nogo-related components are not present in every subject may give an indication of substantial inter-individual differences as state or trait related differences in cognitive strategy when performing the task which are present in controls, ADHD, and BPD patients equally. This emphasizes that both EEG and fMRI data analysis should take into account that both intra-individual variability (i.e., trial-to-trial fluctuations) and inter-individual differences (i.e., neurophysiological phenotypes) may have an impact on the detectability of the neural signals leading to rather larger variability of results.

Study 3 (cf. Chapter 5) demonstrated that the existence or absence of such early Nogo-related ICs is indeed related to substantial inter-individual differences. Group comparisons of behavioral data revealed significantly higher intra-individual variability of RT and enhanced omission errors in IC− subjects, i.e., subjects characterized by the absence of early Nogo-related ICs. As these subjects were also characterized by enhanced scores on subscales of self-rated impulsivity measures and clinical ADHD questionnaires, this may indicate a higher impulsivity trait comparable to ADHD patients. Unimodal ERP group analysis revealed significantly reduced Nogo-P3 amplitudes in these subjects, while unimodal fMRI group comparison revealed a completive activation of left IFG and left putamen/insula in IC− subjects. This could be interpreted as indicating that subjects with a less impulsive personality trait have access to an effective impulse control network that is based on the recruitment of only few key areas of inhibitory control in favor of an effective and well-orchestrated (higher P3 amplitudes) network performance.

In line with this, in IC+ subjects (i.e., the group characterized by the presence of early Nogo-related ICs) relative to IC− subjects the single-trial ERP/fMRI correlation yielded stronger correlations in two central regions of the neural impulse control network: in pre-SMA with N2-derived regressor and in right IFG and insula lobe with P3-derived regressor. The inverse comparison (IC− > IC+) revealed stronger correlations with P3-derived regressors in the left pregenual ACC and superior medial gyrus a region associated with attention, emotion regulation, working memory, and response selection (Bush et al., 2000; Criaud and Boulinguez, 2013; Drevets et al., 2008; Simmonds et al., 2007). Thus despite of no differences in inhibitory performance, i.e., commission error rate, the IC+ and IC− groups showed different phenotypes on various levels: IC− subjects displayed higher impulsivity trait, were characterized by higher intra-individual variability of RT and enhanced omission error rates, and differed significantly from IC+ subjects in neurophysiological (fMRI, ERP) measures. This indicates that the presence or absence of identifiable Nogo-related ICs represents different neurophysiological phenotypes of response inhibition. With this, Study 3 demonstrated that applying the automated IC-selection procedure increases sensitivity for inter-individual differences by incorporating intra-individual variability, and that the resultant group classification (IC+ and IC−) are related to important inter-individual differences in inhibitory control.

6.3. Future directions

The research presented in this thesis showed that combined analysis of simultaneous EEG and fMRI data is a powerful tool to disentangle the spatio-temporal dynamics of neural processes of response inhibition. Single-trial correlations of automatically selected inhibition-related ICs with fMRI responses revealed activity in fronto-striatal regions which were more pronounced in an early compared to a late phase of task execution (Study 1, Chapter 3). This was present in HC subjects and in BPD patients but not in ADHD patients leading to the assumption that the neural response inhibition network was only mildly affected in BPD patients while critical regions of this network are temporally not well orchestrated in adult ADHD patients potentially pointing at an ADHD-specific pathomechanism (Study 2, Chapter 4). Furthermore, unimodal EEG and ERP analysis as well as conventional single-trial ERP/fMRI analysis revealed that the presence or absence of specific inhibition-related ICs in HC subjects was correlated with distinct neural activity pointing towards electrophysiologically dissociable phenotypes of behavioral and neural motor response inhibition (Study 3, Chapter 5). Thus using an approach sensitive to inter-individual differences allows for subgroup classification and hence to identify and characterize the neural correlates of inter-individual differences in response inhibition in healthy subjects.

However, as raised in the discussion of Study 3 (Chapter 5), based on the current data we cannot unambiguously distinguish whether the identified phenotypes were state (short term

strategy adaptation) or trait (static individual neurobiologically determined differences). Although the behavioral data together with psychological data seem to support a trait hypothesis, it would be interesting to test the stability of this finding. In favor of the trait hypothesis of different neurophysiological phenotypes of response inhibition group assignment and the related neural activation pattern should be stable across distinct times of measurement. In addition, it would be interesting to test whether the IC− phenotype is associated with a higher vulnerability towards ADHD pathophysiology. Since the IC− group showed significantly higher scores on the Conners' Adult ADHD Rating Scale (CAARS-S:L) questionnaires, it could be expected to find a disproportionately high number of ADHD patients among close relatives of IC− subjects. Since the same percentage of IC−/IC+ phenotypes were also found in BPD and ADHD patients, it could be argued that the IC− phenotype is independent of ADHD pathology. However, in line with the dimensional measures of Research Domain Criteria (RDoC), it could be argued, that the IC− phenotype represents a hyperactive/impulsive subtype that is present across different human subgroups. Moreover, the higher scores in self-rated impulsivity, i.e., BIS-11 as well as in the clinical ADHD ratings, i.e., CAARS-S:L and Wender Utah Rating Scale (WURS-k) in the non-clinical IC− subjects, may indicate that this IC− phenotype tends towards the hyperactive/impulsive ADHD subtype as diagnosed by the conventional categorical diagnostic criteria Diagnostic and Statistical Manual of Mental Disorders (DSM)-IV. To test this, the same experiment should be repeated in a larger cohort of HC subjects, ADHD and BPD patients. In the end this may provide important information for our understanding of deficits in response inhibition in heterogeneous psychiatric disorders such as ADHD or BPD.

Within the scope of this thesis my research was focused on one subcomponent of response inhibition, i.e., the withholding of a prepotent motor response in HC subjects compared to medication naive ADHD and BPD patients. Thus, with respect to the identified phenotypes of response inhibition (IC+/IC−) it would be also interesting to see whether this phenotype is only present in the action withholding subcomponent of response inhibition or whether this phenotype has impact on other components such as action cancellation (Stop-Signal) and inference inhibition (Simon). The other way round, it would also be an interesting approach to train the algorithm to identify ICs reliably related to stop (Stop-Signal task) or interference (Simon task) processes. This in turn would allow to assess whether the findings of this thesis are specific to the Nogo process or whether it is a more global effect. If applied on data of BPD and ADHD patients, this allows to test whether the deficits in the early phase of response inhibition are ADHD-specific for action withholding (Go/Nogo) or also present in action cancellation (Stop-Signal) and inference inhibition (Simon). In the end this may enable to further delineate the group specific pathomechanisms.

It has been said that—under emotionally neutral conditions—the neural response inhibition network is most widely intact in BPD patients. It is further proposed, that the clinical relevant finding of impulsive behavior results from an interaction of impulse control and emotional stress/deficits in emotion regulation (van Eijk et al., 2015; Lampe et al., 2007; Prada et al., 2014; Sebastian et

al., 2013b, 2014; van Zutphen et al., 2015). In this context, a simultaneous EEG/fMRI study on the subject of an emotional Go/Nogo task may help to disentangle the temporal dynamics of this interaction of emotion (dys-)regulation and impulse control—again in HC subjects compared to BPD and ADHD patients.

Pursuing the objective of deficits in the early phase of response inhibition in ADHD patients— as presented in Study 2 (Chapter 4)—more in-depth analyses are recommended. As raised before, it should be disentangled whether these difficulties within the temporal dynamics or orchestration of neural processes are specific for response inhibition (either only action withholding, or more globally impulse control) or whether this is a universal marker of ADHD. It is assumed that deficits in inhibitory control and behavioral temporal processing in ADHD patients are related to dopamine dysregulation which can be normalized by administration of dopamine re-uptake inhibitors such as methylphenidate (Aron et al., 2003b; Coghill et al., 2014; Cubillo et al., 2014; Nandam et al., 2014; Rubia et al., 2011; Smith et al., 2013a; Vaidya et al., 1998).

Finally, it has also been proposed that treatment effects of methylphenidate in ADHD patients may be related to overall normalization of functional interaction in neural networks (Cooper et al., 2014), indicating an association between dopaminergic dysregulation and neural synchronization. It has also been suggested that rhythmic motor abnormalities in ADHD patients may be related to an oscillatory pathology in the fronto-striatal network (Ben-Pazi et al., 2006). Hence, it could be argued that in ADHD patients the observed timing deficits on the neuronal level of inhibitory control are probably related to or even possibly caused by imprecise neural synchronization on the striatal level and by dopaminergic imbalances. This, however, is purely hypothetical and thus calls for further studies.

In a first step, one would investigate whether the early phase of response inhibition can be normalized by administration of dopamine re-uptake inhibitors such as methylphenidate. In addition, it would be also interesting to compare this with the effect of EEG-based neurofeedback. EEG-based neurofeedback is an alternative treatment method for ADHD that should enable the patient to influence the brain's state of up- and down-regulation of cortical excitability (Zuberer et al., 2015). If EEG-based neurofeedback indeed has a longterm impact on the cortical excitability this may also result in a normalization of the deficient early activity in ADHD. Subsequently data analysis in the time-frequency domain may provide further insights into the question whether the observed timing deficits are indeed related to disturbed neural synchronization. This however requires EEG data with high data qualities and a sufficient amount of trials, which is not provided by the data used in this thesis. Finally, if these data are provided we could reach evidence whether the finding that critical regions of the neural response inhibition network are temporally not well orchestrated in adult ADHD patients is indeed pointing at an ADHD-specific pathomechanism.

7. References

Aghakhani, Y., Beers, C.A., Pittman, D.J., Gaxiola-Valdez, I., Goodyear, B.G., and Federico, P. (2015). Co-localization between the BOLD response and epileptiform discharges recorded by simultaneous intracranial EEG-fMRI at 3 T. NeuroImage Clin. 7, 755-763.

Aguirre, G.K., Zarahn, E., and D'Esposito, M. (1998). The Variability of Human, BOLD Hemodynamic Responses. NeuroImage 8, 360-369.

Albrecht, B., Brandeis, D., Uebel, H., Valko, L., Heinrich, H., Drechsler, R., Heise, A., Müller, U.C., Steinhausen, H.-C., Rothenberger, A., et al. (2013). Familiality of neural preparation and response control in childhood attention deficit-hyperactivity disorder. Psychol. Med. 43, 1997-2011.

Allen, P.J., Polizzi, G., Krakow, K., Fish, D.R., and Lemieux, L. (1998). Identification of EEG events in the MR scanner: the problem of pulse artifact and a method for its subtraction. NeuroImage 8, 229-239.

Allen, P.J., Josephs, O., and Turner, R. (2000). A Method for Removing Imaging Artifact from Continuous EEG Recorded during Functional MRI. NeuroImage 12, 230-239.

de-Almeida, C.P., Wenzel, A., de-Carvalho, C.S., Powell, V.B., Araújo-Neto, C., Quarantini, L.C., and de-Oliveira, I.R. (2012). Amygdalar Volume in Borderline Personality Disorder With and Without Comorbid Post-traumatic Stress Disorder: A Meta-analysis. CNS Spectr. 17, 70-75.

American Psychiatric Association (1994). Diagnostic and Statistical Manual of Mental Disorders DSM-IV. (Washington, DC: American Psychiatric Association).

American Psychiatric Association (2013). Diagnostic and statistical manual of mental disorders: DSM-5. (Washington, DC: American Psychiatric Association).

Anami, K., Mori, T., Tanaka, F., Kawagoe, Y., Okamoto, J., Yarita, M., Ohnishi, T., Yumoto, M., Matsuda, H., and Saitoh, O. (2003). Stepping stone sampling for retrieving artifact-free electroencephalogram during functional magnetic resonance imaging. NeuroImage 19, 281-295.

Ances, B.M. (2004). Coupling of changes in cerebral blood flow with neural activity: what must initially dip must come back up. J. Cereb. Blood Flow Metab. Off. J. Int. Soc. Cereb. Blood Flow Metab. 24, 1-6.

Ardila, A. (2008). On the evolutionary origins of executive functions. Brain Cogn. 68, 92-99.

Arieli, A., Sterkin, A., Grinvald, A., and Aertsen, A. (1996). Dynamics of Ongoing Activity: Explanation of the Large Variability in Evoked Cortical Responses. Science 273, 1868-1871.

Arnsten, A.F. (2009). Toward a new understanding of attention-deficit hyperactivity disorder pathophysiology. CNS Drugs 23, 33-41.

Arnsten, A.F., and Rubia, K. (2012). Neurobiological circuits regulating attention, cognitive control, motivation, and emotion: disruptions in neurodevelopmental psychiatric disorders. J. Am. Acad. Child Adolesc. Psychiatry 51, 356-367.

Arntz, A., van den Hoorn, M., Cornelis, J., Verheul, R., van den Bosch, W.M., and de Bie, A.J. (2003). Reliability and validity of the borderline personality disorder severity index. J. Personal. Disord. 17, 45-59.

Aron, A.R. (2007). The Neural Basis of Inhibition in Cognitive Control. The Neuroscientist 13, 214-228.

Aron, A.R. (2011). From Reactive to Proactive and Selective Control: Developing a Richer Model for Stopping Inappropriate Responses. Biol. Psychiatry 69, e55-e68.

Aron, A.R., and Poldrack, R.A. (2006). Cortical and Subcortical Contributions to Stop Signal Response Inhibition: Role of the Subthalamic Nucleus. J. Neurosci. 26, 2424-2433.

Aron, A.R., Fletcher, P.C., Bullmore, E.T., Sahakian, B.J., and Robbins, T.W. (2003a). Stop-signal inhibition disrupted by damage to right inferior frontal gyrus in humans. Nat. Neurosci. 6, 115-116.

Aron, A.R., Dowson, J.H., Sahakian, B.J., and Robbins, T.W. (2003b). Methylphenidate improves response inhibition in adults with attention-deficit/hyperactivity disorder. Biol. Psychiatry 54, 1465-1468.

Asahi, S., Okamoto, Y., Okada, G., Yamawaki, S., and Yokota, N. (2004). Negative correlation between right prefrontal activity during response inhibition and impulsiveness: A fMRI study. Eur. Arch. Psychiatry Clin. Neurosci. 254.

Attwell, D., and Iadecola, C. (2002). The neural basis of functional brain imaging signals. Trends Neurosci. 25, 621-625.

Attwell, D., Buchan, A.M., Charpak, S., Lauritzen, M., MacVicar, B.A., and Newman, E.A. (2010). Glial and neuronal control of brain blood flow. Nature 468, 232-243.

Bagshaw, A.P., and Warbrick, T. (2007). Single trial variability of EEG and fMRI responses to visual stimuli. NeuroImage 38, 280-292.

Bagshaw, A.P., Kobayashi, E., Dubeau, F., Pike, G.B., and Gotman, J. (2006). Correspondence between EEG-fMRI and EEG dipole localisation of interictal discharges in focal epilepsy. NeuroImage 30, 417-425.

Bailes, D.R., Young, I.R., Thomas, D.J., Straughan, K., Bydder, G.M., and Steiner, R.E. (1982). NMR imaging of the brain using spin-echo sequences. Clin. Radiol. 33, 395-414.

Banaschewski, T., Brandeis, D., Heinrich, H., Albrecht, B., Brunner, E., and Rothenberger, A. (2003). Association of ADHD and conduct disorder-brain electrical evidence for the existence of a distinct subtype. J. Child Psychol. Psychiatry 44, 356-376.

Barkley, R.A. (1997). Behavioral inhibition, sustained attention, and executive functions: constructing a unifying theory of ADHD. Psychol. Bull. 121, 65-94.

Barkley, R.A. (1998). Attention-Deficit Hyperactivity Disorder. Sci. Am.

Barry, R.J., Johnstone, S.J., and Clarke, A.R. (2003). A review of electrophysiology in attention-deficit/hyperactivity disorder: II. Event-related potentials. Clin. Neurophysiol. 114, 184-198.

Bartels, A., Logothetis, N.K., and Moutoussis, K. (2008). fMRI and its interpretations: an illustration on directional selectivity in area V5/MT. Trends Neurosci. 31, 444-453.

Baumeister, S., Hohmann, S., Wolf, I., Plichta, M.M., Rechtsteiner, S., Zangl, M., Ruf, M., Holz, N., Boecker, R., Meyer-Lindenberg, A., et al. (2014). Sequential inhibitory control processes assessed through simultaneous EEG-fMRI. NeuroImage 94, 349-359.

Beauducel, A., Strobel, A., and Brocke, B. (2003). Psychometrische Eigenschaften und Normen einer deutschsprachigen Fassung der Sensation Seeking-Skalen, Form V. Diagnostica 49, 61-72.

Becker, R., Ritter, P., Moosmann, M., and Villringer, A. (2005). Visual evoked potentials recovered from fMRI scan periods. Hum. Brain Mapp. 26, 221-230.

Becker, R., Reinacher, M., Freyer, F., Villringer, A., and Ritter, P. (2011). How ongoing neuronal oscillations account for evoked fMRI variability. J. Neurosci. Off. J. Soc. Neurosci. 31, 11016-11027.

Bekker, E.M., Overtoom, C.C., Kooij, J.S., Buitelaar, J.K., Verbaten, M.N., and Kenemans, J.L. (2005). Disentangling deficits in adults with attention-deficit/hyperactivity disorder. Arch. Gen. Psychiatry 62, 1129-1136.

Bell, A.J., and Sejnowski, T.J. (1995). An Information-Maximization Approach to Blind Separation and Blind Deconvolution. Neural Comput. 7, 1129-1159.

Bellgrove, M.A., Hester, R., and Garavan, H. (2004). The functional neuroanatomical correlates of response variability: evidence from a response inhibition task. Neuropsychologia 42, 1910-1916.

Bénar, C.-G., Aghakhani, Y., Wang, Y., Izenberg, A., Al-Asmi, A., Dubeau, F., and Gotman, J. (2003). Quality of EEG in simultaneous EEG-fMRI for epilepsy. Clin. Neurophysiol. 114, 569-580.

Bénar, C.-G., Schön, D., Grimault, S., Nazarian, B., Burle, B., Roth, M., Badier, J.-M., Marquis, P., Liegeois-Chauvel, C., and Anton, J.-L. (2007). Single-trial analysis of oddball event-related potentials in simultaneous EEG-fMRI. Hum. Brain Mapp. 28, 602-613.

Ben-Pazi, H., Shalev, R.S., Gross-Tsur, V., and Bergman, H. (2006). Age and medication effects on rhythmic responses in ADHD: possible oscillatory mechanisms? Neuropsychologia 44, 412-416.

Berdahl, C.H. (2010). A neural network model of Borderline Personality Disorder. Neural Netw. 23, 177-188.

Beste, C., Willemssen, R., Saft, C., and Falkenstein, M. (2010). Response inhibition subprocesses and dopaminergic pathways: Basal ganglia disease effects. Neuropsychologia 48, 366-373.

Beste, C., Ness, V., Falkenstein, M., and Saft, C. (2011). On the role of fronto-striatal neural synchronization processes for response inhibition–evidence from ERP phase-synchronization analyses in pre-manifest Huntington's disease gene mutation carriers. Neuropsychologia 49, 3484-3493.

Birn, R.M. (2007). The behavioral significance of spontaneous fluctuations in brain activity. Neuron 56, 8-9.

Bland, A., Mushtaq, F., and Smith, D.V. (2011). Exploiting trial-to-trial variability in multimodal experiments. Front. Hum. Neurosci. 80.

Blinowska, K., Müller-Putz, G., Kaiser, V., Astolfi, L., Vanderperren, K., Van Huffel, S., and Lemieux, L. (2009). Multimodal imaging of human brain activity: rational, biophysical aspects and modes of integration. Comput. Intell. Neurosci. 813607.

Bloch, F. (1946). Nuclear Induction. Phys. Rev. 70, 460-474.

Bokura, H., Yamaguchi, S., and Kobayashi, S. (2001). Electrophysiological correlates for response inhibition in a Go/NoGo task. Clin. Neurophysiol. 112, 2224-2232.

Bollimunta, A., Knuth, K.H., and Ding, M. (2007). Trial-by-trial estimation of amplitude and latency variability in neuronal spike trains. J. Neurosci. Methods 160, 163-170.

Bonmassar, G., Anami, K., Ives, J., and Belliveau, J.W. (1999). Visual evoked potential (VEP) measured by simultaneous 64-channel EEG and 3T fMRI. Neuroreport 10, 1893-1897.

Bonmassar, G., Schwartz, D.P., Liu, A.K., Kwong, K.K., Dale, A.M., and Belliveau, J.W. (2001). Spatiotemporal Brain Imaging of Visual-Evoked Activity Using Interleaved EEG and fMRI Recordings. NeuroImage 13, 1035-1043.

Boonstra, A.M., Oosterlaan, J., Sergeant, J.A., and Buitelaar, J.K. (2005). Executive functioning in adult ADHD: a meta-analytic review. Psychol. Med. 35, 1097-1108.

Bornovalova, M.A., Hicks, B.M., Iacono, W.G., and McGue, M. (2009). Stability, change, and heritability of borderline personality disorder traits from adolescence to adulthood: A longitudinal twin study. Dev. Psychopathol. 21, 1335.

Boynton, G.M., Engel, S.A., Glover, G.H., and Heeger, D.J. (1996). Linear Systems Analysis of Functional Magnetic Resonance Imaging in Human V1.

Brandeis, D., van Leeuwen, T.., Rubia, K., Vitacco, D., Steger, J., Pascual-Marqui, R.., and Steinhausen, H.-C. (1998). Neuroelectric mapping reveals precursor of stop failures in children with attention deficits. Behav. Brain Res. 94, 111-125.

Brendel, G.R., Stern, E., and Silbersweig, D.A. (2005). Defining the neurocircuitry of borderline personality disorder: functional neuroimaging approaches. Dev. Psychopathol. 17, 1197-1206.

Brown, A.B., Biederman, J., Valera, E.M., Doyle, A.E., Bush, G., Spencer, T., Monuteaux, M.C., Mick, E., Whitfield-Gabrieli, S., Makris, N., et al. (2010). Effect of dopamine transporter gene (SLC6A3) variation on dorsal anterior cingulate function in attention-deficit/hyperactivity disorder. Am. J. Med. Genet. B Neuropsychiatr. Genet. 153B, 365-375.

Brown, M.R.G., Benoit, J.R.A., Juhás, M., Lebel, R.M., MacKay, M., Dametto, E., Silverstone, P.H., Dolcos, F., Dursun, S.M., and Greenshaw, A.J. (2015). Neural correlates of high-risk behavior tendencies and impulsivity in an emotional Go/NoGo fMRI task. Front. Syst. Neurosci. 9.

Bruin, K.J., Wijers, A.A., and Van Staveren, A.S.J. (2001). Response priming in a go/nogo task: do we have to explain the go/nogo N2 effect in terms of response activation instead of inhibition? Clin. Neurophysiol. 112, 1660-1671.

Brunner, R., Henze, R., Parzer, P., Kramer, J., Feigl, N., Lutz, K., Essig, M., Resch, F., and Stieltjes, B. (2010). Reduced prefrontal and orbitofrontal gray matter in female adolescents with borderline personality disorder: Is it disorder specific? NeuroImage 49, 114-120.

Bucci, P., and Galderisi, S. (2011). Physiologic Basis of the EEG Signal. In Standard Electroencephalography in Clinical Psychiatry: A Practical Handbook, (Wiley-Blackwell), pp. 7-12.

Buckner, R.L., Andrews-Hanna, J.R., and Schacter, D.L. (2008). The Brain's Default Network. Ann. N. Y. Acad. Sci. 1124, 1-38.

Bush, G., Luu, P., and Posner, M.I. (2000). Cognitive and emotional influences in anterior cingulate cortex. Trends Cogn. Sci. 4, 215-222.

Buxton, R.B. (2009). Part IB Introduction to functional magnetic resonance imaging. In Introduction to Functional Magnetic Resonance Imaging: Principles and Techniques, (Cambridge?; New York: Cambridge University Press), pp. 65-116.

Buxton, R.B. (2013). The physics of functional magnetic resonance imaging (fMRI). Rep. Prog. Phys. Phys. Soc. G. B. 76, 096601.

Bydder, G.M., and Steiner, R.E. (1982). NMR imaging of the brain. Neuroradiology 23, 231-240.

Cackowski, S., Reitz, A.-C., Ende, G., Kleindienst, N., Bohus, M., Schmahl, C., and Krause-Utz, A. (2014). Impact of stress on different components of impulsivity in borderline personality disorder. Psychol. Med. 44, 3329-3340.

Carandini, M. (2004). Amplification of Trial-to-Trial Response Variability by Neurons in Visual Cortex. PLoS Biol. 2, e264.

Carmona, S., Hoekzema, E., Ramos-Quiroga, J.A., Richarte, V., Canals, C., Bosch, R., Rovira, M., Carlos Soliva, J., Bulbena, A., Tobeña, A., et al. (2012). Response inhibition and reward anticipation in medication-naïve adults with attention-deficit/hyperactivity disorder: A within-subject case-control neuroimaging study. Hum. Brain Mapp. 33, 2350-2361.

Castellanos, F.X., and Tannock, R. (2002). Neuroscience of attention-deficit/hyperactivity disorder: the search for endophenotypes. Nat. Rev. Neurosci. 3, 617-628.

Caswell, A.J., Bond, R., Duka, T., and Morgan, M.J. (2015). Further evidence of the heterogeneous nature of impulsivity. Personal. Individ. Differ. 76, 68-74.

Chamberlain, S.R., and Sahakian, B.J. (2007). The neuropsychiatry of impulsivity. Curr. Opin. Psychiatry 20, 255-261.

Chambers, C.D., Garavan, H., and Bellgrove, M.A. (2009). Insights into the neural basis of response inhibition from cognitive and clinical neuroscience. Neurosci. Biobehav. Rev. 33, 631-646.

Chester, D.S., and DeWall, C.N. (2014). Prefrontal recruitment during social rejection predicts greater subsequent self-regulatory imbalance and impairment: neural and longitudinal evidence. NeuroImage 101, 485-493.

Chikazoe, J. (2010). Localizing performance of go/no-go tasks to prefrontal cortical subregions. Curr. Opin. Psychiatry 23, 267-272.

Chikazoe, J., Jimura, K., Asari, T., Yamashita, K., Morimoto, H., Hirose, S., Miyashita, Y., and Konishi, S. (2009). Functional Dissociation in Right Inferior Frontal Cortex during Performance of Go/No-Go Task. Cereb. Cortex 19, 146-152.

Christiansen, H., Kis, B., Hirsch, O., Philipsen, A., Henneck, M., Panczuk, A., Pietrowsky, R., Hebebrand, J., and Schimmelmann, B.G. (2011). German validation of the Conners Adult ADHD Rating Scales-self-report (CAARS-S) I: Factor structure and normative data. Eur. Psychiatry 26, 100-107.

Christiansen, H., Kis, B., Hirsch, O., Matthies, S., Hebebrand, J., Uekermann, J., Abdel-Hamid, M., Kraemer, M., Wiltfang, J., Graf, E., et al. (2012). German validation of the Conners Adult ADHD Rating Scales (CAARS) II: Reliability, validity, diagnostic sensitivity and specificity. Eur. Psychiatry 27, 321-328.

Coffey, S.F., Schumacher, J.A., Baschnagel, J.S., Hawk, L.W., and Holloman, G. (2011). Impulsivity and risk-taking in borderline personality disorder with and without substance use disorders. Personal. Disord. Theory Res. Treat. 2, 128-141.

Coghill, D.R., Seth, S., Pedroso, S., Usala, T., Currie, J., and Gagliano, A. (2014). Effects of methylphenidate on cognitive functions in children and adolescents with attention-deficit/hyperactivity disorder: evidence from a systematic review and a meta-analysis. Biol. Psychiatry 76, 603-615.

Coid, J., Yang, M., Tyrer, P., Roberts, A., and Ullrich, S. (2006). Prevalence and correlates of personality disorder in Great Britain. Br. J. Psychiatry 188, 423-431.

Collins, H.R., Corbly, C.R., Liu, X., Kelly, T.H., Lynam, D., and Joseph, J.E. (2012). Too little, too late or too much, too early? Differential hemodynamics of response inhibition in high and low sensation seekers. Brain Res. 1481, 1-12.

Congdon, E., Altshuler, L.L., Mumford, J.A., Karlsgodt, K.H., Sabb, F.W., Ventura, J., McGough, J.J., London, E.D., Cannon, T.D., Bilder, R.M., et al. (2014). Neural activation during response inhibition in adult attention-deficit/hyperactivity disorder: Preliminary findings on the effects of medication and symptom severity. Psychiatry Res. Neuroimaging 222, 17-28.

Cooper, R.E., Skirrow, C., Tye, C., McLoughlin, G., Rijsdijk, F., Banaschweski, T., Brandeis, D., Kuntsi, J., and Asherson, P. (2014). The effect of methylphenidate on very low frequency electroencephalography oscillations in adult ADHD. Brain Cogn. 86, 82-89.

Cortese, S., Kelly, C., Chabernaud, C., Proal, E., Di Martino, A., Milham, M.P., and Castellanos, F.X. (2012). Toward Systems Neuroscience of ADHD: A Meta-Analysis of 55 fMRI Studies. Am. J. Psychiatry 169, 1038-1055.

Criaud, M., and Boulinguez, P. (2013). Have we been asking the right questions when assessing response inhibition in go/no-go tasks with fMRI? A meta-analysis and critical review. Neurosci. Biobehav. Rev. 37, 11-23.

Cubillo, A., Halari, R., Ecker, C., Giampietro, V., Taylor, E., and Rubia, K. (2010). Reduced activation and inter-regional functional connectivity of fronto-striatal networks in adults with childhood Attention-Deficit Hyperactivity Disorder (ADHD) and persisting symptoms during tasks of motor inhibition and cognitive switching. J. Psychiatr. Res. 44, 629-639.

Cubillo, A., Smith, A.B., Barrett, N., Giampietro, V., Brammer, M.J., Simmons, A., and Rubia, K. (2014). Shared and Drug-Specific Effects of Atomoxetine and Methylphenidate on Inhibitory Brain Dysfunction in Medication-Naive ADHD Boys. Cereb. Cortex N. Y. NY 24, 174-185.

Cyders, M.A., and Coskunpinar, A. (2011). Measurement of constructs using self-report and behavioral lab tasks: Is there overlap in nomothetic span and construct representation for impulsivity? Clin. Psychol. Rev. 31, 965-982.

Dalley, J.W., Everitt, B.J., and Robbins, T.W. (2011). Impulsivity, Compulsivity, and Top-Down Cognitive Control. Neuron 69, 680-694.

Davidson, M.A. (2007). Literature Review: ADHD in Adults: A Review of the Literature. J. Atten. Disord. 11, 628-641.

Debener, S., Ullsperger, M., Siegel, M., Fiehler, K., Cramon, D.Y. von, and Engel, A.K. (2005). Trial-by-Trial Coupling of Concurrent Electroencephalogram and Functional Magnetic Resonance Imaging Identifies the Dynamics of Performance Monitoring. J. Neurosci. 25, 11730-11737.

Debener, S., Ullsperger, M., Siegel, M., and Engel, A.K. (2006). Single-trial EEG-fMRI reveals the dynamics of cognitive function. Trends Cogn. Sci. 10, 558-563.

Delorme, A., Sejnowski, T., and Makeig, S. (2007). Enhanced detection of artifacts in EEG data using higher-order statistics and independent component analysis. NeuroImage 34, 1443-1449.

Depue, B.E., Burgess, G.C., Bidwell, L.C., Willcutt, E.G., and Banich, M.T. (2010). Behavioral performance predicts grey matter reductions in the right inferior frontal gyrus in young adults with combined type ADHD. Psychiatry Res. Neuroimaging 182, 231-237.

De Vos, M., Thorne, J.D., Yovel, G., and Debener, S. (2012). Let's face it, from trial to trial: Comparing procedures for N170 single-trial estimation. NeuroImage 63, 1196-1202.

Dhar, M., Been, P.H., Minderaa, R.B., and Althaus, M. (2010). Information processing differences and similarities in adults with dyslexia and adults with Attention Deficit Hyperactivity Disorder during a Continuous Performance Test: A study of cortical potentials. Neuropsychologia 48, 3045-3056.

Diamond, A. (2013). Executive Functions. Annu. Rev. Psychol. 64, 135-168.

Dibbets, P., Evers, L., Hurks, P., Marchetta, N., and Jolles, J. (2009). Differences in feedback- and inhibition-related neural activity in adult ADHD. Brain Cogn. 70, 73-83.

Dickstein, S.G., Bannon, K., Xavier Castellanos, F., and Milham, M.P. (2006). The neural correlates of attention deficit hyperactivity disorder: an ALE meta-analysis. J. Child Psychol. Psychiatry 47, 1051-1062.

Dillo, W., Göke, A., Prox-Vagedes, V., Szycik, G.R., Roy, M., Donnerstag, F., Emrich, H.M., and Ohlmeier, M.D. (2010). Neuronal correlates of ADHD in adults with evidence for compensation strategies-a functional MRI study with a Go/No-Go paradigm. Ger. Med. Sci. 8.

Dimoska, A., Johnstone, S.J., Barry, R.J., and Clarke, A.R. (2003). Inhibitory motor control in children with attention-deficit/hyperactivity disorder: event-related potentials in the stop-signal paradigm. Biol. Psychiatry 54, 1345-1354.

Di Russo, F., Martínez, A., Sereno, M.I., Pitzalis, S., and Hillyard, S.A. (2002). Cortical sources of the early components of the visual evoked potential. Hum. Brain Mapp. 15, 95-111.

Di Russo, F., Pitzalis, S., Spitoni, G., Aprile, T., Patria, F., Spinelli, D., and Hillyard, S.A. (2005). Identification of the neural sources of the pattern-reversal VEP. NeuroImage 24, 874-886.

Doehnert, M., Brandeis, D., Imhof, K., Drechsler, R., and Steinhausen, H.-C. (2010). Mapping Attention-Deficit/Hyperactivity Disorder from Childhood to Adolescence-No Neurophysiologic Evidence for a Developmental Lag of Attention but Some for Inhibition. Biol. Psychiatry 67, 608-616.

Domes, G., Winter, B., Schnell, K., Vohs, K., Fast, K., and Herpertz, S.C. (2006). The influence of emotions on inhibitory functioning in borderline personality disorder. Psychol. Med. 36, 1163.

Doñamayor, N., Heilbronner, U., and Münte, T.F. (2012). Coupling electrophysiological and hemodynamic responses to errors. Hum. Brain Mapp. 33, 1621-1633.

Donegan, N.H., Sanislow, C.A., Blumberg, H.P., Fulbright, R.K., Lacadie, C., Skudlarski, P., Gore, J.C., Olson, I.R., McGlashan, T.H., and Wexler, B.E. (2003). Amygdala hyperreactivity in borderline personality disorder: implications for emotional dysregulation. Biol. Psychiatry 54, 1284-1293.

Donkers, F.C.L., and van Boxtel, G.J.M. (2004). The N2 in go/no-go tasks reflects conflict monitoring not response inhibition. Brain Cogn. 56, 165-176.

Doyle, A.E. (2006). Executive functions in attention-deficit/hyperactivity disorder. J. Clin. Psychiatry 67 Suppl 8, 21-26.

Doyle, A.E. (2015). Commentary: Insights from across diagnostic boundaries: ADHD in the RDoC era - a commentary on Scerif and Baker (2015). J. Child Psychol. Psychiatry 56, 274-277.

Doyle, A.E., Willcutt, E.G., Seidman, L.J., Biederman, J., Chouinard, V.-A., Silva, J., and Faraone, S.V. (2005). Attention-deficit/hyperactivity disorder endophenotypes. Biol. Psychiatry 57, 1324-1335.

Doyle, F.H., Gore, J.C., Pennock, J.M., Bydder, G.M., Orr, J.S., Steiner, R.E., Young, I.R., Burl, M., Clow, H., Gilderdale, D.J., et al. (1981). Imaging of the brain by nuclear magnetic resonance. Lancet 2, 53-57.

Drevets, W.C., Savitz, J., and Trimble, M. (2008). The Subgenual Anterior Cingulate Cortex in Mood Disorders. CNS Spectr. 13, 663-681.

Duann, J.-R., Jung, T.-P., Kuo, W.-J., Yeh, T.-C., Makeig, S., Hsieh, J.-C., and Sejnowski, T.J. (2002). Single-Trial Variability in Event-Related BOLD Signals. NeuroImage 15, 823-835.

Durston, S., Tottenham, N.T., Thomas, K.M., Davidson, M.C., Eigsti, I.-M., Yang, Y., Ulug, A.M., and Casey, B.. (2003). Differential patterns of striatal activation in young children with and without ADHD. Biol. Psychiatry 53, 871-878.

Durston, S., Pol, H.E.H., Schnack, H.G., Buitelaar, J.K., Steenhuis, M.P., Minderaa, R.B., Kahn, R.S., and Van Engeland, H. (2004). Magnetic Resonance Imaging of Boys With Attention-Deficit/Hyperactivity Disorder and Their Unaffected Siblings. J. Am. Acad. Child Adolesc. Psychiatry 43, 332-340.

Eagle, D.M., and Baunez, C. (2010). Is there an inhibitory-response-control system in the rat? Evidence from anatomical and pharmacological studies of behavioral inhibition. Neurosci. Biobehav. Rev. 34, 50-72.

Eagle, D.M., Bari, A., and Robbins, T.W. (2008). The neuropsychopharmacology of action inhibition: cross-species translation of the stop-signal and go/no-go tasks. Psychopharmacology (Berl.) 199, 439-456.

Eichele, T., Specht, K., Moosmann, M., Jongsma, M.L.A., Quiroga, R.Q., Nordby, H., and Hugdahl, K. (2005). Assessing the spatiotemporal evolution of neuronal activation with single-trial event-related potentials and functional MRI. Proc. Natl. Acad. Sci. U. S. A. 102, 17798-17803.

Eichele, T., Calhoun, V.D., Moosmann, M., Specht, K., Jongsma, M.L.A., Quiroga, R.Q., Nordby, H., and Hugdahl, K. (2008). Unmixing concurrent EEG-fMRI with parallel independent component analysis. Int. J. Psychophysiol. Off. J. Int. Organ. Psychophysiol. 67, 222-234.

Eichele, T., Calhoun, V.D., and Debener, S. (2009). Mining EEG-fMRI using independent component analysis. Int. J. Psychophysiol. 73, 53-61.

van Eijk, J., Sebastian, A., Krause-Utz, A., Cackowski, S., Demirakca, T., Biedermann, S.V., Lieb, K., Bohus, M., Schmahl, C., Ende, G., et al. (2015). Women with borderline personality disorder do not show altered BOLD responses during response inhibition. Psychiatry Res. Neuroimaging 234, 378-389.

Ellison-Wright, I., Ellison-Wright, Z., and Bullmore, E. (2008). Structural brain change in Attention Deficit Hyperactivity Disorder identified by meta-analysis. BMC Psychiatry 8, 51.

Enriquez-Geppert, S., Konrad, C., Pantev, C., and Huster, R.J. (2010). Conflict and inhibition differentially affect the N200/P300 complex in a combined go/nogo and stop-signal task. NeuroImage 51, 877-887.

Epstein, J.N., Casey, B.J., Tonev, S.T., Davidson, M.C., Reiss, A.L., Garrett, A., Hinshaw, S.P., Greenhill, L.L., Glover, G., Shafritz, K.M., et al. (2007). ADHD- and medication-related brain activation effects in concordantly affected parent-child dyads with ADHD: ADHD frontostriatal dysfunction. J. Child Psychol. Psychiatry 48, 899-913.

Epstein, J.N., Langberg, J.M., Rosen, P.J., Graham, A., Narad, M.E., Antonini, T.N., Brinkman, W.B., Froehlich, T., Simon, J.O., and Altaye, M. (2011). Evidence for higher reaction time variability for children with ADHD on a range of cognitive tasks including reward and event rate manipulations. Neuropsychology 25, 427-441.

Esposito, F., Mulert, C., and Goebel, R. (2009). Combined distributed source and single-trial EEG-fMRI modeling: application to effortful decision making processes. NeuroImage 47, 112-121.

Eysenck, S.B.G., Eysenck, H.J., and Barrett, P. (1985). A revised version of the psychoticism scale. Personal. Individ. Differ. 6, 21-29.

Falkenstein, M., Hoormann, J., and Hohnsbein, J. (1999). ERP components in Go/Nogo tasks and their relation to inhibition. Acta Psychol. (Amst.) 101, 267-291.

Fallgatter, A.J., Ehlis, A.-C., Seifert, J., Strik, W.K., Scheuerpflug, P., Zillessen, K.E., Herrmann, M.J., and Warnke, A. (2004). Altered response control and anterior cingulate function in attention-deficit/hyperactivity disorder boys. Clin. Neurophysiol. 115, 973-981.

Fallgatter, A.J., Ehlis, A.-C., Rösler, M., Strik, W.K., Blocher, D., and Herrmann, M.J. (2005). Diminished prefrontal brain function in adults with psychopathology in childhood related to attention deficit hyperactivity disorder. Psychiatry Res. Neuroimaging 138, 157-169.

Faraone, S.V. (2005). What Is the Prevalence of Adult ADHD? Results of a Population Screen of 966 Adults. J. Atten. Disord. 9, 384-391.

Faraone, S.V., and Mick, E. (2010). Molecular genetics of attention deficit hyperactivity disorder. Psychiatr. Clin. North Am. 33, 159-180.

Faraone, S.V., Doyle, A.E., Mick, E., and Biederman, J. (2001). Meta-analysis of the association between the 7-repeat allele of the dopamine D(4) receptor gene and attention deficit hyperactivity disorder. Am. J. Psychiatry 158, 1052-1057.

Faraone, S.V., Sergeant, J.A., Gilberg, C., and Biederman, J. (2003). The worldwide prevalence of ADHD: is it an American condition? World Psychiatry 2, 104-113.

Faraone, S.V., Perlis, R.H., Doyle, A.E., Smoller, J.W., Goralnick, J.J., Holmgren, M.A., and Sklar, P. (2005). Molecular Genetics of Attention-Deficit/Hyperactivity Disorder. Biol. Psychiatry 57, 1313-1323.

Fayyad, J., De Graaf, R., Kessler, R., Alonso, J., Angermeyer, M., Demyttenaere, K., De Girolamo, G., Haro, J.M., Karam, E.G., Lara, C., et al. (2007). Cross-national prevalence and correlates of adult attention-deficit hyperactivity disorder. Br. J. Psychiatry J. Ment. Sci. 190, 402-409.

Feige, B. (1999). Oscillatory brain activity and its analysis on the basis for MEG and EEG (Münster: Waxmann).

Feige, B., Scheffler, K., Esposito, F., Di Salle, F., Hennig, J., and Seifritz, E. (2005). Cortical and Subcortical Correlates of Electroencephalographic Alpha Rhythm Modulation. J. Neurophysiol. 93, 2864-2872.

Feige, B., Biscaldi, M., Saville, C.W.N., Kluckert, C., Bender, S., Ebner-Priemer, U., Hennighausen, K., Rauh, R., Fleischhaker, C., and Klein, C. (2013). On the Temporal Characteristics of Performance Variability in Attention Deficit Hyperactivity Disorder (ADHD). PLoS ONE 8, e69674.

First, M., Spitzer, R., Gibbon, M., and Williams, J. (1996). User's Guide for the Structured Clinical Interview for DSM-IV Personality Disorders (SCID-II). (Washington (DC): American Psychiatric Press).

First, M., Spitzer, R., Gibbon, M., and Williams, J. (1997). Structured Clinical Interview for DSM-IV® Axis I Disorders (SCID-I), Clinician Version, User's Guide. (Washington (DC): American Psychiatric Press).

Fisher, T., Aharon-Peretz, J., and Pratt, H. (2011). Dis-regulation of response inhibition in adult Attention Deficit Hyperactivity Disorder (ADHD): An ERP study. Clin. Neurophysiol. 122, 2390-2399.

Fontanini, A., and Katz, D.B. (2008). Behavioral States, Network States, and Sensory Response Variability. J. Neurophysiol. 100, 1160-1168.

Fox, M.D., Snyder, A.Z., Vincent, J.L., Corbetta, M., Van Essen, D.C., and Raichle, M.E. (2005). The human brain is intrinsically organized into dynamic, anticorrelated functional networks. Proc. Natl. Acad. Sci. U. S. A. 102, 9673-9678.

Freese, S., and Kröger, C. (1999). Borderline Personality Disorder Severity Index (BPDSI) (Braunschweig (Germany): Christoph-Dornier-Stiftung, Institut für Psychologie).

Freitag, C.M., Rohde, L.A., Lempp, T., and Romanos, M. (2010). Phenotypic and measurement influences on heritability estimates in childhood ADHD. Eur. Child Adolesc. Psychiatry 19, 311-323.

Friedman, L.A., and Rapoport, J.L. (2015). Brain development in ADHD. Curr. Opin. Neurobiol. 30, 106-111. Friedman, D., Cycowicz, Y.M., and Gaeta, H. (2001). The novelty P3: an event-related brain potential (ERP) sign of the brain's evaluation of novelty. Neurosci. Biobehav. Rev. 25, 355-373.

Friston, K.J., Jezzard, P., and Turner, R. (1994a). Analysis of functional MRI time-series. Hum. Brain Mapp. 1, 153-171.

Friston, K.J., Worsley, K.J., Frackowiak, R.S.J., Mazziotta, J.C., and Evans, A.C. (1994b). Assessing the significance of focal activations using their spatial extent. Hum. Brain Mapp. 1, 210-220.

Friston, K. (2007). Statistical parametric mapping: the analysis of funtional brain images (Amsterdam; Boston: Elsevier/Academic Press).

Frodl, T., and Skokauskas, N. (2012). Meta-analysis of structural MRI studies in children and adults with attention deficit hyperactivity disorder indicates treatment effects: Meta-analysis of structural MRI ADHD studies. Acta Psychiatr. Scand. 125, 114-126.

Fuglø, D., Pedersen, H., Rostrup, E., Hansen, A.E., and Larsson, H.B.W. (2012). Correlation between single-trial visual evoked potentials and the blood oxygenation level dependent response in simultaneously recorded electroencephalography-functional magnetic resonance imaging. Magn. Reson. Med. 68, 252-260.

Fydrich, T., Renneberg, B., Schmitz, B., and Wittchen, H.-U. (1997). Strukturiertes Klinisches Interview für DSM-IV, Achse II: Persönlichkeitsstörungen. (Göttingen (Germany): Hogrefe).

Garavan, H. (2002). Dissociable Executive Functions in the Dynamic Control of Behavior: Inhibition, Error Detection, and Correction. NeuroImage 17, 1820-1829.

Garavan, H., Hester, R., Murphy, K., Fassbender, C., and Kelly, C. (2006). Individual differences in the functional neuroanatomy of inhibitory control. Control Atten. Actions 1105, 130-142.

Gizer, I.R., Ficks, C., and Waldman, I.D. (2009). Candidate gene studies of ADHD: a meta-analytic review. Hum. Genet. 126, 51-90.

Gloor, P. (1969). The work of Hans Berger?: P. Gloor (Montreal, Canada). Electroencephalogr. Clin. Neurophysiol. 27, 649.

Goldman, R.I., Stern, J.M., Engel, J., Jr, and Cohen, M.S. (2000). Acquiring simultaneous EEG and functional MRI. Clin. Neurophysiol. Off. J. Int. Fed. Clin. Neurophysiol. 111, 1974-1980.

Goldman, R.I., Stern, J.M., Engel, J., Jr, and Cohen, M.S. (2002). Simultaneous EEG and fMRI of the alpha rhythm. Neuroreport 13, 2487-2492.

Goldman, R.I., Wei, C.-Y., Philiastides, M.G., Gerson, A.D., Friedman, D., Brown, T.R., and Sajda, P. (2009). Single-trial discrimination for integrating simultaneous EEG and fMRI: Identifying cortical areas contributing to trial-to-trial variability in the auditory oddball task. NeuroImage 47, 136-147.

Gotman, J., Bénar, C.-G., and Dubeau, F. (2004). Combining EEG and FMRI in epilepsy: methodological challenges and clinical results. J. Clin. Neurophysiol. Off. Publ. Am. Electroencephalogr. Soc. 21, 229-240.

Gow, R.V., Rubia, K., Taylor, E., Vallée-Tourangeau, F., Matsudaira, T., Ibrahimovic, A., and Sumich, A. (2012). Abnormal centroparietal ERP response in predominantly medication-naive adolescent boys with ADHD during both response inhibition and execution. J. Clin. Neurophysiol. 29, 181-189.

van Graan, L.A., Lemieux, L., and Chaudhary, U.J. (2015). Methods and utility of EEG-fMRI in epilepsy. Quant. Imaging Med. Surg. 5, 300-312.

Grant, B.F., Chou, S.P., Goldstein, R.B., Huang, B., Stinson, F.S., Saha, T.D., Smith, S.M., Dawson, D.A., Pulay, A.J., Pickering, R.P., et al. (2008). Prevalence, correlates, disability, and comorbidity of DSM-IV borderline personality disorder: results from the Wave 2 National Epidemiologic Survey on Alcohol and Related Conditions. J. Clin. Psychiatry 69, 533-545.

Grech, R., Cassar, T., Muscat, J., Camilleri, K.P., Fabri, S.G., Zervakis, M., Xanthopoulos, P., Sakkalis, V., and Vanrumste, B. (2008). Review on solving the inverse problem in EEG source analysis. J. Neuroengineering Rehabil. 5, 25.

Greven, C.U., Bralten, J., Mennes, M., O'Dwyer, L., van Hulzen, K.J.E., Rommelse, N., Schweren, L.J.S., Hoekstra, P.J., Hartman, C.A., Heslenfeld, D., et al. (2015). Developmentally Stable Whole-Brain Volume Reductions and Developmentally Sensitive Caudate and Putamen Volume Alterations in Those With Attention-Deficit/Hyperactivity Disorder and Their Unaffected Siblings. JAMA Psychiatry 72, 490-499.

Hagenhoff, M., Franzen, N., Koppe, G., Baer, N., Scheibel, N., Sammer, G., Gallhofer, B., and Lis, S. (2013). Executive functions in borderline personality disorder. Psychiatry Res. 210, 224-231.

Hart, H., Radua, J., Mataix-Cols, D., and Rubia, K. (2012). Meta-analysis of fMRI studies of timing in attention-deficit hyperactivity disorder (ADHD). Neurosci. Biobehav. Rev. 36, 2248-2256.

Hart, H., Radua, J., Nakao, T., Mataix-Cols, D., and Rubia, K. (2013). Meta-analysis of Functional Magnetic Resonance Imaging Studies of Inhibition and Attention in Attention-deficit/Hyperactivity Disorder: Exploring Task-Specific, Stimulant Medication, and Age Effects. JAMA Psychiatry 70, 185.

Hautzinger, M., Bailer, M., Worall, H., and Keller, F. (1995). Beck-Depressions-Inventar (BDI) (Bern: Hans Huber).

Hawkes, R.C., Holland, G.N., Moore, W.S., and Worthington, B.S. (1980). Nuclear magnetic resonance (NMR) tomography of the brain: a preliminary clinical assessment with demonstration of pathology. J. Comput. Assist. Tomogr. 4, 577-586.

Hazlett, E.A., New, A.S., Newmark, R., Haznedar, M.M., Lo, J.N., Speiser, L.J., Chen, A.D., Mitropoulou, V., Minzenberg, M., Siever, L.J., et al. (2005). Reduced anterior and posterior cingulate gray matter in borderline personality disorder. Biol. Psychiatry 58, 614-623.

Hazlett, E.A., Zhang, J., New, A.S., Zelmanova, Y., Goldstein, K.E., Haznedar, M.M., Meyerson, D., Goodman, M., Siever, L.J., and Chu, K.-W. (2012). Potentiated Amygdala Response to Repeated Emotional Pictures in Borderline Personality Disorder. Biol. Psychiatry 72, 448-456.

Helenius, P., Laasonen, M., Hokkanen, L., Paetau, R., and Niemivirta, M. (2011). Impaired engagement of the ventral attentional pathway in ADHD. Neuropsychologia 49, 1889-1896.

Hendee, W.R., and Morgan, C.J. (1984). Magnetic resonance imaging Part I-Physical principles. West. J. Med. 141, 491-500.

Herpertz, S.C., Dietrich, T.M., Wenning, B., Krings, T., Erberich, S.G., Willmes, K., Thron, A., and Sass, H. (2001). Evidence of abnormal amygdala functioning in borderline personality disorder: a functional MRI study. Biol. Psychiatry 50, 292-298.

Hillman, E.M.C. (2014). Coupling mechanism and significance of the BOLD signal: a status report. Annu. Rev. Neurosci. 37, 161-181.

Holland, G.N., Moore, W.S., and Hawkes, R.C. (1980). Nuclear magnetic resonance tomography of the brain. J. Comput. Assist. Tomogr. 4, 1-3.

Holtmann, J., Herbort, M.C., Wüstenberg, T., Soch, J., Richter, S., Walter, H., Roepke, S., and Schott, B.H. (2013). Trait anxiety modulates fronto-limbic processing of emotional interference in borderline personality disorder. Front. Hum. Neurosci. 7.

Horn, N.R., Dolan, M., Elliott, R., Deakin, J.F.W., and Woodruff, P.W.R. (2003). Response inhibition and impulsivity: an fMRI study. Neuropsychologia 41, 1959-1966.

Howarth, C. (2014). The contribution of astrocytes to the regulation of cerebral blood flow. Front. Neurosci. 8.

Huang-Hellinger, F.R., Breiter, H.C., McCormack, G., Cohen, M.S., Kwong, K.K., Sutton, J.P., Savoy, R.L., Weisskoff, R.M., Davis, T.L., Baker, J.R., et al. (1995). Simultaneous functional magnetic resonance imaging and electrophysiological recording. Hum. Brain Mapp. 3, 13-23.

Huettel, S.A., Song, A.W., and McCarthy, G. (2008). Functional Magnetic Resonance Imaging, Second Edition (Sunderland, Mass: Sinauer Associates).

Huster, R.J., Westerhausen, R., Pantev, C., and Konrad, C. (2010). The role of the cingulate cortex as neural generator of the N200 and P300 in a tactile response inhibition task. Hum. Brain Mapp. 31, 1260-1271.

Huster, R.J., Eichele, T., Enriquez-Geppert, S., Wollbrink, A., Kugel, H., Konrad, C., and Pantev, C. (2011). Multimodal imaging of functional networks and event-related potentials in performance monitoring. NeuroImage 56, 1588-1597.

Huster, R.J., Debener, S., Eichele, T., and Herrmann, C.S. (2012). Methods for Simultaneous EEG-fMRI: An Introductory Review. J. Neurosci. 32, 6053-6060.

Huster, R.J., Enriquez-Geppert, S., Lavallee, C.F., Falkenstein, M., and Herrmann, C.S. (2013). Electroencephalography of response inhibition tasks: Functional networks and cognitive contributions. Int. J. Psychophysiol. 87, 217-233.

Huster, R.J., Plis, S.M., Lavallee, C.F., Calhoun, V.D., and Herrmann, C.S. (2014). Functional and effective connectivity of stopping. NeuroImage 94, 120-128.

Hyvärinen, A., and Oja, E. (2000). Independent component analysis: algorithms and applications. Neural Netw. 13, 411-430.

Insel, T., Cuthbert, B., Garvey, M., Heinssen, R., Pine, D.S., Quinn, K., Sanislow, C., and Wang, P. (2010). Research domain criteria (RDoC): toward a new classification framework for research on mental disorders. Am. J. Psychiatry 167, 748-51.

Ivanov, I., Bansal, R., Hao, X., Zhu, H., Kellendonk, C., Miller, L., Sanchez-Pena, J., Miller, A.M., Chakravarty, M.M., Klahr, K., et al. (2010). Morphological Abnormalities of the Thalamus in Youths With Attention Deficit Hyperactivity Disorder. Am. J. Psychiatry 167, 397-408.

Ives, J.R., Warach, S., Schmitt, F., Edelman, R.R., and Schomer, D.L. (1993). Monitoring the patient's EEG during echo planar MRI. Electroencephalogr. Clin. Neurophysiol. 87, 417-420.

Jacob, G.A., Gutz, L., Bader, K., Lieb, K., Tüscher, O., and Stahl, C. (2010). Impulsivity in Borderline Personality Disorder: Impairment in Self-Report Measures, but Not Behavioral Inhibition. Psychopathology 43, 180-188

Jacob, G.A., Zvonik, K., Kamphausen, S., Sebastian, A., Maier, S., Philipsen, A., Tebartz van Elst, L., Lieb, K., and Tüscher, O. (2013). Emotional modulation of motor response inhibition in women with borderline personality disorder: an fMRI study. J. Psychiatry Neurosci. JPN 38, 164-172.

Jacobs, J., Levan, P., Moeller, F., Boor, R., Stephani, U., Gotman, J., and Siniatchkin, M. (2009). Hemodynamic changes preceding the interictal EEG spike in patients with focal epilepsy investigated using simultaneous EEG-fMRI. NeuroImage 45, 1220-1231.

Jahfari, S., Waldorp, L., van den Wildenberg, W.P.M., Scholte, H.S., Ridderinkhof, K.R., and Forstmann, B.U. (2011). Effective connectivity reveals important roles for both the hyper-direct (fronto-subthalamic) and the indirect (fronto-striatal-pallidal) fronto-basal ganglia pathways during response inhibition. J. Neurosci. Off. J. Soc. Neurosci. 31, 6891-6899.

Jodo, E., and Kayama, Y. (1992). Relation of a negative ERP component to response inhibition in a Go/No-go task. Electroencephalogr. Clin. Neurophysiol. 82, 477-482.

Johnson, J.S., and Olshausen, B.A. (2003). Timecourse of neural signatures of object recognition. J. Vis. 3, 499-512.

Johnstone, S.J., Barry, R.J., and Clarke, A.R. (2013). Ten years on: A follow-up review of ERP research in attention-deficit/hyperactivity disorder. Clin. Neurophysiol. 124, 644-657.

Juckel, G., Karch, S., Kawohl, W., Kirsch, V., Jäger, L., Leicht, G., Lutz, J., Stammel, A., Pogarell, O., Ertl, M., et al. (2012). Age effects on the P300 potential and the corresponding fMRI BOLD-signal. NeuroImage 60, 2027-2034.

Jung, T., Makeig, S., Lee, T., Mckeown, M.J., Brown, G., Bell, A.J., and Sejnowski, T.J. (2000). Independent component analysis of biomedical signals. In In Proc. 2nd Int. Workshop on Independent Component Analysis and Blind Signal Separation (ICA2000, pp. 633-644.

Jung, T.-P., Makeig, S., Bell, A.J., and Sejnowski, T.J. (1998). Independent Component Analysis of Electroencephalographic and Event-Related Potential Data. In Central Auditory Processing and Neural Modeling, P.W.F. Poon, and J.F. Brugge, eds. (Springer US), pp. 189-197.

Jung, T.-P., Makeig, S., Westerfield, M., Townsend, J., Courchesne, E., and Sejnowski, T.J. (2001). Analysis and visualization of single-trial event-related potentials. Hum. Brain Mapp. 14, 166-185.

Kam, J.W.Y., Dominelli, R., and Carlson, S.R. (2012). Differential relationships between sub?traits of BIS-11 impulsivity and executive processes: An ERP study. Int. J. Psychophysiol. 85, 174-187.

Kanai, R., and Rees, G. (2011). The structural basis of inter-individual differences in human behaviour and cognition. Nat. Rev. Neurosci. 12, 231-242.

Karch, S., Jäger, L., Karamatskos, E., Graz, C., Stammel, A., Flatz, W., Lutz, J., Holtschmidt-Täschner, B., Genius, J., Leicht, G., et al. (2008). Influence of trait anxiety on inhibitory control in alcohol-dependent patients: Simultaneous acquisition of ERPs and BOLD responses. J. Psychiatr. Res. 42, 734-745.

Karch, S., Thalmeier, T., Lutz, J., Cerovecki, A., Opgen-Rhein, M., Hock, B., Leicht, G., Hennig-Fast, K., Meindl, T., Riedel, M., et al. (2010). Neural correlates (ERP/fMRI) of voluntary selection in adult ADHD patients. Eur. Arch. Psychiatry Clin. Neurosci. 260, 427-440.

Karch, S., Segmiller, F., Hantschk, I., Cerovecki, A., Opgen-Rhein, M., Hock, B., Dargel, S., Leicht, G., Hennig-Fast, K., Riedel, M., et al. (2012). Increased gamma oscillations during voluntary selection processes in adult patients with attention deficit/hyperactivity disorder. J. Psychiatr. Res. 46, 1515-1523.

Karch, S., Voelker, J., Thalmeier, T., Ertl, M., Leicht, G., Pogarell, O., and Mulert, C. (2014). Deficits during voluntary selection in adult patients with ADHD: new insights from single-trial coupling of simultaneous EEG/fMRI. Neuropsychiatr. Imaging Stimul. 5, 41.

Kelly, A.M.C., Uddin, L.Q., Biswal, B.B., Castellanos, F.X., and Milham, M.P. (2008). Competition between functional brain networks mediates behavioral variability. NeuroImage 39, 527-537.

Kendler, K.S., Aggen, S.H., Czajkowski, N., Røysamb, E., Tambs, K., Torgersen, S., Neale, M.C., and Reichborn-Kjennerud, T. (2008). The structure of genetic and environmental risk factors for DSM-IV personality disorders: a multivariate twin study. Arch. Gen. Psychiatry 65, 1438-1446.

Kendler, K.S., Myers, J., and Reichborn-Kjennerud, T. (2011). Borderline personality disorder traits and their relationship with dimensions of normative personality: a web-based cohort and twin study: Borderline disorder and normative personality. Acta Psychiatr. Scand. 123, 349-359.

Kenemans, J.L., Bekker, E.M., Lijffijt, M., Overtoom, C.C.E., Jonkman, L.M., and Verbaten, M.N. (2005). Attention deficit and impulsivity: Selecting, shifting, and stopping. Int. J. Psychophysiol. 58, 59-70.

Kessler, R.C., Adler, L., Ames, M., Barkley, R.A., Birnbaum, H., Greenberg, P., Johnston, J.A., Spencer, T., and Ustün, T.B. (2005). The prevalence and effects of adult attention deficit/hyperactivity disorder on work performance in a nationally representative sample of workers. J. Occup. Environ. Med. Am. Coll. Occup. Environ. Med. 47, 565-572.

Keune, P.M., Wiedemann, E., Schneidt, A., and Schönenberg, M. (2015). Frontal brain asymmetry in adult attention-deficit/hyperactivity disorder (ADHD): extending the motivational dysfunction hypothesis. Clin. Neurophysiol. Off. J. Int. Fed. Clin. Neurophysiol. 126, 711-720.

Key, A.P.F., Dove, G.O., and Maguire, M.J. (2005). Linking brainwaves to the brain: an ERP primer. Dev. Neuropsychol. 27, 183-215.

Kim, S.-G., and Ogawa, S. (2012). Biophysical and physiological origins of blood oxygenation level-dependent fMRI signals. J. Cereb. Blood Flow Metab. Off. J. Int. Soc. Cereb. Blood Flow Metab. 32, 1188-1206.

Kisley, M.A., and Gerstein, G.L. (1999). Trial-to-Trial Variability and State-Dependent Modulation of Auditory-Evoked Responses in Cortex. J. Neurosci. 19, 10451-10460.

Kitayama, N., Vaccarino, V., Kutner, M., Weiss, P., and Bremner, J.D. (2005). Magnetic resonance imaging (MRI) measurement of hippocampal volume in posttraumatic stress disorder: A meta-analysis. J. Affect. Disord. 88, 79-86.

Klein, C., Wendling, K., Huettner, P., Ruder, H., and Peper, M. (2006). Intra-subject variability in attention-deficit hyperactivity disorder. Biol. Psychiatry 60, 1088-1097.

Klem, G.H., Lüders, H.O., Jasper, H.H., and Elger, C. (1999). The ten-twenty electrode system of the International Federation. The International Federation of Clinical Neurophysiology. Electroencephalogr. Clin. Neurophysiol. Suppl. 52, 3-6.

Kóbor, A., Takács, Á., Honbolygó, F., and Csépe, V. (2014). Generalized lapse of responding in trait impulsivity indicated by ERPs: The role of energetic factors in inhibitory control. Int. J. Psychophysiol. 92, 16-25.

Koch, S.P., Werner, P., Steinbrink, J., Fries, P., and Obrig, H. (2009). Stimulus-induced and state-dependent sustained gamma activity is tightly coupled to the hemodynamic response in humans. J. Neurosci. Off. J. Soc. Neurosci. 29, 13962-13970.

Köchel, A., Leutgeb, V., and Schienle, A. (2012). Affective inhibitory control in adults with attention deficit hyperactivity disorder: Abnormalities in electrocortical late positivity. Neurosci. Lett. 530, 47-52.

Konishi, S., Nakajima, K., Uchida, I., Sekihara, K., and Miyashita, Y. (1998). No-go dominant brain activity in human inferior prefrontal cortex revealed by functional magnetic resonance imaging. Eur. J. Neurosci. 10, 1209-1213.

Konrad, K., and Eickhoff, S.B. (2010). Is the ADHD brain wired differently? A review on structural and functional connectivity in attention deficit hyperactivity disorder. Hum. Brain Mapp. 31, 904-916.

Kooistra, L., van der Meere, J.J., Edwards, J.D., Kaplan, B.J., Crawford, S., and Goodyear, B.G. (2010). Preliminary fMRI findings on the effects of event rate in adults with ADHD. J. Neural Transm. 117, 655-662.

Kopp, B., Mattler, U., Goertz, R., and Rist, F. (1996). N2, P3 and the lateralized readiness potential in a nogo task involving selective response priming. Electroencephalogr. Clin. Neurophysiol. 99, 19-27.

Krause-Utz, A., Oei, N.Y.L., Niedtfeld, I., Bohus, M., Spinhoven, P., Schmahl, C., and Elzinga, B.M. (2012). Influence of emotional distraction on working memory performance in borderline personality disorder. Psychol. Med. 42, 2181-2192.

Krause-Utz, A., Winter, D., Niedtfeld, I., and Schmahl, C. (2014). The Latest Neuroimaging Findings in Borderline Personality Disorder. Curr. Psychiatry Rep. 16.

Kruggel, F., Wiggins, C. j., Herrmann, C. s., and von Cramon, D. y. (2000). Recording of the event-related potentials during functional MRI at 3.

Kruggel, F., Herrmann, C.S., Wiggins, C.J., and von Cramon, D.Y. (2001). Hemodynamic and electroencephalographic responses to illusory figures: recording of the evoked potentials during functional MRI. NeuroImage 14, 1327-1336.

Kwong, K.K., Belliveau, J.W., Chesler, D.A., Goldberg, I.E., Weisskoff, R.M., Poncelet, B.P., Kennedy, D.N., Hoppel, B.E., Cohen, M.S., and Turner, R. (1992). Dynamic magnetic resonance imaging of human brain activity during primary sensory stimulation. Proc. Natl. Acad. Sci. 89, 5675-5679.

Lampe, K., Konrad, K., Kroener, S., Fast, K., Kunert, H.J., and Herpertz, S.C. (2007). Neuropsychological and behavioural disinhibition in adult ADHD compared to borderline personality disorder. Psychol. Med. 37.

Laufs, H. (2008). Endogenous brain oscillations and related networks detected by surface EEG-combined fMRI. Hum. Brain Mapp. 29, 762-769.

Laufs, H., Kleinschmidt, A., Beyerle, A., Eger, E., Salek-Haddadi, A., Preibisch, C., and Krakow, K. (2003). EEG-correlated fMRI of human alpha activity. NeuroImage 19, 1463-1476.

Lavallee, C.F., Herrmann, C.S., Weerda, R., and Huster, R.J. (2014). Stimulus-Response Mappings Shape Inhibition Processes: A Combined EEG-fMRI Study of Contextual Stopping. PLoS ONE 9, e96159.

Lavric, A., Pizzagalli, D.A., and Forstmeier, S. (2004). When "go" and "nogo" are equally frequent: ERP components and cortical tomography. Eur. J. Neurosci. 20, 2483-2488.

Lawrence, M.A. (2013). ez: Easy analysis and visualization of factorial experiments. R package version 4.

Lazar, N.A. (2008). The Science of fMRI. In The Statistical Analysis of Functional MRI Data, (Springer New York), pp. 1-15.

Ledberg, A., Montagnini, A., Coppola, R., and Bressler, S.L. (2012). Reduced Variability of Ongoing and Evoked Cortical Activity Leads to Improved Behavioral Performance. PLoS ONE 7, e43166.

Lee, J.-H., Oh, S., Jolesz, F.A., Park, H., and Yoo, S.-S. (2009). Application of Independent Component Analysis for the Data Mining of Simultaneous EEG-fMRI: Preliminary Experience on Sleep Onset. Int. J. Neurosci. 119, 1118-1136.

Lee, T.-W., Girolami, M., and Sejnowski, T.J. (1999). Independent Component Analysis Using an Extended Infomax Algorithm for Mixed Subgaussian and Supergaussian Sources. Neural Comput. 11, 417-441.

van Leeuwen, T.H., Steinhausen, H.-C., Overtoom, C.C.E., Pascual-Marqui, R.D., van't Klooster, B., Rothenberger, A., Sergeant, J.A., and Brandeis, D. (1998). The continuous performance test revisited with neuroelectric mapping: impaired orienting in children with attention deficits. Behav. Brain Res. 94, 97-110.

Lehrl, S. (1995). Manual zum MWT-B (Balingen: Spitta-Verl.).

Leichsenring, F., Leibing, E., Kruse, J., New, A.S., and Leweke, F. (2011). Borderline personality disorder. The Lancet 377, 74-84.

Li, D., Sham, P.C., Owen, M.J., and He, L. (2006). Meta-analysis shows significant association between dopamine system genes and attention deficit hyperactivity disorder (ADHD). Hum. Mol. Genet. 15, 2276-2284.

Lieb, K., Zanarini, M.C., Schmahl, C., Linehan, M.M., and Bohus, M. (2004). Borderline personality disorder. The Lancet 364, 453-461.

Liebenthal, E., Ellingson, M.L., Spanaki, M.V., Prieto, T.E., Ropella, K.M., and Binder, J.R. (2003). Simultaneous ERP and fMRI of the auditory cortex in a passive oddball paradigm. NeuroImage 19, 1395-1404.

Liotti, M., Pliszka, S.R., Perez, R., Kothmann, D., and Woldorff, M.G. (2005). Abnormal brain activity related to performance monitoring and error detection in children with ADHD. Cortex J. Devoted Study Nerv. Syst. Behav. 41, 377-388.

Liotti, M., Pliszka, S.R., Higgins, K., Perez III, R., and Semrud-Clikeman, M. (2010). Evidence for specificity of ERP abnormalities during response inhibition in ADHD children: A comparison with reading disorder children without ADHD. Brain Cogn. 72, 228-237.

Lis, E., Greenfield, B., Henry, M., Guilé, J.M., and Dougherty, G. (2007). Neuroimaging and genetics of borderline personality disorder: a review. J. Psychiatry Neurosci. JPN 32, 162-173.

Logothetis, N.K. (2002). The neural basis of the blood-oxygen-level-dependent functional magnetic resonance imaging signal. Philos. Trans. R. Soc. B Biol. Sci. 357, 1003-1037.

Logue, S.F., and Gould, T.J. (2014). The Neural and Genetic Basis of Executive Function: Attention, Cognitive Flexibility, and Response Inhibition. Pharmacol. Biochem. Behav. 0, 45-54.

Luck, S. (2004). Ten Simple Rules for Designing and Interpreting ERP Experiments. In Event-Related Potentials: A Methods Handbook, T. Handy, ed. (MIT Press), p. 430.

Luck, S.J. (2005). An Introduction to the Event-Related Potential Technique (Cambridge, Mass: The Mit Press). Lutz, A., Lachaux, J.-P., Martinerie, J., and Varela, F.J. (2002). Guiding the study of brain dynamics by using first-person data: Synchrony patterns correlate with ongoing conscious states during a simple visual task. Proc. Natl. Acad. Sci. 99, 1586-1591.

van Maanen, L., Brown, S.D., Eichele, T., Wagenmakers, E.-J., Ho, T., Serences, J., and Forstmann, B.U. (2011). Neural correlates of trial-to-trial fluctuations in response caution. J. Neurosci. Off. J. Soc. Neurosci. 31, 17488-17495.

MacDonald, S.W.S., Nyberg, L., and Bäckman, L. (2006). Intra-individual variability in behavior: links to brain structure, neurotransmission and neuronal activity. Trends Neurosci. 29, 474-480.

Maier, S., Perlov, E., Graf, E., Dieter, E., Sobanski, E., Rump, M., Warnke, A., Ebert, D., Berger, M., Matthies, S., et al. (2015). Discrete Global but No Focal Gray Matter Volume Reductions in Unmedicated Adult Patients with Attention-Deficit/Hyperactivity Disorder. Biol Psychiatry 0.

Magistretti, P.J., and Pellerin, L. (1999). Cellular mechanisms of brain energy metabolism and their relevance to functional brain imaging. Philos. Trans. R. Soc. Lond. B. Biol. Sci. 354, 1155-1163.

Makeig, S., and Onton, J. (2011). ERP Features and EEG Dynamics. In The Oxford Handbook of Event-Related Potential Components, E.S. Kappenman, and S.J. Luck, eds. (Oxford University Press).

Makeig, S., Bell, A.J., Jung, T., and Sejnowski, T.J. (1996). Independent Component Analysis of Electroencephalographic Data. In In Advances in Neural Information Processing Systems, (MIT Press), pp. 145-151.

Makeig, S., Westerfield, M., Jung, T.-P., Covington, J., Townsend, J., Sejnowski, T.J., and Courchesne, E. (1999). Functionally Independent Components of the Late Positive Event-Related Potential during Visual Spatial Attention. J. Neurosci. 19, 2665-2680.

Makeig, S., Westerfield, M., Jung, T.-P., Enghoff, S., Townsend, J., Courchesne, E., and Sejnowski, T.J. (2002). Dynamic Brain Sources of Visual Evoked Responses. Science 295, 690-694.

Makris, N., Biederman, J., Valera, E.M., Bush, G., Kaiser, J., Kennedy, D.N., Caviness, V.S., Faraone, S.V., and Seidman, L.J. (2007). Cortical Thinning of the Attention and Executive Function Networks in Adults with Attention-Deficit/Hyperactivity Disorder. Cereb. Cortex 17, 1364-1375.

Makris, N., Buka, S.L., Biederman, J., Papadimitriou, G.M., Hodge, S.M., Valera, E.M., Brown, A.B., Bush, G., Monuteaux, M.C., Caviness, V.S., et al. (2008). Attention and Executive Systems Abnormalities in Adults with Childhood ADHD: A DT-MRI Study of Connections. Cereb. Cortex 18, 1210-1220.

Mayhew, S.D., Macintosh, B.J., Dirckx, S.G., Iannetti, G.D., and Wise, R.G. (2010). Coupling of simultaneously acquired electrophysiological and haemodynamic responses during visual stimulation. Magn. Reson. Imaging 28, 1066-1077.

McCloskey, M.S., New, A.S., Siever, L.J., Goodman, M., Koenigsberg, H.W., Flory, J.D., and Coccaro, E.F. (2009). Evaluation of behavioral impulsivity and aggression tasks as endophenotypes for borderline personality disorder. J. Psychiatr. Res. 43, 1036-1048.

McLoughlin, G., Albrecht, B., Banaschewski, T., Rothenberger, A., Brandeis, D., Asherson, P., and Kuntsi, J. (2010). Electrophysiological evidence for abnormal preparatory states and inhibitory processing in adult ADHD. Behav. Brain Funct. 6, 66.

Meares, R., Melkonian, D., Gordon, E., and Williams, L. (2005). Distinct pattern of P3a event-related potential in borderline personality disorder. Neuroreport 16, 289-293.

Meares, R., Schore, A., and Melkonian, D. (2011). Is borderline personality a particularly right hemispheric disorder? A study of P3a using single trial analysis. Aust. N. Z. J. Psychiatry 45, 131-139.

Menzer, D.L., Bokil, H., Ryou, J.W., Schiff, N.D., Purpura, K.P., and Mitra, P.P. (2010). Characterization of trial-to-trial fluctuations in local field potentials recorded in cerebral cortex of awake behaving macaque. J. Neurosci. Methods 186, 250-261.

Michel, C.M. (2009). Electrical neuroimaging (Cambridge; New York: Cambridge University Press).

Michels, L., Lüchinger, R., Koenig, T., Martin, E., and Brandeis, D. (2012). Developmental changes of BOLD signal correlations with global human EEG power and synchronization during working memory. PloS One 7, e39447.

Milner, R., Rusiniak, M., Lewandowska, M., Wolak, T., Ganc, M., Piatkowska-Janko, E., Bogorodzki, P., and Skarzynski, H. (2014). Towards neural correlates of auditory stimulus processing: A simultaneous auditory evoked potentials and functional magnetic resonance study using an odd-ball paradigm. Med. Sci. Monit. 20, 35-46.

Minzenberg, M., Fan, J., New, A., Tang, C., and Siever, L. (2008). Frontolimbic structural changes in borderline personality disorder. J. Psychiatr. Res. 42, 727-733.

Mitchell, J.T. (2010). Behavioral Approach in ADHD Testing a Motivational Dysfunction Hypothesis. J. Atten. Disord. 13, 609-617.

Mitchell, J.T., and Nelson-Gray, R.O. (2006). Attention-Deficit/Hyperactivity Disorder symptoms in adults: Relationship to Gray's Behavioral Approach System. Personal. Individ. Differ. 40, 749-760.

Miyake, A. (2000). The Unity and Diversity of Executive Functions and Their Contributions to Complex "Frontal Lobe" Tasks: A Latent Variable Analysis. Cognit. Psychol. 41, 49-100.

Mobascher, A., Brinkmeyer, J., Warbrick, T., Musso, F., Wittsack, H.J., Saleh, A., Schnitzler, A., and Winterer, G. (2009). Laser-evoked potential P2 single-trial amplitudes covary with the fMRI BOLD response in the medial pain system and interconnected subcortical structures. NeuroImage 45, 917-926.

Möcks, J., Gasser, T., and Tuan, P.D. (1984). Variability of single visual evoked potentials evaluated by two new statistical tests. Electroencephalogr. Clin. Neurophysiol. 57, 571-580.

Möcks, J., Gasser, T., Tuan, P.D., and Köhler, W. (1987). Trial-to-Trial Variability of Single Potentials: Methodological Concepts and Results. Int. J. Neurosci. 33, 25-32.

Montgomery, S.A., and Asberg, M. (1979). A new depression scale designed to be sensitive to change. Br. J. Psychiatry J. Ment. Sci. 134, 382-389.

Moore, W.S., and Holland, G.N. (1980). Nuclear magnetic resonance imaging. Br. Med. Bull. 36, 297-299.

Morein-Zamir, S., Dodds, C., van Hartevelt, T.J., Schwarzkopf, W., Sahakian, B., Müller, U., and Robbins, T. (2014). Hypoactivation in right inferior frontal cortex is specifically associated with motor response inhibition in adult ADHD: Inhibition-Specific Hypoactivation in ADHD. Hum. Brain Mapp. 35, 5141-5152.

Mostofsky, S.H., and Simmonds, D.J. (2008). Response Inhibition and Response Selection: Two Sides of the Same Coin. J. Cogn. Neurosci. 20, 751-761.

Mulert, C., Jäger, L., Schmitt, R., Bussfeld, P., Pogarell, O., Möller, H.-J., Juckel, G., and Hegerl, U. (2004). Integration of fMRI and simultaneous EEG: towards a comprehensive understanding of localization and time-course of brain activity in target detection. NeuroImage 22, 83-94.

Mulert, C., Seifert, C., Leicht, G., Kirsch, V., Ertl, M., Karch, S., Moosmann, M., Lutz, J., Möller, H.-J., Hegerl, U., et al. (2008). Single-trial coupling of EEG and fMRI reveals the involvement of early anterior cingulate cortex activation in effortful decision making. NeuroImage 42, 158-168.

Mulligan, R.C., Knopik, V.S., Sweet, L.H., Fischer, M., Seidenberg, M., and Rao, S.M. (2011). Neural correlates of inhibitory control in adult attention deficit/hyperactivity disorder: Evidence from the Milwaukee longitudinal sample. Psychiatry Res. Neuroimaging 194, 119-129.

Munakata, Y., Herd, S.A., Chatham, C.H., Depue, B.E., Banich, M.T., and O'Reilly, R.C. (2011). A unified framework for inhibitory control. Trends Cogn. Sci. 15, 453-459.

Naito, E., and Matsumura, M. (1994). Movement-related potentials associated with motor inhibition as determined by use of a stop signal paradigm in humans. Cogn. Brain Res. 2, 139-146.

Nandam, L.S., Hester, R., and Bellgrove, M.A. (2014). Dissociable and common effects of methylphenidate, atomoxetine and citalopram on response inhibition neural networks. Neuropsychologia 56, 263-270.

Nee, D.E., Wager, T.D., and Jonides, J. (2007). Interference resolution: Insights from a meta-analysis of neuroimaging tasks. Cogn. Affect. Behav. Neurosci. 7, 1-17.

Negishi, M., Pinus, B.I., Pinus, A.B., and Constable, R.T. (2007). Origin of the radio frequency pulse artifact in simultaneous EEG-fMRI recording: rectification at the carbon-metal interface. IEEE Trans. Biomed. Eng. 54, 1725-1727.

Neumann, N.U., and Schulte, R.M. (1988). Bestimmung der Validität und Interrater-Reliabilität der deutschen Fassung der Montgomery-Asberg-Depression-Rating-Skala(MADRS). Psycho 911-924.

Nieuwenhuis, S., Yeung, N., and Cohen, J.D. (2004). Stimulus modality, perceptual overlap, and the go/no-go N2.

Nigg, J.T. (2001). Is ADHD a disinhibitory disorder? Psychol. Bull. 127, 571-598.

Nigg, J.T. (2010). Attention-Deficit/Hyperactivity Disorder: Endophenotypes, Structure, and Etiological Pathways. Curr. Dir. Psychol. Sci. 19, 24-29.

Nigg, J.T., Stavro, G., Ettenhofer, M., Hambrick, D.Z., Miller, T., and Henderson, J.M. (2005a). Executive functions and adhd in adults: Evidence for selective effects on ADHD symptom domains. J. Abnorm. Psychol. 114, 706-717.

Nigg, J.T., Silk, K.R., Stavro, G., and Miller, T. (2005b). Disinhibition and borderline personality disorder. Dev. Psychopathol. 17, 1129-1149.

Noreika, V., Falter, C.M., and Rubia, K. (2013). Timing deficits in attention-deficit/hyperactivity disorder (ADHD): Evidence from neurocognitive and neuroimaging studies. Neuropsychologia 51, 235-266.

Novitskiy, N., Ramautar, J.R., Vanderperren, K., De Vos, M., Mennes, M., Mijovic, B., Vanrumste, B., Stiers, P., Van den Bergh, B., Lagae, L., et al. (2011). The BOLD correlates of the visual P1 and N1 in single-trial analysis of simultaneous EEG-fMRI recordings during a spatial detection task. NeuroImage 54, 824-835.

Ogawa, S., Lee, T.M., Kay, A.R., and Tank, D.W. (1990). Brain magnetic resonance imaging with contrast dependent on blood oxygenation. Proc. Natl. Acad. Sci. 87, 9868-9872.

Ogawa, S., Tank, D.W., Menon, R., Ellermann, J.M., Kim, S.G., Merkle, H., and Ugurbil, K. (1992). Intrinsic signal changes accompanying sensory stimulation: functional brain mapping with magnetic resonance imaging. Proc. Natl. Acad. Sci. 89, 5951-5955.

Oldendorf, W.H. (1981). Nuclear medicine in clinical neurology: An update. Ann. Neurol. 10, 207-213.

Oldfield, R.C. (1971). The assessment and analysis of handedness: The Edinburgh inventory. Neuropsychologia 9, 97-113.

O'Neill, A., and Frodl, T. (2012). Brain structure and function in borderline personality disorder. Brain Struct. Funct. 217, 767-782.

O'Neill, A., D'Souza, A., Carballedo, A., Joseph, S., Kerskens, C., and Frodl, T. (2013). Magnetic resonance imaging in patients with borderline personality disorder: A study of volumetric abnormalities. Psychiatry Res. Neuroimaging 213, 1-10.

Ou, W., Nummenmaa, A., Ahveninen, J., Belliveau, J.W., Hämäläinen, M.S., and Golland, P. (2010). Multimodal functional imaging using fMRI-informed regional EEG/MEG source estimation. NeuroImage 52, 97-108.

Paris, J. (2005). Borderline personality disorder. Can. Med. Assoc. J. 172, 1579-1583.

Pascual-Marqui, R.D. (1999). Review of methods for solving the EEG inverse problem. Int. J. Bioelectromagn. 1, 75-86.

Pasley, B., and Freeman, R. (2008). Neurovascular coupling. Scholarpedia 3, 5340, revision #91581.

Passarotti, A.M., Sweeney, J.A., and Pavuluri, M.N. (2010). Neural correlates of response inhibition in pediatric bipolar disorder and attention deficit hyperactivity disorder. Psychiatry Res. Neuroimaging 181, 36-43.

Patton, J.H., Stanford, M.S., and Barratt, E.S. (1995). Factor structure of the barratt impulsiveness scale. J. Clin. Psychol. 51, 768-774.

Pessoa, L., and Padmala, S. (2005). Quantitative prediction of perceptual decisions during near-threshold fear detection. Proc. Natl. Acad. Sci. U. S. A. 102, 5612-5617.

Picton, T.W. (1992). The P300 wave of the human event-related potential. J. Clin. Neurophysiol. Off. Publ. Am. Electroencephalogr. Soc. 9, 456-479.

Picton, T. w., Bentin, S., Berg, P., Donchin, E., Hillyard, S. a., Johnson, R., Miller, G. a., Ritter, W., Ruchkin, D. s., Rugg, M. d., et al. (2000). Guidelines for using human event-related potentials to study cognition: Recording standards and publication criteria. Psychophysiology 37, 127-152.

Pironti, V.A., Lai, M.-C., Müller, U., Dodds, C.M., Suckling, J., Bullmore, E.T., and Sahakian, B.J. (2014). Neuroanatomical abnormalities and cognitive impairments are shared by adults with attention-deficit/hyperactivity disorder and their unaffected first-degree relatives. Biol. Psychiatry 76, 639-647.

Plichta, M.M., and Scheres, A. (2014). Ventral-striatal responsiveness during reward anticipation in ADHD and its relation to trait impulsivity in the healthy population: A meta-analytic review of the fMRI literature. Neurosci. Biobehav. Rev. 38, 125-134.

Pliszka, S.R., Liotti, M., and Woldorff, M.G. (2000). Inhibitory control in children with attention-deficit/hyperactivity disorder: event-related potentials identify the processing component and timing of an impaired right-frontal response-inhibition mechanism. Biol. Psychiatry 48, 238-246.

Pliszka, S.R., Liotti, M., Bailey, B.Y., Perez III, R., Glahn, D., and Semrud-Clikeman, M. (2007). Electrophysiological Effects of Stimulant Treatment on Inhibitory Control in Children with Attention-Deficit/Hyperactivity Disorder. J. Child Adolesc. Psychopharmacol. 17, 356-366.

Polich, J. (2007). Updating P300: an integrative theory of P3a and P3b. Clin. Neurophysiol. Off. J. Int. Fed. Clin. Neurophysiol. 118, 2128-2148.

Polich, J., and Criado, J.R. (2006). Neuropsychology and neuropharmacology of P3a and P3b. Int. J. Psychophysiol. 60, 172-185.

Poustchi-Amin, M., Mirowitz, S.A., Brown, J.J., McKinstry, R.C., and Li, T. (2001). Principles and Applications of Echo-planar Imaging: A Review for the General Radiologist1. Radiographics 21, 767-779.

Prada, P., Hasler, R., Baud, P., Bednarz, G., Ardu, S., Krejci, I., Nicastro, R., Aubry, J.-M., and Perroud, N. (2014). Distinguishing borderline personality disorder from adult attention deficit/hyperactivity disorder: A clinical and dimensional perspective. Psychiatry Res. 217, 107-114.

Prox, V., Dietrich, D.E., Zhang, Y., Emrich, H.M., and Ohlmeier, M.D. (2007). Attentional processing in adults with ADHD as reflected by event-related potentials. Neurosci. Lett. 419, 236-241.

Purcell, E.M., Torrey, H.C., and Pound, R.V. (1946). Resonance Absorption by Nuclear Magnetic Moments in a Solid. Phys. Rev. 69, 37-38.

Raichle, M.E., MacLeod, A.M., Snyder, A.Z., Powers, W.J., Gusnard, D.A., and Shulman, G.L. (2001). A default mode of brain function. Proc. Natl. Acad. Sci. 98, 676-682.

Railo, H., Koivisto, M., and Revonsuo, A. (2011). Tracking the processes behind conscious perception: a review of event-related potential correlates of visual consciousness. Conscious. Cogn. 20, 972-983.

Rathakrishnan, R., Moeller, F., Levan, P., Dubeau, F., and Gotman, J. (2010). BOLD signal changes preceding negative responses in EEG-fMRI in patients with focal epilepsy. Epilepsia 51, 1837-1845.

R Core Team (2014). R: A language and environment for statistical computing. (Vienna, Austria: R Foundation for Statistical Computing).

Reed, T.E. (1998). Causes of intraindividual variability in reaction times: a neurophysiologically oriented review and a new suggestion. Personal. Individ. Differ. 25, 991-998.

Reich, D.S., Victor, J.D., Knight, B.W., Ozaki, T., and Kaplan, E. (1997). Response Variability and Timing Precision of Neuronal Spike Trains In Vivo. J. Neurophysiol. 77, 2836-2841.

Rentrop, M., Backenstrass, M., Jaentsch, B., Kaiser, S., Roth, A., Unger, J., Weisbrod, M., and Renneberg, B. (2008). Response Inhibition in Borderline Personality Disorder: Performance in a Go/Nogo Task. Psychopathology 41, 50-57.

Retz, W., Retz-Junginger, P., Supprian, T., Thome, J., and Rösler, M. (2004). Association of serotonin transporter promoter gene polymorphism with violence: relation with personality disorders, impulsivity, and childhood ADHD psychopathology. Behav. Sci. Law 22, 415-425.

Retz-Junginger, P., Retz, W., Blocher, D., Stieglitz, R.-D., Georg, T., Supprian, T., Wender, P.H., and Rösler, M. (2003). Reliabilität und Validität der Wender-Utah-Rating-Scale-Kurzform. Nervenarzt 74, 987-993.

Reynolds, B., Ortengren, A., Richards, J.B., and de Wit, H. (2006). Dimensions of impulsive behavior: Personality and behavioral measures. Personal. Individ. Differ. 40, 305-315

Rietdijk, W.J.R., Franken, I.H.A., and Thurik, A.R. (2014). Internal Consistency of Event-Related Potentials Associated with Cognitive Control: N2/P3 and ERN/Pe. PLoS ONE 9, e102672.

Rodrigues, E., Wenzel, A., Ribeiro, M.P., Quarantini, L.C., Miranda-Scippa, A., de Sena, E.P., and de Oliveira, I.R. (2011). Hippocampal volume in borderline personality disorder with and without comorbid posttraumatic stress disorder: A meta-analysis. Eur. Psychiatry 26, 452-456.

Rosa-Neto, P., Lou, H.C., Cumming, P., Pryds, O., Karrebaek, H., Lunding, J., and Gjedde, A. (2005). Methylphenidate-evoked changes in striatal dopamine correlate with inattention and impulsivity in adolescents with attention deficit hyperactivity disorder. NeuroImage 25, 868-876.

Rösler, K.M., Roth, D.M., and Magistris, M.R. (2008). Trial-to-trial size variability of motor-evoked potentials. A study using the triple stimulation technique. Exp. Brain Res. 187, 51-59.

Rubia, K. (2011). "Cool" inferior frontostriatal dysfunction in attention-deficit/hyperactivity disorder versus "hot" ventromedial orbitofrontal-limbic dysfunction in conduct disorder: a review. Biol. Psychiatry 69, e69-e87.

Rubia, K., Russell, T., Overmeyer, S., Brammer, M.J., Bullmore, E.T., Sharma, T., Simmons, A., Williams, S.C., Giampietro, V., Andrew, C.M., et al. (2001a). Mapping motor inhibition: conjunctive brain activations across different versions of go/no-go and stop tasks. NeuroImage 13, 250-261.

Rubia, K., Taylor, E., Smith, A.B., Oksannen, H., Overmeyer, S., and Newman, S. (2001b). Neuropsychological analyses of impulsiveness in childhood hyperactivity. Br. J. Psychiatry 179, 138-143.

Rubia, K., Smith, A.B., Brammer, M.J., Toone, B., and Taylor, E. (2005). Abnormal Brain Activation During Inhibition and Error Detection in Medication-Naive Adolescents With ADHD. Am. J. Psychiatry 162, 1067-1075.

Rubia, K., Halari, R., Christakou, A., and Taylor, E. (2009a). Impulsiveness as a timing disturbance: neurocognitive abnormalities in attention-deficit hyperactivity disorder during temporal processes and normalization with methylphenidate. Philos. Trans. R. Soc. B Biol. Sci. 364, 1919-1931.

Rubia, K., Smith, A.B., Halari, R., Matsukura, F., Mohammad, M., Taylor, E., and Brammer, M.J. (2009b). Disorder-specific dissociation of orbitofrontal dysfunction in boys with pure conduct disorder during reward and ventrolateral prefrontal dysfunction in boys with pure ADHD during sustained attention. Am. J. Psychiatry 166, 83-94.

Rubia, K., Halari, R., Smith, A.B., Mohammad, M., Scott, S., and Brammer, M.J. (2009c). Shared and disorder-specific prefrontal abnormalities in boys with pure attention-deficit/hyperactivity disorder compared to boys with pure CD during interference inhibition and attention allocation. J. Child Psychol. Psychiatry 50, 669-678.

Rubia, K., Halari, R., Cubillo, A., Mohammad, A.-M., Scott, S., and Brammer, M. (2010a). Disorder-specific inferior prefrontal hypofunction in boys with pure attention-deficit/hyperactivity disorder compared to boys with pure conduct disorder during cognitive flexibility. Hum. Brain Mapp. 31, 1823-1833.

Rubia, K., Cubillo, A., Smith, A.B., Woolley, J., Heyman, I., and Brammer, M.J. (2010b). Disorder-specific dysfunction in right inferior prefrontal cortex during two inhibition tasks in boys with attention-deficit hyperactivity disorder compared to boys with obsessive-compulsive disorder. Hum. Brain Mapp. 31, 287-299.

Rubia, K., Halari, R., Cubillo, A., Smith, A.B., Mohammad, A.-M., Brammer, M., and Taylor, E. (2011). Methylphenidate Normalizes Fronto-Striatal Underactivation During Interference Inhibition in Medication-Naïve Boys with Attention-Deficit Hyperactivity Disorder. Neuropsychopharmacology 36, 1575-1586.

Rubia, K., Alegría, A.A., and Brinson, H. (2014a). Brain abnormalities in attention-deficit hyperactivity disorder: a review. Rev. Neurol. 58 Suppl 1, S3-S16.

Rubia, K., Alegria, A.A., Cubillo, A.I., Smith, A.B., Brammer, M.J., and Radua, J. (2014b). Effects of Stimulants on Brain Function in Attention-Deficit/Hyperactivity Disorder: A Systematic Review and Meta-Analysis. Biol. Psychiatry 76, 616-628.

Ruchsow, M., Groen, G., Kiefer, M., Hermle, L., Spitzer, M., and Falkenstein, M. (2008a). Impulsiveness and ERP components in a Go/Nogo task. J. Neural Transm. 115, 909-915.

Ruchsow, M., Groen, G., Kiefer, M., Buchheim, A., Walter, H., Martius, P., Reiter, M., Hermle, L., Spitzer, M., Ebert, D., et al. (2008b). Response inhibition in borderline personality disorder: event-related potentials in a Go/Nogo task. J. Neural Transm. 115, 127-133.

Ruchsow, M., Groen, G., Kiefer, M., Beschoner, P., Hermle, L., Ebert, D., and Falkenstein, M. (2008c). Electrophysiological evidence for reduced inhibitory control in depressed patients in partial remission: A Go/Nogo study. Int. J. Psychophysiol. 68, 209-218.

Ruocco, A.C., Amirthavasagam, S., and Zakzanis, K.K. (2012). Amygdala and hippocampal volume reductions as candidate endophenotypes for borderline personality disorder: A meta-analysis of magnetic resonance imaging studies. Psychiatry Res. Neuroimaging 201, 245-252.

Russo, P.M., De Pascalis, V., Varriale, V., and Barratt, E.S. (2008). Impulsivity, intelligence and P300 wave: An empirical study. Int. J. Psychophysiol. 69, 112-118.

Sadeh, B., Podlipsky, I., Zhdanov, A., and Yovel, G. (2010). Event-related potential and functional MRI measures of face-selectivity are highly correlated: a simultaneous ERP-fMRI investigation. Hum. Brain Mapp. 31, 1490-1501.

Sajda, P. (2009). Signal processing challenges for single-trial analysis of simultaneous EEG/fMRI. In Annual International Conference of the IEEE Engineering in Medicine and Biology Society, 2009. EMBC 2009, pp. 29-30.

Saville, C.W.N., Dean, R.O., Daley, D., Intriligator, J., Boehm, S., Feige, B., and Klein, C. (2011a). Electrocortical correlates of intra-subject variability in reaction times: Average and single-trial analyses. Biol. Psychol. 87, 74-83.

Saville, C.W.N., Pawling, R., Trullinger, M., Daley, D., Intriligator, J., and Klein, C. (2011b). On the stability of instability: Optimising the reliability of intra-subject variability of reaction times. Personal. Individ. Differ. 51, 148-153.

Scerif, G., and Baker, K. (2015). Annual Research Review: Rare genotypes and childhood psychopathology - uncovering diverse developmental mechanisms of ADHD risk. J. Child Psychol. Psychiatry 56, 251-273.

Schachar, R., Logan, G.D., Robaey, P., Chen, S., Ickowicz, A., and Barr, C. (2007). Restraint and Cancellation: Multiple Inhibition Deficits in Attention Deficit Hyperactivity Disorder. J. Abnorm. Child Psychol. 35, 229-238.

Scheeringa, R., Fries, P., Petersson, K.-M., Oostenveld, R., Grothe, I., Norris, D.G., Hagoort, P., and Bastiaansen, M.C.M. (2011a). Neuronal dynamics underlying high- and low-frequency EEG oscillations contribute independently to the human BOLD signal. Neuron 69, 572-583.

Scheeringa, R., Mazaheri, A., Bojak, I., Norris, D.G., and Kleinschmidt, A. (2011b). Modulation of visually evoked cortical FMRI responses by phase of ongoing occipital alpha oscillations. J. Neurosci. Off. J. Soc. Neurosci. 31, 3813-3820.

Scheibe, C., Ullsperger, M., Sommer, W., and Heekeren, H.R. (2010). Effects of Parametrical and Trial-to-Trial Variation in Prior Probability Processing Revealed by Simultaneous Electroencephalogram/Functional Magnetic Resonance Imaging. J. Neurosci. 30, 16709-16717.

Schmajuk, M., Liotti, M., Busse, L., and Woldorff, M.G. (2006). Electrophysiological activity underlying inhibitory control processes in normal adults. Neuropsychologia 44, 384-395.

Schmüser, L., Sebastian, A., Mobascher, A., Lieb, K., Tüscher, O., and Feige, B. (2014). Data-driven analysis of simultaneous EEG/fMRI using an ICA approach. Front. Neurosci. 8, 175.

Schmüser, L., Sebastian, A., Mobascher, A., Lieb, K., Feige, B., and Tüscher, O. (2016). Data-driven analysis of simultaneous EEG/fMRI reveals neurophysiological phenotypes of impulse control. Hum. Brain Mapp.. doi: 10.1002/hbm.23230.

Schneider, M.F., Krick, C.M., Retz, W., Hengesch, G., Retz-Junginger, P., Reith, W., and Rösler, M. (2010). Impairment of fronto-striatal and parietal cerebral networks correlates with attention deficit hyperactivity disorder (ADHD) psychopathology in adults - a functional magnetic resonance imaging (fMRI) study. Psychiatry Res. 183, 75-84.

Schuch, V., Utsumi, D.A., Costa, T.V.M.M., Kulikowski, L.D., and Muszkat, M. (2015). Attention Deficit Hyperactivity Disorder in the Light of the Epigenetic Paradigm. Front. Psychiatry 6, 126.

Sebastian, A., Gerdes, B., Feige, B., Klöppel, S., Lange, T., Philipsen, A., Tebartz van Elst, L., Lieb, K., and Tüscher, O. (2012). Neural correlates of interference inhibition, action withholding and action cancelation in adult ADHD. Psychiatry Res. Neuroimaging 202, 132-141.

Sebastian, A., Pohl, M.F., Klöppel, S., Feige, B., Lange, T., Stahl, C., Voss, A., Klauer, K.C., Lieb, K., and Tüscher, O. (2013a). Disentangling common and specific neural subprocesses of response inhibition. NeuroImage 64, 601-615.

Sebastian, A., Jacob, G., Lieb, K., and Tüscher, O. (2013b). Impulsivity in Borderline Personality Disorder: A Matter of Disturbed Impulse Control or a Facet of Emotional Dysregulation? Curr. Psychiatry Rep. 15.

Sebastian, A., Baldermann, C., Feige, B., Katzev, M., Scheller, E., Hellwig, B., Lieb, K., Weiller, C., Tüscher, O., and Klöppel, S. (2013c). Differential effects of age on subcomponents of response inhibition. Neurobiol. Aging 34, 2183-2193.

Sebastian, A., Jung, P., Krause-Utz, A., Lieb, K., Schmahl, C., and Tüscher, O. (2014). Frontal dysfunctions of impulse control - a systematic review in borderline personality disorder and attention-deficit/hyperactivity disorder. Front. Hum. Neurosci. 8, 698.

Sebastian, A., Jung, P., Neuhoff, J., Wibral, M., Fox, P.T., Lieb, K., Fries, P., Eickhoff, S.B., Tüscher, O., and Mobascher, A. (2015). Dissociable attentional and inhibitory networks of dorsal and ventral areas of the right inferior frontal cortex: a combined task-specific and coordinate-based meta-analytic fMRI study. Brain Struct. Funct. 1-17.

Sharma, A., and Couture, J. (2014). A review of the pathophysiology, etiology, and treatment of attention-deficit hyperactivity disorder (ADHD). Ann. Pharmacother. 48, 209-225.

Sharp, D.J., Bonnelle, V., Boissezon, X.D., Beckmann, C.F., James, S.G., Patel, M.C., and Mehta, M.A. (2010). Distinct frontal systems for response inhibition, attentional capture, and error processing. Proc. Natl. Acad. Sci. 107, 6106-6111.

Shen, I.-H., Lee, D.-S., and Chen, C. (2014). The role of trait impulsivity in response inhibition: Event-related potentials in a stop-signal task. Int. J. Psychophysiol. 91, 80-87.

Sijbers, J., Van Audekerke, J., Verhoye, M., Van der Linden, A., and Van Dyck, D. (2000). Reduction of ECG and gradient related artifacts in simultaneously recorded human EEG/MRI data. Magn. Reson. Imaging 18, 881-886.

Silbersweig, D., Clarkin, J.F., Goldstein, M., Kernberg, O.F., Tuescher, O., Levy, K.N., Brendel, G., Pan, H., Beutel, M., Pavony, M.T., et al. (2007). Failure of frontolimbic inhibitory function in the context of negative emotion in borderline personality disorder. Am. J. Psychiatry 164, 1832-1841.

Simmonds, D.J., Fotedar, S.G., Suskauer, S.J., Pekar, J.J., Denckla, M.B., and Mostofsky, S.H. (2007). Functional brain correlates of response time variability in children. Neuropsychologia 45, 2147-2157.

Simmonds, D.J., Pekar, J.J., and Mostofsky, S.H. (2008). Meta-analysis of Go/No-go tasks demonstrating that fMRI activation associated with response inhibition is task-dependent. Neuropsychologia 46, 224-232.

Simson, R., Vaughan Jr., H.G., and Ritter, W. (1977). The scalp topography of potentials in auditory and visual Go/NoGo tasks. Electroencephalogr. Clin. Neurophysiol. 43, 864-875.

Smith, A., Taylor, E., Brammer, M., Toone, B., and Rubia, K. (2006). Task-specific hypoactivation in prefrontal and temporoparietal brain regions during motor inhibition and task switching in medication-naive children and adolescents with attention deficit hyperactivity disorder. Am. J. Psychiatry 163, 1044-1051.

Smith, A., Cubillo, A., Barrett, N., Giampietro, V., Simmons, A., Brammer, M., and Rubia, K. (2013a). Neurofunctional Effects of Methylphenidate and Atomoxetine in Boys with Attention-Deficit/Hyperactivity Disorder During Time Discrimination. Biol. Psychiatry 74, 615-622.

Smith, J.L., Johnstone, S.J., and Barry, R.J. (2004). Inhibitory processing during the Go/NoGo task: an ERP analysis of children with attention-deficit/hyperactivity disorder. Clin. Neurophysiol. Off. J. Int. Fed. Clin. Neurophysiol. 115, 1320-1331.

Smith, J.L., Johnstone, S.J., and Barry, R.J. (2008). Movement-related potentials in the Go/NoGo task: The P3 reflects both cognitive and motor inhibition. Clin. Neurophysiol. 119, 704-714.

Smith, J.L., Jamadar, S., Provost, A.L., and Michie, P.T. (2013b). Motor and non-motor inhibition in the Go/NoGo task: An ERP and fMRI study. Int. J. Psychophysiol. 87, 244-253.

Snyder, H.R., Miyake, A., and Hankin, B.L. (2015). Advancing understanding of executive function impairments and psychopathology: bridging the gap between clinical and cognitive approaches. Front. Psychol. 6, 328.

Soloff, P., Nutche, J., Goradia, D., and Diwadkar, V. (2008). Structural brain abnormalities in borderline personality disorder: A voxel-based morphometry study. Psychiatry Res. Neuroimaging 164, 223-236.

Soloff, P.H., White, R., Omari, A., Ramaseshan, K., and Diwadkar, V.A. (2015). Affective context interferes with brain responses during cognitive processing in borderline personality disorder: fMRI evidence. Psychiatry Res. 233, 23-35.

Sommer, M., Meinhardt, J., and Volz, H.-P. (2003). Combined measurement of event-related potentials (ERPs) and fMRI. Acta Neurobiol. Exp. (Warsz.) 63, 49-53.

Sonuga-Barke, E.J.S. (2005). Causal models of attention-deficit/hyperactivity disorder: from common simple deficits to multiple developmental pathways. Biol. Psychiatry 57, 1231-1238.

Sonuga-Barke, E.J., Houlberg, K., and Hall, M. (1994). When is "impulsiveness" not impulsive? The case of hyperactive children's cognitive style. J. Child Psychol. Psychiatry 35, 1247-1253.

Srivastava, G., Crottaz-Herbette, S., Lau, K.M., Glover, G.H., and Menon, V. (2005). ICA-based procedures for removing ballistocardiogram artifacts from EEG data acquired in the MRI scanner. NeuroImage 24, 50-60.

Stahl, C., Voss, A., Schmitz, F., Nuszbaum, M., Tüscher, O., Lieb, K., and Klauer, K.C. (2014). Behavioral components of impulsivity. J. Exp. Psychol. Gen. 143, 850-886.

Steiger, H., Joober, R., Israël, M., Young, S.N., Ng Ying Kin, N.M.K., Gauvin, L., Bruce, K.R., Joncas, J., and Torkaman-Zehi, A. (2005). The 5HTTLPR polymorphism, psychopathologic symptoms, and platelet [3H-] paroxetine binding in bulimic syndromes. Int. J. Eat. Disord. 37, 57-60.

Stone, M.H. (2013). The Brain in Overdrive: A New Look at Borderline and Related Disorders. Curr. Psychiatry Rep. 15.

Stuss, D.T. (2003). Staying on the job: the frontal lobes control individual performance variability. Brain 126, 2363-2380.

Sun, L., and Hinrichs, H. (2009). Simultaneously recorded EEG-fMRI: removal of gradient artifacts by subtraction of head movement related average artifact waveforms. Hum. Brain Mapp. 30, 3361-3377.

Suskauer, S.J., Simmonds, D.J., Fotedar, S., Blankner, J.G., Pekar, J.J., Denckla, M.B., and Mostofsky, S.H. (2007). Functional Magnetic Resonance Imaging Evidence for Abnormalities in Response Selection in Attention Deficit Hyperactivity Disorder: Differences in Activation Associated with Response Inhibition but Not Habitual Motor Response. J. Cogn. Neurosci. 20, 478-493.

Swick, D., Ashley, V., and Turken, U. (2011). Are the neural correlates of stopping and not going identical? Quantitative meta-analysis of two response inhibition tasks. NeuroImage 56, 1655-1665.

Tamm, L., Menon, V., Ringel, J., and Reiss, A.L. (2004). Event-Related fMRI Evidence of Frontotemporal Involvement in Aberrant Response Inhibition and Task Switching in Attention-Deficit/Hyperactivity Disorder. J. Am. Acad. Child Adolesc. Psychiatry 43, 1430-1440.

Tamm, L., Narad, M.E., Antonini, T.N., O'Brien, K.M., Hawk, L.W., and Epstein, J.N. (2012). Reaction Time Variability in ADHD: A Review. Neurotherapeutics 9, 500-508.

Tebartz van Elst, L., Hesslinger, B., Thiel, T., Geiger, E., Haegele, K., Lemieux, L., Lieb, K., Bohus, M., Hennig, J., and Ebert, D. (2003). Frontolimbic brain abnormalities in patients with borderline personality disorder: a volumetric magnetic resonance imaging study. Biol. Psychiatry 54, 163-171.

Thesen, S., Heid, O., Mueller, E., and Schad, L.R. (2000). Prospective acquisition correction for head motion with image-based tracking for real-time fMRI. Magn. Reson. Med. 44, 457-465.

Torgersen, S., Lygren, S., Oien, P.A., Skre, I., Onstad, S., Edvardsen, J., Tambs, K., and Kringlen, E. (2000). A twin study of personality disorders. Compr. Psychiatry 41, 416-425.

Truccolo, W.A., Ding, M., Knuth, K.H., Nakamura, R., and Bressler, S.L. (2002). Trial-to-trial variability of cortical evoked responses: implications for the analysis of functional connectivity. Clin. Neurophysiol. 113, 206-226.

Trull, T.J., Jahng, S., Tomko, R.L., Wood, P.K., and Sher, K.J. (2010). Revised NESARC Personality Disorder Diagnoses: Gender, Prevalence, and Comorbidity with Substance Dependence Disorders. J. Personal. Disord. 24, 412-426.

Turetsky, B.I., Raz, J., and Fein, G. (1989). Estimation of Trial-to-Trial Variation in Evoked Potential Signals by Smoothing Across Trials. Psychophysiology 26, 700-712.

Ullsperger, M., and Debener, S. (2010). Simultaneous EEG and fMRI: recording, analysis, and application (New York: Oxford University Press).

Vaidya, C.J., Austin, G., Kirkorian, G., Ridlehuber, H.W., Desmond, J.E., Glover, G.H., and Gabrieli, J.D. (1998). Selective effects of methylphenidate in attention deficit hyperactivity disorder: a functional magnetic resonance study. Proc. Natl. Acad. Sci. 95, 14494-14499.

Vaidya, C.J., Bunge, S.A., Dudukovic, N.M., Zalecki, C.A., Elliott, G.R., and Gabrieli, J.D. (2005). Altered neural substrates of cognitive control in childhood ADHD: evidence from functional magnetic resonance imaging. Am. J. Psychiatry 1605-1613.

Valera, E.M., Faraone, S.V., Murray, K.E., and Seidman, L.J. (2007). Meta-Analysis of Structural Imaging Findings in Attention-Deficit/Hyperactivity Disorder. Biol. Psychiatry 61, 1361-1369.

Valera, E.M., Spencer, R.M.C., Zeffiro, T.A., Makris, N., Spencer, T.J., Faraone, S.V., Biederman, J., and Seidman, L.J. (2010). Neural Substrates of Impaired Sensorimotor Timing in Adult Attention-Deficit/Hyperactivity Disorder. Biol. Psychiatry 68, 359-367.

Vaurio, R.G., Simmonds, D.J., and Mostofsky, S.H. (2009). Increased intra-individual reaction time variability in attention-deficit/hyperactivity disorder across response inhibition tasks with different cognitive demands. Neuropsychologia 47, 2389-2396.

Vigário, R., Särelä, J., Jousmäki, V., Hämäläinen, M., and Oja, E. (2000). Independent component approach to the analysis of EEG and MEG recordings. IEEE Trans. Biomed. Eng. 47, 589-593.

Villemonteix, T., De Brito, S.A., Kavec, M., Balériaux, D., Metens, T., Slama, H., Baijot, S., Mary, A., Peigneux, P., and Massat, I. (2015). Grey matter volumes in treatment naïve vs. chronically treated children with attention deficit/hyperactivity disorder: a combined approach. Eur. Neuropsychopharmacol. 0.

Völker, K., Spitzer, C., Limberg, A., Grabe, H.J., Freyberger, H.J., and Barnow, S. (2009). Exekutive Dysfunktionen bei Patientinnen mit Borderline-Persönlichkeitsstörung unter Berücksichtigung von Impulsivität und Depressivität. Psychother. Psychosom. Med. Psychol. 59, 264-272.

Volkow, N.D., Wang, G.J., Fowler, J.S., Gatley, S.J., Logan, J., Ding, Y.S., Hitzemann, R., and Pappas, N. (1998). Dopamine transporter occupancies in the human brain induced by therapeutic doses of oral methylphenidate. Am. J. Psychiatry 155, 1325-1331.

Walz, J.M., Goldman, R.I., Carapezza, M., Muraskin, J., Brown, T.R., and Sajda, P. (2013). Simultaneous EEG-fMRI Reveals Temporal Evolution of Coupling between Supramodal Cortical Attention Networks and the Brainstem. J. Neurosci. 33, 19212-19222.

Walz, J.M., Goldman, R.I., Carapezza, M., Muraskin, J., Brown, T.R., and Sajda, P. (2014). Simultaneous EEG-fMRI reveals a temporal cascade of task-related and default-mode activations during a simple target detection task. NeuroImage 102, 229-239.

Warbrick, T., Mobascher, A., Brinkmeyer, J., Musso, F., Richter, N., Stoecker, T., Fink, G.R., Shah, N.J., and Winterer, G. (2009). Single-trial P3 amplitude and latency informed event-related fMRI models yield different BOLD response patterns to a target detection task. NeuroImage 47, 1532-1544.

Warbrick, T., Arrubla, J., Boers, F., Neuner, I., and Shah, N.J. (2013). Attention to Detail: Why Considering Task Demands Is Essential for Single-Trial Analysis of BOLD Correlates of the Visual P1 and N1.

Wessel, J.R., and Aron, A.R. (2015). It's not too late: The onset of the frontocentral P3 indexes successful response inhibition in the stop-signal paradigm: Onset latency indexes response inhibition. Psychophysiology 52, 472-480.

Wessel, J.R., and Ullsperger, M. (2011). Selection of independent components representing event-related brain potentials: A data-driven approach for greater objectivity. NeuroImage 54, 2105-2115.

Whiteside, S.P., and Lynam, D.R. (2001). The Five Factor Model and impulsivity: using a structural model of personality to understand impulsivity. Personal. Individ. Differ. 30, 669-689.

Wiersema, R., van der Meere, J., Roeyers, H., Van, Coster, R., and Baeyens, D. (2006a). Event rate and event-related potentials in ADHD. J. Child Psychol. Psychiatry 47, 560-567.

Wiersema, R., van der Meere, J., Antrop, I., and Roeyers, H. (2006b). State regulation in adult ADHD: an event-related potential study. J. Clin. Exp. Neuropsychol. 28, 1113-1126.

Willcutt, E.G., Doyle, A.E., Nigg, J.T., Faraone, S.V., and Pennington, B.F. (2005). Validity of the Executive Function Theory of Attention-Deficit/Hyperactivity Disorder: A Meta-Analytic Review. Biol. Psychiatry 57, 1336-1346.

Wingenfeld, K., Rullkoetter, N., Mensebach, C., Beblo, T., Mertens, M., Kreisel, S., Toepper, M., Driessen, M., and Woermann, F.G. (2009a). Neural correlates of the individual emotional Stroop in borderline personality disorder. Psychoneuroendocrinology 34, 571-586.

Wingenfeld, K., Mensebach, C., Rullkoetter, N., Schlosser, N., Schaffrath, C., Woermann, F.G., Driessen, M., and Beblo, T. (2009b). Attentional bias to personally relevant words in borderline personality disorder is strongly related to comorbid posttraumatic stress disorder. J. Personal. Disord. 23, 141-155.

Wittchen, H.-U., First, M.B., Zaudig, M., and Fydrich, T. (1997). SKID: Strukturiertes klinisches Interview für DSM-IV: Achse I und II (Göttingen (Germany): Hogrefe).

Woltering, S., Liu, Z., Rokeach, A., and Tannock, R. (2013). Neurophysiological differences in inhibitory control between adults with ADHD and their peers. Neuropsychologia 51, 1888-1895.

Woo, C.-W., Krishnan, A., and Wager, T.D. (2014). Cluster-extent based thresholding in fMRI analyses: Pitfalls and recommendations. NeuroImage 91, 412-419.

Woodman, G.F. (2010). A brief introduction to the use of event-related potentials in studies of perception and attention. Atten. Percept. Psychophys. 72, 2031-2046.

Woon, F.L., and Hedges, D.W. (2009). Amygdala volume in adults with posttraumatic stress disorder: a meta-analysis. J. Neuropsychiatry Clin. Neurosci. 21, 5-12.

Woon, F.L., Sood, S., and Hedges, D.W. (2010). Hippocampal volume deficits associated with exposure to psychological trauma and posttraumatic stress disorder in adults: A meta-analysis. Prog. Neuropsychopharmacol. Biol. Psychiatry 34, 1181-1188.

Wu, Y., and Zhou, X. (2009). The P300 and reward valence, magnitude, and expectancy in outcome evaluation. Brain Res. 1286, 114-122.

Yang, B., Chan, R.C.K., Jing, J., Li, T., Sham, P., and Chen, R.Y.L. (2007). A meta-analysis of association studies between the 10-repeat allele of a VNTR polymorphism in the 3'-UTR of dopamine transporter gene and attention deficit hyperactivity disorder. Am. J. Med. Genet. Part B Neuropsychiatr. Genet. Off. Publ. Int. Soc. Psychiatr. Genet. 144B, 541-550.

Young, I.R., Hall, A.S., Pallis, C.A., Legg, N.J., Bydder, G.M., and Steiner, R.E. (1981). Nuclear magnetic resonance imaging of the brain in multiple sclerosis. Lancet 2, 1063-1066.

Zaitsev, M., Hennig, J., and Speck, O. (2004). Point spread function mapping with parallel imaging techniques and high acceleration factors: Fast, robust, and flexible method for echo-planar imaging distortion correction. Magn. Reson. Med. 52, 1156-1166.

Zuberer, A., Brandeis, D., and Drechsler, R. (2015). Are treatment effects of neurofeedback training in children with ADHD related to the successful regulation of brain activity? A review on the learning of regulation of brain activity and a contribution to the discussion on specificity. Front. Hum. Neurosci. 9

van Zutphen, L., Siep, N., Jacob, G.A., Goebel, R., and Arntz, A. (2015). Emotional sensitivity, emotion regulation and impulsivity in borderline personality disorder: a critical review of fMRI studies. Neurosci. Biobehav. Rev. 51, 64-76.

de Zwaan, M., Gruß, B., Müller, A., Graap, H., Martin, A., Glaesmer, H., Hilbert, A., and Philipsen, A. (2012). The estimated prevalence and correlates of adult ADHD in a German community sample. Eur. Arch. Psychiatry Clin. Neurosci. 262, 79-86.

A. Schmüser et al. (2014) Frontiers in Neuroscience

Schmüser, L., Sebastian, A., Mobascher, A., Lieb, K., Tüscher, O., and Feige, B. (2014). Data-driven analysis of simultaneous EEG/fMRI using an ICA approach. Front. Neurosci. 8, 175.

B. Schmüser et al. (2016) Human Brain Mapping

Schmüser, L., Sebastian, A., Mobascher, A., Lieb, K., Feige, B., and Tüscher, O. (2016). Data-driven analysis of simultaneous EEG/fMRI reveals neurophysiological phenotypes of impulse control. Hum. Brain Mapp.. doi: 10.1002/hbm.23230.

C. Curriculum Vitae

The CV was removed for data privacy protection reasons.

The CV was removed for data privacy protection reasons.

The CV was removed for data privacy protection reasons.